Научном већу Института за физику у Београду

ПРЕДМЕТ: Молба за покретање поступка за реизбор у звање виши научни сарадник

Молим Научно веће Института за физику да у складу са Правилником о поступку и начину вредновања и квантитативном исказивању научно-истраживачких резултата истраживача покрене мој реизбор у звање виши научни сарадник.

У прилогу достављам:

1. Мишљење руководиоца са предлогом чланова комисије
2. Кратку стручну биографију
3. Преглед научне активности
4. Елементе за квалитативну оцену научног доприноса
5. Елементе за квантитативну оцену научног доприноса
6. Списак објављених радова и њихове копије
7. Податке о цитираности
8. Копију решења о претходном избору у звање
9. Додатне прилоге са доказима

У Београду,

14.12.2021

С поштовањем,

Зоран Мијић

др Зоран Мијић

Научном већу Института за физику у Београду

ПРЕДМЕТ: Мишљење руководиоца о реизбору др Зорана Мијића у звање виши научни сарадник

Др Зоран Мијић је запослен у Лабораторији за физику животне средине Института за физику у Београду од 2003. године, и руководилац је поменуте лабораторије од 2016. године.

У претходном периоду др Зоран Мијић је био ангажован на пројектима интегралних интердисциплинарних истраживања Министарства просвете, науке и технолошког развоја, као и на неколико међународних пројеката. Бави се темама из области даљинске детекције атмосферских аеросола и њихових оптичких карактеристика, анализом транспорта полутаната као и испитивањима карактеристика атмосфере.

С обзиром да др Зоран Мијић испуњава све критеријуме прописане Правилником о поступку, начину вредновања и квантитативном исказивању научноистраживачких резултата Министарства просвете, науке и технолошког развоја сагласан сам са покретањем поступка за реизбор др Зорана Мијића у звање виши научни сарадник.

За састав Комисије за реизбор др Зорана Мијића у звање виши научни сарадник предлажем:

1. др Владимира Срећковића, научног саветника Института за физику у Београду,
2. др Горана Попарића, редовног професора Физичког факултета Универзитета у Београду,
3. др Владимира Удовичића, вишег научног сарадника Института за физику у Београду

др Александар Богојевић
директор Института за физику

У Београду,
14.12.2021.

2. БИОГРАФСКИ ПОДАЦИ КАНДИДАТА

Зоран Мијић је рођен 15.08.1976. године у Бијељини, Босна и Херцеговина. Основне студије на Физичком факултету Универзитета у Београду завршава 2003. године са просечном оценом 9,14 одбранивши дипломски рад под називом "Методе мерења и узорковања суспендованих честица ПМ10 и ПМ2.5 у ваздуху Београда". У Институту за физику запослен је од 1. јула 2003. године када и уписује последипломске студије на Физичком факултету Универзитета у Београду, смер примењена и компјутерска физика које завршава са просечном оценом десет (10). Магистарски рад под називом "Мерење концентрација суспендованих честица у ваздуху и примена статистичких модела за процену утицаја различитих извора емисије", урађен у Лабораторији за физику околине, под руководством др Мирјане Тасић, одбранио је 24. новембра 2006. године чиме је стекао академски назив магистра физичких наука.

Зоран Мијић је 25. марта 2011. године на Физичком факултету Универзитета у Београду одбранио докторску дисертацију под називом "Одређивање физичко-хемијских карактеристика, просторне и временске расподеле тропосферског аеросола: LIDAR систем и рецепторски модели" под менторством др Мирјане Тасић.

Добитник је награде „проф. др Љубомир Ћирковић" за најбољи магистарски рад одбрањен на Физичком факултету у Београду за 2006/2007. годину.

Од 2007. до 2013. године Зоран Мијић је био активни члан Комисије за такмичење из физике ученика средњих школа Друштва физичара Србије, као аутор задатака. У име Друштва физичара Србије је као стручни руководилац предводио екипе наше земље на Међународним олимпијадама из физике 2009. године у Мексику и 2011. године на Тајланду.

Руководилац је Лабораторије за физику животне средине Института за физику у Београду од 2016. године и био је ангажован на више националних пројеката финансираних од стране Министарства просвете, науке и технолошког развоја. Руководио је потпројектом у оквиру пројекта интегралних интердисциплинарних истраживања ИИИ43007 "Истраживања климатских промена и њиховог утицаја на животну средину. Праћење утицаја, адаптација и ублажавање".

Учествовао је у више међународних пројеката и руководио је тимом из Института за физику у два EU H2020 пројекта: GEO-CRADLE (Coordinating and integRating state-of-the-art Earth Observation Activities in the regions of North Africa, Middle East, and Balkans and Developing Links with GEO related initiatives towards GEOSS), и ACTRIS-2 (Aerosols, Clouds, and Trace gases Research InfraStructure Network) Integrated Activities (IA). Одговорни је истраживач у оквиру Европске мреже лидар мерних станица EARLINET (the European Aerosol Research Lidar Network).

Од 2021. године обавља функцију националног координатора у оквиру Европског програма за сарадњу у домену научних и технолошких истраживања - COST (European Cooperation in Science and Technology).

Др Зоран Мијић је објавио 21 рад у међународним часописима који су на основу базе SCOPUS цитирани 442 пута (без самоцитата) уз h-index 11.

3. ПРЕГЛЕД НАУЧНЕ АКТИВНОСТИ

Своје досадашње научне активности и истраживања др Зоран Мијић је развијао у области

физике атмосфере, даљинске детекције и мултидисциплинарних истраживања у области заштите животне средине. Правац истраживања у претходном периоду је био усмерен ка експерименталним мерењима карактеристика атмосферских аеросола, испарљивих органских једињења, као и примени хибридних модела за анализу транспорта загађујућих материја. Управо испитивање транспорта атмосферских загађујућих материја, са посебним фокусом на атмосферске аеросоле, као и коришћење даљинске детекције (активне и пасивне) за одређивање оптичких карактеристика аеросола (вертикалних профила коефицијената екстинкције, расејања) у основи су истраживачких активности др Зорана Мијића.

У наставку су укратко описане активности кандидата у оквиру истраживачких тема:

Напомена: Звездицом (*) су означени радови публиковани у периоду након претходног избора у звање

3.1 Примена даљинске детекције за испитивање атмосферских аеросола и карактеристика атмосфере

Атмосферски аеросоли се у основи дефинишу као мултифазни системи сачињени од чврстих и/или течних честица суспендованих у гасној средини, односно ваздуху. Потреба за континуалним мерењима аеросола је последица њиховог утицаја на многе аспекте живота: заједно са гасовима стаклене баште имају кључну улогу у климатским променама и велики утицај на хемијске процесе у атмосфери као површине за одвијање реакција које доводе до смањења озонског слоја; утичу на укупни биланс зрачења и расподелу температуре, као и на оптичке карактеристике атмосфере. Од 2014. године Зоран Мијић је одговорни истраживач за лидар мерну станицу у Београду у оквиру EARLINET мреже. Поред мерења вертикалних профила аеросола у циљу испитивања оптичких карактеристика и климатолошких студија у протеклом периоду је Раман лидар систем коришћен и за одређивање висине и динамике планетарног граничног слоја (ПГС). Специфичан случај делимичног помрачења Сунца је искоришћен за испитивање параметара атмосфере у пертурбованим условима. Метод градијента је употребљен за анализу динамике ПГС-а користећи еластично расејано зрачење уназад на 355 nm и аеросоле као трасере. Истовремено у вишим слојевима атмосфере у сарадњи са др Владимиром Срећковићем вршена је анализа експериментално забележених података релевантних за електромагнетне сигнале врло ниских фреквенција (VLF сигнали). У даљем раду је урађено моделовање просторних и временских расподела електронске концентрације посебно развијеном техником упоређивања регистрованих амплитуда и фаза са одговарајућим вредностима добијеним нумеричким моделовањем простирања VLF сигнала. Такође уведен је једноставан израз за висинску и временску расподелу електронске концентрације и вршено је нумеричко моделовање плазме ниске јоносфере услед јаких Сунчевих пертубација. У оквиру EARLINET мреже развијен је и тестиран јединствен процес прорачуна Single Calculus Chain (SCC) којим се омогућава процесуирање података добијених лидар мерењима са високом резолуцијом. Имплементиран је итеративни метод чиме се прорачунава вертикалан профил коефицијената расејања уназад и односа деполаризације расејаног зрачења на честицама. Тиме се омогућава идентификација честица неправилног облика као што су вулканска или пустињска прашина што представља основу за успостављање система за рано упозорење. Добијени резултати у оквиру описане сарадње су приказани у следећим радовима:

- *Papagiannopoulos, N., D'Amico, G., Gialitaki, A., Ajtai, N., Alados-Arboledas, L., Amodeo, A., Amiridis, V., Baars, H., Balis, D., Binietoglou, I., Comerón, A., Dionisi, D., Falconieri, A., Fréville, P., Kampouri, A., Mattis, I., **Mijić**, **Z.**, Molero, F., Papayannis, A., Pappalardo, G., Rodríguez-Gómez, A., Solomos, S., and Mona, L. (2020). An EARLINET early warning system for atmospheric aerosol aviation hazards, Atmospheric Chemistry and Physics (20) 10775–10789. doi:10.5194/acp-20-10775-2020
- *L. Ilić, M. Kuzmanoski, P. Kolarž, A. Nina, V. Srećković, **Z. Mijić**, J. Bajčetić, M. Andrić, (2018). Changes of atmospheric properties over Belgrade, observed using remote sensing and in situ methods during the partial solar eclipse of 20 March 2015, Journal of Atmospheric and Solar-Terrestrial Physics, 171, 250-259. doi:10.1016/j.jastp.2017.10.001
- *Srećković V.A, Šulić D.M, Vujčić V, **Mijić Z.R,** Ignjatović L.M. (2021). Novel Modelling Approach for Obtaining the Parameters of Low Ionosphere under Extreme Radiation in X-Spectral Range. Applied Sciences 11(23):11574. doi:10.3390/app112311574
- *Kolarski A, Srećković V.A, **Mijić Z.R**. (2022). Response of the Earth's Lower Ionosphere to Solar Flares and Lightning-Induced Electron Precipitation Events by Analysis of VLF Signals: Similarities and Differences. Applied Sciences 12(2):582. doi:10.3390/app12020582

3.2 Примена рецепторског моделирања за идентификацију и квантификацију доприноса извора емисије

Једна од основних потешкоћа у процесу осмишљавања стратегије за контролу квалитета ваздуха јесте идентификација и квантификација утицаја појединих извора емисије на концентрације загађујућих материја у ваздуху. Потешкоће у примени дисперзионих модела настају услед непотпуне или нетачне информације о појединим изворима емисије одређених загађујућих материја. У оваквим случајевима потребно је имати алтернативне моделе који ће допринети идентификацији извора емисије. Такви модели се називају рецепторски модели, јер су оријентисани на амбијенталне концентрације на месту мерења (место рецептора) за разлику од дисперзионих модела који су оријентисани на извор емисије, транспорт и трансформације загађујућих материја од места извора па све до места мерења. На основу измерених вредности масених концентрација одређеног броја хемијских компоненти у саставу атмосферских аеросола и испарљивих органских једињења (ИОЈ) помоћу рецепторских модела је могуће одредити највероватнији број извора емисије, састав извора, као и допринос појединог извора у укупно измереној концентрацији сваког узорка.

Први резултати су добијени применом анализе главних компонената (PCA – Principal component analysis) над честицама PM_{10} и $PM_{2.5}$ и публиковани су у радовима:

- Slavica Rajsic, **Zoran Mijic,** Mirjana Tasic, Mirjana Radenkovic and Jasminka Joksic, (2008). Evaluation of the levels and sources of trace elements in urban particulate matter, Environmental Chemistry Letters, 6(2), 95-100. doi: 10.1007/s 10311-007-0115-0
- Dragan M. Markovic, Dragan A. Markovic, Anka Jovanovic, Lazar Lazic, **Zoran Mijic,** (2008), Determination of Oз, N02, S02, CO and PM10 measured in Belgrade urban area, Environmental Monitoring and Assessment 145 (1), 349-359. doi: 10.1007/s 10661-007-0044-1

Упоредо је вршена и физичко-хемијска карактеризација појединачних PM честица анализом репрезентативних PM_{10} и $PM_{2.5}$ узорака коришћењем електронске микроскопије (SEM/EDX-анализа). Кандидат је руководио експерименталном поставком мерења и активно учествовао у анализи узорака помоћу електронске микроскопије. Одређене су расподеле честица по величини, фактору облика, као и карактеристичне групе честица у односу на њихов хемијски састав и облик. Извршено је и поређење наведених карактеристика честица током различитих временских периода чиме је указано на порекло честица и резултати су публиковани у следећим радовима.

- Tasic M., Duric-Stanojevic B., Rajsic S.F., **Mijic** Z., Novakovic V.T., (2006) Physico-chemical Characterization of PM10 and PM2.5 in the Belgrade Urban Area, Acta Chimica Slovenica 53, 401-405.
- **Zoran Mijic,** Slavica Rajsic, Andrijana Zekic, Mirjana Perisic, Andreja Stojic and Mirjana Tasic (2010). Characteristics and application of receptor models to the atmospheric aerosols research, Book chapter in Air quality edited by Ashok Kumar, pp.143-167. ISBN 978-953-307-131-2.

У свом даљем раду кандидат наставља рад на развоју и примени нових рецепторских модела, посебно UNMIX и PMF (Positive Matrix Factorization). UNMIX се базира на анализи својствених вектора корелационе матрице података, док за процену грешке приликом рачунања састава појединачних извора емисије користи метод узорковања са понављањем (bootstrap). PMF за одређивање састава и доприноса појединих извора емисије користи једначину одржања масе и метод најмањег квадрата за минимизирање разлике између мерених података и података предвиђених моделом. Уз услов постојања ненегативних састава и доприноса појединих извора PMF омогућава и појединачно пондерисање сваког мерења чиме се недостајући подаци могу третирати као мерења са великом грешком. Модели су успешно примењивани на вишегодишњу базу концентрација PM_{10} честица и њиховог хемијског састава (As, Cd, Cr, Mn, Ni, Pb, Cl^-, Na^+, K^+, Mg, Ca, NO_3^-, SO_4^{2-}, NH_4^+ и бензо(а)пирен) као и укупну атмосферску депозицију. Упоредо са идентификацијом и проценом доприноса појединих извора емисије анализирана је и динамика и периодичност њиховог доприноса коришћем Фуријеове спектралне анализе. Резултати су објављени у следећим радовима:

- **Mijic,** Z., Stojic, A., Perisic, M., Rajsic, S., Tasic, M. (2012). Receptor modeling studies for the characterization of PM 10 pollution sources in Belgrade. Chemical Industry and Chemical Engineering Quarterly, 18(4-2), 623-634.
- Lazic L., Urosevic M.A., **Mijic** Z., Vukovic G., Ilic L. (2016). Traffic contriЬution to air pollution in urban street canyons: Integrated application of the OSPM, moss biomonitoring and spectral analysis, Atmospheric Environment, 141, 347-360.
- Stojic, A., Stanisic Stojic, S., Reljin, 1., Cabarkapa, M., Sostaric, A., Perisic, M., **Mijic, Z**. (2016). Comprehensive analysis of PM10 in Belgrade urban area on the basis of long term measurements. Environmental Science and Pollution Research, 23, 10722-10732.
- **Mijic, Z**., Stojic, A., Perisic, M., Rajsic, S., Tasic, M., Radenkovic, M., Joksic, J. (2010). Seasonal variability and source apportionment of metals in the atmospheric deposition in Belgrade. Atmospheric Environment, 44(30), 3630-3637.

Заједно са колегом др Андрејом Стојићем, коме је кандидат био ментор, Зоран Мијић проширује примену рецепторских модела и прилагођава њихову примену на испарљива органска једињења и неорганске гасове у атмосфери. Мерењем концентрација испарљивих органских једињења на великом броју молекулских маса методом масене спектрометрије са трансфером протона *(Proton Transfer Reaction Mass Spectrometry* – PTR-MS), јединствене у земљама Западног Балкана, установљена је репрезентативна база података у урбаној и семи-урбаној средини Београда. Резултати истраживања су приказани у радовима:

- *Šoštaric, S. Stanišic Stojic, G. Vukovic, **Z. Mijic**, A. Stojic, Gržetic I. (2017). Rainwater capacities for BTEX scavenging from ambient air, Atmospheric Environment, 168, 46-54, doi:10.1016/j.atmosenv.2017.08.045
- Stojic, A., Stanisic Stojic, S., Sostaric, A., Ilic, L., **Mijic Z**., Rajsic S. (2015). Characterization of VOC sources in urban area based on PTR-MS measurements and receptor modelling, Environmental Science and Pollution Research, 22, 13137-13152.
- Stojic, S. Stanisic Stojic, **Z. Mijic**, L. Ilic, M. Tomasevic, Marija Todorovic, and Mirjana Perisic (2015). Comprehensive Analysis of VOC Emission Sources in Belgrade Urban Area, In: Urban and Built Environments: Sustainable Developments, Health Implications and Challenges, Editor: Alexis Cohen, Nova Science Publishers, NY, USA, pp. 55-87, ISBN: 978- 1-63483-117-8
- Tomasevic, M., **Z. Mijic**, M. Anicic, A. Stojic, M. Perisic, M. Kuzmanoski, M. Todorovic, and S. Rajsic (2013). Air Quality Study in Belgrade: Particulate Matter and Volatile Organic Compounds as Threats to Human Health, In: Air Pollution: Sources, Prevention and Health Effects, Editor: Rajat Sethi, Nova Science Publishers, NY, USA, pp. 315-346, 2013. ISBN: 978-1-62417- 735-4

3.3 Испитивање транспорта атмосферских загађујућих материја

Присуство атмосферских полутаната, првенствено атмосферских аеросола и испарљивих органских једињења (ИОЈ) у одређеној области зависе од извора емисије, али и од транспорта ваздушних маса. Као алтернатива дисперзионим моделима за анализу транспорта полутаната развијени су хибридни рецепторски модели који омогућавају анализу и просторну идентификацију извора емисије и њихов допринос на регионалном нивоу. Фокус истраживања кандидата је на анализи транспорта атмосферских аеросола и ИОЈ помоћу хибридних модела функције потенцијалних доприноса PSCF (Potential Source Contribution Function) и CWT (Concentration Weighted Trajectory) који подразумевају одређивање трајекторија делића ваздуха на регионалном нивоу, као и CPF (Conditional Probability Function) и CBF (Conditional Bivariate Function) за локалну просторну анализу извора емисије. За одређивање просторне вероватноће расподеле потенцијалних извора емисије и квантификације њиховог доприноса на месту рецептора неопходно је израчунати трајекторије делића ваздуха и утврдити њихову репрезентативност вршењем селекције у зависности од висине планетарног граничног слоја (ПГС). Управо одређивање висине ПГС-а је први пут рађено на простору Балкана помоћу новог Раман лидар система детекцијом еластично расејаног повратног зрачења на таласној дужини 355 nm и Рамановог расејања на 387 nm. Принцип рада лидар система се заснива на емитовању импулсног ласерског зрачења у атмосферу и детектовању дела зрачења расејаног уназад. Висока временска и просторна резолуција мерења, могућност осматрања и праћења у реалном времену и

амбијенталним условима, као и могућност мерења на раздаљинама до више километара допринели су атрактивности примене лидар система. Зоран Мијић је у Институту за физику радио на развоју лидар система заснованог на детекцији еластично расејаног зрачења уназад на таласној дужини 532 nm и био је водећи истраживач за увођење и покретање новог Раман лидар система, јединственог на овим просторима. Одговорни је истраживач за интеграцију и мерења у оквиру европске мреже лидар станица чиме је започето добијање квантитативне базе података о вертикалној расподели и кретањима аеросола изнад нашег региона. Резултати добијени експерименталним мерењима помоћу лидар система су коришћени за унапређење хибридних модела и добијање прецизније слике о транспорту загађујућих материја у региону. Недавно је започета сарадња са др Слободаном Ничковићем на унапређењу и валидацији дисперзионог модела за прогнозу транспорта честица полена у који су укључени додатни процеси који доприносе стварању субполенских честица за које се показује да представљају изузетну опасност, посебно за настајање астме.

- *S. Ničković, L. Ilić, S. Petković, G. Pejanović, A. Huete, **Z. Mijić**. A Numerical Model For Pollen Prediction: Thunderstorm Asthma Case Study, The 8th International WeBIOPATR Workshop & Conference, 29th November to 1st December 2021, Abstracts of Keynote Invited Lectures and Contributed papers, p. 37
- **Zoran Mijic**, Andreja Stojic, Mirjana Perisic, Slavica Rajsic and Mirjana Tasic (2012). In: Air Quality - New Perspective, Statistical Character and Transport Pathways of Atmospheric Aerosols in Belgrade, pp. 199 - 226, Editors: Gustavo Lopez Badilla, Benjamin Valdez and Michael Schorr, Published by InTech, ISBN: 978-953-51-0674-6.
- Stojic, A., Stojic, S. S., **Mijic, Z**., Sostaric, A., Rajsic, S. (2015). Spatio-temporal distribution of VOC emissions in urban area based оп receptor modeling. Atmospheric Environment, 106, 71-79.
- **Z. Mijic**, M. Kuzmanoski, D. Nicolau, L. Belegante (2013). The use of hybrid receptor models and ground based remote sensing of particulate matter for identification of potential source regions, Proceedings from the 4th WeBIOPATR Workshop, pp. 52-59.
- Kuzmanoski M., L. Ilic, **Z. Mijic**, Aerosol remote sensing study of a Saharan dust intrusion episode in Belgrade, Serbia, XIX International Eco-conference, Environmental protection of urban and suburban settlements, Proceedings, pp. 73-81. September 23-25, 2015. Novi Sad, Serbia.
- **Mijic Z.,** M. Perisic, A. Stojic, M. Kuzmanoski, L. Ilic, Estimation of atmospheric aerosol transport by ground-based remote sensing and modeling, XIX International Eco-conference, Environmental protection of urban and suburban settlements, Proceedings, pp. 375-382. September 23-25, 2015. Novi Sad, Serbia.

3.4 Примена статистичких модела за процену и прогнозу концентрација атмосферских загађујућих материја

Различити статистички модели су примењивани за анализу постојећих база података које се односе на мерења концентрација атмосферских загађујућих материја у Србији у циљу квантитативног одређивања и процене усаглашености постојећег стања са важећим регулативама. На основу података добијених у експерименталним кампањама моделиране су различите фунције расподеле појединих полутаната које су искоришћене за процену

неопходне редукције емисије, као и анализу екстремних вредности измерених концентрација полутаната и њихову вероватноћу појављивања у различитим условима. Тестиране су различите функције расподеле масених концентрација PM честица, и показано је да Пирсонова типа V и логнормална расподела у већини случајева најбоље репрезентују измерене масене концентрације. Особине ових функција су даље искоришћене за предвиђање вероватноће премашивања критичних вредности концентрација у наредном периоду као и процену неопходне редукције емисије. У циљу бољег описивања области високих концентрација PM честица из теорије екстремних вредности су изведена два типа расподела, двопараметарска експоненцијална и асимптотска функција које боље описују расподелу измерених високих концентрација PM честица и дају приближнију вероватноћу премашивања критичних вредности. Овако развијени приступ има практичну примену (коришћен је и за припрему званичног плана управљања квалитетом ваздуха на територији града Београда) и добијени резултати су публиковани у следећим радовима:

- **Zoran Mijic**, Mirjana Tasic, Slavica Rajsic, Velibor Novakovic, (2009). The statistical characters of PM10 in Belgrade area, Atmospheric Research, 92 (4), 420-426. doi:10.1016/ j.atmosres.2009.01.002
- Perisic, M, Stojic, A., Stojic, S. S., Sostaric, A., **Mijic, Z**., Rajsic, S. (2015). Estimation of required PM10 emission source reduction on the basis of a 10-year period data. Air Quality, Atmosphere & Health, 8, 379-389. doi: 10. 1007/ sl1869-014-0292-5
- Marija N. Todorovic, Mirjana D. Perisic, Maja Kuzmanoski, Andreja M. Stojic, Andrej I. Sostaric, **Zoran R. Mijic** and Slavica F. Rajsic (2015) Assessment of PM10 pollution level and required source emission reduction in Belgrade area.
  Journal of Environmental Science and Health Part A, 50(13), 1351-1359. doi: 10.1080/10934529 .2015 .1059110

Упоредо са претходним, предложена је и нова метода прогнозе квантитативног доприноса појединих извора емисије заснована на мултиваријационим моделима који као улазне параметре могу да користе саставе извора који су претходно добијени помоћу рецепторских модела. Показано је да се на такав начин може извршити прогноза појављивања високих конценрација загађујућих материја у појединим областима само на основу стандардних метеоролошких мерења. Метода је тестирана на бази података измерених концентрација већег броја испарљивих органских једињења применом масене спектрометрије са трансфером протона, а резултат је приказан у раду

- Stojic, A., Maletic, D., Stojic, S. S., **Mijic, Z**., Sostaric, A. (2015). Forecasting of VOC emissions from traffic and industry using classification and regression multivariate methods, Science of the Total Environment, 521-522, 19-26.

4. ЕЛЕМЕНТИ ЗА КВАЛИТАТИВНУ ОЦЕНУ НАУЧНОГ ДОПРИНОСА КАНДИДАТА

4.1 Квалитет научних резултата

4.1.1 Научни ниво и значај резултата, утицај научних радова

Др Зоран Мијић је у свом досадашњем научном раду објавио укупно 21 радова у међународним часописима са ISI листе, од чега 9 категорије М21 (2 рада у међународном часопису изузетних вредности М21а и 7 радова у врхунском међународном часопису М21), 8 категорије М22 (истакнути међународни часописи), 4 категорије М23 (међународни часописи), 2 категорије М31, 22 категорије М33 (саопштења са међународних скупова штампана у целини) и 29 категорије М34 (саопштења са међународних скупова штампана у изводу), 2 категорије М53, 1 категорије М61, 15 категорије М63, 2 категорије М64, као и 3 поглавља у књизи категорије М13 и 3 у категорији М14.

Након претходног избора у звање објављено је 5 радова у међународним часописима са ISI листе, од чега 2 категорије М21 (1 рад у међународном часопису изузетних вредности М21а и 1 рад у врхунском међународном часопису М21), 3 категорије М22 (истакнути међународни часописи), 6 категорије М33 (саопштења са међународних скупова штампана у целини) и 9 категорије М34 (саопштења са међународних скупова штампана у изводу), 1 категорије М63. Као пет најзначајнијих радова кандидата могу се узети:

1. **Zoran Mijic**, Mirjana Tasic, Slavica Rajsic, Velibor Novakovic, (2009). The statistical characters of PM10 in Belgrade area, Atmospheric Research, 92 (4), 420-426. doi:10.1016/ j.atmosres.2009.01.002 (ИФ= l,811, цитиран 24 пута)
2. **Mijic, Z**., Stojic, A., Perisic, M., Rajsic, S., Tasic, M., Radenkovic, M., Joksic, J. (2010). Seasonal variability and source apportionment of metals in the atmospheric deposition in Belgrade. Atmospheric Environment, 44(30), 3630-3637 (ИФ= 3,459, цитиран 84 пута)
3. Stojic, A., Stojic, S. S., **Mijic, Z**., Sostaric, A., Rajsic, S. (2015). Spatio-temporal distribution of VOC emissions in urban area based on receptor modeling, Atmospheric Environment, 106, 71-79. doi:10.1016/j.atmosenv.2015.01.071 (ІФ = 3,459, цитиран 19 пута)
4. Lazic L., Urosevic M.A., **Mijic** Z., Vukovic G., Ilic L. (2016). Traffic contriЬution to air pollution in urban street canyons: Integrated application of the OSPM, moss biomonitoring and spectral analysis, Atmospheric Environment, 141, 347-360. (ИФ=3,459, цитиран 19 пута)
5. Papagiannopoulos, N., D'Amico, G., Gialitaki, A., Ajtai, N., Alados-Arboledas, L., Amodeo, A., Amiridis, V., Baars, H., Balis, D., Binietoglou, I., Comerón, A., Dionisi, D., Falconieri, A., Fréville, P., Kampouri, A., Mattis, I., **Mijić**, **Z**., Molero, F., Papayannis, A., Pappalardo, G., Rodríguez-Gómez, A., Solomos, S., and Mona, L. (2020). An EARLINET early warning system for atmospheric aerosol aviation hazards, Atmospheric Chemistry and Physics (20) 10775–10789. doi:10.5194/acp-20-10775-2020 (ИФ= 6,133, цитиран 4 пута)

Наведених пет научних радова репрезентују области којима се кандидат активно бави и у којима је дао значајан научни допринос.

Радови 1. и 2. су настали током припреме докторске дисертације. У раду 1 анализиране су статистичке карактеристике PM_{10} честица и тестирано је неколико функција расподеле за процену неопходне редукције емисије, као и анализу екстремних вредности измерених концентрација и њихову вероватноћу појављивања. Особине ових функција су даље искоришћене за предвиђање вероватноће премашивања критичних вредности концентрација као и процену неопходне редукције емисије. У циљу бољег описивања области високих концентрација PM честица из теорије екстремних вредности су изведена два типа расподела, двопараметарска експоненцијална и асимптотска функција које дају приближнију вероватноћу премашивања критичних вредности. Слична метода је широко коришћена у практичној примени за процену стања квалитета ваздуха.

Други рад се односи на четворогодишњу студију процене утицаја антропогених извора емисије на животну средину анализирањем месечних узорака укупне депозиције. Атомском апсорпционом спектрометријом анализиране су концентрације Al, V, Cr, Mn, Fe, Ni, Cu, Zn, Cd и Pb и примењен је мултиваријанти рецепторски модел за идентификацију и квантификацију утицаја главних извора емисије. Један је од најцитиранијих радова имајући у виду презентовану базу података и почетак примене рецепторских модела у овој области.

У трећем раду је проширена примена хибридних рецепторских модела (Unmix, PMF) на концентрације испарљивих органских једињења, аеросола и гасова NO_x, NO_2, NO, SO_2, CO, and PM_{10} добијене током кампање мерења у Београду. Поуздана идентификација извора загађивача, опис њихових карактеристика и процена њихове просторно-временске дистрибуције приказани су кроз свеобухватну анализу и поређење решења рецепторског модела, с обзиром на метеоролошке податке, висину планетарног граничног слоја и регионални и транспорт на даљину.

У четвртом раду се испитивала расподела загађујућих материја у амбијенту урбаног уличног кањона. Коришћен је Operational Street Pollution Model (OSPM) за часовну прогнозу садржаја NO_X, NO, NO_2, O_3, CO, BNZ and PM_{10}. Студија је спроведена у пет уличних кањона у Београду током 10-недељног летњег периода. Тестиране су могућности биомонитора за компарацију и анализу тренда промена концентрација са висином у урбаним условима. Примењена је спектрална анализа за испитивање варијација и периодичности антропогеног утицаја.

У петом раду је представљен потпуно нов метод за откривање потенцијалних опасности у ваздуху услед присуства атмосферских аеросола. Метод је заснован на мерењима помоћу лидар система у скоро реалном времену (near real time - NRT). У оквиру EARLINET мреже развијен је и тестиран јединствен процес прорачуна The Single Calculus Chain (SCC) којим се омогућава процесуирање података добијених лидар мерењима са високом резолуцијом. Имплементиран је итеративни метод чиме се прорачунава вертикалан профил коефицијената расејања уназад и односа деполаризације расејаног зрачења на честицама. Тиме се омогућава идентификација честица неправилног облика као што су вулканска или пустињска прашина што представља основу за успостављање система за рано упозорење.

4.1.2 Позитивна цитираност научних радова кандидата

Подаци о цитираности радова кандидата према базама података Scopus и Web of Science су сумирани у наредној табели.

База података	Број цитата	Број цитата без самоцитата	h-index
Scopus	517	442	11
Web of Science	463	417	11

Прилог: подаци о цитираности са интернет странице ISI Web of Science и Scopus

4.1.3 Параметри квалитета часописа

За процену квалитета часописа у којима су радови публиковани у наставку су приказане категорије часописа и њихов фактор утицаја, односно импакт фактор – ИФ (наведена је најбоља вредност из периода до две године уназад од када је рад објављен). Подвучени су они фактори утицаја за часописе у којима је кандидат објављивао након претходног избора у звање:
У категорији М21а (међународни часопис изузетних вредности) кандидат је објавио радове у следећем часопису:

1 рад у *Science of the Total Environment* (ИФ=4,099)
1 рад у *Atmospheric Chemistry and Physics* (ИФ=6,133)

У категорији М21 (врхунски међународни часопис) кандидат је објавио радове у следећим часописима:
1 рад у *Environmental Pollution* (ИФ=3,426)
рада у *Atmospheric Environment* (ИФ=3,459 за 2 рада, ИФ=3,226 за 1 рад, ИФ=3,705 за 1 рад)
2 рада у *Environmental Science and Pollution Research* (ИФ=2,828 за 2 рада)

У категорији М22 (истакнути међународни часопис) кандидат је објавио радове у следећим часописима:
2 рада у Applied Sciences (ИФ= 2.679 за 2 рада)
1 рад у *Journal of Atmospheric and Solar-Terrestrial Physics* (ИФ= 1,79)
2 рада у *Air Quality, Atmosphere & Health* (ИФ=2,324 за 2 рада)
1 рад у *Atmospheric Research* (ИФ= l,811)
1 рад у *Environmental Chemistry Letters* (ИФ= 1,584)
1 рад у *Physica Scripta* (ИФ= 1,920)

У категорији М23 (међународни часопис) кандидат је објавио радове у следећим часописима:
1 рад у *Journal of Environmental Science and Health Part A* (ИФ= 1,276)
1 рад у *Environmental Monitoring and Assessment* (ИФ= 1,035)
1 рад у *Acta Chimica Slovenica* (ИФ=О,703)
1 рад у *Chemical Industry and Chemical Engineering Quarterly* (ИФ=О,610)

Укупан фактор утицаја радова кандидата износи 53,003, а у периоду након претходног избора у звање фактор утицаја је 16,989.

Часописи у којима је кандидат објављивао радове су по свом угледу цењени и водећи у областима којима припадају, а посебно се истичу часописи *Atmospheric Environment, Atmospheric Research* у области физике атмосфере и метеорологије, *Atmospheric Chemistry*

and Physics, *Science of the Total Environment, Environmental Science and Pollution Research* у области заштите животне средине и климатских промена.

Додатни библиометријски показатељи у вези са објављеним радовима кандидата након претходног избора у научно звање дати су у доњој табели. Она садржи импакт факторе (ИФ) радова, М20 бодове радова по категоризацији научноистраживачких резултата, као и импакт фактор нормализован по импакту цитирајућег чланка (СНИП) (најбоља вредност из периода до две године уназад од објаве рада). У табели су дате укупне вредности, као и вредности свих фактора усредњених по броју чланака и по броју аутора по чланку, за радове објављене у М20 категоријама

	ИФ	М	СНИП
Укупно	16,989	33	6,4
Усредњено по чланку	3,398	6,6	1,28
Усредњено по аутору	2,537	1,435	1,04

4.1.4 Степен самосталности и степен учешћа у реализацији радова у научним центрима у земљи и иностранству

Др Зоран Мијић има изражену самосталност у научном раду и значајан допринос у већини публикација. Покренуо је истраживања у области транспорта различитих загађујућих материја у атмосфери применом хибридних атмосферских модела у Лабораторији за физику животне средине Института за физику. У истраживања која се односе на анализу транспорта загађујућих материја у атмосфери су били укључени и докторанти, до сада су одбрањене две докторске дисертације на Физичком факултету Универзитетата у Београду, а једном од њих је кандидат руководио и био ментор. У радовима који су објављени у периоду након избора у претходно звање кандидат је учествовао у свим експерименталним поставкама, и активно учествовао у истраживањима. Посебно треба истаћи самосталност кандидата у развоју и примени хибридних модела. Заједно са својим студентом, др Андрејом Стојићем коме је био ментор, проширио је истраживања на примену масене спектрометрије са трансфером протона на испитивања динамике и транспорта испарљивих органских једињења у атмосфери.

У истраживањима која се односе на примену ласера за даљинску детекцију атмосферских аеросола и испитивање њихових оптичких карактеристика кандидат је као докторанд у Институту за физику учествовао у развоју лидар система заснованог на детекцији еластично расејаног зрачења уназад на таласној дужини 532 nm. Након боравка у National Institute of Research&Development for Optoelectronics у Букурешту и успостављања сарадње са лабораторијом за даљинска осматрања у атмосфери, Зоран Мијић стиче експериментално искуство и иницира даље унапређење даљинске детекције атмосферских аеросола применом Раман лидар система. Тренутно је водећи истраживач и одговоран за експерименталну поставку и рад овог јединственог система у региону.

4.1.5 Награде и признања за научни рад

Кандидат је добитник награде "Др Љубомир Ћирковић " за најбољи магистарски рад одбрањен на Физичком факултету Универзитета у Београду за 2006/2007 годину.

4.2 Ангажованост у формирању научних кадрова и развоју услова за научни рад

Др Зоран Мијић је од 2016. године руководилац Лабораторије за физику животне средине у Институту за физику, а у периоду од 2012-2018. г. био је ангажован и у оквиру активности Центра изузетних вредности за примену плазме у нанотехнологијама, биомедицини и екологији. Активно је учествовао у обезбеђивању средстава за опремање лабораторије и био је одговоран за набавку капиталне опреме (Раман лидар систем) као и за инсталацију, конфигурацију и изградњу пратеће инфраструктуре. Раман лидар систем је успешно тестиран и пуштен у рад почетком 2014. године. Успостављена је прва мерна станица у Србији и региону која је придружена Европској мрежи лидар мерних станица (EARLINET-European Aerosol Research Lldar Network), а др Зоран Мијић је именован за одговорног истраживача (PI). У оквиру међународне сарадње др Зоран Мијић предводи тим који је укључен у два пројекта из програма EU H2020 (ACTRIS2 Integrated Activities - Aerosols, Clouds, and Trace gases Research InfraStructure Network, и GEO-CRADLE - Coordinating and integRating state-of-the-art Earth Observation Activities in the regions of North Africa, Middle East, and Balkans and Developing Links with GEO related initiatives towards GEOSS) чиме је обезбеђено додатно финансирање за рад Лабораторије за физику животне средине због чега 2017. године добија награду за финансијски допринос Института за физику. Претходне активности су омогућиле значајан искорак у новом правцу истраживања оптичких карактеристика и транспорта атмосферских аеросола. Упоредо са покренутом новом истраживачком темом о примени хибридних рецепторских модела за анализу транспорта полутаната у атмосфери, даљинска детекција и испитивања у атмосфери представљају главну тему научног рада др Зорана Мијића у оквиру које је одбрањена једна докторска дисертација, а у току је рад на изради још једне докторске дисертације.

4.3. Нормирање броја коауторских радова, патената и техничких решења

У свим публикованим радовима кандидата су комбинована експериментална истраживања са теоријским и нумеричким симулацијама па.се рачунају са пуном тежином у односу на 7 коаутора . Од укупно 16 публикација које су објављене у периоду након претходног избора у звање одговарајуће нормирање на основу броја коаутора зе извршено за 1 рад категорије М21а, 1 рад категорије М22, 1 рад категорије М33 и 1 рад категорије М63. Број М бодова је 44.5, а након нормирања је 35,15 што је изнад захтеваног броја бодова за реизбор у звање виши научни сарадник.

4.4 Руковођење пројектима, потпројектима и пројектним задацима

Др Зоран Мијић је од 2016. руководилац Лабораторије за физику животне средине Институза за физику у Београду.

- Др Зоран Мијић је у оквиру пројекта ИИИ43007 "Истраживање климатских промена и њиховог утицаја на животну средину- праћење утицаја, адаптација и ублажавње" (2011- 2019), финансираном од стране Министарства просвете, науке и технолошког развоја Републике Србије, руководио потпројектом 3 "Интегрална истраживања квалитета ваздуха у урбаним срединама".
- У оквиру у EU H2020 пројекта GEO-CRADLE (Coordinating and integRating state-of-the- art Earth Observation Activities in the regions of North Africa, Middle East, and Balkans

and Developing Links with GEO related initiatives towards GEOSS), the European Union's Horizon 2020 (H2020) research and innovation programme under grant agreement No 690133 (2016 – 2018) др Зоран Мијић је руководилац активности под називом "Modelling and computing facilities".

- Др Зоран Мијић је руководио тимом из Србије у оквиру кампање мерења 2020. године "COVID-19 NRT lidar measurement campaign" која је организована у оквиру ACTRIS евопрске иницијативе за проучавање промена у атмосфери.
- У Институту за физику у оквиру Центра изузетних вредности за примену плазме у нанотехнологијама, биомедицини и екологији кандидат је руководио пројектним задатком "Даљинско мерење оптичких карактеристика аеросола и моделовање у атмосфери" (2013)
- У Институту за физику у оквиру Центра изузетних вредности за примену плазме у нанотехнологијама, биомедицини и екологији кандидат је руководио пројектним задатком "Примена рецепторских модела за идентификацију и квантитативну процену доприноса извора емисије" (2014).

Прилози:

Копије анекса уговора о реализацији пројекта ИИИ43007
Копије годишњих извештаја Центра изузетних вредности за примену плазме у нанотехнологијама, биомедицини и екологији
Копија уговора пројекта GEO-CRADLE
Извод извештаја COVID-19 Actris
Одлука о именовању руководиоца лабораторије

4.5 Активност у научним и научно-стручним друштвима

Кандидат је учествовао у раду (2007-2013) Државне комисије за такмичења из физике за ученике средњих школа у оквиру Друштва физичара Србије које је опуномоћено од стране Министарства за просвету, науку и технолошки развој да организује такмичења из физике за ученике средњих школа у Републици Србији

- У име Друштва физичара Србије др Зоран Мијић је предводио тим ученика из Србије на међународним олимпијадама из физике за ученике средњих школа 2009. године у Мексику и 2011. године на Тајланду.
- Од 2007. до 2013. године био је члан Комисије за такмичење из физике ученика средњих школа Друштва физичара Србије и аутор задатака за такмичења за 1. разред.
- Од 2007. до 2013. године кандидат је као члан Друштва физичара Србије учествовао у организацији више републичких такмичења из физике за ученике основних и средњих школа и учествовао у раду комисија за преглед задатака

Члан је EUROPLANET SOCIETY, Europlanet South Eastern European Hub, Serbia

4.6 Утицајност научних резултата

Утицајност научних радова кандидата је наведена у одељцима 4.1. Пун списак радова дат је у одељку 6, док су подаци о цитираности наведени са доступне базе података након списка свих радова.

4.7 Конкретан допринос кандидата у реализацији радова у научним центрима у земљи и иностранству

Зоран Мијић је дао кључни допринос у развоју и примени нове области истраживања код нас, даљинској детекцији атмосферских аеросола и примени хибридних модела за анализу транспорта загађујућих материја. За више детаља о доприносу кандидата погледати део *Степен самосталности и степен учешћа у реализацији радова у научним центрима у земљи и иностранству.*

4.8 Уводна предавања на конференцијама и друга предавања по позиву

Предавања по позиву на конференцијама одржана у периоду пре претходног избора у звање

- **Z. Mijic**, M. Kuzmanoski, D. Nicolau, L. Belegante (2013). The use of hybrid receptor models and ground based remote sensing of particulate matter for identification of potential source regions, Proceedings from the 4th WeBIOPATR Workshop Conference, 4th WeBIOPATR2013, October 2-6, Belgrade, Serbia.
- **Zoran Mijic**, Darko Vasiljevic, Aleksander Kovacevic, Bratimir Panic, Milan Minic, Mirjana Tasic, Branislav Jelenkovic, Ilija Belic, Ana Vukovic, (2011). Investigation of transport pathways and potential source regions of atmospheric aerosols in Belgrade: receptor modeling and LIDAR system, 5th International Workshop on Optoelectronic for Environmental Monitoring, 28-30 September, Magurele, Romania

Прилог:
Копије позивног писма и програма конференције у којима се види да је кандидат био предавач

4.9 Педагошки рад

Др Зоран Мијић је веома активан у педагошком раду и формирању научног подмлатка и у наставку су наведене најважније активности:

- У име Друштва физичара Србије др Зоран Мијић је предводио тим ученика из Србије на међународним олимпијадама из физике за ученике средњих школа 2009. године у Мексику и 2011. године на Тајланду.
- Од 2007. до 2013. године члан Комисије за такмичење из физике ученика средњих школа Друштва физичара Србије и био аутор задатака за такмичења.
- Од 2007. до 2013. године кандидат је као члан Друштва физичара Србије учествовао у организацији више републичких такмичења из физике за ученике основних и средњих школа и учествовао у раду комисија за преглед задатака
- 2012. године је сарађивао је са Регионалним центром за таленте Београд 1-Земун где је радио на изради експерименталних радова са ученицима који су учествовали на Републичком такмичењу младих талената за основне школе.
- Школске 2014/2015 и 2015/2016. године је био ангажован за одржавање предавања и вежби из предмета Физика на Техничком факултету Универзитета Сингидунум у

Београду, смер Елеткротехника и рачунарство.

- На позив Министарства просвете и науке Републике Српске у Бања Луци учествовао у припреми ученика средњих школа за учешће на такмичењима из физике и међународној олимпијади.
- Учесник на пројекту Научна визуелизација у школском простору и на паметном телефону Центар за промоцију науке Београд, главни реализатор Институт за физику Београд, број уговора: 667/15, 24.09.2015.
- Од 2011. до 2014. године учествује на пројекту Подстицајна околина за активно учење природних наука – ПОКО, Центар за промоцију науке Београд, главни реализатор Институт за физику Београд.
- Као предавач учествовао у више акредитованих семинара за наставнике физике чији је реализатор био Институт за физику, Београд

4.9.1 Менторство при изради мастер, магистарских и докторских радова

- Др Зоран Мијић је био ментор при изради докторске дисертације др Андреје Стојића под називом "Анализа расподела и динамике испарљивих органских једињења и аеросола у тропосфери – лидар и масена спектрометрија " која је одбрањена 7.07.2015. године на Физичком факултету Универзитета у Београду.
- Др Зоран Мијић је био члан комисије за одбрану докторске дисертације др Андреја Шоштарића под називом Механизми уклањања лако испарљивих моноароматичних угљоводоника (BTEX) из амбијенталног ваздуха мокром депозицијом која је одбрањена 27.12.2017. године на Хемијском факултету Универзитета у Београду.

Прилог:
Одлука Наставно-научног већа Физичког факултета Универзитета у Београду о одређивању ментора за докторску дисертацију дрАндреје Стојића и одговарајући документи за чланство у комисији за одбрану докторске дисертације др Андреја Шоштарића

4.10 Међународна сарадња

- Од 2021. године др Зоран Мијић обавља функцију националног координатора у оквиру Европског програма за сарадњу у домену научних и технолошких истраживања - COST (European Cooperation in Science and Technology).

- Др Зоран Мијић је учествовао у више међународних пројеката у којима је и руководио појединим активностима:
- 2017−2021. године као заменик члана управљачког одбора учествује у COST акцији inDUST: International Network to Encourage the Use of Monitoring and Forecasting Dust Products; European Cooperation in Science and Technology, COST Action CA16202;
- 2016 - 2018. године учествује у EU H2020 пројекту GEO-CRADLE (Coordinating and integRating state-of-the-art Earth Observation Activities in the regions of North Africa, Middle East, and Balkans and Developing Links with GEO related initiatives towards GEOSS), the European Union's Horizon 2020 (H2020) research and innovation programme

under grant agreement No 690133. Координатор пројекта је National Observatory of Athens (NOA). У оквиру пројекта руководи радом тима из Института за физику у Београду.

- 2015 - 2019. године учествује у EU H2020 пројекту ACTRIS-2 Integrated Activities (IA). ACTRIS-2 је финансиран у оквиру the European Union 's Horizon 2020 research and innovation programme (grant agreement No 654109). Координатор пројекта је Consiglio Nazionale delle Ricerche, CNR, Italy. У оквиру пројекта руководи радом српског тима.
- 2019 - Одговорни је представник у име тима из Србије у оквиру пројекта Aeolus L2A aerosol and cloud product validation using the European Aerosol Research Lidar Network EARLINET, којим руководи Европска свемирска агенција (ESA)
- 2014 – Одговорни је представник у оквиру EARLINET (the European Aerosol Research Lidar Neћvork) мреже.
- 2011 - 2015. године учествује у EU FP7 пројекту ACTRIS (Aerosols, Clouds, and Trace gases Research InfraStructure Network). ACTRIS је финансиран у оквиру the EC 7th Framework Programme under "Research Infrastructures for Atmospheric Research". Координатор пројекта је Consiglio Nazionale delle Ricerche, CNR, Italy. У оквиру пројекта руководи радом српског тима.
- 2015 - 2016. године учествује у раду пројекта iSPEX-EU. iSPEX-EU је део пројекта LIGHT2015, финансираног у оквиру the European Union 's innovation programme under grant agreement No 644964.
- 2006 - 2009. године учествује на пројекту IPB-CNP Reinforcing Experimental Centre for Non-equilibrium Studies with Application in Nano-technologies, Etching of Integrated circuits and Environmental Research у оквиру FP6 програма Европске уније (2006-2009.).
- 2008 - 2009. године учествује на пројекту билатералне сарадње између Србије и Словеније: Development of complementary photothermal and optical spectroscopy methods and techniques.
- 2006 - 2007. године учествује на пројекту билатералне сарадње између Србије и Словеније: Ласерске технике за праћење аеросола и испитивање гасова стаклене баште.

Прилози:
Копије одговарајућих уговора пројеката и интернет страница у којима се документује учешће на пројектима

4.11 Организација научних скупова

- Чланство у Научном одбору међународне конференције III Meeting on Astrophysical Spectroscopy - A&M DATA, која је одржана од 6-9. децембра 2021. године, Палић,
- Чланство у Научном одбору међународне конференције The Eighth Intemational WeBIOPATR Workshop and Conference Particulate Matter: Research and Management (WeBIOPATR2021) која је одржана од 29. Новембра до 1. Децембра 2021. године у Београду. https://www.vin .bg.ac.rs/webiopatr/#Workshop/
- Чланство у Научном одбору међународне конференције The Seventh Intemational WeBIOPATR Workshop and Conference Particulate Matter: Research and Management (WeBIOPATR2019) која је одржана од 1. до 3. октобра 2019. године у Београду. https://www.vin .bg.ac.rs/webiopatr/#Workshop/

- Чланство у Научном одбору међународне конференције The Sixt Intemational WeBIOPATR Workshop and Conference Particulate Matter: Research and Management (WeBIOPATR2017) која је одржана од 6. до 9. септембра 2017. године у Београду. https://www.vin .bg.ac.rs/webiopatr/#Workshop/
- Чланство у Организационом одбору међународне конференције 18th International Conference on Photoacoustic and Photothennal Phenomena (ICPPP18) која је одржана од 1. до 6. септембра 2015. године у Новом Саду.
- Чланство у Научном одбору међународне конференције The Fifth Intemational WeBIOPATR Workshop and Conference Particulate Matter: Research and Management (WeBIOPATR2015) која је одржана од 14. до 16. октобра 2015. године у Београду. https://www.vin .bg.ac.rs/webiopatr/#Workshop/
- Чланство у Научном одбору међународне конференције The Fourth Intemational WeBIOPATR Workshop and Conference Particulate Matter: Research and Management (WeBIOPATR2013) која је одржана од 2. до 4. октобра 2013. године у Београду. http://www.vin.bg.ac.rs /webiopatr/4th-workshop/
- Чланство у Организационом одбору конференције Фотоника 2010 Теорија и експеримент у Србији, која је одржана од 21. до 23. априла 2010. године у Београду.

Прилози:

Одговарајуће копије и изводи књига апстракатά и публикација са наведеним саставом научног и организационог одбора

4.12 Чланства у уређивачким одборима часописа, уређивање монографија, рецензије научних радова и пројеката

Кандидат је урадио укупно 57 резензија радова за неколико међународних часописа. У периоду након претходног избора у звање урадио је 41 рецензију. Рецензију је радио за следеће научне часописе (у загради је наведен број радова за сваку часопис):
Atmospheric Pollution Research (12), Science of the Total Environment (11), Remote Sensing (5), Atmospheric Environment (4), Atmosphere (9), Sustainability (3), Applied Sciences (2), Optical and Quantum Electronics (1), Journal of Cleaner Production (3), Atmospheric Research (2), International Journal of Environment (1), Environmental Pollution (1), Air Quality, Atmosphere and Health (1)

Др Зоран Мијић је био гост уредник за часопис *Atmosphere* за специјалан број под називом *"Atmospheric Aerosol Hazards".*

Прилози:

Копије и потврде уредништва часописа и одговарајући извод из базе података Publons

5. ЕЛЕМЕНТИ ЗА КВАНТИТАТИВНУ ОЦЕНУ НАУЧНОГ ДОПРИНОСА КАНДИДАТА

Остварени резултати у периоду након претходног избора у звање

Категорија	М бодова по раду	Број радова	Укупно М бодова	Нормиран број М бодова
М21а	10	1	10	2,381
М21	8	1	8	8
М22	5	3	15	14,166
М33	1	6	6	5,555
М34	0,5	9	4,5	4,5
М63	1	1	1	0,555

Поређење са минималним квантитативним условима за реизбор у звање виши научни сарадник*

Минимални број М бодова*		Остварено М бодова без нормирања	Остварено М бодова са нормирањем
Укупно	50/2	44,5	35,157
М10+М20+М31+М32+М33+М41+М42+М90	40/2	39	30,102
М11+М12+М21+М22+М23	30/2	33	24,547

За резизбор у звање виши научни сарадник потребно је 50% од минималног броја М бодова

6. Списак публикација по категоријама

Монографска студија/поглавље у књизи М11 или рад у тематском зборнику водећег међународног значаја (М13)

Радови објављени пре претходног избора у звање

А.1.А. Stojić, S. Stanišić Stojić**, Z. Mijić**, L. Ilić, M. Tomašević, Marija Todorović, and Mirjana Perišić (2015). Comprehensive Analysis of VOC Emission Sources in Belgrade Urban Area, In: Urban and Built Environments: Sustainable Developments, Health Implications and Challenges , Editor: Alexis Cohen, Nova Science Publishers, NY, USA, pp. 55-87, ISBN: 978-1-63483-117-8
https://www.novapublishers.com/catalog/product_info.php?products_id=55296&osCsid=02f84bd86252250cc78d9293d753be8b

А.2. Tomašević, M., **Z. Mijić**, M. Aničić, A. Stojić, M. Perišić, M. Kuzmanoski, M. Todorović, and S. Rajšić (2013). Air Quality Study in Belgrade: Particulate Matter and Volatile Organic Compounds as Threats to Human Health, In: Air Pollution: Sources, Prevention and Health Effects, Editor: Rajat Sethi, Nova Science Publishers, NY, USA, pp. 315-346, 2013. ISBN: 978-1-62417-735-4
https://www.novapublishers.com/catalog/product_info.php?products_id=38962&osCsid=cc956b5e1008d06c56c891f47982d91c

А.3. Aničić M., **Z. Mijić**, M. Kuzmanoski, A. Stojić, M. Tomašević, S. Rajšić, and M. Tasić (2012). A Study of Airborne Trace Elements in Belgrade Urban Area: Instrumental and Active Biomonitoring Approach, In: Trace Elements: Environmental Sources, Geochemistry and Human Health, Editors: Diego Alejandro De Leon and Paloma Raquel Aragon, Nova Science Publishers, NY, USA, pp.1-30, ISBN: 978-1-62081-401-7
https://www.novapublishers.com/catalog/product_info.php?products_id=30058&osCsid=cc956b5e1008d06c56c891f47982d91c

Монографска студија/поглавље у књизи М12 или рад у тематском зборнику водећег међународног значаја (М14)

Радови објављени пре претходног избора у звање

Б.1. **Zoran Mijić**, Andreja Stojić, Mirjana Perišić, Slavica Rajšić and Mirjana Tasić (2012). In: Air Quality - New Perspective, Statistical Character and Transport Pathways of Atmospheric Aerosols in Belgrade, pp. 199 - 226, Editors: Gustavo Lopez Badilla, Benjamin Valdez and Michael Schorr, Published by InTech, ISBN: 978-953-51-0674-6.
http://www.intechopen.com/books/air-quality-new-perspective/statistical-character-and-transport-pathways-of-atmospheric-aerosols-in-belgrade

Б.2. **Zoran Mijić**, Slavica Rajšić, Andrijana Žekić, Mirjana Perišić, Andreja Stojić and Mirjana Tasić (2010). Characteristics and application of receptor models to the atmospheric aerosols research, Book chapter in Air quality edited by Ashok Kumar, pp. 143-167. ISBN 978-953-307-131-2.
http://www.intechopen.com/books/air-quality/characteristics-and-application-of-receptor-models-to-the-atmospheric-aerosols-research

Б.3. Mirjana Tasić, Slavica Rajšic, Milica Tomašević, **Zoran Mijić**, Mira Aničić, Velibor Novaković, Dragan M Marković, Dragan A Marković, Lazar Lazić, Mirjana Radenković, Jasminka Joksić (2008). Assessment of Air Quality in an Urban Area of Belgrade, Serbia, In: Environmental technologies, New Developments, Edited by E. Burcu Ozkaraova Gungor, I-Tech Education and Publishing, Vienna, Austria, ISBN 978-3-902613-10-3, pp. 209-244. Available from: http://www.intechopen.com/books/environmental_technologies/assessment_of_air_quality_in_an_urban_area_of_belgrade__serbia

РАДОВИ ОБЈАВЉЕНИ У НАУЧНИМ ЧАСОПИСИМА МЕЂУНАРОДНОГ ЗНАЧАЈА (М20)

Рад у међународном часопису изузетних вредности (М21а)

Радови објављени након претходног избора у звање

1. Papagiannopoulos, N., D'Amico, G., Gialitaki, A., Ajtai, N., Alados-Arboledas, L., Amodeo, A., Amiridis, V., Baars, H., Balis, D., Binietoglou, I., Comerón, A., Dionisi, D., Falconieri, A., Fréville, P., Kampouri, A., Mattis, I., **Mijić, Z**., Molero, F., Papayannis, A., Pappalardo, G., Rodríguez-Gómez, A., Solomos, S., and Mona, L. (2020). An EARLINET early warning system for atmospheric aerosol aviation hazards,
Atmospheric Chemistry and Physics (20) 10775–10789.
doi:10.5194/acp-20-10775-2020

Радови објављени пре претходног избора у звање

1. Stojić, A., Maletić, D., Stojić, S. S., **Mijić, Z**., Šoštarić, A. (2015). Forecasting of VOC emissions from traffic and industry using classification and regression multivariate methods, Science of the Total Environment, 521-522, 19-26.
doi:10.1016/j.scitotenv.2015.03.098

Рад у врхунском међународном часопису (М21)

Радови објављени након претходног избора у звање

1. Šoštarić, S. Stanišić Stojić, G. Vuković, **Z. Mijić**, A. Stojić, Gržetić I. (2017). Rainwater capacities for BTEX scavenging from ambient air,
Atmospheric Environment, 168, 46-54,
doi:10.1016/j.atmosenv.2017.08.045.

Радови објављени пре претходног избора у звање

1. Lazić, L., Urošević M.A., Mijić, Z., Vuković G., Ilić L. (2016). Traffic contribution to airpollution in urban street canyons: Integrated application of the OSPM, moss biomonitoring and spectral analysis
   Atmospheric Environment, 141, 347-360.
   doi:10.1016/j.atmosenv.2016.07.008
2. Stojić, A., Stanišić Stojić, S., Reljin, I., Čabarkapa, M., Šoštarić, A., Perišić, M., **Mijić, Z**. (2016). Comprehensive analysis of PM_{10} in Belgrade urban area on the basis of long term measurements.
   Environmental Science and Pollution Research, 23, 10722-10732
   doi:10.1007/s11356-016-6266-4
3. Stojić, A., Stojić, S. S., **Mijić, Z**., Šoštarić, A., Rajšić, S. (2015). Spatio-temporal distribution of VOC emissions in urban area based on receptor modeling.
   Atmospheric Environment, 106, 71-79.
   doi:10.1016/j.atmosenv.2015.01.071
4. Stojić, A., Stanišić Stojić, S., Šoštarić, A., Ilić, L., **Mijić Z**., Rajšić S. (2015). Characterization of VOC sources in urban area based on PTR-MS measurements and receptor modelling, Environmental Science and Pollution Research, 22, 13137-13152.
   doi:10.1007/s11356-015-4540-5
5. **Mijić, Z**., Stojić, A., Perišić, M., Rajšić, S., Tasić, M., Radenković, M., Joksić, J. (2010). Seasonal variability and source apportionment of metals in the atmospheric deposition in Belgrade.
   Atmospheric Environment, 44(30), 3630-3637.
   doi:10.1016/j.atmosenv.2010.06.045
6. M. Aničić, M. Tasić, M.V. Frontasyeva, M. Tomašević, S. Rajšić, **Z.Mijić**, A. Popović, (2009). Active Moss Biomonitoring of Trace Elements with *Sphagnum girgensohnii* Moss Bags in Relation to Atmospheric Bulk Deposition in Belgrade, Serbia,
   Environmental Pollution 157 (2), 673-679.
   doi:10.1016/j.envpol.2008.08.003

Рад у истакнутом међународном часопису (М22)

Радови објављени након претходног избора у звање

1. L. Ilić, M. Kuzmanoski, P. Kolarž, A. Nina, V. Srećković, **Z. Mijić**, J. Bajčetić, M. Andrić, (2018). Changes of atmospheric properties over Belgrade, observed using remote sensing and in situ methods during the partial solar eclipse of 20 March 2015,
   Journal of Atmospheric and Solar-Terrestrial Physics, 171, 250-259.
   doi:10.1016/j.jastp.2017.10.001.

2. Srećković V.A, Šulić D.M, Vujčić V, **Mijić Z.R**, Ignjatović L.M. (2021). Novel Modelling Approach for Obtaining the Parameters of Low Ionosphere under Extreme Radiation in X-Spectral Range.
   Applied Sciences 11(23):11574.
   doi:10.3390/app112311574

3. Kolarski A, Srećković V.A, **Mijić Z.R**. (2022). Response of the Earth's Lower Ionosphere to Solar Flares and Lightning-Induced Electron Precipitation Events by Analysis of VLF Signals: Similarities and Differences.
Applied Sciences 12(2):582.
doi:10.3390/app12020582

Радови објављени пре претходног избора у звање

1. Perišić M, Rajšić S, Šoštarić A, **Mijić Z**, Stojić A., (2016) Levels of PM_{10} bound species in Belgrade, Serbia: spatio-temporal distributions and related human health risk estimation Air Quality, Atmosphere & Health
doi: 10.1007/s11869-016-0411-6

2. Perišić, M., Stojić, A., Stojić, S. S., Šoštarić, A., **Mijić, Z**., Rajšić, S. (2015). Estimation of required PM_{10} emission source reduction on the basis of a 10-year period data. Air Quality, Atmosphere & Health, 8, 379-389.
doi:10.1007/s11869-014-0292-5

3. **Zoran Mijić**, Mirjana Tasić, Slavica Rajšić, Velibor Novaković, (2009). The statistical characters of PM_{10} in Belgrade area,
Atmospheric Research, 92 (4), 420-426.
doi:10.1016/j.atmosres.2009.01.002

4. Slavica Rajšić, **Zoran Mijić**, Mirjana Tasić, Mirjana Radenković and Jasminka Joksić, (2008). Evaluation of the levels and sources of trace elements in urban particulate matter, Environmental Chemistry Letters, 6(2), 95-100.
doi:10.1007/s10311-007-0115-0

5. M.D.Tasić, S.F.Rajšić, V.T.Novaković. **Z.R.Mijić**, M.N.Tomašević, (2005). PM_{10} and $PM_{2.5}$ Mass Concentration Measurements in Belgrade Urban Area,
Physica Scripta, Vol.T118, 29-30.

Рад у међународном часопису (М23)

1. Marija N. Todorović, Mirjana D. Perišić, Maja M. Kuzmanoski, Andreja M. Stojić, Andrej I. Šoštarić, **Zoran R. Mijić** and Slavica F. Rajšić (2015) Assessment of PM10 pollution level and required source emission reduction in Belgrade area.
Journal of Environmental Science and Health Part A, 50(13), 1351-1359.
doi:10.1080/10934529.2015.1059110

2. **Mijić, Z**., Stojić, A., Perišić, M., Rajšić, S., Tasić, M. (2012). Receptor modeling studies for the characterization of PM_{10} pollution sources in Belgrade.
Chemical Industry and Chemical Engineering Quarterly, 18(4-2), 623-634.
doi: 10.2298/CICEQ120104108M

3. Dragan M. Marković, Dragan A. Marković, Anka Jovanović, Lazar Lazić, **Zoran Mijić**, (2008), Determination of O_3, NO_2, SO_2, CO and PM_{10} measured in Belgrade urban area,
Environmental Monitoring and Assessment 145 (1), 349–359.
doi:10.1007/s10661-007-0044-1

4. Tasić M., Đurić-Stanojević B., Rajšić S.F., **Mijić Z.**, Novaković V.T., (2006) Physico-chemical Characterization of PM_{10} and $PM_{2.5}$ in the Belgrade Urban Area, Acta Chimica Slovenica 53, 401-405.

ЗБОРНИЦИ МЕЂУНАРОДНИХ НАУЧНИХ СКУПОВА (М30)

Предавање по позиву са међународног скупа штампано у целини (М31)

Радови објављени пре претходног избора у звање

1. **Z. Mijić**, M. Kuzmanoski, D. Nicolau, L. Belegante (2013). The use of hybrid receptor models and ground based remote sensing of particulate matter for identification of potential source regions, Proceedings from the 4th WeBIOPATR Workshop Conference, 4th WeBIOPATR2013, October 2-6, Belgrade, Serbia, pp. 52-59.
2. **Zoran Mijić**, Darko Vasiljević, Aleksander Kovačević, Bratimir Panić, Milan Minić, Mirjana Tasić, Branislav Jelenković, Ilija Belić, Ana Vuković, (2011). Investigation of transport pathways and potential source regions of atmospheric aerosols in Belgrade: receptor modeling and LIDAR system, 5th International Workshop on Optoelectronic Techiques for Environmental Monitoring, pg. 109-116. 28-30 September, Magurele, Romania.

Саопштење са међународног скупа штампано у целини (М33)

Радови објављени након претходног избора у звање

1. **Z.Mijić**, L. Ilić, M. Kuzmanoski, Raman lidar for atmospheric aerosol profiling in Serbia, 49th International October Conference on Mining and Metallurgy, 49th International October Conference on Mining and Metallurgy, pp. 65 - 68, Bor, 18. - 21. Oct, 2017
2. **Z.Mijić**, M. Perišić, L. Ilić, A. Stojić, M. Kuzmanoski, Air mass transport over Balkan region identified by atmospheric modeling and aerosol lidar technique, 49th International October Conference on Mining and Metallurgy, 49th International October Conference on Mining and Metallurgy, pp. 69 - 72, Bor, Serbia, 18. - 21. Oct, 2017
3. Maja Kuzmanoski, Luka Ilić, Marija Todorović, **Zoran Mijić**, A study of a dust intrusion event over Belgrade, Serbia, Proceedings from the Sixth International WeBIOPATR Workshop & Conference / Particulate Matter: Research and Management, pp. 103 - 108, Belgrade, 6. - 8. Sep, 2017
4. Mirjana Perišić, Gordana Vuković, **Zoran Mijić**, Andrej Šoštarić, Andreja Stojić, Relative importance of gaseous pollutants and aerosol constituents for identification of PM10 sources of variability, Proceedings from the Sixth international WeBIOPATR workshop and conference Particulate Matter: Research and Management, pp. 109 - 112, 9, Belgrade, 6. - 8. Sep, 2017
5. Andreja Stojić, Svetalna Stanišić Stojić, Mirjana Perišić, **Zoran Mijić**, Multiscale multifractal analysis of nonlinearity in particulate matter time series, Proceedings from the Sixth

international WeBIOPATR workshop and conference Particulate Matter: Research and Management, pp. 114 - 118, Belgrade, 6. - 8. Sep, 2017

6. Aleksandra Nina, Milan Radovanović, Luka Popović, Ana Černok, Bratislav Marinković, Vladimir Srećković, Anđelka Kovačević, Jelena Radović, Vladan Čelebonović, Ivana Milić Žitnik, **Zoran Mijić**, Nikola Veselinović, Aleksandra Kolarski, Alena Zdravković, Activities Of Serbian Scientists In Europlanet, Proceedings of the XII Serbian-Bulgarian Astronomical Conference, 107-121, 2020.

Радови објављени пре претходног избора у звање

1. Kuzmanoski M., L. Ilić, **Z. Mijić**, Aerosol remote sensing study of a Saharan dust intrusion episode in Belgrade, Serbia, XIX International Eco-conference, Environmental protection of urban and suburban settlements, Proceedings, pp. 73-81. September 23-25, 2015. Novi Sad, Serbia.
2. **Mijić Z**., M. Perišić, A. Stojić, M. Kuzmanoski, L. Ilić, Estimation of atmospheric aerosol transport by ground-based remote sensing and modeling, XIX International Eco-conference, Environmental protection of urban and suburban settlements, Proceedings, pp. 375-382. September 23-25, 2015. Novi Sad, Serbia.
3. Šoštarić, A. Stojić, S. Stanišić Stojić and **Z. Mijić**, Traffic-related VOC dynamics in Belgrade urban area, Physical Chemistry 2014: proceedings. Vol. 1. 12th International Conference on Fundamental and Applied Aspects of Physical Chemistry, September 22-26, 2014, Belgrade, Serbia, pp. 945-948.
4. S. Stanišić Stojić, Šoštarić, A. **Z. Mijić,** M. Perišić, The contribution of chemical industry to ambient VOC levels in Belgrade, Physical Chemistry 2014: proceedings. Vol. 1. 12th International Conference on Fundamental and Applied Aspects of Physical Chemistry, September 22-26, 2014, Belgrade, Serbia, pp. 949-952.
5. Šoštarić, M. Perišić, A. Stojić, **Z. Mijić** and S. Rajšić, Dynamics of gaseous pollutants in Belgrade urban area, Physical Chemistry 2014: proceedings. Vol. 1. 12th International Conference on Fundamental and Applied Aspects of Physical Chemistry, September 22-26, 2014, Belgrade, Serbia, pp. 953-956.
6. M. Perišić, **Z. Mijić**, A. Stojić, Frequency analysis of PM10 time series and assessing source reduction for air quality compliance in Serbia, Proceedings from the 4th WeBIOPATR Workshop Conference, 4th WeBIOPATR2013, October 2-6, Belgrade, Serbia, pp. 64-68, 2013.
7. Šoštarić, M. Perišić, A. Stojić, **Z. Mijić**, S. Rajšić, M. Tasić, The influence of air mass origin and potential source contributions on PM10 in Belgrade, Proceedings from the 4th WeBIOPATR Workshop Conference, 4th WeBIOPATR2013, October 2-6, 2013, Belgrade, Serbia, pp.39-43.
8. Mirjana Perišić, Andreja Stojić, **Zoran Mijić**, MarijaTodorovic and Slavica Rajšić, Source apportionment of ambient VOCs in Belgrade semi-urban area, 6th International Conference on Proton Transfer Reaction Mass Spectrometry and Its Application, Book of Contributions, 2013, Innsbruck, Austria, pp. 204-208.

9. Andreja Stojić, Mirjana Perišić, **Zoran Mijić**, Slavica Rajšić, Ambient VOCs measurements in winter: Belgrade semi-urban area, 5th International Conference on Proton Transfer Reaction Mass Spectrometry and Its Application, Book of Contributions, 2011, Innsbruck, Austria, pp. 248-251.
10. M. Perišic, **A. Stojić**, S. Rajšic and Z. Mijic: Assessment of VOCs concentrations in Belgrade semi-urban area, Proceedings of the 10th International Conference of Fundamental and Applied aspects of Physical Chemistry, September 21-24, 2010, Belgrade, Serbia, pp. 579-581.
11. A. Stojić, S.Rajšić, M.Perišić, **Z.Mijić**, M.Tasić, Assessment of ambient VOCs levels in Belgrade semiurban area, 4th International Conference on Proton Transfer Reaction Mass Spectrometry and its Applications, IUP Insbruck University Press, Conference Series, Eds. Tilmann D.Mark, Birgit Holzner, Contributions, February 16-21, 2009, Obergurgl, Austria, pp. 289- 293.
12. Tasić, M., **Mijić, Z.**, Rajšić, S., Stojić, A., Radenković, M., & Joksić, J. Source apportionment of atmospheric bulk deposition in the Belgrade urban area using positive matrix factorization. In Journal of Physics: Conference Series, IOP Publishing, April, 2009, Vol. 162, No. 1, pp. 012018.
13. **Zoran Mijić**, Lazar Lazić, Slavica Rajšić, Mirjana Tasić and Velibor Novaković, Air Back Trajectories Analysis for High PM Concentration Episodes, The Changing Chemical Climate of the Atmosphere, 1st Accent Symposium, Urbino, September 12-16 (2005), Proceedings, editors: Sandro Fuzzi, Michela Maione, 1st edition: November 2006, CD, ISBN 88-548-0851-2
14. M.D.Tasić, **Z.R.Mijić**, D.S.Đorđević, D.J.Radmanović, V.T.Novaković, M.N.Tomašević, Atmospheric deposition of heavy metals in Belgrade urban area, Proceedings Of The 7th International Conference on Fundamental and Applied Aspects of Physical Chemistry, pg. 640-642; Belgrade, (2004)
15. M.D.Tasić,S.F.Rajšić, V.T.Novaković, **Z.R.Mijić**, M.N.Tomašević, Particulate matter mass concentrations in the ambient air of Belgrade, Proceedings Of The 7th International Conference on Fundamental and Applied Aspects of PhysicalChemistry, pg. 643-645; Belgrade, (2004)
16. M.D.Tasić, S.F.Rajšić, V.T.Novaković, **Z.R.Mijić**, and M.N.Tomašević, Characterization of PM_{10} and $PM_{2.5}$ particulate matter in the ambient air of Belgrade, Fifth Balkan Physics Union Conference (BPU-5), Vrnjacka Banja, Serbia and Montenegro, (2003), CD r.

Саопштење са међународног скупа штампано у изводу (М34)

Радови објављени након претходног избора у звање

1. **Z.Mijić**, L. Ilić, M. Kuzmanoski, Vertical Raman LIDAR profiling of atmospheric aerosol optical properties over Belgrade, Book of Abstracts PHOTONICA2017, The Sixth International School and Conference on Photonics, Belgrade, Serbia, 28. Aug - 01. Sep, 2017, pp. 210
2. **Z. Mijić**, A. Jovanović, M. Kuzmanoski, L. Ilić; A climatology of satellite derived aerosol optical depth over Belgrade region, Serbia; The 7th International WeBIOPATR Workshop & Conference, October 1–3, 2019, Book of Abstracts, p. 74.

3. A. Jovanović, L. Ilić, M. Kuzmanoski, **Z. Mijić**, Case study of the vertical distribution of Saharan dust over Belgrade; The 7th International WeBIOPATR Workshop & Conference, October 1–3, 2019, Book of Abstracts, p. 80.
4. **Zoran Mijić**, Mirjana Perišić, Comparison of MODIS aerosol observations and ground-based PM measurement for the Belgrade region, Integration of satellite and ground-based observations and multi-disciplinary in research and prediction of different types of hazards in Solar system, Petnica, 10. - 13. May, 2019, Book of Abstracts, pp. 51 – 52.
5. **Zoran Mijić**, Demonstration of the EARLINET Capacity to Provide Near Real Time Data, Book Of Abstracts And Contributed Papers, III Meeting on Astrophysical Spectroscopy - A&M DATA, December 6 to 9, 2021, Palić, Serbia, pp.46-47.
6. **Zoran Mijić**, Usage of High-Resolution Satellite Products in Atmospheric modeling, Book Of Abstracts And Contributed Papers, III Meeting on Astrophysical Spectroscopy - A&M DATA, December 6 to 9, 2021, Palić, Serbia, pp.48.
7. Aleksandra Kolarski, Vladimir Srećković**, Zoran Mijić**, Lower ionosphere under high-energy events: observations and model parameters, Book of Abstracts And Contributed Papers, III Meeting on Astrophysical Spectroscopy - A&M DATA, December 6 to 9, 2021, Palić, Serbia, pp.18.
8. S. Ničković, L. Ilić, S. Petković, G. Pejanović, A. Huete, **Z. Mijić**. A Numerical Model For Pollen Prediction: Thunderstorm Asthma Case Study, The 8th International WeBIOPATR Workshop & Conference, 29th November to 1st December 2021, Abstracts of Keynote Invited Lectures and Contributed papers, p. 37.
9. **Z. Mijić,** M. Kuzmanoski, L. Ilić , A Study On Tropospheric Aerosols Change During The Covid-19 Lockdown Period: Experience From Earlinet Measurement Campaign, The 8th International WeBIOPATR Workshop & Conference, 29th November to 1st December 2021, Abstracts of Keynote Invited Lectures and Contributed papers, p.54.

Радови објављени пре претходног избора у звање

1. L. Ilić, M. Kuzmanoski, **Z. Mijić**, Planetary boundary layer and elevated aerosol layer height estimation from lida signal in Belgrade, Proceedings of the 5th International WeBIOPATR Workshop & Conference, Particulate Matter: Researh and Management, Public Health Institute of Belgrade, 14-16 October 2015, Belgrade Serbia.
2. M. Perišić, A. Stojić, M. Todorović, **Z. Mijić**, A. Šoštarić, Transport contribution to $PM_{2.5}$ mass concentration in Belgrade sub-urban area, Proceedings of the 5th International WeBIOPATR Workshop & Conference, Particulate Matter: Researh and Management, Public Health Institute of Belgrade, 14-16 October 2015, Belgrade Serbia.
3. Lazar Lazić, Mira Aničić, Gordana Vuković, Mirjana Tasić, Slavica Rajšić and **Zoran Mijić**, Modelling of local traffic contributions to particulate air pollution in Belgrade street canyons using WinOSPM model, Urban Environmental Pollution – Create healthy, liveable cities, 17-20 June, (2012), Amsterdam, The Netherlands, CD-P2.112. http://www.uepconference.com/
4. **Z. Mijic**, M. Tasic, S. Rajšic, A. Stojic, Receptor modeling studies for the characterization of PM_{10} pollution sources in Belgrade, Proceedings of the 3rd International WeBIOPATR Workshop & Conference, CD, 15-17 November, 2011, Belgrade, Serbia.

5. **Z. Mijic**, M. Kuzmanoski, A. Stojic, A. Žekic, S. Rajšic, M. Tasic, Investigation of regional transport and health risk effects of metals in PM2.5 air particulate matter in Belgrade, Proceedings of the 3rd International WeBIOPATR Workshop & Conference, CD, 15-17 November, 2011, Belgrade, Serbia.
6. A.Stojic, M. Perišic, **Z. Mijic**, S. Rajšic, D. Ristic, Ambient VOCs measurement in Belgrade semi-urban area: winter case study, EUROanalysis, The 16th European conference on analytical chemistry Challenges in modern analytical chemistry, September 11-15, 2011, Belgrade, Serbia.
7. Mirjana Perišic, Andreja Stojic, **Zoran Mijic** and Slavica Rajšić, Source apportionment of volatile organic compounds in Belgrade semi-urban area, Book of Abstracts, 11th European Meeting on Environmental Chemistry EMEC 11, Portoroz, December 8-11, 2010, Slovenia, pp. 232.
8. A. Stojic, M. Perišić, **Z. Mijić**, S. Rajšić and D. Ristić, Ambient VOCs Measurement In Belgrade Semi-Urban Area Using Proton Transfer Reaction Mass Spectrometer, 1st Center of Excellence for Food Safety and Emerging Risk (CEFSER) Workshop "Regional perspectives in food safety", 12th Danube-Kris-Mures-Tisa (DKMT) Euroregion Conference on Food, Environment and Health, CD Book of Abstracts, Faculty of Technology, University of Novi Sad, September 2010, Novi Sad, Serbia.
9. Andreja Stojic, Mirjana Perišić, **Zoran Mijić**, Slavica Rajšić, Proton Transfer Reaction Mass Spectrometry: Ambient Air VOCs Measurement In Belgrade Semi-urban Area, 20th ESCAMPIG, July, 2010, Novi Sad, Serbia.
10. A.Stojić, M.Nešić, **Z.Mijić**, V.Novaković, S.Rajšić, M.Tasić, Heavy metal concentrations in streat dust and soils adjacent to roads in Belgrade, Serbia, 9th Highway and Urban Environment Symposium, Books of abstracts, June, 9-11, 2008, Madrid, Spain, pp. 87.
11. M.Nešic, A. Stojic, **Z. Mijic**, V. Novakovic, S. Rajšic, First results of outdoor and indoor VOCs measurements using PTR-MS i Belgrade, Serbia, 8th European Meeting on Environmental Chemistry (EMEC8), Book of abstracts, December 5-8, 2007, Inverness, Scotland, pp. 37.
12. Slavica Rajšić, **Zoran Mijić**, Mirjana Tasić, Mirjana Radenković, Jasminka Joksić, Source identification of trace elements in urban particulate matter, The First International WeBIOPATR Workshop: Particulate Matter: Research and Management, Book of extended abstracts pg.50-53, Belgrade, 20-22 May (2007).
13. Nesic Mirjana, Stojic Andreja, **Mijic Zoran,** Novakovic Velibor, Rajsic Slavica, First results of outdoor and indoor VOCs measurements using PTR-MS in Belgrade, Serbia, The 8th European Meeteng on Environmental Chemistry (EMEC8) Book of Abstracts pg. 37., December 5-8 (2007), Inverness, Scotland
14. **Z.R.Mijić**, L.A.Lazić, S.F. Rajšić, M.D. Tasić and V.T. Novaković, Some Characteristic Air Back Trajectories For High PM_{10} and $PM_{2.5}$ Concentration Episodes, 6th International Conference of the Balkan Physical Union, Book of Abstracts, pg. 1006, 22-26 August, Istanbul, Turkey, (2006)
15. V.T. Novaković, M.D. Tasić, B.Djurić-Stanojević, S.F. Rajšić and **Z.R.Mijić**, Physical Characterisation of PM_{10} and $PM_{2.5}$ in Belgrade Atmosphere by SEM/EDX and Image

Analysis System, 6th International Conference of the Balkan Physical Union, Book of Abstracts, pg. 1008, 22-26 August, Istanbul, Turkey, (2006)

16. V.T. Novaković, M.D. Tasić, B.Djurić-Stanojević, S.F. Rajšić and **Z.R.Mijić**, Physical Characterisation of PM10 and PM2.5 in Belgrade Atmosphere by SEM/EDX and Image Analysis System, AIP Conference Proceedings Volume 899 pg. 743. Sixth International Conference Of The Balkan Physical Union, Istanbul (Turkey), 22-26 August (2006) ISBN: 978-0-7354-0404-5
17. **Z.R.Mijić**, L.A.Lazić, S.F. Rajšić, M.D. Tasić and V.T. Novaković, Some Characteristic Air Back Trajectories For High PM10 and PM2.5 Concentration Episodes, AIP Conference Proceedings Volume 899 pg. 741. Sixth International Conference Of The Balkan Physical Union, Istanbul (Turkey), 22-26 August 2006 ISBN: 978-0-7354-0404-5
18. S. Rajšić, **Z. Mijić**, M. Tasić, M. Radenković, J. Joksić Assessment of the levels and sources of trace elements in PM_{10} and $PM_{2.5}$ in Belgrade, The Seventh European Meeting on Environmental Chemistry EMEC 7, The book of Abstracts pg. 175. , December 6-9. (2006) Brno, Czech Republic,
19. M. Tasić, B.Đurić-Stanojević, S.Rajšić, **Z.Mijić**, V. Novaković, Physico-chemical characterization of PM_{10} and $PM_{2.5}$ particles in the Belgrade urban area, 14th International Symposium Spectroscopy in theory and practice, Book of Abstracts pg. 109, Nova Gorica 10-13 april (2005)
20. S.Rajšić, **Z. Mijić,** L. Lazić, M. Tasić and V. Novaković, Analysis PM_{10} and $PM_{2.5}$ Air Pollution Episodes in Belgrade The Sixth European Meeting on Environmental Chemistry (EMEC6), Book of Abstracts, pg. 276, December 6-10th (2005), Belgrade, Serbia and Montenegro

ЧАСОПИСИ НАЦИОНАЛНОГ ЗНАЧАЈА (М 50)

Радови у научном часопису (М53)

Радови објављени пре претходног избора у звање

1. **Z. Mijić**, M. Tasić, S. Rajšić, A. Stojić, (2012). Primena hibridnih receptorskih modela za ispitivanje transporta PM_{10} čestica na područje Beograda, Glasnik Hemičara, Tehnologa i ekologa Republike Srpske, 4(7), 41- 48.
2. M.Tasić, S.Rajšić, V.Novaković, **Z.Mijić**. (2006). Atmospheric aerosols and their influence on air quality in urban area, Facta Universitatis-Physics, Chemistry and Technology Vol. 4, No1, 83-91,

ЗБОРНИЦИ СКУПОВА НАЦИОНАЛНОГ ЗНАЧАЈА (М60)

Предавање по позиву са скупа националног значаја штампано у целини (М61)

Радови објављени пре претходног избора у звање

1. Mirjana Tasić, Slavica Rajšić, Velibor Novaković, Zoran Mijić, Atmosferski aerosoli i njihov uticaj na kvalitet vazduha u urbanim sredinama, uvodno predavanje Zbornik radova Eko Fizika 37-46, Kruševac 21-22. maj (2005).

Саопштење са скупа националног значаја штампано у целини (M63)

Радови објављени након претходног избора у звање

1. I. Milić Žitnik, A. Nina, V. A. Srećković, B. P. Marinković, **Z. Mijić**, D. Šević, M. Budiša, D. Marčeta, A. Kovačević, J. Radović and A. Kolarski, Activities of the Serbian EUROPLANET group within EUROPLANET society, Proceedings of the XIX Serbian Astronomical Conference Belgrade, October 13 – 17, 2020, pp. 315 – 321.

Радови објављени пре претходног избора у звање

1. **Z. Mijić**, D. Vasiljević, A. Kovačević, M. Tasić i B. Panić, Ispitivanje transporta atmosferskih aerosola pomocu CWT modela i LIDAR sistema, XII Kongres fizičara Srbije, Zbornik radova, 2013, Vrnjačka Banja, Srbija, str. 428-432.
2. Mirjana Perišic, Andreja Stojić, Marija Todorovic, **Zoran Mijić** , Slavica Rajšić, Analiza dinamike i transporta CO, NO_x i SO_2 u urbanoj sredini Beograda, XII Kongres fizičara Srbije, Zbornik radova, 2013, Vrnjačka Banja, Srbija, str. 444-447.
3. Andreja Stojić, Mirjana Perišić, **Zoran Mijić**, Marija Todorovic, Slavica Rajšić. Odredjivanje izvora emisije isparljivih organskih jedinjenja u Beogradu, XII Kongres fizičara Srbije, Zbornik radova, 2013, Vrnjačka Banja, Srbija, str. 453-456.
4. **Zoran Mijić**, Mirjana Tasić, Bratimir Panić, Aleksander Kovačević, Darko Vasiljević, Brana Jelenković, Ilija Belić, Daljinska detekcija aerosola – LIDAR sistem, Savremene tehnologije za održivi razvoj gradova, Zbornik radova pp. 243-251, Banja Luka, 14-15 novembar (2008).
5. Aleksander Kovačević, Bratimir Panić, Milan Minić, Darko Vasiljević, **Zoran Mijić**, Mirjana Tasić, Branislav Jelenković, Ilija Belić, Detekcija povratnog rasejanog zračenja LIDAR sistema na 532 nm Zbornik radova ETRAN CD, Palić (2008)
6. Prvi rezultati merenja isparljivih organskih jedinjenja u ambijentalnom vazduhu Beograda korišćenjem uređaja PTR-MS , M. Nešić, A. Stojić, **Z. Mijić**, S. Rajšić, M. Tasić, 5th Symposium Chemistry and Environmental Protection with international participation, Book of Abstracts pp.40-41, 27-30 maj (2008), Tara, Srbija
7. Belić, D. Vasiljević, A. Kovačević, B. Panić, **Z. Mijić**, V. Novaković, M. Tasić, B. Jelenković, D. Pantelić, Primena LIDAR-a u detekciji aero-zagađenja, Zbornik radova Kongresa metrologa Srbije, (2007), pp. 181-189.
8. **Mijić Zoran**, Lazić Lazar, Rajšić Slavica, Velibor Novaković, Analiza transporta za vreme epizoda sa visokim koncentracijama PM čestica, Zbornik radova Eko Fizika 230-233, Kruševac 21-22. maj (2005).

9. Branislava Đurić-Stanojević, Mirjana Tasić, Slavica Rajšić, **Zoran Mijić**, Velibor Novaković, Milica Tomašević, Fizičko-hemijska karakterizacija PM2.5 i PM10 čestica u urbanoj sredini Beograda, Zbornik radova Eko Fizika 234-237, Kruševac 21-22. maj (2005).
10. P.Kolarž, **Z.Mijić**, D.M.Marković, D.A.Marković, Epizoda merenja ozona, aerosola i nanometarskih brzih jona vazduha na obali Dunava jula 2003. godine, Zbornik radova sa Kongresa fizicara Srbije i Crne Gore, Petrovac na Moru, 3-5.jun (2004), 8-87,8-90
11. **Z.R.Mijić**, V.T. Novaković, M.D.Tasić, S.F.Rajšić, Procena raspodele učestanosti masenih koncentracija PM10 i PM2.5, Zbornik radova sa Kongresa fizicara Srbije i Crne Gore, Petrovac na Moru, 3-5.jun (2004), 8-115,8-118
12. V.T.Novaković, **Z.R.Mijić**, M.D.Tasić, S.F.Rajšić, M.N.Tomašević, Merenje koncentracije PM10 čestica u suburbanoj oblasti Beograda, Zbornik radova sa Kongresa fizicara Srbije i Crne Gore, Petrovac na Moru, 3-5.jun (2004), 8-147,8-150
13. M.D.Tasić, S.F.Rajšić, V.T.Novaković, **Z.R.Mijić**, M.N.Tomašević, Ispitivanje kvaliteta vazduha u urbanim sredinama:PM10 i PM2.5, Zbornik radova sa Kongresa fizicara Srbije i Crne Gore, Petrovac na Moru, 3-5.jun (2004), 8-173,8-176
14. M.Tasić, S. Rajšić, D.Marković, V. Novaković**, Z. Mijić**, D. Marković, Ispitivanje kvaliteta vazuha na području grada Beograda-suspendovane čestice i ozon, Zbornik radova Ekološki problemi gradova, Beograd, 22-23.04. (2004) 93-94.

Саопштење са скупа националног значаја штампано у изводу (М64)

Радови објављени пре претходног избора у звање

1. A.Stojić**,** S Stojić Stanišic, A. Šoštarić, **Z. Mijić**, M. Todorović, Contribution of transported pollution to traffic-related VOC concentrations in Belgrade urban area, Book of abstracts, the 7th Symposium Chemistry and Environmental Protection, June 9-12, 2015, Palic, Serbia, pp. 167-168.
2. M.Nesić, A.Stojić, **Z.Mijić**, S.Rajšić, M.Tasić, First results of ambient VOCs measurements using PTR/MS IN Belgrade, 5th Symposium Chemistry and Environmental Protection, Ed. The Serbian Chemical Society, Book of abstracts, June, 27-30, 2008, Tara, Serbia, pp. 41.

7. МАГИСТАРСКЕ И ДОКТОРСКЕ ТЕЗЕ (М70)

Одбрањена докторска дисертација (М71)

1. Zoran Mijić, (2011), Određivanje fizičko-hemijskih karakteristika, prostorne i vremenske raspodele troposferskog aerosola: LIDAR sistem i receptorski modeli, doktorska disertacija, Fizički fakultet, Univerzitet u Beogradu

Одбрањен магистарски рад (М72)

1. Zoran Mijić, (2006), Merenje koncentracija suspendovanih čestica u vazduhu i primena statističkih modela za procenu uticaja različitih izvora emisije, magistarski rad, Fizički fakultet, Univerzitet u Beogradu

Atmos. Chem. Phys., 20, 10775–10789, 2020
https://doi.org/10.5194/acp-20-10775-2020

Atmospheric Chemistry and Physics
Open Access
EGU

An EARLINET early warning system for atmospheric aerosol aviation hazards

Nikolaos Papagiannopoulos[1,2], Giuseppe D'Amico[1], Anna Gialitaki[3,4], Nicolae Ajtai[5], Lucas Alados-Arboledas[6], Aldo Amodeo[1], Vassilis Amiridis[3], Holger Baars[7], Dimitris Balis[4], Ioannis Binietoglou[8], Adolfo Comerón[2], Davide Dionisi[9], Alfredo Falconieri[1], Patrick Fréville[10], Anna Kampouri[3,4], Ina Mattis[11], Zoran Mijić[12], Francisco Molero[13], Alex Papayannis[14], Gelsomina Pappalardo[1], Alejandro Rodríguez-Gómez[2], Stavros Solomos[3], and Lucia Mona[1]

[1]Consiglio Nazionale delle Ricerche – Istituto di Metodologie per l'Analisi Ambientale (CNR-IMAA), C. da S. Loja, Tito Scalo (PZ), Italy
[2]CommSensLab, Dept. of Signal Theory and Communications, Universitat Politècnica de Catalunya, Barcelona, Spain
[3]IAASARS, National Observatory of Athens, Athens, Greece
[4]Laboratory of Atmospheric Physics, Physics Department, Aristotle University of Thessaloniki, Thessaloniki, Greece
[5]Faculty of Environmental Science and Engineering, Babes–Bolyai University of Cluj Napoca, Cluj, Romania
[6]Department of Applied Physics, University of Granada, Granada, Spain
[7]Leibniz Institute for Tropospheric Research (TROPOS), Leipzig, Germany
[8]National Institute of R&D for Optoelectronics (INOE), Magurele, Romania
[9]Consiglio Nazionale delle Ricerche – Istituto di Scienze Marine (CNR-ISMAR), Rome, Italy
[10]Observatoire de Physique du Globe (OPGC-LaMP), Clermont-Ferrand, France
[11]Deutscher Wetterdienst, Meteorologisches Observatorium Hohenpeißenberg, Hohenpeissenberg, Germany
[12]Institute of Physics Belgrade, University of Belgrade, Belgrade, Serbia
[13]Centro de Investigaciones Energéticas, Medioambientales y Tecnológicas, Department of Environment, Madrid, Spain
[14]Laser Remote Sensing Unit, Physics Department, National Technical University of Athens, Athens, Greece

Correspondence: Nikos Papagiannopoulos (nikolaos.papagiannopoulos@imaa.cnr.it)

Received: 24 February 2020 – Discussion started: 27 February 2020
Revised: 5 June 2020 – Accepted: 3 August 2020 – Published: 15 September 2020

Abstract. A stand-alone lidar-based method for detecting airborne hazards for aviation in near real time (NRT) is presented. A polarization lidar allows for the identification of irregular-shaped particles such as volcanic dust and desert dust. The Single Calculus Chain (SCC) of the European Aerosol Research Lidar Network (EARLINET) delivers high-resolution preprocessed data: the calibrated total attenuated backscatter and the calibrated volume linear depolarization ratio time series. From these calibrated lidar signals, the particle backscatter coefficient and the particle depolarization ratio can be derived in temporally high resolution and thus provide the basis of the NRT early warning system (EWS). In particular, an iterative method for the retrieval of the particle backscatter is implemented. This improved capability was designed as a pilot that will produce alerts for imminent threats for aviation. The method is applied to data during two diverse aerosol scenarios: first, a record breaking desert dust intrusion in March 2018 over Finokalia, Greece, and, second, an intrusion of volcanic particles originating from Mount Etna, Italy, in June 2019 over Antikythera, Greece. Additionally, a devoted observational period including several EARLINET lidar systems demonstrates the network's preparedness to offer insight into natural hazards that affect the aviation sector.

Published by Copernicus Publications on behalf of the European Geosciences Union.

1 Introduction

During the aviation crisis related to the volcanic eruption of Eyjafjallajökull, Iceland, in 2010, the European Aerosol Research Lidar Network (EARLINET; Pappalardo et al., 2014) provided range-resolved information to the World Meteorological Organization (WMO) on a daily basis (reports available at: https://www.earlinet.org, last access: 31 October 2019). The reports communicated the altitude, time, and location of the volcanic clouds over Europe. Furthermore, the time–height evolution of the lidar returns was freely available in near real time (NRT) on the EARLINET website. The nonautomated, non-harmonized, and non-homogenized process and the lack of tailored products for natural hazards made the EARLINET data disregarded in the decision-making process.

The lessons learned from the Eyjafjallajökull crisis emphasized the vulnerability of air transportation to natural hazards (Bolic and Sivcev, 2011). Volcanic ash plumes, as well as desert dust outbreaks, present an imminent threat to aviation as they lead, among others, to poor visibility with considerable consequences to flight operations (Bolic and Sivcev, 2011; Middleton, 2017). Aircraft that do fly in volcanic/desert dust conditions can have a variety of damage from scouring of surfaces to engine failure (Eliasson et al., 2016). The aftermath of an encounter can be immediate, reducing flight safety; furthermore, it can financially affect the airlines due to higher maintenance costs and the replacement of mechanical equipment.

Furthermore, the Eyjafjallajökull eruption highlighted the gap in the availability of real-time measurements and monitoring information for airborne hazards. Specifically, the lack of height-resolved information, a key aspect in flight planning and mitigation strategies, became evident. In the frame of the Horizon 2020 research project EUNADICS-AV (European Natural Disaster Coordination and Information System for Aviation; https://www.eunadics.eu, last access: 31 October 2019) funded by the European Commission, different organizations worked together in a consortium to provide relevant data during situations when aviation is affected by airborne hazards (e.g., volcanic ash, desert dust, biomass burning, radionuclide). Crucial for the overall success of the project and the early warning system (EWS) design were the review of the available observations and the collection of specific requirements from the different stakeholders that once more pointed out the importance of height-resolved information.

A polarization lidar is an important tool to characterize the different aerosols. This system permits the discrimination of light-depolarizing coarse-mode particles such as volcanic and desert dust and fine-mode particles such as smoke particles and anthropogenic pollution (e.g., Tesche et al., 2011; Mamouri and Ansmann, 2017). Further, the lidar setup allows for the retrieval of coarse-mode and fine-mode backscatter coefficients for wavelengths of 532 and 1064 nm (e.g., Tesche et al., 2009). When synergistically used with a photometer, it is possible to retrieve their mass concentration profile (e.g., Ansmann et al., 2012; Lopatin et al., 2013; Chaikovsky et al., 2016).

During the last years, EARLINET has strongly increased its observing capacity with the addition of new stations and a system upgrade, namely, the installation of depolarization channels. In addition, the further development of the Single Calculus Chain (SCC) (D'Amico et al., 2015, 2016; Mattis et al., 2016) under the ACTRIS (Aerosols, Clouds and Trace gases Research InfraStructure Network) umbrella eliminated the inconsistencies in the retrieval procedures and in the signal error calculation, automated the data evaluation, and now allows for NRT data processing and the generation of tailored products network-wide. EARLINET has already demonstrated the network's NRT capabilities, as well as assisted modeling studies in NRT evaluation and assimilation (Wang et al., 2014; Sicard et al., 2015). As a consequence, EARLINET is prepared to provide prompt, height-resolved information and tailored products that were greatly missed during the 2010 aviation crisis. Therefore, a methodology for an early warning system based solely on EARLINET data is developed.

In Sect. 2, we present the EARLINET remote sensing network and the data that we used in this study. In Sect. 3, we introduce the methodology of the EARLINET-based EWS. In Sect. 4, we present the results obtained by applying the methodology to real measurements and the lessons learned from a multi-station EARLINET observational period. Finally, in Sect. 5, we give our conclusions and indicate directions for future work.

2 EARLINET

The European Aerosol Research Lidar Network (EARLINET; Pappalardo et al., 2014) was established in 2000, provides aerosol profiling data on a continental scale, and is now part of the Aerosols, Clouds, and Trace gases Research InfraStructure (ACTRIS; https://www.actris.eu, last access: 31 October 2019). Nowadays, more than 30 stations are active and perform measurements according to the network's schedule (one daytime and two nighttime measurements per week). Figure 1 illustrates the network's geographic extent and the location of the active EARLINET stations (green squares) and the joining EARLINET stations (yellow squares), together with the non-active site of Finokalia (red square), for which lidar data are used in this study. Further measurements are devoted to special events, such as volcanic eruptions, forest fires, and desert dust outbreaks (e.g., Mona et al., 2012; Pappalardo et al., 2013; Ortiz-Amezcua et al., 2017; Granados-Muñoz et al., 2016). The majority of the EARLINET stations operate multi-wavelength Raman lidars that combine a set of elastic and nitrogen inelastic channels and are equipped with depolarization channels. This li-

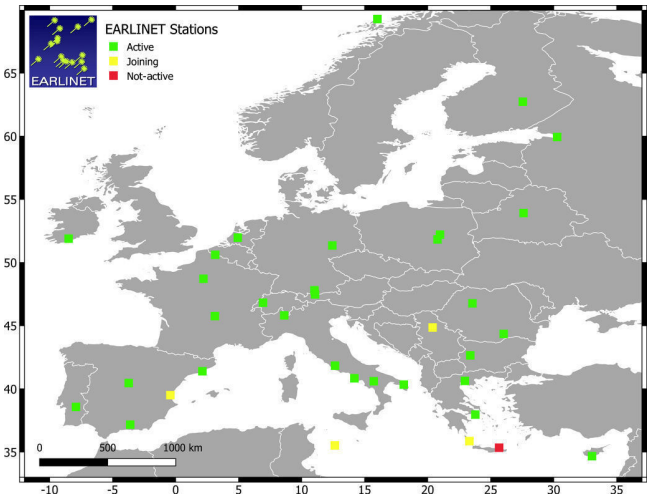

Figure 1. The EARLINET network in Europe. The green squares indicate the active stations, the yellow squares indicate the joining stations, and the red square indicates the non-active Finokalia, Greece, station.

dar configuration allows for the retrieval of intensive aerosol profiles, such as the particle lidar ratio, particle Ångström exponent, and particle depolarization ratio. These variables are shown to vary with the aerosol type and location, and, consequently, EARLINET stations are able to characterize the aerosol load (Müller et al., 2007). Accordingly, EARLINET has established tools for automatic aerosol characterization (Nicolae et al., 2018; Papagiannopoulos et al., 2018).

To ensure a homogeneous, traceable, and quality-controlled analysis of raw lidar data across the network, a centralized and fully automated analysis tool, called the Single Calculus Chain (SCC), has been developed within EARLINET (D'Amico et al., 2015, 2016; Mattis et al., 2016). Raw lidar data are first submitted to the central SCC server by each EARLINET station, and several lidar products are generated automatically. In particular, low-resolution (in both time and space) uncalibrated preprocessed products provided by the SCC EARLINET Lidar Pre-Processor (ELPP) module (D'Amico et al., 2016) and aerosol optical properties vertical profiles provided by the SCC EARLINET Lidar Data Analyzer (ELDA) module (Mattis et al., 2016) are made available. Recently a new version of the SCC has been released providing also standardized high-resolution preprocessed lidar products. These new products include the calibrated attenuated backscatter coefficient and volume linear depolarization ratio time series at instrumental time and space resolution. Particular attention has been paid to the calibration of the high-resolution products; an automatic and fully traceable calibration procedure using the low-resolution SCC-retrieved particle backscatter and extinction coefficients has been designed and implemented in the SCC framework.

The cloud screening module is responsible for cloud identification in uncalibrated lidar signals and especially with low clouds since such clouds do not permit the aerosol optical property retrieval by ELDA. Note that the cloud removal is also essential in our EWS methodology. The input of the algorithm is the high-resolution preprocessed signals produced by the SCC HiRELPP (High-Resolution EARLINET Pre-Processor) module. The current cloud screening detects clouds as bins with irregularly high values in signal and edge strength (Nixon and Aguado, 2019; Tramutoli, 1998). The algorithm works well with uncalibrated signals recorded by multiple lidar systems across EARLINET. However, the false detection of aerosol-laden bins as cloud can occur, especially in cases where there is high contrast between an aerosol layer and the rest of the atmosphere. For this reason, the development of a cloud screening module based on calibrated lidar signals and quantitative criteria is foreseen.

The calibrated high-resolution data along with the cloud screening output are essential for the proposed methodology and are used in the EWS. The methodology to derive the particle high-resolution data that are described in Sect. 3 is first cloud cleared and second based on 5 min and 30 m averaged profiles in order to increase the signal-to-noise ratio.

2.1 The sites of Finokalia and Antikythera, Greece

The EARLINET component of NOA (National Observatory of Athens) for the period of April 2017 until May 2018 was deployed through the NOA lidar system on the north coast of Crete. The Finokalia Atmospheric Observatory (35.34° N, 25.67° E) is a research infrastructure with activities covering in situ aerosol characterization, 3-D aerosol distribution, and gas precursors. Since June 2018, the system has been located on the island of Antikythera, where a suite of remote sensing sensors are installed in order to study the properties of natural aerosol particles (e.g., sea salt, dust, volcanic ash) in Mediterranean background conditions. The islands of Crete and Antikythera are very often affected by windblown dust originating from the Sahara due to their proximity to the African coastline, and this can be along the traveled path of volcanic dust and sulfate aerosols from the Italian active volcanoes (e.g., Hughes et al., 2016).

The NOA lidar system Polly^{XT} (e.g., Engelmann et al., 2016) operates in the frame of EARLINET and under the umbrella of ACTRIS. The system is equipped with three elastic channels at 355, 532, and 1064 nm, two vibration-rotation Raman channels at 387 and 607 nm, two linear depolarization channels at 355 and 532 nm, and one water vapor channel at 407 nm. Depending on the atmospheric conditions, the combined use of its near-range and far-range telescopes provides reliable vertical profiles of aerosol optical properties from 0.2–0.4 km to almost 16 km in height.

2.2 Additional data

For the detection of the desert dust plume, satellite imagery from the Spinning Enhanced Visible Infrared Imager (SE-

VIRI) is used. SEVIRI is a line-by-line scanning radiometer on board the Meteosat Second Generation (MSG) geostationary satellite. It provides data in 12 spectral bands every 15 min for the full Earth disk area. The spatial resolution is around 3 km at the nadir, which is different from the high-resolution visible (HRV) band (1 km). In this study, we used a largely accepted multi-temporal scheme of satellite data analysis (Tramutoli, 2007) to detect the dust plume over the Mediterranean basin. In particular, we used the $\mathrm{eRST_{DUST}}$ (enhanced robust satellite technique for dust detection) algorithm (Marchese et al., 2017), which combines an index analyzing the visible radiance (at around 0.6 µm) to another one based on the brightness temperature difference (BTD) of the signal measured by the SEVIRI spectral channels centered at 10.8 and 12 µm wavelengths.

For the detection of the volcanic dust, we use the Lagrangian transport model FLEXPART (FLEXible PARTicle dispersion model; Brioude et al., 2013; Stohl et al., 2005) in a forward mode to simulate the dispersion of volcanic emissions from Mount Etna, Italy. Dispersion simulations are driven by hourly meteorological fields from the Weather Research and Forecasting model (WRF; Skamarock et al., 2008) at 36 km × 36 km horizontal resolution. The initial and boundary conditions for the off-line coupled WRF–FLEXPART runs are taken from the National Center for Environmental Prediction (NCEP) final analysis (FNL) dataset at a $1^\circ \times 1^\circ$ resolution at 6-hourly intervals. The sea surface temperature (SST) is taken from the NCEP $0.5^\circ \times 0.5^\circ$ analysis. The simulated case study did not include an eruptive stage; therefore, the initial injection height is set from the crater level (3.3 km at sea level, a.s.l.) up to 4 km a.s.l. A total of 10 000 tracer particles are released for this simulation. Dry and wet deposition processes are also enabled in these runs. Saharan dust transport is also described in WRF with the Air Force Weather Agency (AFWA) scheme (Jones et al., 2012).

3 Methodology

3.1 Retrieval of the particle parameters in temporally high resolution

The delivery of an alert using EARLINET data is based on a two-step approach. In the first step, the high-resolution calibrated data are used to estimate the particle backscatter coefficient and the particle linear depolarization ratio. In order to retrieve the particle backscatter coefficient, an iterative methodology is adapted. The methodology, described in Di Girolamo et al. (1999), is able to retrieve a particle backscatter coefficient with an overall error of no more than 50 %. Prior to that, the cloud contaminated pixels are removed from the data using the cloud screening algorithm developed for the SCC (see Sect. 2).

The method is similar to that of Mattis et al. (2016) in which SCC is employed to derive optical products from elastic backscatter signals. For an ever-available NRT and automated aerosol retrieval, we use channels for elastic backscattering, including depolarization, since Raman observations during daytime have been hitherto challenging.

The calibrated attenuated backscatter coefficient provided by the SCC can be written as

$$\beta_{\mathrm{att}}(\lambda, r) = \left[\beta_{\mathrm{molec.}}(\lambda, r) + \beta_{\mathrm{par}}(\lambda, r)\right] T^2_{\mathrm{molec.}}(\lambda, r) T^2_{\mathrm{par}}(\lambda, r), \quad (1)$$

where $\beta_{\mathrm{par}}(\lambda, r)$ and $\beta_{\mathrm{molec.}}(\lambda, r)$ are, respectively, the backscatter coefficient for particles (par) and molecules (molec.); $T^2_{\mathrm{par}}(\lambda, r)$ and $T^2_{\mathrm{molec.}}(\lambda, r)$ represent the two-way attenuation to and from range r due to, respectively, particles and molecules at wavelength λ. The latter can be expressed as

$$T^{-2}_{\mathrm{par/molec.}}(\lambda, r) = \exp\left[-2\int_0^R \alpha^{-1}_{\mathrm{par/molec.}}(\lambda, r)\mathrm{d}r\right], \quad (2)$$

where $\alpha_{\mathrm{par}}(\lambda, r)$ and $\alpha_{\mathrm{molec.}}(\lambda, r)$ are the particle and molecular extinction coefficients, respectively. The term λ is omitted from the subsequent expressions as the analysis explicitly focuses on 532 nm. The terms $\alpha_{\mathrm{molec.}}(r)$ and $\beta_{\mathrm{molec.}}(r)$ can be estimated from temperature and pressure profiles.

In an initial step, the attenuation in the atmosphere is neglected, $\alpha^{(0)}_{\mathrm{par}}(r) = 0\,\mathrm{m}^{-1} \Rightarrow T^{(0)^2}_{\mathrm{par}}(r) = 1$, which reduces Eq. (1) to

$$\beta^{(1)}_{\mathrm{par}}(r) = \beta_{\mathrm{molec.}}(r)\left[\frac{\beta_{\mathrm{att}}(r)}{\beta_{\mathrm{molec.}}(r) T^2_{\mathrm{molec.}}(r)} - 1\right]. \quad (3)$$

The particle extinction coefficient is estimated by multiplying $\beta^{(1)}_{\mathrm{par}}(r)$ with a constant lidar ratio, S_{par}. Using the particle extinction coefficient in Eq. (1) we derive a new backscatter coefficient given by

$$\beta^{(2)}_{\mathrm{par}}(r) = \beta_{\mathrm{molec.}}(r)\left[\frac{\beta_{\mathrm{att}}(r)}{\beta_{\mathrm{molec.}}(r) T^2_{\mathrm{molec.}}(r) T^{(1)^2}_{\mathrm{par}}(r)} - 1\right]. \quad (4)$$

Baars et al. (2017) developed a method to derive atmospheric parameters in temporally high resolution, and they refer to the product of Eq. (4) as the quasi-particle backscatter coefficient, which serves as the best estimate for the particle backscatter coefficient. However, here the particle backscatter,

$$\beta^{(i)}_{\mathrm{par}}(r) = \beta_{\mathrm{molec.}}(r)\left[\frac{\beta_{\mathrm{att}}(r)}{\beta_{\mathrm{molec.}}(r) T^2_{\mathrm{molec.}}(r) T^{(i-1)^2}_{\mathrm{par}}(r)} - 1\right], \quad (5)$$

is calculated in the ith iteration step from the calibrated attenuated backscatter coefficient. The procedure is successfully terminated if the absolute difference between the backscatter coefficient of two subsequent profiles is smaller than a fixed threshold. The absolute difference, Δ_β, is defined as

$$\Delta\beta^{(i)} = \left|\int \beta^{(i)}_{\mathrm{par}}\mathrm{d}r - \int \beta^{(i-1)}_{\mathrm{par}}\mathrm{d}r\right|. \quad (6)$$

We found that fewer than 10 steps are required for a difference of 1 % for the cases examined herein.

The particle depolarization ratio at 532 nm can be defined as (Baars et al., 2017)

$$\delta_{\mathrm{par}} = [\delta_{\mathrm{vol}}(r) + 1] \times \left(\frac{\beta_{\mathrm{molec.}}(r)\,[\delta_{\mathrm{molec.}} - \delta_{\mathrm{vol}}(r)]}{\beta_{\mathrm{par}}(r)\,[1 + \delta_{\mathrm{molec.}}]} \right)^{-1} - 1, \quad (7)$$

where $\delta_{\mathrm{molec.}}$ is the molecular depolarization ratio and is calculated theoretically (Behrendt and Nakamura, 2002). The term $\delta_{\mathrm{vol}}(r)$ denotes the volume depolarization ratio, and it is the output of SCC.

The input lidar ratio value used in the retrieval could significantly affect the results. Papagiannopoulos et al. (2018) used 48 ± 13 sr for fresh volcanic particles and 55 ± 7 sr for desert dust particles observed over EARLINET sites in their aerosol classification, which illustrates the variability of this intensive parameter. The uncertainty induced due to the assumption of the lidar ratio can easily exceed 20 % (Sasano et al., 1985) and presents an important source that affects the retrieval. In this study, $S_{\mathrm{par}} = 50$ sr is chosen for the backscatter coefficient retrieval as it is a good compromise for many EARLINET sites and different aerosol conditions (Papayannis et al., 2008; Müller et al., 2007; Mona et al., 2014; Papagiannopoulos et al., 2016). Figure 2 shows a desert dust layer around 3 km over the Potenza EARLINET station on 4 April 2016, 18:47–22:15 UTC. The backscatter coefficient at 532 nm retrieved for 30, 50, and 70 sr along with the backscatter coefficient from the Raman method is shown (Fig. 2a). The three curves almost coincide in the upper part (relative difference is around 5 %) and deviate from one another by less than 35 % in the lower portion of the profile where local aerosol is mixed with dust particles.

The performance of the iterative method for $S_{\mathrm{par}} = 50$ sr can be assessed in Fig. 2b. The overall agreement is very good with the relative difference being around 4 %; however, the iterative method underestimates almost everywhere the Raman method due to the assumption of $S_{\mathrm{par}} = 50$ sr instead of the measured 43 ± 7 sr. Figure 2c highlights the effect when the directly measured lidar ratio is plotted against the fixed lidar ratio. Evidently, the curves agree fairly well for the aerosol layer (e.g., desert dust) in the free troposphere and deviate from the layer below (i.e., values over 50 sr). As discussed above, the inference of the lidar ratio is an important factor, yet a lidar ratio value valid for a common volcanic dust and desert dust layer will provide a robust solution for this approach.

3.2 Aviation alert delivery

In the second step, the location and the intensity of the volcanic dust and desert dust event are identified. Mona and Marenco (2016) reported that particle depolarization ratio values were around 35 % for freshly emitted particles from various volcanoes and that the values decrease with time. Similarly, pure Saharan dust particles are supposed

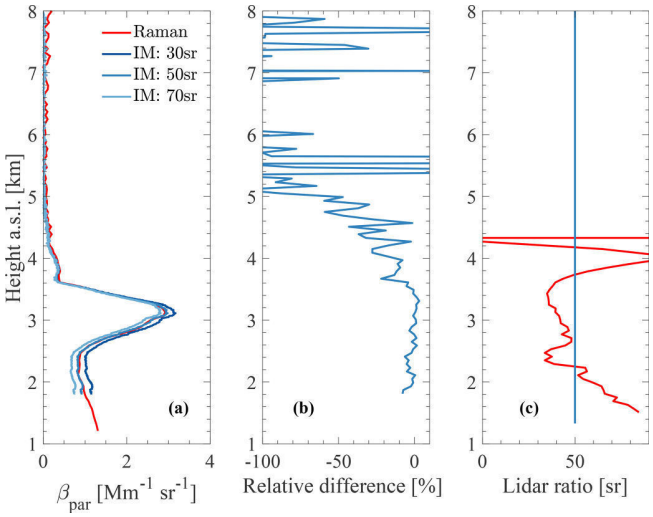

Figure 2. (a) The 532 nm backscatter coefficient retrieved with the iterative method (IM) for 30, 50, and 70 sr along with the backscatter coefficient determined with the Raman method (standard SCC product) measured at Potenza (760 m a.s.l.), Italy, on 4 April 2016, 18:47–22:15 UTC. The lidar system of Potenza has a full overlap at around 1.15 km a.s.l. for 532 nm (Madonna et al., 2018). **(b)** The relative difference between the iterative method (IM: 50 sr) and the Raman method backscatter coefficient. **(c)** The lidar ratio profile measured with the Raman method and the fixed lidar ratio used for the iterative method.

to have a slightly smaller particle depolarization ratio of 31 % (Freudenthaler et al., 2009). Since nonspherical particles such as volcanic and desert dust particles yield high particle depolarization ratio values, the one-step polarization-lidar photometer networking (POLIPHON) method is used (e.g., Ansmann et al., 2012).

The particle depolarization ratio is used to separate the nonspherical particles contribution to the particle backscatter coefficient. Mamouri and Ansmann (2014) describe in detail the retrieval process; however, here we treat volcanic dust and desert dust inextricably. The volcanic dust and desert dust backscatter coefficient can be expressed by

$$\beta_{\mathrm{c}} = \beta_{\mathrm{par}} \frac{(\delta_{\mathrm{par}} - \delta_{\mathrm{nc}})\,(1 + \delta_{\mathrm{c}})}{(\delta_{\mathrm{c}} - \delta_{\mathrm{nc}})\,(1 + \delta_{\mathrm{par}})}, \quad (8)$$

where the coarse (c) and non-coarse (nc) depolarization ratios are set to $\delta_{\mathrm{c}} = 0.31$ and $\delta_{\mathrm{nc}} = 0.05$, respectively. For values $\delta_{\mathrm{par}} < \delta_{\mathrm{nc}}$, we need to set $\beta_{\mathrm{nc}} = \beta_{\mathrm{par}}$. Similarly, when $\delta_{\mathrm{par}} > \delta_{\mathrm{c}}$, we set $\beta_{\mathrm{c}} = \beta_{\mathrm{par}}$.

Until the aviation crisis in 2010, planes were advised to avoid the volcanic plumes regardless of the aerosol concentration (Guffanti et al., 2010). Recently, the International Civil Aviation Organization (ICAO, 2014) established three ash concentration thresholds which play a key role in the decision-making process. Aircraft are allowed to fly below 0.2 mg m^{-3}, whereas they are forbidden to fly over 2 and 4 mg m^{-3} (depending on the aircraft's resilience).

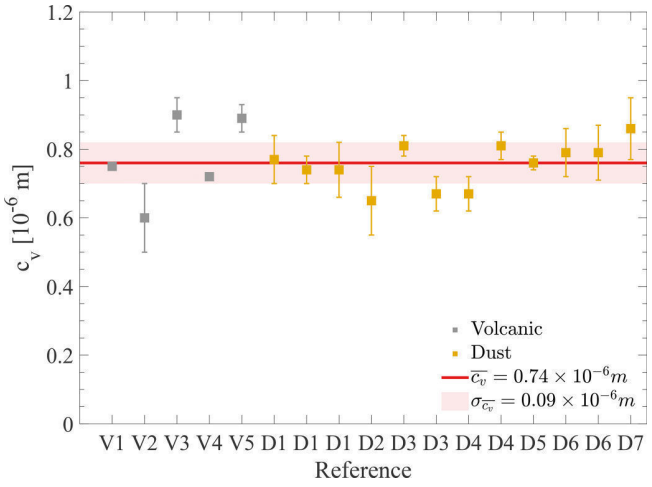

Figure 3. The scatter plot indicates the mean and the standard deviation of the conversion factor, c_v, for the different literature references. The plot is color coded with respect to "Volcanic" (gray) and "Dust" (orange) observations. The red line highlights the overall mean conversion factor and the reddish-pink rectangle shows the standard deviation – i.e., $(0.76 \pm 0.06) \times 10^{-6}$ m.

Table 1. The code used in Fig. 3 and the respective reference.

Code	Reference
V1	Ansmann et al. (2010)
V2	Ansmann et al. (2011)
V3	Ansmann et al. (2012)
V4	Devenish et al. (2012)
V5	Sicard et al. (2012)
D1	Ansmann et al. (2012)
D2	Binietoglou (2014)
D3	Córdoba-Jabonero et al. (2018)
D4	Mamali et al. (2018)
D5	Mamouri and Ansmann (2014)
D6	Mamouri and Ansmann (2017)
D7	Ansmann et al. (2019)

The methodology proposed by Ansmann et al. (2012) for the estimation of aerosol mass concentration profiles employs data from a single-wavelength polarization lidar. The methodology retrieves mass concentration profiles with an uncertainty of 20 %–30 %, and it has proven to be robust and applicable to very different scenarios (e.g., Mamali et al., 2018; Córdoba-Jabonero et al., 2018) that need one wavelength and can be applied to cloudy skies. We chose to convert the three ash concentration thresholds into particle backscatter coefficient. The threshold values for the particle backscatter coefficient, β_{th}, are estimated as

$$\beta_{\text{th}} = M \frac{1}{\rho c_{\text{v}} S}, \tag{9}$$

where M is the mass concentration given by ICAO, ρ the volcanic and desert dust bulk density, c_{v} the mass-to-extinction conversion factor, and S the volcanic and desert dust lidar ratio. All the terms have to be assumed constant, and they are selected from the literature. The above concentration thresholds (e.g., 0.2, 2, 4 mg m^{-3}) are used for the term M. For the ρ, we used the value 2.6 g cm^{-3} that corresponds to a commonly used value for volcanic and desert dust applications (e.g., Gasteiger et al., 2011; Ansmann et al., 2012; Binietoglou et al., 2015; Mamali et al., 2018). The term S is chosen to be 50 sr as a good compromise for fresh volcanic particles (e.g., Ansmann et al., 2011) and Saharan dust (e.g., Wiegner et al., 2012).

The term c_{v} can be estimated using Aerosol Robotic Network (AERONET) observations as being the ratio of the coarse column volume concentration, υ_{c}, to the coarse mode aerosol optical thickness, τ_{c}. More information on the different retrievals and AERONET data processing can be found in Ansmann et al. (2012), Mamouri and Ansmann (2017), and Ansmann et al. (2019). However, for an EWS and day–night availability, we have to select a constant value for volcanic dust and desert dust. Figure 3 shows an overview of AERONET-based c_{v} values. To interpret the horizontal axis of the figure, one should also look at Table 1. The figure is separated into volcanic (gray points) and desert (orange points) dust and depicts the range of the observed values; furthermore, the plot shows the mean and standard deviation for the overall average of the conversion factors. It is evident from Fig. 3 that for both volcanic and desert dust the values accumulate between 0.6 and 0.9×10^{-6} m with a mean of $(0.76 \pm 0.06) \times 10^{-6}$ m. It is worth noting that although most of the conversion factors were estimated using carefully selected AERONET observations, Mamouri and Ansmann (2017) and Ansmann et al. (2019) use a climatology to derive the conversion factor.

The conversion factor for the coarse particles (i.e., volcanic and desert dust) varies strongly with the distance from the source and, in the case of volcanic eruptions, with the eruption type. Ansmann et al. (2012) highlight that, when particles larger than 15 µm (i.e., the higher limit of the assumed particles radii for the AERONET data analysis scheme) are present, the mass concentration may be underestimated by more than 100 %. The conversion factor in the case of dense and coarser plumes should be much higher and, consequently, will have an adverse impact on our EWS approach. For instance, Pisani et al. (2012) used a conversion factor of 0.6×10^{-5} m for a freshly erupted volcanic plume near Mount Etna in Italy. A similar increase, although less pronounced, in the conversion factor can be observed in Mamouri and Ansmann (2017) and Ansmann et al. (2019), in which the authors retrieve a dust coarse-mode conversion factor (i.e., the values reported in Fig. 3). It is believed that particles bigger than 10 µm usually fall quickly to the ground, whereas smaller particles can travel over long distances (Goudie and Middleton, 2006; Wilson et al., 2012). Conversely, van der Does et al. (2016) and Ryder et al. (2018)

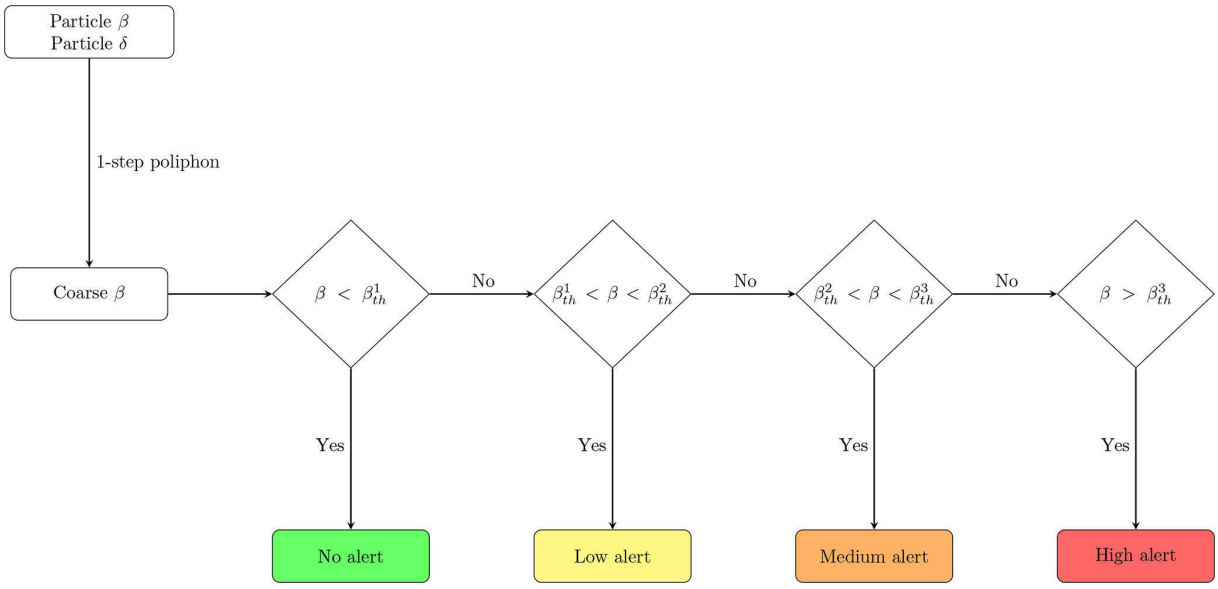

Figure 4. The EARLINET alert delivery scheme for aviation. The particle backscatter coefficient and depolarization ratio are used to estimate the coarse backscatter coefficient (one-step POLIPHON method). Three levels are considered that correspond to "Low alert" for particle concentrations higher than $0.2\,\mathrm{mg\,m^{-3}}$ and lower than $2\,\mathrm{mg\,m^{-3}}$, "Medium alert" for concentrations higher than $2\,\mathrm{mg\,m^{-3}}$ and lower than $4\,\mathrm{mg\,m^{-3}}$, and "High alert" for mass concentrations higher than $4\,\mathrm{mg\,m^{-3}}$. The three backscatter coefficient thresholds are $\beta^1_{\mathrm{th}} = 1.7 \times 10^{-6}\,\mathrm{m^{-1}sr^{-1}}$, $\beta^2_{\mathrm{th}} = 1.7 \times 10^{-5}\,\mathrm{m^{-1}sr^{-1}}$, and $\beta^3_{\mathrm{th}} = 3.4 \times 10^{-5}\,\mathrm{m^{-1}sr^{-1}}$.

have illustrated that the desert dust size far away from its source is much coarser than previously suggested, and this has been incorporated into climate models. In light of the above, we chose as the conversion factor in our approach the maximum retrieved value, which is 0.9×10^{-6} m (Ansmann et al., 2012). Hence, the thresholds for the particle backscatter coefficient become 1.7×10^{-6} (for $0.2\,\mathrm{mg\,m^{-3}}$), 1.7×10^{-5} (for $2\,\mathrm{mg\,m^{-3}}$), and $3.4 \times 10^{-5}\,\mathrm{m^{-1}\,sr^{-1}}$ (for $4\,\mathrm{mg\,m^{-3}}$). Given also that the EARLINET stations are far from the active European volcanoes (i.e., Mount Etna and the Icelandic volcanoes), we consider that the selected AERONET-derived conversion factor holds for most of the situations.

Figure 4 illustrates the decision flowchart for the aviation alert delivery in which three alert levels are available: low alert ($0.2 < M_{\mathrm{c}} < 2\,\mathrm{mg\,m^{-3}}$), medium alert ($2 < M_{\mathrm{c}} < 4\,\mathrm{mg\,m^{-3}}$), and high alert ($M_{\mathrm{c}} > 4\,\mathrm{mg\,m^{-3}}$), indicating the increasing amount of dust particles that are likely dangerous for flight operations. The coarse backscatter coefficient due to the highly depolarizing particles is estimated first. Next, the coarse backscatter coefficient is checked, and the level of alert is decided. Furthermore, to avoid isolated false alarms in the EWS product, we incorporated a linear spatial smoothing filter. It is the average of the pixels contained in the neighborhood of each pixel, for which we defined a 3 pixel × 3 pixel grid. A similar methodology has been demonstrated within an international demonstration exercise for the purpose of the EUNADICS-AV project, in which an artificial Mount Etna eruption was simulated (Hirtl et al., 2020).

4 Results

In this section, we apply the described methodology to potential perilous events recently detected by the stations of Finokalia and Antikythera, Greece. The observations refer to the same lidar system that was initially deployed in Finokalia and later moved to the island of Antikythera. The aim is not to present a detailed analysis of investigated cases but instead to demonstrate the potential of this methodology to be integrated as a tailored EARLINET product for the fast alerting of airborne hazards relevant to flight operations.

4.1 Desert dust particle case

During March 2018, frequent intense dust storms affected Greece with the region of Libya being the originating source (Kaskaoutis et al., 2019). Strong surface and middle and upper troposphere Khamsin winds transported dust northwards for four distinct periods (i.e., 4–7, 17, 21–22, 25–26 March). Solomos et al. (2018) examined in detail the record-breaking episode of 21–22 March, when surface concentrations exceeded $6\,\mathrm{mg\,m^{-3}}$ on 22 March and resulted in the closure of the Heraklion airport.

Here we focus on 21 March when the dust cloud initially appeared over Crete. Figure 5 shows the dust map derived from SEVIRI data along with the cloud cover at 12:00 UTC. The dusty pixels are depicted in two different colors as a function of the confidence levels of the dust detection scheme (i.e., brown means high confidence and orange mid–low con-

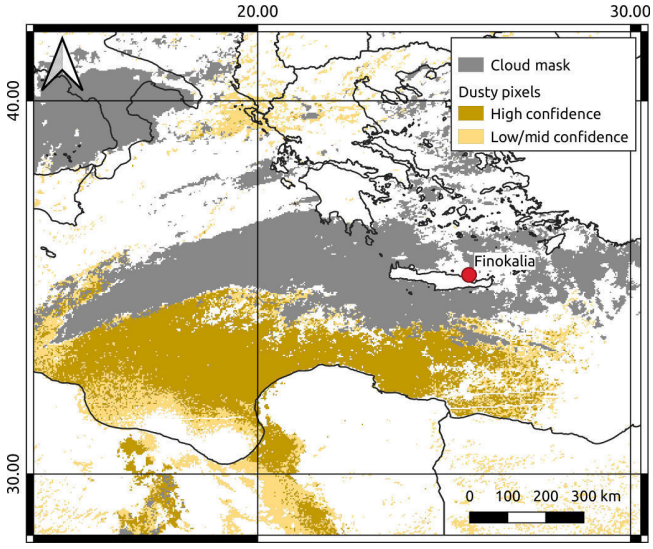

Figure 5. The dust SEVIRI product (Marchese et al., 2017) at 12:00 UTC on 21 March 2018 is represented in confidence levels (i.e., brown pixels refer to high confidence and orange pixels to mid–low confidence). The gray pixels indicate the cloud cover.

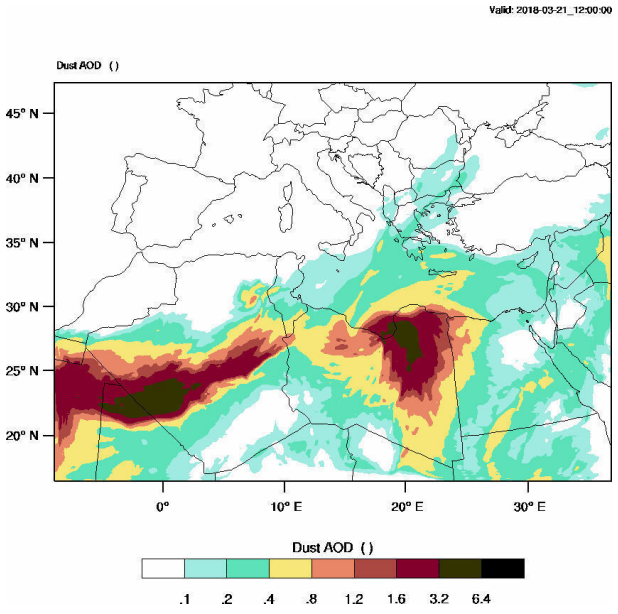

Figure 6. WRF-Chem dust aerosol optical depth (AOD) on 21 March 2018 12:00 UTC.

fidence). In particular, the dust cloud moves from northern Africa towards the eastern Mediterranean, where the cloud cover impedes the dust detection over insular Greece, although the map demonstrates the intensity and the geographic extent of the dust event. The situation of the dust transport at 12:00 UTC on 21 March 2018 is also evident from the WRF-Chem (WRF model coupled with Chemistry) dust aerosol optical depth (AOD) in Fig. 6. The entire eastern

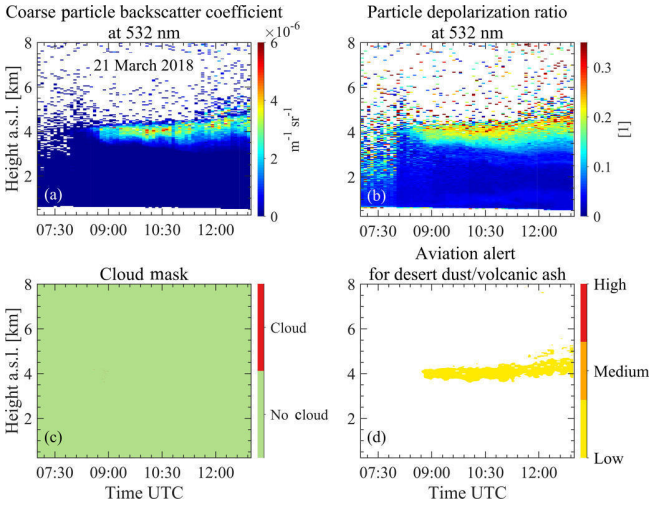

Figure 7. EARLINET observations at Finokalia on 21 March 2018: **(a)** the coarse particle backscatter coefficient at 532 nm, **(b)** the particle depolarization ratio at 532 nm, **(c)** the cloud screening output, and **(d)** the alert for aviation. Note that the cloud screening product is given at its full resolution – i.e., the vertical resolution is 7.5 m, and the temporal resolution is 30 s – and all the other products have a resolution of 30 m and 5 min instead.

Mediterranean is affected by this episode, and the simulated AOD exceeds 0.4 over certain parts of eastern Crete near the Finokalia station.

The coarse particle backscatter coefficient, the particle depolarization ratio at 532 nm (as described in Sect. 3.1), the cloud mask, and the tailored product for the period 07:00–13:00 UTC are shown in Fig. 7. The dust particles arrive over Finokalia around 08:00 UTC in a filament-like layer of about 4 km, wherein the dust particles exhibit high values of the particle depolarization ratio. Figure 7d shows the alert product for aviation, which demonstrates a low level alert indicating a considerable amount of dust particles in the troposphere that are likely dangerous for flight operations. In particular, the coarse particle backscatter coefficient at 532 nm exhibits values up to 6×10^{-6} m^{-1} sr^{-1}, which exceeds the threshold value of 1.7×10^{-6} m^{-1} sr^{-1}. In addition, this case illustrates the advantage of a ground-based lidar system to operate below high clouds that obstruct satellite observations (see Fig. 5) and, therefore, provides important insight.

As the event was aggravated in the following hours, the lidar signal is most likely attenuated which highlights the limitation of the methodology. However, the alert delivery could act as a pre-alerting tool for aviation by pinpointing the specific aerosol conditions. A similar approach for airport operations has been developed using automatic lidars and ceilometers for the prediction of fog formation (Haeffelin et al., 2016).

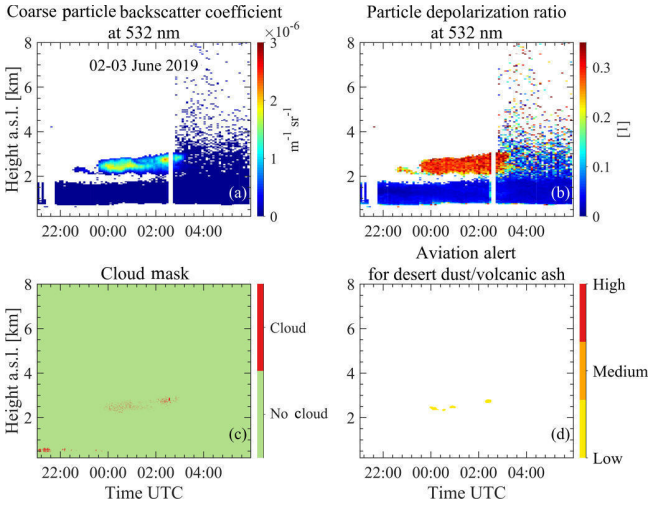

Figure 8. EARLINET observations at Antikythera on 2–3 June 2019: **(a)** the coarse particle backscatter coefficient at 532 nm, **(b)** the particle depolarization ratio at 532 nm, **(c)** the cloud screening output, and **(d)** the alert for aviation. Note that the cloud screening product is given at its full resolution – i.e., the vertical resolution is 7.5 m, and the temporal resolution is 30 s – and all the other products have a resolution of 30 m and 5 min instead.

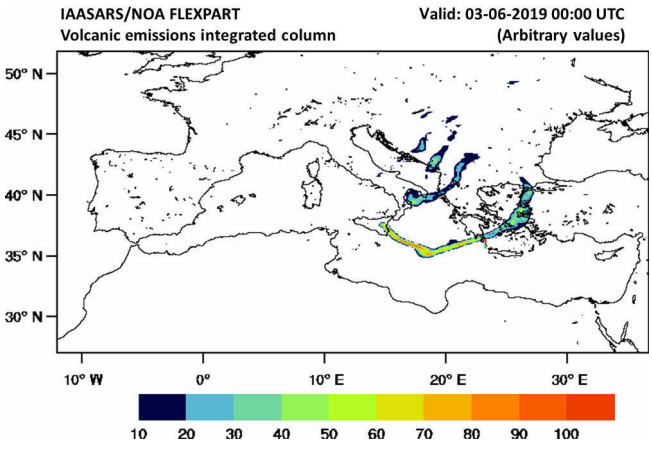

Figure 9. FLEXPART vertically integrated volcanic ash particles (arbitrary values) originating from Mount Etna on 3 June 2019 at 00:00 UTC. The green star indicates the location of Antikythera, and the red line is the misplacement of the simulated plume from the lidar station.

4.2 Volcanic and desert dust particle case

The eruption of the volcano Mount Etna which began in the early hours of 30 May 2019 injected ash into the atmosphere at an altitude of 3.5–4.0 km (Toulouse Volcanic Ash Advisory Center report at 11:21 UTC, 30 May). The volcanic activity ceased most likely on 3 June (https://ingvvulcani.wordpress.com, last access: 31 October 2019). This volcanic activity did not lead to any air traffic disruption, as was the case for the explosion on 20 July. The latter caused flight rerouting and delays (Amato, 2019).

Aerosol particles of possibly volcanic origin were monitored with the multi-wavelength lidar of NOA over Antikythera, Greece. The eastward advection of volcanic particles from Mount Etna presents a common pathway and has been previously investigated by means of active remote sensing (e.g., Hughes et al., 2016; Zerefos et al., 2006). The presence of these elevated layers above Greece could be a result of the continuous Mount Etna activity of the past few days. Figure 8 shows two distinct layers with different characteristics for the period from 21:00 UTC on 2 June to 06:00 UTC on 3 June. The first layer is initially observed between 1 and 2 km on 2 June and remains visible for the rest of the temporal window. The particle backscatter coefficient is around $1 \times 10^{-6}\,\mathrm{m^{-1}\,sr^{-1}}$, and the particle depolarization ratio is below 5 % and differentiates from the second layer above. The second layer is seen after 23:30 UTC on 2 June until 03:00 UTC on 3 June and resides in the range of 2–3 km. The layer particle depolarization ratio is well above 20 % and indicates non-spherical particles. Moreover, it exhibits a higher particle backscatter coefficient ($\sim 3 \times 10^{-6}\,\mathrm{m^{-1}\,sr^{-1}}$). As a result, the alert is triggered for the latter. It is noteworthy that, as seen in the cloud mask, few pixels within the same aerosol layer are wrongly classified as clouds and are used instead in the alert delivery. The improvement of the cloud masking module is currently ongoing and is expected to eliminate false cloud detection, but nonetheless the aerosol layer is very well captured by the method.

The identification of the source of the two aerosol layers is made through an analysis of FLEXPART and WRF-Chem simulations. Figure 9 indicates the eastward transport of a relatively thin ($\sim$ 60 km horizontal width) volcanic ash plume from Mount Etna towards Greece. As shown by the FLEXPART simulation, this plume propagated eastwards from Sicily towards the Ionian Sea, reaching parts of southern Greece. The simulated plume is misplaced by about 70 km towards the north from the EARLINET Antikythera station; however, its vertical structure is still evident in the cross section of Fig. 10. The eastward motion and the vertical profile of simulated aerosol volcanic plume corroborate the existence of volcanic particles in the upper layer of Fig. 8. The non-depolarizing structures below 2 km are sea-salt particles possibly mixed with dust particles. Limited concentrations ($> 0.04\,\mathrm{mg\,m^{-3}}$) of dust are simulated at these heights by the WRF-Chem model (Fig. 11) and are accompanied by increased relative humidity near the surface, thus implying hygroscopic growth and more spherical particles in this area. In synthesis, both observations and model simulations advocate for the identification of likely volcanic dust and aged desert dust particles in the same aerosol scene but in separate layers. Consequently, the alert delivered refers to volcanic dust.

Table 2. EARLINET stations that participated in the EUNADICS-AV exercise during 5–6 March 2019. The percentage of the measurements made for the 2 consecutive days and the specific temporal windows is reported. The "X" denotes the stations for which it was possible to derive the alert for aviation – i.e., the availability of a calibrated backscatter coefficient and depolarization ratio of 532 nm.

EARLINET station	Measurements performed (%)		EWS
	5 March, 11:00–17:00 UTC	6 March, 07:00–12:00 UTC	
Antikythera (GR)	100	100	X
Athens* (GR)	100	100	
Barcelona (ES)	100	0	X
Belgrade* (SRB)	100	100	
Clermont-Ferrand* (FR)	33	40	
Cluj* (RO)	100	80	
Granada (ES)	17	20	X
Hohenpeissenberg (DE)	100	100	X
Leipzig (DE)	100	100	X
Madrid (ES)	33	0	
Potenza (IT)	100	100	X
Rome – Tor Vergata (IT)	100	100	
Thessaloniki* (GR)	83	100	

The * indicates the stations equipped with a depolarization channel, although this information was not available during the exercise.

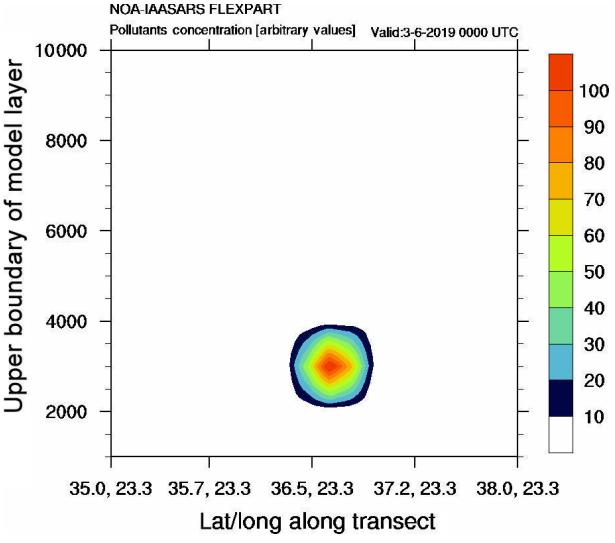

Figure 10. FLEXPART vertical cross section of the simulated volcanic particles (in arbitrary values) over the greater Antikythera region. The exact location of the cross section is indicated by the red line in Fig. 9.

4.3 Lessons learned from the EUNADICS-AV exercise

The application of the EWS and the timely delivery of the EARLINET data were tested in real time during the EUNADICS-AV exercise, in which EARLINET stations performed synchronous measurements. The EUNADICS-AV demonstration exercise in March 2019, based on a fictitious volcanic eruption, demonstrated that tailored observations, as well as model services, can profitably support aviation stakeholders (Hirtl et al., 2020).

In particular, 13 EARLINET stations contributed to the exercise according to a predefined measurement schedule – i.e., from 11:00 to 17:00 UTC on 5 March 2019 and from 07:00 to 11:00 UTC on 6 March 2019 – independent of the station's capabilities with respect to the EWS. This decision stems from the opportunity to assess the sequence of procedures for real-time data retrieval and data visualization. In addition, the measurements schedule, the stations submitted raw lidar data to the SCC server every hour, which were automatically available on the EARLINET Quicklook Interface (https://quicklooks.earlinet.org/, last access: 16 January 2019). For the majority of the stations and temporal windows, low clouds and cirrus clouds were observed. Table 2 summarizes the measurements gathered per hour segment and the station capabilities with respect to the EWS. In total, 73 % of the measurements were performed successfully, whereas rain and staffing the stations mostly inhibited the rest. Moreover, only for six of the stations was it possible to retrieve the tailored product mainly because of the lack of the depolarization information during the exercise. The tailored product did not produce any alert as the aerosol layers were neither volcanic dust nor desert dust, and they did not yield high backscatter coefficient values. Hence, results of the exercise are not shown here; nonetheless, the EARLINET observations are available through the EARLINET Quicklook Interface.

Overall, the raw lidar data were streamed and processed in less than 30 min from the measurement, enabling the timely delivery of the lidar data and the tailored product when pos-

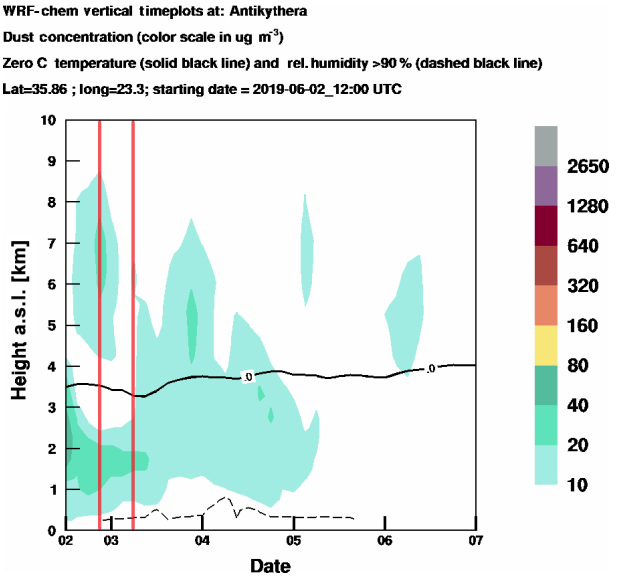

Figure 11. WRF-Chem time–height cross section of simulated dust concentration ($\mu g\,m^{-3}$) over Antikythera starting on 2 June at 12:00 UTC. The solid black line is the 0 °C isotherm, and the dashed black line indicates 90 % relative humidity. The red lines correspond to the time domain of the lidar observations – i.e., from 21:00 UTC on 2 June 2019 until 06:00 UTC on 3 June 2019.

sible. Furthermore, the demonstration exercise was the first occasion in which the proposed methodology was tested in NRT, and the obtained results suggest that the network could actively support stakeholders in decision-making during an aviation crisis.

5 Conclusions

A tailored product for aviation hazards by means of high-resolution lidar data has been proposed for the first time to our knowledge. In particular, the methodology employs single-wavelength EARLINET high-resolution data (i.e., 532 nm calibrated backscatter coefficient and 532 nm calibrated volume linear depolarization ratio) and yields NRT alerts based on established aerosol mass concentration thresholds. The methodology aims to provide an EARLINET EWS for the fast alerting of airborne hazards exploiting the SCC advancements and to mitigate the effects of a future aviation crisis. The application on EARLINET data from the eastern Mediterranean demonstrated the strength of the methodology in identifying possible dangers for aviation from volcanic ash and desert dust plumes.

One of the key challenges for a NRT automated alert delivery is the calibration of the backscatter and depolarization profiles as the elastic and depolarization channels are used. The EARLINET SCC ensures the absolute calibration of the lidar signals. As a source of high uncertainties in the retrieval of the particle backscatter coefficient, the inference of the lidar ratio was acknowledged. Accordingly, an iterative method has been developed to work with high-resolution lidar data, which compares well with particle backscatter coefficient profiles retrieved with the Raman method.

Additionally, and equally important in the alert delivery approach, there is the conversion factor with which the mass concentration thresholds are converted into a particle backscatter coefficient. The AERONET-derived conversion factors are known to be restricted by the AERONET data inversion scheme and to underestimate large to giant particles. Therefore, the selected conversion factor was chosen (i.e., 0.9×10^{-6} m) as the maximum value of the literature review with reference to fresh volcanic and desert dust observations.

The NRT operation of EARLINET during the EUNADICS-AV exercise was successfully demonstrated. The successful application of the method in NRT has been achieved during the EUNADICS-AV exercise. The raw data, upon being uploaded to the SCC server, were automatically processed and became freely accessible through the EARLINET portal and available in order to initiate the alert delivery. The exercise demonstrated the strength of the network, which, if promptly triggered, can enable measurements in the case of natural hazards for aviation.

In addition, a similar approach can be extended to lidar systems operated by the European volcano observatories. Two examples of such observatories in Europe are the Istituto Nazionale di Geofisica e Vulcanologia – Osservatorio Etneo (INGV-OE) and the Icelandic Meteorological Office (IMO). INGV-OE is responsible for monitoring Mount Etna, while IMO is responsible for monitoring all volcanic activity in Iceland.

This method is highly versatile as it can adapt to other wavelengths, and the aerosol backscatter thresholds can be set to accommodate different volcanic and desert dust scenarios by adjusting the conversion factor, the lidar ratio, the bulk density, and the mass concentration levels. In addition, even if developed on the basis of EARLINET, it can be applied to such lidar systems as those that are part of Galion (ADNet, LALINET, MPLNET), as well as to current (CALIPSO; Cloud-Aerosol Lidar and Infrared Pathfinder Satellite Observation) and future (EarthCARE; Earth Clouds, Aerosols and Radiation Explorer) lidar-based satellite missions.

Code availability. The code is available upon request (contact mail: nikolaos.papagiannopoulos@imaa.cnr.it).

Data availability. The EARLINET data are accessible through the EARLINET database web portal https://data.earlinet.org (login required, last access: 10 September 2020).

Author contributions. The conceptualization and design of this study were carried out by NP and LM. GD is the lead scientist and

curator of the EARLINET SCC data. IM and IB created the calibration and cloud mask module for the EARLINET SCC, respectively. VA and AG are the principal investigator (PI) and data originator for the EARLINET stations of Finokalia and Antikythera, respectively. SS and AK performed FLEXPART model simulations for the Antikythera case study. AF retrieved the dust product from SEVIRI data for the Finokalia case study. AA, AC, AP, ARG, DD, DM, FM, HB, IM, LAA, NA, PF, VM, and ZM are either the PIs or the key personnel of the stations involved in the measurements exercise and ensured the high-quality operation of the respective lidars. The interpretation of results was determined from discussions involving all authors. The original draft of the paper was written by NP and reviewed and edited by all the coauthors.

Competing interests. The authors declare that they have no conflict of interest.

Special issue statement. This article is part of the special issue "EARLINET aerosol profiling: contributions to atmospheric and climate research". It is not associated with a conference.

Acknowledgements. The authors acknowledge EARLINET for providing aerosol lidar profiles (https://www.earlinet.org, last access: 31 October 2019). We thank the ACTRIS-2 and ACTRIS preparatory phase projects that have received funding from the European Union's Horizon 2020 Framework Program for Research and Innovation (grant agreement no. 654109) and from European Union's Horizon 2020 Coordination and Support Action (grant agreement no. 739530), respectively. This work has been conducted within the framework of the EUNADICS-AV project, which has received funding from the European Union's Horizon 2020 research program for Societal Challenges – Smart, Green and Integrated Transport under grant agreement no. 723986. Furthermore, the research leading to these results has received funding from the COST Action CA16202, supported by the COST Association (European Cooperation in Science and Technology). The project e-shape (EuroGEOSS Showcases: Applications Powered by Europe), funded under the European Union's Horizon 2020 program (grant agreement no. 820852), is also acknowledged. Part of the work performed for this study was funded by the Ministry of Research and Innovation through Program I – Development of the National Research-Development System, subprogram 1.2 – Institutional Performance – Projects of Excellence Financing in RDI (grant no. 19PFE/17.10.2018) and by the Romanian National Core Program (grant no. 18N/2019). VA acknowledges support of this work by the European Research Council (ERC) under the European Community's Horizon 2020 Framework Program for Research and Innovation grant agreement 725698 (D-10 TECT).

Financial support. This research has been supported by the ACTRIS-2 (grant no. 654109), the ACTRIS preparatory phase (grant no. 739530), the EUNADICS-AV (grant no. 723986), the E-shape (EuroGEOSS Showcases: Applications Powered by Europe) (grant no. 820852), the Ministry of Research and Innovation through Program I – Development of the National Research-Development System, Subprogram 1.2 – Institutional Performance – Projects of Excellence Financing in RDI (grant no. 19PFE/17.10.2018), the Romanian National Core Program (grant no. 18N/2019), and the European Commission, H2020 Research Infrastructures (D-TECT (grant no. 725698)).

Review statement. This paper was edited by Eduardo Landulfo and reviewed by three anonymous referees.

References

Amato, G.: Cenere dall'Etna, disagi in mattinata all'aeroporto di Catania, La Repubblica, available at: https://palermo.repubblica.it/cronaca/2019/07/20/news/cenere_dall_etna_disagi_all_aeroporto_di_catania-231613901/?ref=search (last access: 10 September 2020), 2019 (in Italian).

Ansmann, A., Tesche, M., Groß, S., Freudenthaler, V., Seifert, P., Hiebsch, A., Schmidt, J., Wandinger, U., Mattis, I., Müller, D., and Wiegner, M.: The 16 April 2010 major volcanic ash plume over central Europe: EARLINET lidar and AERONET photometer observations at Leipzig and Munich, Germany, Geophys. Res. Lett., 37, L13810, https://doi.org/10.1029/2010GL043809, 2010.

Ansmann, A., Tesche, M., Seifert, P., Groß, S., Freudenthaler, V., Apituley, A., Wilson, K. M., Serikov, I., Linné, H., Heinold, B., Hiebsch, A., Schnell, F., Schmidt, J., Mattis, I., Wandinger, U., and Wiegner, M.: Ash and fine-mode particle mass profiles from EARLINET-AERONET observations over central Europe after the eruptions of the Eyjafjallajökull volcano in 2010, J. Geophys. Res.-Atmos., 116, D00U02, https://doi.org/10.1029/2010JD015567, 2011.

Ansmann, A., Seifert, P., Tesche, M., and Wandinger, U.: Profiling of fine and coarse particle mass: case studies of Saharan dust and Eyjafjallajökull/Grimsvötn volcanic plumes, Atmos. Chem. Phys., 12, 9399–9415, https://doi.org/10.5194/acp-12-9399-2012, 2012.

Ansmann, A., Mamouri, R.-E., Hofer, J., Baars, H., Althausen, D., and Abdullaev, S. F.: Dust mass, cloud condensation nuclei, and ice-nucleating particle profiling with polarization lidar: updated POLIPHON conversion factors from global AERONET analysis, Atmos. Meas. Tech., 12, 4849–4865, https://doi.org/10.5194/amt-12-4849-2019, 2019.

Baars, H., Seifert, P., Engelmann, R., and Wandinger, U.: Target categorization of aerosol and clouds by continuous multiwavelength-polarization lidar measurements, Atmos. Meas. Tech., 10, 3175–3201, https://doi.org/10.5194/amt-10-3175-2017, 2017.

Behrendt, A. and Nakamura, T.: Calculation of the calibration constant of polarization lidar and its dependency on atmospheric temperature, Opt. Express, 10, 805–817, https://doi.org/10.1364/OE.10.000805, 2002.

Binietoglou, I.: Synergies of ground-based remote sensing techniques for aerosol mass profiling, PhD thesis, University of Basilicata, 139 pp., 2014.

Binietoglou, I., Basart, S., Alados-Arboledas, L., Amiridis, V., Argyrouli, A., Baars, H., Baldasano, J. M., Balis, D., Belegante, L., Bravo-Aranda, J. A., Burlizzi, P., Carrasco, V., Chaikovsky, A., Comerón, A., D'Amico, G., Filioglou, M., Granados-

Muñoz, M. J., Guerrero-Rascado, J. L., Ilic, L., Kokkalis, P., Maurizzi, A., Mona, L., Monti, F., Muñoz Porcar, C., Nicolae, D., Papayannis, A., Pappalardo, G., Pejanovic, G., Perreira, S., Perrone, M., Pietruczuk, A., Posyniak, M., Rocadenbosch, F., Rodríguez-Gómez, A., Sicard, M., Siomos, N., Szkop, A., Taradellas, E., Tsekeri, A., Vukovic, A., Wandinger, U., and Wagner, J.: A methodology for investigating dust model performance using synergistic EARLINET/AERONET dust concentration retrievals, Atmos. Meas. Tech., 8, 3577–3600, https://doi.org/10.5194/amt-8-3577-2015, 2015.

Bolic, T. and Sivcev, Z.: Eruption of Eyjafjallajökull in Iceland: Experience of European Air Traffic Management, Trans. Res. Record, 2214, 136–143, https://doi.org/10.3141/2214-17, 2011.

Brioude, J., Arnold, D., Stohl, A., Cassiani, M., Morton, D., Seibert, P., Angevine, W., Evan, S., Dingwell, A., Fast, J. D., Easter, R. C., Pisso, I., Burkhart, J., and Wotawa, G.: The Lagrangian particle dispersion model FLEXPART-WRF version 3.1, Geosci. Model Dev., 6, 1889–1904, https://doi.org/10.5194/gmd-6-1889-2013, 2013.

Chaikovsky, A., Dubovik, O., Holben, B., Bril, A., Goloub, P., Tanré, D., Pappalardo, G., Wandinger, U., Chaikovskaya, L., Denisov, S., Grudo, J., Lopatin, A., Karol, Y., Lapyonok, T., Amiridis, V., Ansmann, A., Apituley, A., Alados-Arboledas, L., Binietoglou, I., Boselli, A., D'Amico, G., Freudenthaler, V., Giles, D., Granados-Muñoz, M. J., Kokkalis, P., Nicolae, D., Oshchepkov, S., Papayannis, A., Perrone, M. R., Pietruczuk, A., Rocadenbosch, F., Sicard, M., Slutsker, I., Talianu, C., De Tomasi, F., Tsekeri, A., Wagner, J., and Wang, X.: Lidar-Radiometer Inversion Code (LIRIC) for the retrieval of vertical aerosol properties from combined lidar-radiometer data: development and distribution in EARLINET, Atmos. Meas. Tech., 9, 1181–1205, https://doi.org/10.5194/amt-9-1181-2016, 2016.

Córdoba-Jabonero, C., Sicard, M., Ansmann, A., del Águila, A., and Baars, H.: Separation of the optical and mass features of particle components in different aerosol mixtures by using POLIPHON retrievals in synergy with continuous polarized Micro-Pulse Lidar (P-MPL) measurements, Atmos. Meas. Tech., 11, 4775–4795, https://doi.org/10.5194/amt-11-4775-2018, 2018.

D'Amico, G., Amodeo, A., Baars, H., Binietoglou, I., Freudenthaler, V., Mattis, I., Wandinger, U., and Pappalardo, G.: EARLINET Single Calculus Chain–overview on methodology and strategy, Atmos. Meas. Tech., 8, 4891–4916, https://doi.org/10.5194/amt-8-4891-2015, 2015.

D'Amico, G., Amodeo, A., Mattis, I., Freudenthaler, V., and Pappalardo, G.: EARLINET Single Calculus Chain – technical – Part 1: Pre-processing of raw lidar data, Atmos. Meas. Tech., 9, 491–507, https://doi.org/10.5194/amt-9-491-2016, 2016.

Devenish, B., Thomson, D., Marenco, F., Leadbetter, S., Ricketts, H., and Dacre, H.: A study of the arrival over the United Kingdom in April 2010 of the Eyjafjallajökull ash cloud using ground-based lidar and numerical simulations, Atmos. Environ., 48, 152–164, 2012.

Di Girolamo, P., Ambrico, P. F., Amodeo, A., Boselli, A., Pappalardo, G., and Spinelli, N.: Aerosol observations by lidar in the nocturnal boundary layer, Appl. Opt., 38, 4585–4595, https://doi.org/10.1364/AO.38.004585, 1999.

Eliasson, J., Watson, I. M., and Weber, K.: Volcanic Ash: Hazard Observation, In Situ Observations of Airborne Ash From Manned Aircraft, Elsevier, 89–98, 2016.

Engelmann, R., Kanitz, T., Baars, H., Heese, B., Althausen, D., Skupin, A., Wandinger, U., Komppula, M., Stachlewska, I. S., Amiridis, V., Marinou, E., Mattis, I., Linné, H., and Ansmann, A.: The automated multiwavelength Raman polarization and water-vapor lidar Polly$_{XT}$: the neXT generation, Atmos. Meas. Tech., 9, 1767–1784, https://doi.org/10.5194/amt-9-1767-2016, 2016.

Freudenthaler, V., Esselborn, M., Wiegner, M., Heese, B., Tesche, M., Ansmann, A., Müller, D., Althausen, D., Wirth, M., Fix, A., Ehret, G., Knippertz, P., Toledano, C., Gasteiger, J., Garhammer, M., and Seefeldner, M.: Depolarization ratio profiling at several wavelengths in pure Saharan dust during SAMUM 2006, Tellus B, 61, 165–179, https://doi.org/10.1111/j.1600-0889.2008.00396.x, 2009.

Gasteiger, J., Groß, S., Freudenthaler, V., and Wiegner, M.: Volcanic ash from Iceland over Munich: mass concentration retrieved from ground-based remote sensing measurements, Atmos. Chem. Phys., 11, 2209–2223, https://doi.org/10.5194/acp-11-2209-2011, 2011.

Goudie, A. and Middleton, N. J.: Desert Dust in the Global System, Springer-Verlag Berlin Heidelberg, 287 pp., https://doi.org/10.1007/3-540-32355-4, 2006.

Granados-Muñoz, M. J., Navas-Guzmán, F., Guerrero-Rascado, J. L., Bravo-Aranda, J. A., Binietoglou, I., Pereira, S. N., Basart, S., Baldasano, J. M., Belegante, L., Chaikovsky, A., Comerón, A., D'Amico, G., Dubovik, O., Ilic, L., Kokkalis, P., Muñoz Porcar, C., Nickovic, S., Nicolae, D., Olmo, F. J., Papayannis, A., Pappalardo, G., Rodríguez, A., Schepanski, K., Sicard, M., Vukovic, A., Wandinger, U., Dulac, F., and Alados-Arboledas, L.: Profiling of aerosol microphysical properties at several EARLINET/AERONET sites during the July 2012 ChArMEx/EMEP campaign, Atmos. Chem. Phys., 16, 7043–7066, https://doi.org/10.5194/acp-16-7043-2016, 2016.

Guffanti, M., Schneider, D. J., Wallace, K. L., Hall, T., Bensimon, D. R., and Salinas, L. J.: Aviation response to a widely dispersed volcanic ash and gas cloud from the August 2008 eruption of Kasatochi, Alaska, USA, J. Geophys. Res.-Atmos., 115, D00L19, https://doi.org/10.1029/2010JD013868, 2010.

Haeffelin, M., Laffineur, Q., Bravo-Aranda, J.-A., Drouin, M.-A., Casquero-Vera, J.-A., Dupont, J.-C., and De Backer, H.: Radiation fog formation alerts using attenuated backscatter power from automatic lidars and ceilometers, Atmos. Meas. Tech., 9, 5347–5365, https://doi.org/10.5194/amt-9-5347-2016, 2016.

Hirtl, M., Arnold, D., Baro, R., Brenot, H., Coltelli, M., Eschbacher, K., Hard-Stremayer, H., Lipok, F., Maurer, C., Meinhard, D., Mona, L., Mulder, M. D., Papagiannopoulos, N., Pernsteiner, M., Plu, M., Robertson, L., Rokitansky, C.-H., Scherllin-Pirscher, B., Sievers, K., Sofiev, M., Som de Cerff, W., Steinheimer, M., Stuefer, M., Theys, N., Uppstu, A., Wagenaar, S., Winkler, R., Wotawa, G., Zobl, F., and Zopp, R.: A volcanic-hazard demonstration exercise to assess and mitigate the impacts of volcanic ash clouds on civil and military aviation, Nat. Hazards Earth Syst. Sci., 20, 1719–1739, https://doi.org/10.5194/nhess-20-1719-2020, 2020.

Hughes, E. J., Yorks, J., Krotkov, N. A., da Silva, A. M., and McGill, M.: Using CATS near-real-time lidar observations to monitor and

constrain volcanic sulfur dioxide (SO2) forecasts, Geophys. Res. Lett., 43, 11089–11097, https://doi.org/10.1002/2016GL070119, 2016.

Jones, S. L., Adams-Selin, R., Hunt, E. D., Creighton, G. A., and Cetola, J. D.: Update on modifications to WRF-CHEM GOCART for fine-scale dust forecasting at AFWA, in: AGU Fall Meeting Abstracts, A33D-0188, 2012.

Kaskaoutis, D., Rashki, A., Dumka, U., Mofidi, A., Kambezidis, H., Psiloglou, B., Karagiannis, D., Petrinoli, K., and Gavriil, A.: Atmospheric dynamics associated with exceptionally dusty conditions over the eastern Mediterranean and Greece in March 2018, Atmos. Res., 218, 269–284, https://doi.org/10.1016/j.atmosres.2018.12.009, 2019.

Lopatin, A., Dubovik, O., Chaikovsky, A., Goloub, P., Lapyonok, T., Tanré, D., and Litvinov, P.: Enhancement of aerosol characterization using synergy of lidar and sun-photometer coincident observations: the GARRLiC algorithm, Atmos. Meas. Tech., 6, 2065–2088, https://doi.org/10.5194/amt-6-2065-2013, 2013.

Madonna, F., Rosoldi, M., Lolli, S., Amato, F., Vande Hey, J., Dhillon, R., Zheng, Y., Brettle, M., and Pappalardo, G.: Intercomparison of aerosol measurements performed with multiwavelength Raman lidars, automatic lidars and ceilometers in the framework of INTERACT-II campaign, Atmos. Meas. Tech., 11, 2459–2475, https://doi.org/10.5194/amt-11-2459-2018, 2018.

Mamali, D., Marinou, E., Sciare, J., Pikridas, M., Kokkalis, P., Kottas, M., Binietoglou, I., Tsekeri, A., Keleshis, C., Engelmann, R., Baars, H., Ansmann, A., Amiridis, V., Russchenberg, H., and Biskos, G.: Vertical profiles of aerosol mass concentration derived by unmanned airborne in situ and remote sensing instruments during dust events, Atmos. Meas. Tech., 11, 2897–2910, https://doi.org/10.5194/amt-11-2897-2018, 2018.

Mamouri, R. E. and Ansmann, A.: Fine and coarse dust separation with polarization lidar, Atmos. Meas. Tech., 7, 3717–3735, https://doi.org/10.5194/amt-7-3717-2014, 2014.

Mamouri, R.-E. and Ansmann, A.: Potential of polarization/Raman lidar to separate fine dust, coarse dust, maritime, and anthropogenic aerosol profiles, Atmos. Meas. Tech., 10, 3403–3427, https://doi.org/10.5194/amt-10-3403-2017, 2017.

Marchese, F., Sannazzaro, F., Falconieri, A., Filizzola, C., Pergola, N., and Tramutoli, V.: An Enhanced Satellite–Based Algorithm for Detecting and Tracking Dust Outbreaks by Means of SEVIRI Data, Remote Sens., 9, 537, https://doi.org/10.3390/rs9060537, 2017.

Mattis, I., D'Amico, G., Baars, H., Amodeo, A., Madonna, F., and Iarlori, M.: EARLINET Single Calculus Chain – technical – Part 2: Calculation of optical products, Atmos. Meas. Tech., 9, 3009–3029, https://doi.org/10.5194/amt-9-3009-2016, 2016.

Middleton, N. J.: Desert dust hazards: A global review, Aeolian Res., 24, 53–63, https://doi.org/10.1016/j.aeolia.2016.12.001, 2017.

Mona, L. and Marenco, F.: Volcanic Ash: Hazard Observation, Lidar Observations of Volcanic Particles, Elsevier, 161–173, 2016.

Mona, L., Amodeo, A., D'Amico, G., Giunta, A., Madonna, F., and Pappalardo, G.: Multi-wavelength Raman lidar observations of the Eyjafjallajökull volcanic cloud over Potenza, southern Italy, Atmos. Chem. Phys., 12, 2229–2244, https://doi.org/10.5194/acp-12-2229-2012, 2012.

Mona, L., Papagiannopoulos, N., Basart, S., Baldasano, J., Binietoglou, I., Cornacchia, C., and Pappalardo, G.: EARLINET dust observations vs. BSC-DREAM8b modeled profiles: 12-year-long systematic comparison at Potenza, Italy, Atmos. Chem. Phys., 14, 8781–8793, https://doi.org/10.5194/acp-14-8781-2014, 2014.

Müller, D., Ansmann, A., Mattis, I., Tesche, M., Wandinger, U., Althausen, D., and Pisani, G.: Aerosol-type-dependent lidar ratios observed with Raman lidar, J. Geophys. Res., 112, D16202, https://doi.org/10.1029/2006JD008292, 2007.

Nicolae, D., Vasilescu, J., Talianu, C., Binietoglou, I., Nicolae, V., Andrei, S., and Antonescu, B.: A neural network aerosol-typing algorithm based on lidar data, Atmos. Chem. Phys., 18, 14511–14537, https://doi.org/10.5194/acp-18-14511-2018, 2018.

Nixon, M. and Aguado, A.: Feature Extraction and Image Processing for Computer Vision, Academic Press, 632 pp., 2019.

Ortiz-Amezcua, P., Guerrero-Rascado, J. L., Granados-Muñoz, M. J., Benavent-Oltra, J. A., Böckmann, C., Samaras, S., Stachlewska, I. S., Janicka, Ł., Baars, H., Bohlmann, S., and Alados-Arboledas, L.: Microphysical characterization of long-range transported biomass burning particles from North America at three EARLINET stations, Atmos. Chem. Phys., 17, 5931–5946, https://doi.org/10.5194/acp-17-5931-2017, 2017.

Papagiannopoulos, N., Mona, L., Alados-Arboledas, L., Amiridis, V., Baars, H., Binietoglou, I., Bortoli, D., D'Amico, G., Giunta, A., Guerrero-Rascado, J. L., Schwarz, A., Perreira, S., Spinelli, N., Wandinger, U., Wang, X., and Pappalardo, G.: CALIPSO climatological products: evaluation and suggestions from EARLINET, Atmos. Chem. Phys., 16, 2341–2357, https://doi.org/10.5194/acp-16-2341-2016, 2016.

Papagiannopoulos, N., Mona, L., Amodeo, A., D'Amico, G., Gumà Claramunt, P., Pappalardo, G., Alados-Arboledas, L., Guerrero-Rascado, J. L., Amiridis, V., Kokkalis, P., Apituley, A., Baars, H., Schwarz, A., Wandinger, U., Binietoglou, I., Nicolae, D., Bortoli, D., Comerón, A., Rodríguez-Gómez, A., Sicard, M., Papayannis, A., and Wiegner, M.: An automatic observation-based aerosol typing method for EARLINET, Atmos. Chem. Phys., 18, 15879–15901, https://doi.org/10.5194/acp-18-15879-2018, 2018.

Papayannis, A., Amiridis, V., Mona, L., Tsaknakis, G., Balis, D., Bösenberg, J., Chaikovski, A., De Tomasi, F., Grigorov, I., Mattis, I., Mitev, V., Müller, D., Nickovic, S., Pérez, C., Pietruczuk, A., Pisani, G., Ravetta, F., Rizi, V., Sicard, M., Trickl, T., Wiegner, M., Gerding, M., Mamouri, R. E., D'Amico, G., and Pappalardo, G.: Systematic lidar observations of Saharan dust over Europe in the frame of EARLINET (2000–2002), J. Geophys. Res., 113, D10204, https://doi.org/10.1029/2007JD009028, 2008.

Pappalardo, G., Mona, L., D'Amico, G., Wandinger, U., Adam, M., Amodeo, A., Ansmann, A., Apituley, A., Alados Arboledas, L., Balis, D., Boselli, A., Bravo-Aranda, J. A., Chaikovsky, A., Comerón, A., Cuesta, J., De Tomasi, F., Freudenthaler, V., Gausa, M., Giannakaki, E., Giehl, H., Giunta, A., Grigorov, I., Groß, S., Haeffelin, M., Hiebsch, A., Iarlori, M., Lange, D., Linné, H., Madonna, F., Mattis, I., Mamouri, R. E., McAuliffe, M. A. P., Mitev, V., Molero, F., Navas-Guzmán, F., Nicolae, D., Papayannis, A., Perrone, M. R., Pietras, C., Pietruczuk, A., Pisani, G., Preißler, J., Pujadas, M., Rizi, V., Ruth, A. A., Schmidt, J., Schnell, F., Seifert, P., Serikov, I., Sicard, M., Simeonov, V., Spinelli, N., Stebel, K., Tesche, M., Trickl, T., Wang, X., Wagner, F., Wiegner, M., and Wilson, K. M.: Four-dimensional dis-

tribution of the 2010 Eyjafjallajökull volcanic cloud over Europe observed by EARLINET, Atmos. Chem. Phys., 13, 4429–4450, https://doi.org/10.5194/acp-13-4429-2013, 2013.

Pappalardo, G., Amodeo, A., Apituley, A., Comerón, A., Freudenthaler, V., Linné, H., Ansmann, A., Bösenberg, J., D'Amico, G., Mattis, I., Mona, L., Wandinger, U., Amiridis, V., Alados-Arboledas, L., Nicolae, D., and Wiegner, M.: EARLINET: towards an advanced sustainable European aerosol lidar network, Atmos. Meas. Tech., 7, 2389–2409, https://doi.org/10.5194/amt-7-2389-2014, 2014.

Pisani, G., Boselli, A., Coltelli, M., Leto, G., Pica, G., Scollo, S., Spinelli, N., and Wang, X.: Lidar depolarization measurement of fresh volcanic ash from Mt. Etna, Italy, Atmos. Environ., 62, 34–40, https://doi.org/10.1016/j.atmosenv.2012.08.015, 2012.

Ryder, C. L., Marenco, F., Brooke, J. K., Estelles, V., Cotton, R., Formenti, P., McQuaid, J. B., Price, H. C., Liu, D., Ausset, P., Rosenberg, P. D., Taylor, J. W., Choularton, T., Bower, K., Coe, H., Gallagher, M., Crosier, J., Lloyd, G., Highwood, E. J., and Murray, B. J.: Coarse-mode mineral dust size distributions, composition and optical properties from AER-D aircraft measurements over the tropical eastern Atlantic, Atmos. Chem. Phys., 18, 17225–17257, https://doi.org/10.5194/acp-18-17225-2018, 2018.

Sasano, Y., Browell, E. V., and Ismail, S.: Error caused by using a constant extinction/backscattering ratio in the lidar solution, Appl. Opt., 24, 3929–3932, https://doi.org/10.1364/AO.24.003929, 1985.

Sicard, M., Guerrero-Rascado, J. L., Navas-Guzmán, F., Preißler, J., Molero, F., Tomás, S., Bravo-Aranda, J. A., Comerón, A., Rocadenbosch, F., Wagner, F., Pujadas, M., and Alados-Arboledas, L.: Monitoring of the Eyjafjallajökull volcanic aerosol plume over the Iberian Peninsula by means of four EARLINET lidar stations, Atmos. Chem. Phys., 12, 3115–3130, https://doi.org/10.5194/acp-12-3115-2012, 2012.

Sicard, M., D'Amico, G., Comerón, A., Mona, L., Alados-Arboledas, L., Amodeo, A., Baars, H., Baldasano, J. M., Belegante, L., Binietoglou, I., Bravo-Aranda, J. A., Fernández, A. J., Fréville, P., García-Vizcaíno, D., Giunta, A., Granados-Muñoz, M. J., Guerrero-Rascado, J. L., Hadjimitsis, D., Haefele, A., Hervo, M., Iarlori, M., Kokkalis, P., Lange, D., Mamouri, R. E., Mattis, I., Molero, F., Montoux, N., Muñoz, A., Muñoz Porcar, C., Navas-Guzmán, F., Nicolae, D., Nisantzi, A., Papagiannopoulos, N., Papayannis, A., Pereira, S., Preißler, J., Pujadas, M., Rizi, V., Rocadenbosch, F., Sellegri, K., Simeonov, V., Tsaknakis, G., Wagner, F., and Pappalardo, G.: EARLINET: potential operationality of a research network, Atmos. Meas. Tech., 8, 4587–4613, https://doi.org/10.5194/amt-8-4587-2015, 2015.

Skamarock, W. C., Klemp, J. B., Dudhia, J., Gill, D. O., Barker, D. M., Duda, M. G., Huang, X.-Y., Wang, W., and Powers, J. G.: A Description of the Advanced Research WRF Version 3, Ncar technical note 475, National Center for Atmospheric Research, Boulder, Colorado, USA, 125 pp., 2008.

Solomos, S., Kalivitis, N., Mihalopoulos, N., Amiridis, V., Kouvarakis, G., Gkikas, A., Binietoglou, I., Tsekeri, A., Kazadzis, S., Kottas, M., Pradhan, Y., Proestakis, E., Nastos, P. T., and Marenco, F.: From Tropospheric Folding to Khamsin and Foehn Winds: How Atmospheric Dynamics Advanced a Record-Breaking Dust Episode in Crete, Atmosphere, 9, 240, https://doi.org/10.3390/atmos9070240, 2018.

Stohl, A., Forster, C., Frank, A., Seibert, P., and Wotawa, G.: Technical note: The Lagrangian particle dispersion model FLEXPART version 6.2, Atmos. Chem. Phys., 5, 2461–2474, https://doi.org/10.5194/acp-5-2461-2005, 2005.

Tesche, M., Ansmann, A., Müller, D., Althausen, D., Engelmann, R., Freudenthaler, V., and Groß, S.: Vertically resolved separation of dust and smoke over Cape Verde using multiwavelength Raman and polarization lidars during Saharan Mineral Dust Experiment 2008, J. Geophys. Res.-Atmos., 114, D13202, https://doi.org/10.1029/2009JD011862, 2009.

Tesche, M., Müller, D., Groß, S., Ansmann, A., Althausen, D., Freudenthaler, V., Weinzierl, B., Veira, A., and Petzold, A.: Optical and microphysical properties of smoke over Cape Verde inferred from multiwavelength lidar measurements, Tellus B, 63, 677–694, https://doi.org/10.1111/j.1600-0889.2011.00549.x, 2011.

Tramutoli, V.: Robust AVHRR techniques (RAT) for environmental monitoring: theory and applications, in: Earth Surface Remote Sensing II, edited by: Cecchi, G. and Zilioli, E., Vol. 3496, International Society for Optics and Photonics, SPIE, 101–113, https://doi.org/10.1117/12.332714, 1998.

Tramutoli, V.: Robust Satellite Techniques (RST) for Natural and Environmental Hazards Monitoring and Mitigation: Theory and Applications, in: 2007 International Workshop on the Analysis of Multi-temporal Remote Sensing Images, IEEE, 1–6, https://doi.org/10.1109/MULTITEMP.2007.4293057, 2007.

van der Does, M., Korte, L. F., Munday, C. I., Brummer, G.-J. A., and Stuut, J.-B. W.: Particle size traces modern Saharan dust transport and deposition across the equatorial North Atlantic, Atmos. Chem. Phys., 16, 13697–13710, https://doi.org/10.5194/acp-16-13697-2016, 2016.

Wang, Y., Sartelet, K. N., Bocquet, M., Chazette, P., Sicard, M., D'Amico, G., Léon, J. F., Alados-Arboledas, L., Amodeo, A., Augustin, P., Bach, J., Belegante, L., Binietoglou, I., Bush, X., Comerón, A., Delbarre, H., García-Vízcaino, D., Guerrero-Rascado, J. L., Hervo, M., Iarlori, M., Kokkalis, P., Lange, D., Molero, F., Montoux, N., Muñoz, A., Muñoz, C., Nicolae, D., Papayannis, A., Pappalardo, G., Preissler, J., Rizi, V., Rocadenbosch, F., Sellegri, K., Wagner, F., and Dulac, F.: Assimilation of lidar signals: application to aerosol forecasting in the western Mediterranean basin, Atmos. Chem. Phys., 14, 12031–12053, https://doi.org/10.5194/acp-14-12031-2014, 2014.

Wiegner, M., Gasteiger, J., Groß, S., Schnell, F., Freudenthaler, V., and Forkel, R.: Characterization of the Eyjafjallajökull ash-plume: Potential of lidar remote sensing, Phys. Chem. Earth Pt. A/B/C, 45/46, 79–86, https://doi.org/10.1016/j.pce.2011.01.006, 2012.

Wilson, T. M., Stewart, C., Sword-Daniels, V., Leonard, G. S., Johnston, D. M., Cole, J. W., Wardman, J., Wilson, G., and Barnard, S. T.: Volcanic ash impacts on critical infrastructure, Phys. Chem. Earth Pt. A/B/C, 45/46, 5–23, 2012.

Zerefos, C., Nastos, P., Balis, D., Papayannis, A., Kelepertsis, A., Kannelopoulou, E., Nikolakis, D., Eleftheratos, C., Thomas, W., and Varotsos, C.: A complex study of Etna's volcanic plume from ground-based, in situ and space-borne observations, International J. Remote Sens., 27, 1855–1864, https://doi.org/10.1080/01431160500462154, 2006.

Atmospheric Environment 168 (2017) 46–54

Contents lists available at ScienceDirect

Atmospheric Environment

journal homepage: www.elsevier.com/locate/atmosenv

Rainwater capacities for BTEX scavenging from ambient air

A. Šoštarić [a, *], S. Stanišić Stojić [b], G. Vuković [c], Z. Mijić [c], A. Stojić [c], I. Gržetić [d]

[a] Institute of Public Health Belgrade, Bulevar Despota Stefana 54a, 11000 Belgrade, Serbia
[b] Faculty of Physical Chemistry, University of Belgrade, Studentski Trg 12-16, 11000 Belgrade, Serbia
[c] Institute of Physics Belgrade, University of Belgrade, Pregrevica 118, 11080 Belgrade, Serbia
[d] Faculty of Chemistry, University of Belgrade, Studentski Trg 12-16, 11000 Belgrade, Serbia

HIGHLIGHTS

- Potential of rainwater for BTEX scavenging from ambient air was examined.
- BTEX concentrations in rain samples exceeded the theoretically predicted values.
- BTEX retention could be associated with BTEX aerosol fraction.
- Random forest and instance based algorithms provide reliable enrichment predictions.
- Gas mixing ratios, rainwater characteristics and meteorology affect BTEX distribution.

ARTICLE INFO

Article history:
Received 14 March 2017
Received in revised form
15 August 2017
Accepted 18 August 2017
Available online 23 August 2017

Keywords:
BTEX
Wet deposition
Rain
PTR-MS
Multivariate methods
Unmix

ABSTRACT

The contribution of atmospheric precipitation to volatile organic compound (VOC) removal from the atmosphere remains a matter of scientific debate. The aim of this study was to examine the potential of rainwater for benzene, toluene, ethylbenzene and xylene (BTEX) scavenging from ambient air. To that end, air and rainwater samples were collected simultaneously during several rain events that occurred over two distinct time periods in the summer and autumn of 2015. BTEX concentrations in the gaseous and aqueous phases were determined using proton transfer reaction mass spectrometry. The results reveal that the registered amounts of BTEX in rainwater samples were higher than those predicted by Henry's law. Additional analysis, including physico-chemical characterization and source apportionment, was performed and a possible mechanism underlying the BTEX adsorption to the aqueous phase was considered and discussed herein. Finally, regression multivariate methods (MVA) were successfully applied (with relative errors from 20%) to examine the functional dependency of BTEX enrichment factor on gaseous concentrations, physico-chemical properties of rainwater and meteorological parameters.

1. Introduction

Benzene, toluene, ethylbenzene and the three xylene isomers, frequently referred to as BTEX, constitute a group of aromatic hydrocarbon species of particular environmental interest, commonly associated with the petrochemical industry and incomplete fossil fuel oxidation (Stojić et al., 2015a, 2015b). Besides being important photochemical precursors for tropospheric ozone and secondary organic aerosols (SOA) (Chatani et al., 2015), these hazardous air pollutants cause chronic toxicity even in small concentrations (Stojić et al., 2015c). According to the IARC data, benzene is recognized as a significant public health threat and classified as group I carcinogen, ethylbenzene is a suspected IIB carcinogen, while both toluene and the xylene isomers belong to group III neurotoxins (WHO, 1986, 1993, 1997; Durmusoglu et al., 2010).

In the atmosphere, volatile species are distributed between the gaseous, aqueous and particle phase (Matsumoto et al., 2010). In their biogeochemical cycle, it is believed that the role of atmospheric water is quite prominent, but this issue is still subject to continuous scientific debate (McNeill et al., 2012). The concentrations of BTEX in various forms of atmospheric water depend on various factors including their ambient gas mixing ratios, water solubility and Henry's law constant, frequency and intensity of precipitation events (Balla et al., 2014), gas-water surface interactions (Raja and Valsaraj, 2004), content and concentrations of other species in atmospheric water (Okochi et al., 2005; Sato et al.,

* Corresponding author.
E-mail address: andrej.sostaric@zdravlje.org.rs (A. Šoštarić).

http://dx.doi.org/10.1016/j.atmosenv.2017.08.045
1352-2310/

2006; Allou et al., 2011), as well as the origin of air masses (Mullaugh et al., 2015). Previous studies, which primarily focused on wet deposition of BTEX and their partition between gaseous and aqueous phases, were relatively scarce and provided contradictory conclusions.

In the study aimed at investigating the capacity of rainwater for wet scavenging of BTEX, Okochi et al. (2004) reported that the concentrations of species detected in rain samples were higher than those predicted by Henry's law, and concluded that atmospheric precipitation might play significantly greater role in removing BTEX from ambient air than previously thought. Thereby, the observed supersaturation was assumed to be associated with the presence of surface-active agents in rain droplets, whereas the rainfall intensity appeared to be of negligible importance. Accordingly, our previous study confirmed a significant enrichment of BTEX in the aqueous phase in a dynamic equilibrium system designed to resemble the interactions between the gaseous and water phase during rainfall (Šoštarić et al., 2016). Conversely, recent findings of Mullaugh et al. (2015) indicate that BTEX were not efficiently scavenged from the atmosphere by wet deposition processes. Furthermore, the authors concluded that light-mediated reactions with OH· or nitrogen radicals remain the major atmospheric sink for BTEX. Nonetheless, it should be noted that this research was not based on the ambient air measurements, but it mainly relied on the previously published BTEX data from similar locations.

In order to better understand the fate of volatile species in atmospheric, terrestrial and aquatic systems, the present study examines the contribution of rainwater to wet scavenging of atmospheric BTEX, as well as the mechanisms related to their air-water distribution transfer.

2. Materials and methods

A total of 53 sample pairs of air and rainwater samples were collected simultaneously during several rain events that occurred over two distinct time periods in the summer and autumn season of 2015. The sampling was performed at the Institute of Physics (Belgrade, Serbia; 44°49′ N, 20°28′ E), located in the vicinity of the Danube river, in the suburban residential area, with a number of local fireboxes active during the heating season.

Rainwater sampling was performed using a custom-built precipitation collector with the effective sampling area of 9 m^2. The steep collecting panels (45°) were designed to reduce rainfall retention time and minimize possible BTEX volatilization. Such large sampling area enabled collecting a vast number of samples per each rain event. The panels were thoroughly rinsed with 18 MΩ ultrapure water (ELGA PURELAB maxima system) prior to each sampling campaign, and the rinsing water was collected and analyzed as a field blank control sample. No target compounds were detected in the field blank control samples. The samples were collected and stored directly into brown glass bottles of 1 300 mL. All bottles were washed with detergent, thoroughly rinsed with ultrapure water and dried in an oven for 2 h at 105 °C to remove any trace of contamination. During the sampling, the bottles were filled to the top to avoid headspace, and the sampling duration and sample temperature were recorded. Since sampling equipment enables collection of large volumes of rainwater within a short period, the last sample in each sampling campaign was collected in the bottle of 2600 mL and was split into two standard aliquots. The first aliquot was analyzed immediately, whereas the other one was examined after all other samples to determine whether the BTEX levels changed over time. No difference could be observed in the obtained quantity of double samples (Table S1, Supplementary material).

BTEX concentrations in both gas and water phases were measured using proton transfer reaction mass spectrometer (Standard PTR-quad-MS, Ionicon Analytik, GmbH, Austria), whose detailed description is given elsewhere (Lindinger et al., 1998). Since PTR-quad-MS is not capable of distinguishing isobaric ions, the signal detected at m/z 107 referred to C_8 aromatic hydrocarbons, ethylbenzene, o-, m-, and p-xylene. Signals detected at m/z 79 and m/z 93 referred to benzene and toluene, respectively (Warneke et al., 2003).

The air samples were collected as a side flow from a 1/8-inch teflon tube sampling line through which ambient air was drawn at the flow rate of about 50 L min^{-1} to ensure short residence. The sample inlet was located 6 m above ground level with a sampling angle of 360°. Drift tube parameters included: pressure, ranging from 2.04 to 2.14 mbar; temperature, 60 °C; voltage, 600 V; E/N parameter, 145 Td providing reaction time of 90 μs? The count rate of $H_3O^+H_2O$ was 3–8% of the $9.2 \cdot 10^6$ counts s^{-1} count rate of primary H_3O^+ ions. PTR-MS calibration was performed before and after each sampling campaign using an external standard five-point calibration, ranging from 0 to 26 ppbV, 0–25 ppbV and 0–80 ppbV for B, T and EX, respectively. For this purpose, 2.5 ppmV mixture of BTEX (BTEX in nitrogen, Messer Group GmbH) was diluted with high-purity synthetic air (CH free, Messer Group GmbH) by means of HORIBA ASGU 370-P system.

Determination of BTEX concentrations in rainwater was performed immediately after each sampling campaign. A liter of each unfiltered rainwater sample was transferred to the gas washing bottle (GWB) and purged out with synthetic air at a flow rate of 1L min^{-1}. Rainwater filtration was avoided due to potential adsorption of species on the filter. The GWB output was connected with PTR-MS inlet via T-piece, and further analytical procedure, calibration and data processing were conducted as described in Šoštarić et al. (2016). In brief, PTR-MS signal obtained during exsufflation was subject to baseline fitting. The exsufflation time was determined for each sample as the interval required for equilibrium to be achieved (t_{eq}). The obtained exsufflation time was used for determining the amounts of target compounds retained in the analyzed rainwater samples. The aqueous concentrations of analyzed species were calculated by multiplying the obtained amounts by the conversion factor (3.25; 3.83 and 4.41 for B, T and EX, respectively). The detection limits (DL) in rainwater were determined using HC free air and calculated as 10 nM, 10 nM and 20 nM for B, T and EX, respectively. The remaining portion of each rainwater sample was transferred to a 300-mL bottle and stored at 4 °C until further analysis, which included determination of the major inorganic anions (F^-, Cl^-, SO_4^{2-}, NO_2^- and NO_3^-), dissolved cations (Na^+, NH_4^+, K^+, Ca^{2+} and Mg^{2+}), total organic carbon, electrical conductivity, UV extinction, turbidity and pH, in accordance with the standard methods (US EPA 300.1:1993, EN ISO 14911:1998, ISO 8 245:1999, EN 27888:1993, SMEWW 19th method 5 910 B, US EPA 180.1:1993, EN ISO 10523:2008, respectively). More details of the methods and equipment applied for physico-chemical analysis conducted on rainwater samples are presented in Supplementary material.

In order to determine the extent to which Henry's law constant (K_H) describes BTEX distribution between the gaseous and aqueous phase, distribution coefficients (D_{OBS}) were calculated for each sample pair and each species, as the ratio of the corresponding experimentally derived rainwater concentrations in nM (C_R) and ambient gas phase mixing ratios in ppbV (p_g):

$$D_{OBS} = C_R / p_g \left(M\ atm^{-1}\right) \quad (1)$$

Furthermore, the enrichment factors (EF) were calculated as the

ratio of D_{OBS} and K_H.

Considering the K_H temperature dependence, EF were calculated using temperature corrected K_HT for each rain sample by means of the following equation (Sander, 2015):

$$K_HT = K_H(298.15)exp\left\{\frac{-\Delta H}{R}\left(\frac{1}{298.15}-\frac{1}{T}\right)\right\} \quad (2)$$

where K_H is the Henry's law constant at 298.15 K for pure water, ΔH is the enthalpy change of air-water transfer, T is the rainwater temperature, and R is the universal gas constant (8.314 J K^{-1} mol^{-1}). Furthermore, to assess the representativeness of ground level conditions for the atmospheric conditions during rainfall, K_HT and EF altitude profiles were calculated using the temperature profiles obtained from GDAS1 (Global Data Assimilation System, 2015), by replacing the rainwater temperature value by the temperature at the corresponding altitude.

Meteorological parameters during rain events (precipitation (accumulated rainfall, rain current and peak intensity, and the duration of a rain event), wind speed and direction, pressure, humidity and temperature) were measured by Vaisala Weather Transmitter WXT530 Series. Cloud information, including cloud height and type, was obtained from the airport "Nikola Tesla", Belgrade, ICAO code LYBE, located 8.9 km SSW from the sampling site.

The relationships between enrichment factors (EF), physicochemical characteristics and wind characteristics (wind speed and direction) were examined using the bivariate polar plot analyses (Carslaw and Beevers, 2013) implemented in the Openair package (Carslaw and Ropkins, 2012) within the statistical software environment R (Team, 2012).

The neutralization factors (NF) were calculated based on the study of Moreda-Piñeiro et al. (2014), Tiwari et al. (2016) and references therein in order to examine the potential of the cations to balance the rainwater acidic components:

$$[NF_{Ca^{2+}}] = \frac{[nssCa^{2+}]}{NO_3^- + \left[nssSO_4^{2-}\right]} \quad (3)$$

$$\left[NF_{Mg^{2+}}\right] = \frac{[nssMg^{2+}]}{NO_3^- + \left[nssSO_4^{2-}\right]} \quad (4)$$

$$\left[NF_{NH_4^+}\right] = \frac{\left[NH_4^+\right]}{NO_3^- + \left[nssSO_4^{2-}\right]} \quad (5)$$

$$[NF_{K^+}] = \frac{[nssK^+]}{NO_3^- + \left[nssSO_4^{2-}\right]} \quad (6)$$

To calculate the non-sea salt fraction of any particular ion (*nss*), we assumed that all Na originated from marine sources, and used it as a referent element. The nss contribution is given as:

$$[nss-X]_i = [X_i] - \left[Na^+\right]_i \left[\frac{[X]}{Na^+}\right]_{sea\ salt} \quad (7)$$

where [nss - X]$_i$ is the nss concentration of the selected ion in the sample *i*, [X_i] is the total concentration of the ion X measured in the rainwater sample *i*, [Na^+] is the total concentration of Na^+ measured in the rainwater sample, and [[X][Na^+]$^{-1}$]$_{seasalt}$ is the reference ratio determined in the seawater.

Potential remote source regions that might affect the observed BTEX mixing ratios were identified using HYSPLIT-derived 72-h back trajectories (Draxler and Rolph, 2014). The trajectories were computed for each hour UTC a day before and during each rain event, above the sampling location at the half of the planetary boundary layer height calculated from GDAS1 using MeteoInfo (Wang, 2014), as described in Stojić et al. (2016) and Stojić and Stanišić Stojić (2017).

Rainwater source apportionment was performed using Unmix (USEPA, 2007). The maximum number of species selected as input variables was chosen using the trial and error with the overall aim of yielding the most physically meaningful results. For concentrations below the DL, a value equal to the half of the DL was used.

Guided regularized random forest (GRRF) was applied (Deng and Runger, 2013) for the selection of features that are most relevant for EF. Random forest (RF) consists of a number of decision trees which every node represents a condition on a single variable designed to split the dataset in two parts so that similar response values end up in the same set. Variable importance measures how much each variable decreases the weighted impurity across all tress, a measure based on which the optimal condition is chosen. GRFF uses the importance scores from a preliminary RF to guide the feature selection of regularized random forest (RRF), and has several advantages as follows: it is more robust and computationally efficient than RRF, varSelRF and LASSO logistic regression; it can select compact feature subsets moderating the curse of dimensionality; it avoids the effort to analyze irrelevant or redundant features; and it has competitive accuracy performance. Variable importance presented herein was obtained by calculating the average value of 2000 GRRF runs. The appropriate number of trees was determined to assure out-of-bag error convergence. Method performance was tested by 100 times replicated 10-fold cross validation.

To analyze the relationship between EF and features that are considered most relevant for EF prediction, the following 24 regression MVA methods implemented in Weka 3.8 (Hall et al., 2009) were applied: Alternating Model Tree, Conjunctive Rule, Decision Stump, Decision Table, Elastic Net, Gaussian Processes, IBk, IBkLG, Isotonic Regression, K*, Least Median Squared, Linear Regression, Locally Weighted Learning, M5P, M5 Rules, Multilayer Perceptron, Pace Regression, Random Forest, Random Tree, Radial Base Function (RBF) Network, RBF Regressor, REP Tree, Simple Linear Regression and SMOreg Support Vector Machine. A brief description of the methods, including functions (neural network, support vector machine, etc.), clustering techniques, rules and trees, is provided in Supplementary material. Method performance was tested by 10 times replicated 10-fold cross-validation.

3. Results and discussion

Light showers, with occasional thunderstorms, constituted a considerable part of summer rain events. Scattered and broken clouds in the form of cumulonimbus or towering cumulus were observed at the height of 400–1 000 m. In the autumn campaign, the vast majority of rain events were light and sporadically followed by mist. Scattered clouds were registered at levels below 300 m, whereas broken clouds were observed from 100 to 900 m.

As expected, both aqueous and gaseous BTEX concentrations were higher during the cold part of the year. Lower BTEX concentrations in summer can be attributed to intense photochemical removal and washout effects associated with more sunny and rainy days (Lee et al., 2002), whereas higher concentrations of BTEX in autumn can be associated with individual combustion fireboxes widely spread in the vicinity of the sampling site. Furthermore, aqueous B concentrations in summer were below DL.

As can be seen in Fig. 1, each rain event was associated with air

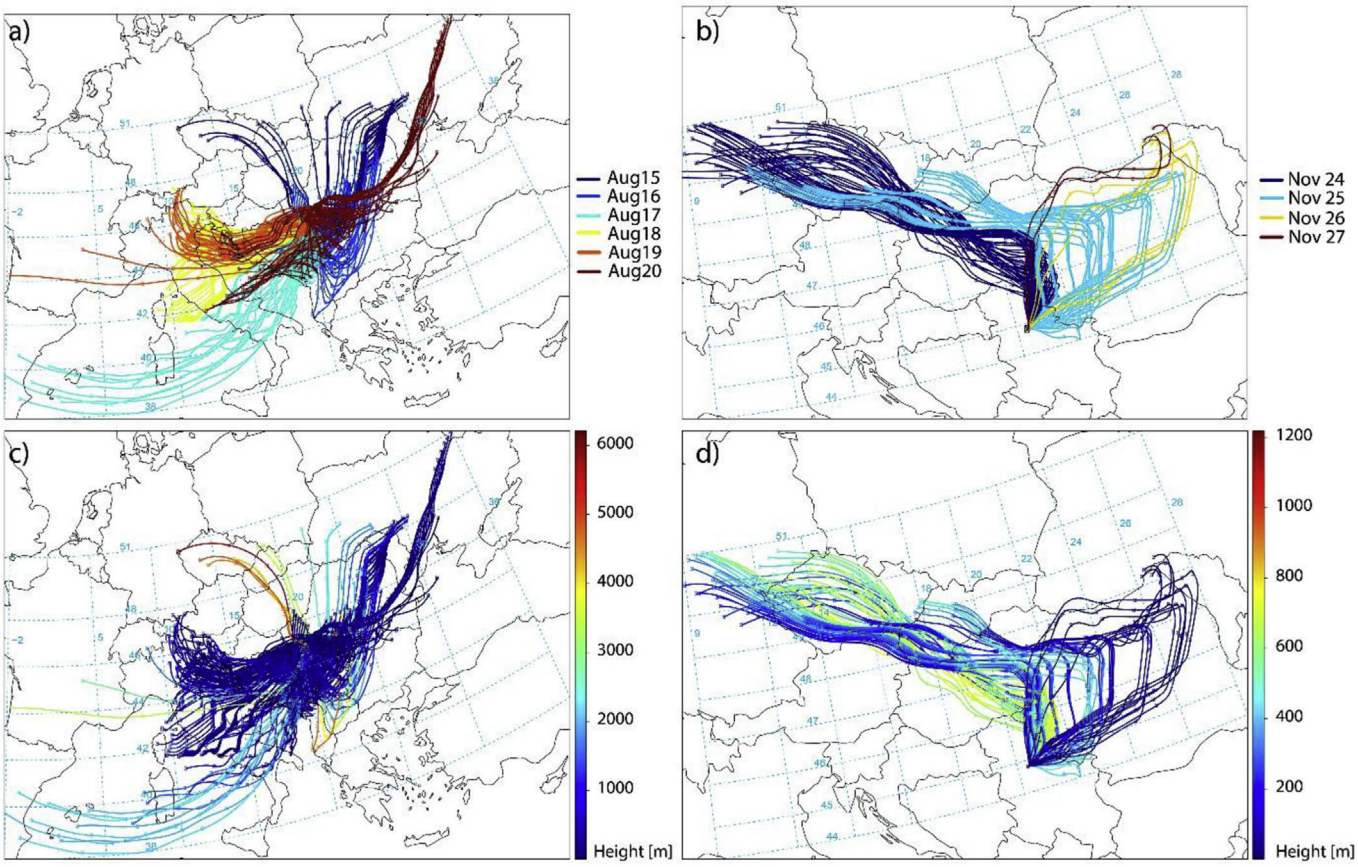

Fig. 1. Back trajectories a day before (August 15 and November 24) and during summer (a) and autumn (b) rain events and corresponding trajectory heights (c, d).

masses coming from different source regions and heights. During summer rain events, air flows from all directions were followed by significant variations in physico-chemical properties of rainwater, whereas N and NE air masses in autumn were associated with a more uniform rainwater composition. Gaseous concentrations of volatile species, particularly B, were relatively stable during rain events, which can be explained by the fact that the sampling site was dominated by local BTEX sources.

3.1. Physico-chemical characteristics of rainwater

Basic statistics for all rainwater parameters and BTEX concentrations is given in Table S2, Supplementary material. The average rainwater pH was 6.01, while the turbidity was below 10 NTU, indicating that the samples contained moderate amounts of suspended particles from the atmosphere. As illustrated in Fig. S1, conductivity, as well as high concentrations of most ions (SO_4^{2-}, NO_3^-, Ca^{2+}, Mg^{2+}, K^+ and Na^+) were influenced by the high-speed SW wind (20–30 m s^{-1}), while only NH_4^+ concentrations were increased with the wind of moderate speed (10 m s^{-1}) from NE direction.

The rainwater pH varied from 3.70 to 8.20 with the volume weighted mean of 6.01, which is mainly due to scavenging of alkaline species (Ca^{2+} and SO_4^{2-}). The average pH value is also close to the 5-year-mean (6.1) obtained as a part of the regular air quality monitoring in Belgrade. The contribution of SO_4^{2-} to the rainwater acidity was confirmed by ($Cl^- + NO_3^-$) and (SO_4^{2-}) ratio below 1 (Tiwari et al., 2016). As shown, Ca^{2+} was the dominant neutralization component, followed by NH_4^+, Mg^{2+} and K^+, with mean of 77%, 14%, 7% and 2.3%, respectively.

As shown in Fig. S2, significant correlations were observed as follows: > 0.80 (NO_3^- – SO_4^{2-}, NH_4^+ – aq. B, NH_4^+ – gas. B, NH_4^+ – EF_B); 0.70–0.80 (F^- – SO_4^{2-}, F^- – NO_3^-, F^- – aq. B, F^- – gas. B, F^- – EF_B, K^+ – Na^+); and 0.60–0.70 (NO_3^- – Mg^{2+}, SO_4^{2-} – Mg^{2+}, SO_4^{2-} – EF_{EX}, Na^+ – Mg^{2+}). Furthermore, high correlations were noted between aq. And gas. BTEX concentrations (≥0.80), as well as between aq. EX and aq. B (0.67) and aq. T (0.67), suggesting that these species might share the common source.

As can be seen in Tables S3, S4 and S5, four factors were derived using Unmix. With high contributions of volatile BTEX species (99%, 44.5% and 52.2%) and a relatively high share of UV extinction (33.3%), the first factor was recognized as organic compounds in the gaseous form. The second factor, characterized by the highest contribution of TOC (71.6%) and turbidity (79.7%), represented the solid fraction dissolved in the atmospheric water. Significant shares of K^+ (58.0%), SO_4^{2-} (42.2%) and NO_3^- (31.3%) were also apportioned to this factor, as a result of fossil fuel burning and traffic exhaust (Rao et al., 2016; Tiwari et al., 2016). The high shares of crustal-related elements, Na^+ (61.8%) and Mg^{2+} (61.4%), were apportioned to the third factor (Cao et al., 2008; Sapek, 2014). Moderate to significant shares (>30%) of all species except Na^+, K^+ and B were apportioned to the fourth factor, being recognized as the aerosol fraction. Apart from gaseous oxides (SO_2 and NO_2), which react with ozone and OH· radicals in the presence of Ca^{2+} and Mg^{2+} (Seinfeld and Pandis, 2006), BTEX are susceptible to photo-oxidation that can also lead to SOA formation. BTEX reactions include oxidation with ozone and OH·, but also with NO_x and SO_2, which results in multi-functional oxy products that are further deposited onto the existing aerosol or initiate the formation of SOA by self-nucleation. BTEX behave differently in the atmosphere due

to differences in the methyl chain substituent and the alkyl chain length. Benzene is considered being extremely stable compared to T and EX (Słomińska et al., 2014), and it is less susceptible to the heterogeneous reactions and formation of SOA in the atmosphere.

The contributions of the gaseous organic- and aerosol-related factors were mostly associated with N wind of moderate speed (<10 m s^{-1}), which clearly reflects their local origin, while the solid- and crustal-related factors were associated with the air masses from SW direction and high wind speed (20–30 m s^{-1}) (Fig. S3). The contribution of the factor assigned to aerosols declined during rain events due to wet deposition, while similar behavior was not observed for other factors.

TEX air mixing ratios and rain concentrations decreased during the first 2 h of the rainfall, but tend to rise afterwards probably as a result of rainfall intensity decrease (Fig. S4, Supplementary material). The highest TEX enrichment, caused by air mixing ratio decrease, was detected during the second hour. Typical washout effect was observed for source contributions related to the rainwater aerosol and solid components, and was less pronounced for crustal factor. Unlike TEX, only a slight decrease in benzene air mixing ratios was noticeable, which is reflected in a constant EF_B increase.

3.2. BTEX distribution between gaseous and aqueous phases

The exsufflation time required for the equilibrium to be achieved was different for rainwater samples and ultrapure water, which suggests that physico-chemical properties and BTEX content distributed between different phases have certain impact on the adsorption to the aqueous phase (Fig. 2, left). However, the correlations were registered only between the concentrations of B, and F^- (−0.72) and NH_4^+ (0.83) (Fig. S2, Supplementary material). The impact of rainwater physico-chemical properties on the BTEX retention was further examined by insufflating 2 ppbV of BTEX in 10 pre-exsufflated rainwater samples, as described in our previous paper (Šoštarić et al., 2016). The results showed slightly longer exsufflation periods for rainwater samples compared to the pure water, indicating that physico-chemical properties are not the main contributor to the extended retention in the rainwater. The comparative qualitative analysis of rainwater and ultrapure water exsufflation time series obtained by real-time PTR-MS measurements showed that different capacities for BTEX retention can be mainly associated with BTEX aerosol fraction (Fig. 2, right).

Generally, due to very small K_H values of aromatic compounds, BTEX concentrations in rainwater are expected to be low (Słomińska et al., 2014). However, according to the results, EF values were in the range from 61 to 128, from 8 to 209, and from 25 to 295 for B, T and EX, respectively, indicating that the BTEX amounts in the aqueous phase significantly exceeded the theoretically predicted levels. Both lower and higher EF values have been reported in the literature. According to the studies dealing with the distribution of chlorinated hydrocarbons and monocyclic aromatic hydrocarbons between air and rainwater, EF ranged from 2.4 to 34 for BTEX (Okochi et al., 2004; Sato et al., 2006), whereas the study of Valsaraj et al. (1993) reported several hundred to a thousand-fold enrichment of hydrophobic organic compounds in fog samples. The enhanced BTEX transfer to urban dew water was also shown by Okochi et al. (2005), with the reported EF values ranging from 7.87 to 20.2. Furthermore, Fries et al. (2007) showed that the concentrations of aromatic hydrocarbons including ethylbenzene, xylenes and 1,2,4-trimethylbenzene, have been significantly lower in rain (15–53 ng L^{-1}) than in snow (71–2 200 ng L^{-1}). In the later study,

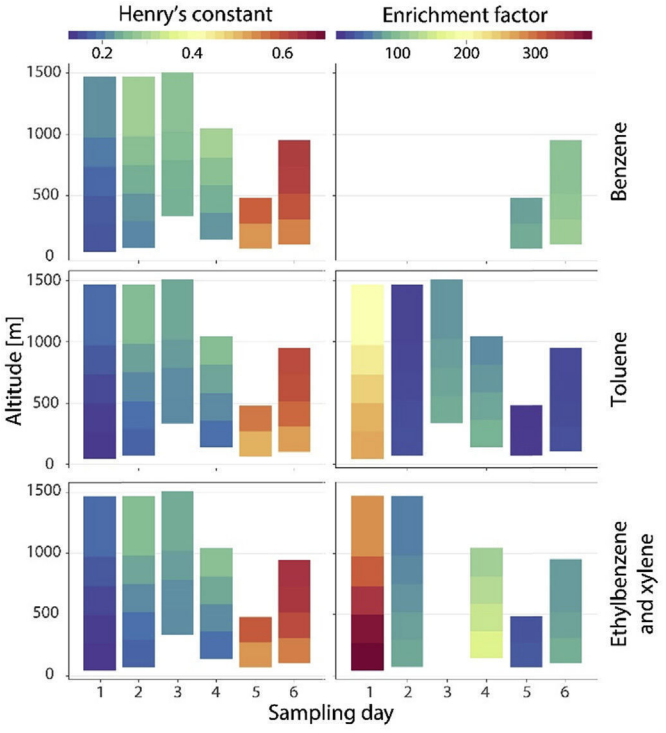

Fig. 3. Henry's constant and EF BTEX altitude distributions.

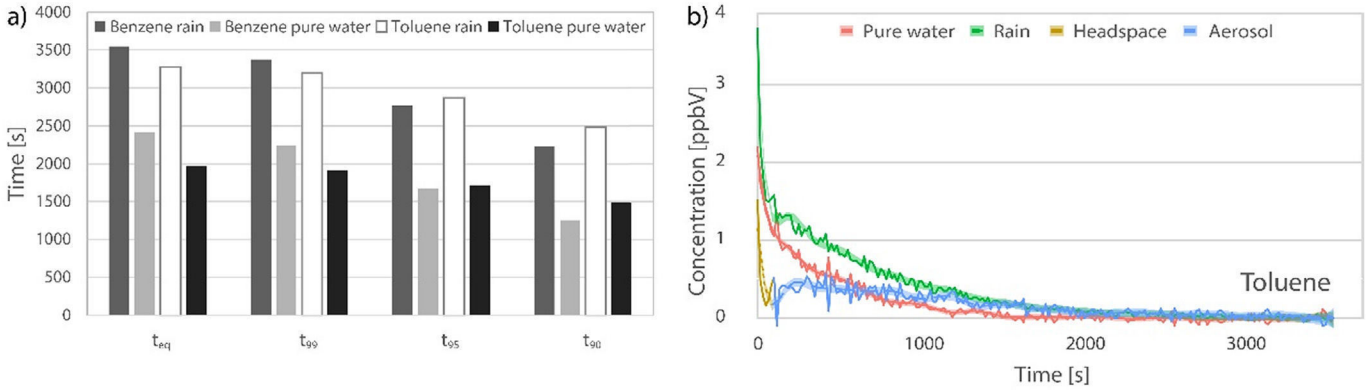

Fig. 2. The time required to reach equilibrium (t_{eq}) and 99, 95 and 90% quantity of benzene and toluene to be exsufflated (left), and toluene exsufflation from ultra-pure water and rainwater (right).

Fries et al. (2008) found that in-cloud scavenging could be a possible explanation for the occurrence of VOC in fallen snow.

Fig. 3 illustrates the K_H and EF altitude distribution for BTEX. It should be mentioned that K_H and EF for B and EX exhibit the similar pattern. As can be seen, K_H and consequently EF, change as the raindrop falls to the ground. K_H values calculated using the average temperature on the path of the raindrop differ ±20% from those obtained using the rainwater temperature. Such agreement indicates that the rainwater temperature measured at the ground level is a good indicator of atmospheric conditions under which reactions with BTEX takes place. Moreover, in the study of Lin et al. (2011), it was concluded that, at higher altitudes in locations with dominant local sources, VOC concentrations were generally lower, and hence, higher K_H values would not be expected to affect C_R, nor calculated values of D_{OBS} and EF.

As suggested by the field studies (Valsaraj et al., 1993; Goss, 1994; Okochi et al., 2004; Starokozhev et al., 2009), as well as the laboratory experiments (Bruant and Conklin, 2000, 2002; Raja et al., 2002; Raja and Valsaraj, 2004; Šoštarić et al., 2016), the interfacial adsorption might be the major mechanism associated with the enhanced VOC transfer to the aqueous phase.

Some previous studies have examined the composition of atmospheric water and the impact of different species, including nitric acid, anionic and nonionic surfactants, as well as the impact of salinity and pH on air-water VOC distribution (O'Sullivan et al., 1996; Vane and Giroux, 2000; Sato et al., 2006; Allou et al., 2011). The supersaturation of VOC in rain samples was explained by decreased rainwater polarity associated with the presence of different organic compounds (Sato et al., 2006). The presence of colloidal organic matter with its large binding capacity for many hydrophobic species was found in fog droplets (Valsaraj et al., 1993). Similarly, in the study of Okochi et al. (2005), the enhanced dissolution of VOC species in urban dew compared to rainwater was explained by the fact that dew forms near the ground and contain more humic-like substances that could lead to a decrease in water surface tension and consequently result in higher VOC enrichment.

The present study considers several factors that could contribute to BTEX enrichment in rainwater, including BTEX concentrations, rainwater physico-chemical properties, rainfall intensity, air masses origin, meteorological conditions and adsorption at the air/water interface.

As regards the physico-chemical characteristics of rainwater, only F^- and SO_4^{2-} can be considered important for the prediction of EF_B (−0.73) and EF_{EX} (0.62), respectively. The latter indicates that SO_2-rich coal burning emissions are also a significant source of EX, while the results for B should be taken with caution due to the small data size.

Higher rainwater T enrichment was mostly observed for low gaseous T concentrations, high TOC (8–12 mg L^{-1}) and turbidity (Supplementary file 1), although the strict link between rainwater enrichment and gaseous concentrations cannot be established. The exsufflation dynamics (Fig. 2) and the EF values suggest that prolonged BTEX retention could also be attributed to the adsorption to aerosol fraction. We have considered T partitioning, not only because T concentrations were in a relatively broad range, but also because of the significant number of samples collected in both seasons with comparable concentrations, despite the fact that similar findings were observed for the rainwater enrichment with EX (Supplementary file 2). As can be observed in Fig. 4 and Table S6 of the Supplementary material, higher T enrichment was mostly associated with a higher wind speed at the sampling site (up to 30 m s^{-1}) and air masses coming from SW area, whereas the lowest rainwater enrichment was registered under relatively stable atmospheric conditions (ws < 5 m s^{-1}). Similar associations were also observed for EX. Higher rainwater enrichment could be the result of the prolonged contact time between the aqueous and the gaseous phases, when strong wind-driven raindrops were falling obliquely.

According to GRRF results (Table S7, Supplementary material), physico-chemical rainwater properties and gaseous T concentrations appear to be of greater importance than meteorological factors for predicting T and EX rainwater enrichment. Furthermore, these findings also indicate that ground level gaseous concentrations have higher impact on the transfer of species to the aqueous phase than the polluted air masses coming from greater atmospheric heights.

Out of 24 examined MVA regression methods, some of which were previously successfully applied for prediction of PM_{10} and VOC emissions (Stojić et al., 2015d; Perišić et al., 2017), it has been shown that RF, IBk and IBkLG can provide predictions of EF_T and EF_{EX} based on the variables of the highest importance derived by GRRF with relative errors of approx. 20%, *i.e.* 27%, and correlation coefficients around 0.95 and 0.87, respectively (Table 1). Conversely, the prediction of EF_T and EF_{EX} based on Unmix derived source contributions was less accurate (K*: 36.3% relative error and correlation coefficient 0.79). As can be concluded, functional description of EF_T and EF_{EX} can be based on certain rainwater properties and gaseous T concentrations. In addition to ambient and rainwater B concentrations, EF_B is affected by meteorological conditions (sample and ambient temperature and Rh), but these results should be taken with caution due to the small B data size.

Fig. 5 represents EF for T and EX as a function of their ambient gas phase mixing ratios. As can be seen, EF values increased in summer, due to ambient air temperature, which is one of the most important factors for the decrease of the surface tension leading to enhanced interfacial adsorption (Bruant and Conklin, 2000, 2002). Another important feature of Fig. 5 is the power functional dependence of EF on ambient gas phase mixing ratios, as adsorption processes are generally more efficient for lower adsorbate concentrations and are characterized by the power functions. These findings are in compliance with the findings of Sato et al. (2006) who showed that rainwater enrichment is especially significant for the species with lower atmospheric concentrations.

4. Conclusions

The transfer of BTEX and other VOC from the atmosphere to various forms of atmospheric water is an important process that affects the global transport of air pollutants, environmental fate and enables the transfer of these species to terrestrial and aquatic systems. The purpose of this study was to investigate the scavenging potential of rainwater and consider the potential mechanisms and factors associated with this phenomenon.

As shown, BTEX concentrations observed in the aqueous phase exceeded the theoretically predicted values. Given that the interfacial adsorption is assumed to be the major mechanism underlying the enhanced rain scavenging of BTEX, the removal process was observed to be more efficient for lower gas mixing ratios, mainly due to equal surface available for smaller number of molecules and the prolonged contact time between the two phases when wind-driven rain drops were falling obliquely. Accordingly, theoretical predictions are probably more accurate in the area of larger gaseous concentrations, whereas in the case of lower concentrations, transfer to the aqueous phase is often underestimated. Furthermore, the results of the presented regression multivariate analysis suggest that multiple factors determine the spatio-temporal BTEX distribution in the environmental multiphase system, including ambient mixing ratios, physico-chemical properties of rainwater and meteorological data. More specifically, the functional description of EF_T and EF_{EX} can be based on certain rainwater properties.

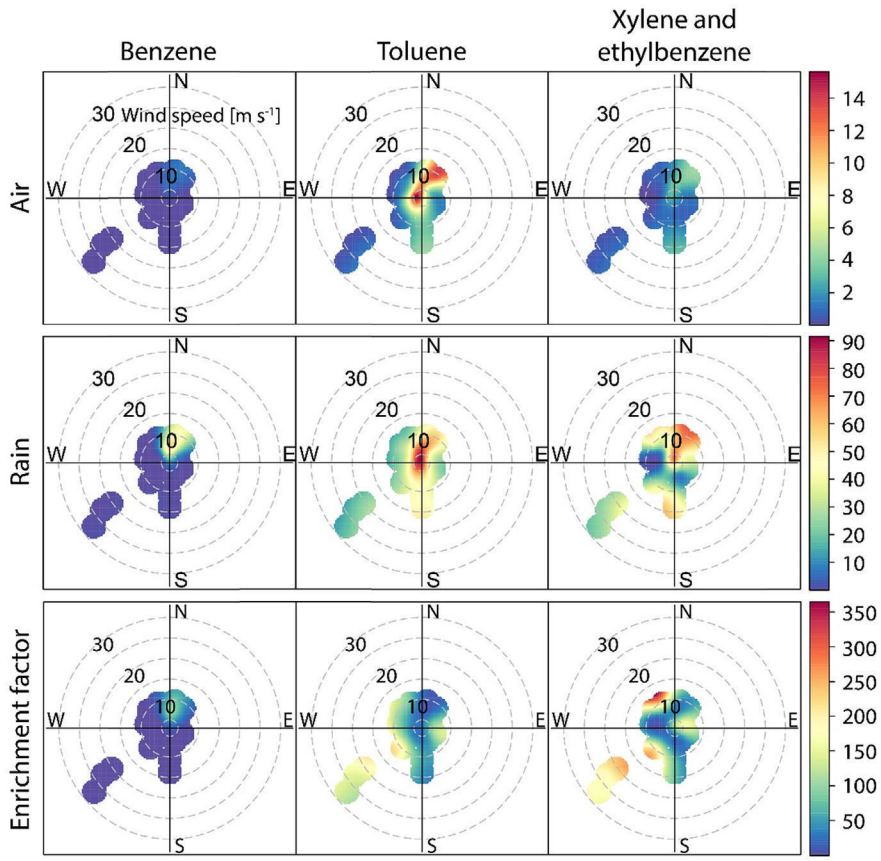

Fig. 4. The relationship between BTEX air mixing ratios (ppb), rain concentrations (nM) and enrichment factor and wind characteristics.

Table 1
MVA method performance comparison for enrichment factor prediction based on the measured parameters and Unmix-derived source contributions: absolute error, relative error and correlation coefficient (r).

Method	EF_T						EF_{EX}					
	Measured parameters			Unmix derived source contributions			Measured parameters			Unmix derived source contributions		
	Abs. error	Rel. error	r	Abs. error	Rel. error	r	Abs. error	Rel. error	r	Abs. error	Rel. error	r
Alternating Model Tree	18.5	34.8	0.88	40.8	76.4	0.67	33.8	42.0	0.78	59.2	111.0	0.53
Conjunctive Rule	26.1	48.9	0.64	32.0	59.9	0.40	39.2	48.7	0.55	43.4	81.2	0.41
Decision Stump	25.5	47.8	0.57	29.3	54.9	0.46	36.4	45.2	0.57	39.4	73.8	0.45
Decision Table	17.8	33.3	0.85	25.3	47.4	0.68	33.9	42.1	0.71	44.8	83.9	0.46
Elastic Net	15.2	28.5	0.88	22.3	41.9	0.77	29.4	36.5	0.74	38.6	72.4	0.62
Gaussian Processes	16.1	30.2	0.88	21.9	41.0	0.79	30.6	38.0	0.72	41.0	76.8	0.60
IBk	11.6	21.7	0.95	20.6	38.5	0.79	22.4	27.8	0.89	31.9	59.8	0.68
IBkLG	11.6	21.7	0.95	20.6	38.5	0.79	22.4	27.8	0.89	31.9	59.8	0.68
Isotonic Regression	13.7	25.7	0.93	31.4	58.9	0.54	34.9	43.3	0.62	39.5	74.0	0.58
K*	11.9	22.3	0.92	19.4	36.3	0.79	22.0	27.4	0.87	31.0	58.1	0.68
Least MedSq	17.4	32.7	0.87	35.6	66.8	0.67	52.7	65.4	0.29	47.4	88.8	0.50
Linear Regression	15.5	29.1	0.89	22.7	42.5	0.78	30.8	38.2	0.74	39.0	73.2	0.61
LWL	15.9	29.7	0.91	26.7	50.0	0.72	35.5	44.1	0.70	39.4	73.9	0.53
M5P	13.9	26.1	0.91	21.6	40.5	0.78	29.7	36.9	0.74	40.4	75.7	0.60
M5Rules	15.0	28.1	0.90	22.9	42.9	0.74	30.8	38.3	0.74	42.2	79.1	0.59
Multilayer Perceptron	17.7	33.1	0.92	24.2	45.4	0.80	37.5	46.5	0.74	49.5	92.7	0.55
Pace Regression	15.9	29.8	0.88	22.7	42.6	0.77	30.1	37.4	0.74	38.6	72.4	0.62
Random Forest	11.6	21.7	0.95	22.5	42.2	0.76	27.8	34.5	0.76	34.9	65.4	0.62
Random Tree	13.8	25.9	0.89	28.6	53.7	0.59	32.8	40.8	0.67	41.7	78.1	0.54
RBF Network	29.9	56.0	0.45	30.4	57.0	0.65	44.8	55.7	0.49	52.8	98.9	0.40
RBF Regressor	14.7	27.6	0.91	23.6	44.2	0.78	28.1	34.9	0.83	40.9	76.6	0.56
REP Tree	13.9	26.1	0.91	22.5	42.1	0.72	36.9	45.8	0.58	42.0	78.8	0.43
Simple Linear Regression	29.9	56.1	0.49	30.3	56.7	0.55	34.3	42.7	0.71	40.5	75.8	0.61
SMOreg	14.7	27.5	0.88	21.5	40.3	0.79	28.8	35.8	0.75	39.0	73.2	0.61

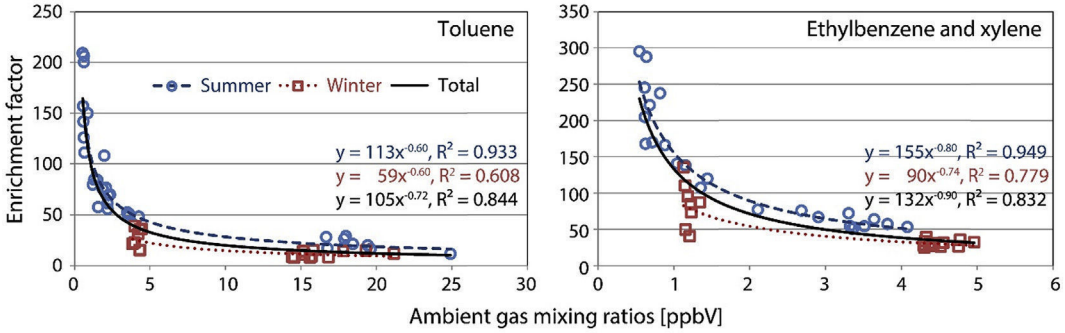

Fig. 5. The relationship between T and EX enrichment factors and their gaseous concentrations.

On the other hand, it has been shown that EF_B is affected by meteorological conditions (sample and ambient temperature, and Rh), as well as B ambient and rainwater concentrations (however, these results should be interpreted with caution due to the small B data size).

Acknowledgments

This paper was realized as part of projects No III43007 and No III41011, which were financed by the Ministry of Education, Science and Technological Development of the Republic of Serbia for the period 2011–17, and was supported by the Institute of Public Health of Belgrade, Serbia.

Appendix A. Supplementary data

Supplementary data related to this article can be found at http://dx.doi.org/10.1016/j.atmosenv.2017.08.045.

References

Allou, L., El Maimouni, L., Le Calve, S., 2011. Henry's law constant measurements for formaldehyde and benzaldehyde as a function of temperature and water composition. Atmos. Environ. 45, 2991–2998.
Balla, D., Papageorgiou, A., Voutsa, D., 2014. Carbonyl compounds and dissolved organic carbon in rainwater of an urban atmosphere. Environ. Sci. Pollut. Res. 21, 12062–12073.
Bruant Jr., R.G., Conklin, M.H., 2000. Dynamic determination of vapor/water interface adsorption for volatile hydrophobic organic compounds (VHOCs) using axisymmetric drop shape analysis: procedure and analysis of benzene adsorption. J. Phys. Chem. B 104, 11146–11152.
Bruant Jr., R.G., Conklin, M.H., 2002. Adsorption of benzene and methyl-substituted benzenes at the vapor/water interface. 3. finite binary-component VHOC adsorption. J. Phys. Chem. B 106, 2232–2239.
Cao, J.J., Chow, J.C., Watson, J.G., Wu, F., Han, Y.M., Jin, Z.D., An, Z.S., 2008. Size-differentiated source profiles for fugitive dust in the Chinese Loess Plateau. Atmos. Environ. 42, 2261–2275.
Carslaw, D.C., Beevers, S.D., 2013. Characterising and understanding emission sources using bivariate polar plots and k-means clustering. Environ. Model. Softw. 40, 325–329.
Carslaw, D.C., Ropkins, K., 2012. Openair - an R package for air quality data analysis. Environ. Model. Softw. 27, 52–61.
Chatani, S., Matsunaga, S.N., Nakatsuka, S., 2015. Estimate of biogenic VOC emissions in Japan and their effects on photochemical formation of ambient ozone and secondary organic aerosol. Atmos. Environ. 120, 38–50.
Deng, H., Runger, G., 2013. Gene selection with guided regularized random forest. Pattern Recognit. 46, 3483–3489.
Draxler, R.R., Rolph, G.D., 2014. HYSPLIT (HYbrid Single-particle Lagrangian Integrated).
Durmusoglu, E., Taspinar, F., Karademir, A., 2010. Health risk assessment of BTEX emissions in the landfill environment. J. Hazard. Mater 176, 870–877.
Fries, E., Starokozhev, E., Haunold, W., Jaeschke, W., Mitra, S.K., Borrmann, S., Schmidt, M.U., 2007. Laboratory studies on the uptake of aromatic hydrocarbons by ice crystals during vapor depositional crystal growth. Atmos. Environ. 41, 6156–6166.
Fries, E., Sieg, K., Püttmann, W., Jaeschke, W., Winterhalter, R., Williams, J., Moortgat, G.K., 2008. Benzene, alkylated benzenes, chlorinated hydrocarbons and monoterpenes in snow/ice at Jungfraujoch (46.6 N, 8.0 E) during CLACE 4 and 5. Sci. Total Environ. 391, 269–277.
Global Data Assimilation System, 2015. https://www.ready.noaa.gov/gdas1.php. (Accessed 27 December 2015).
Goss, K.U., 1994. Predicting the enrichment of organic compounds in fog caused by adsorption on the water surface. Atmos. Environ. 28, 3513–3517.
Hall, M., Frank, E., Holmes, G., Pfahringer, B., Reutemann, P., Witten, I.H., 2009. The WEKA data mining software: an update. SIGKDD Explor 11, 10–18.
Lee, S.C., Chiu, M.Y., Ho, K.F., Zou, S.C., Wang, X., 2002. Volatile organic compounds (VOCs) in urban atmosphere of Hong Kong. Chemosphere 48, 375–382.
Lin, C.C., Lin, C., Hsieh, L.T., Chen, C.Y., Wang, J.P., 2011. Vertical and diurnal characterization of volatile organic compounds in ambient air in urban areas. J. Air Waste. Manag. Assoc. 61, 714–720.
Lindinger, W., Hansel, A., Jordan, A., 1998. On-line monitoring of volatile organic compounds at pptv levels by means of Proton-Transfer-Reaction Mass Spectrometry (PTR-MS). Medical applications, food control and environmental research. Int. J. Mass Spectrom. Ion. Process 173, 191–241.
Matsumoto, K., Matsumoto, K., Mizuno, R., Igawa, M., 2010. Volatile organic compounds in ambient aerosols. Atmos. Res. 97, 124–128.
McNeill, V.F., Grannas, A.M., Abbatt, J.P., Ammann, M., Ariya, P., Bartels-Rausch, T., Domine, F., Donaldson, D.J., Guzman, M.I., Heger, D., Kahan, T.F., 2012. Organics in environmental ices: sources, chemistry, and impacts. Atmos. Chem. Phys. 12, 9653–9678.
Moreda-Piñeiro, J., Rodríguez, E.L., Pérez, C.M., Heras, G.B., Carou, I.T., Mahía, P.L., Lorenzo, S.M., Rodríguez, D.P., 2014. Influence of marine, terrestrial and anthropogenic sources on ionic and metallic composition of rainwater at a suburban site (Northwest Coast of Spain). Atmos. Environ. 88, 30–38.
Mullaugh, K.M., Hamilton, J.M., Avery, G.B., Felix, J.D., Mead, R.N., Willey, J.D., Kieber, R.J., 2015. Temporal and spatial variability of trace volatile organic compounds in rainwater. Chemosphere 134, 203–209.
O'Sullivan, D.W., Lee, M., Noone, B.C., Heikes, B.G., 1996. Henry's law constant determinations for hydrogen peroxide, methyl hydroperoxide, hydroxymethyl hydroperoxide, ethyl hydroperoxide, and peroxyacetic acid. J. Phys. Chem. 100, 3241–3247.
Okochi, H., Sugimoto, D., Igawa, M., 2004. The enhanced dissolution of some chlorinated hydrocarbons and monocyclic aromatic hydrocarbons in rainwater collected in Yokohama. Jpn. Atmos. Environ. 38, 4403–4414.
Okochi, H., Kataniwa, M., Sugimoto, D., Igawa, M., 2005. Enhanced dissolution of volatile organic compounds into urban dew water collected in Yokohama. Jpn. Atmos. Environ. 39, 6027–6036.
Perišić, M., Maletić, D., Stojić, S.S., Rajšić, S., Stojić, A., 2017. Forecasting hourly particulate matter concentrations based on the advanced multivariate methods. Int. J. Environ. Sci. Technol. 14, 1047–1054.
Raja, S., Valsaraj, K.T., 2004. Adsorption and transport of gas-phase naphthalene on micron-size fog droplets in air. Environ. Sci. Technol. 38, 763–768.
Raja, S., Yaccone, F.S., Ravikrishna, R., Valsaraj, K.T., 2002. Thermodynamic parameters for the adsorption of aromatic hydrocarbon vapors at the gas–water interface. J. Chem. Eng. Data 47, 1213–1219.
Rao, P.S.P., Tiwari, S., Matwale, J.L., Pervez, S., Tunved, P., Safai, P.D., Srivastava, A.K., Bisht, D.S., Singh, S., Hopke, P.K., 2016. Sources of chemical species in rainwater during monsoon and nonmonsoonal periods over two megacities in India and dominant source region of secondary aerosols. Atmos. Environ. 146, 90–99.
Sander, R., 2015. Compilation of Henry's law constants (version 4.0) for water as solvent. Atmos. Chem. Phys. 15, 4399–4981.
Sapek, B., 2014. Calcium and magnesium in atmospheric precipitation, groundwater and the soil solution in long-term meadow experiments. J. Eleme 19, 191–208.
Sato, E., Matsumoto, K., Okochi, H., Igawa, M., 2006. Scavenging effect of precipitation on volatile organic compounds in ambient atmosphere. Bull. Chem. Soc. Jpn. 79, 1231–1233.
Seinfeld, J.H., Pandis, S.N., 2006. Atmospheric Chemistry and Physics: from Air Pollution to Climate Change, second ed. J. Wiley & Sons, New York.
Šoštarić, A., Stojić, A., Stanišić, S.S., Gržetić, I., 2016. Quantification and mechanisms of BTEX distribution between aqueous and gaseous phase in a dynamic system. Chemosphere 144, 721–727.
Starokozhev, E., Fries, E., Cycura, A., Püttmann, W., 2009. Distribution of VOCs

between air and snow at the Jungfraujoch high alpine research station, Switzerland, during CLACE 5 (winter 2006). Atmos. Chem. Phys. 9, 3197–3207.
Stojić, A., Stanišić Stojić, S., 2017. The innovative concept of three-dimensional hybrid receptor modeling. Atmos. Environ. 164, 216–223.
Stojić, A., Stanišić, S.S., Šoštarić, A., Ilić, L., Mijić, Z., Rajšić, S., 2015a. Characterization of VOC sources in an urban area based on PTR-MS measurements and receptor modelling. Environ. Sci. Pollut. Res. 22, 13137–13152.
Stojić, A., Stojić, S.S., Mijić, Z., Ilić, L., Tomašević, M., Todorović, M., Perišić, M., 2015b. Comprehensive analysis of VOC emission sources in Belgrade urban area. Urban Built Environ. 55–88.
Stojić, A., Stojić, S.S., Mijić, Z., Šoštarić, A., Rajšić, S., 2015c. Spatio-temporal distribution of VOC emissions in urban area based on receptor modelling. Atmos. Environ. 106, 71–79.
Stojić, A., Maletić, D., Stojić, S.S., Mijić, Z., Šoštarić, A., 2015d. Forecasting of VOC emissions from traffic and industry using classification and regression multivariate methods. Sci. Total. Environ. 521, 19–26.
Stojić, A., Stanišić, S.S., Reljin, I., Čabarkapa, M., Šoštarić, A., Perišić, M., Mijić, Z., 2016. Comprehensive analysis of PM10 in Belgrade urban area on the basis of long term measurements. Environ. Sci. Pollut. Res. 23, 10722–10732.
Słomińska, M., Konieczka, P., Namieśnik, J., 2014. The fate of BTEX compounds in ambient air. Crit. Rev. Env. Sci. Tec. 44, 455–472.
Team, 2012. R: a language and environment for statistical computing. http://cran.case.edu/web/packages/dplR/vignettes/timeseries-dplR.pdf (Accessed 4 December 2015).
Tiwari, S., Hopke, P.K., Thimmiah, D., Dumka, U.C., Srivastava, A.K., Bisht, D.S., Rao, P.S.P., Chate, D.M., Srivastava, M.K., Tripathi, S.N., 2016. Nature and sources of ionic species in precipitation across the Indo-Gangetic Plains, India. Aerosol Air Qual. Res. 16, 943–957.
USEPA, 2007. EPA Unmix 6.0 Fundamentals and User Guide. USEPA Office of Research and Development.
Valsaraj, K.T., Thoma, G.J., Reible, D.D., Thibodeaux, L.J., 1993. On the enrichment of hydrophobic organic compounds in fog droplets. Atmos. Environ. 27, 203–210.
Vane, L.M., Giroux, E.L., 2000. Henry's law constants and micellar partitioning of volatile organic compounds in surfactant solutions. J. Chem. Eng. Data 45, 38–47.
Wang, Y.Q., 2014. MeteoInfo: GIS software for meteorological data visualization and analysis. Meteorol. Appl. 21, 360–368.
Warneke, C., De Gouw, J.A., Kuster, W.C., Goldan, P.D., Fall, R., 2003. Validation of atmospheric VOC measurements by proton-transfer-reaction mass spectrometry using a gas-chromatographic preseparation method. Environ. Sci. Technol. 37, 2494–2501.
WHO, 1986. Toluene Environmental Health Criteria, vol. 52. WHO (International Programme on Chemical Safety).
WHO, 1993. Benzene Environmental Health Criteria, vol. 150. WHO (International Programme on Chemical Safety).
WHO, 1997. Ethylbenzene Environmental Health Criteria, vol. 186. WHO (International Programme on Chemical Safety).

Journal of Atmospheric and Solar-Terrestrial Physics 171 (2018) 250–259

Contents lists available at ScienceDirect

Journal of Atmospheric and Solar-Terrestrial Physics

journal homepage: www.elsevier.com/locate/jastp

Changes of atmospheric properties over Belgrade, observed using remote sensing and in situ methods during the partial solar eclipse of 20 March 2015

L. Ilić [a,*], M. Kuzmanoski [a], P. Kolarž [a], A. Nina [a], V. Srećković [a], Z. Mijić [a], J. Bajčetić [b], M. Andrić [b]

[a] Institute of Physics Belgrade, University of Belgrade, Pregrevica 118, 11080, Belgrade, Serbia
[b] University of Defence, Military Academy, Generala Pavla Jurišića Šturma 33, 11000, Belgrade, Serbia

ARTICLE INFO

Keywords:
Solar eclipse
Lidar
Planetary boundary layer
Ground based observations

ABSTRACT

Measurements of atmospheric parameters were carried out during the partial solar eclipse (51% coverage of solar disc) observed in Belgrade on 20 March 2015. The measured parameters included height of the planetary boundary layer (PBL), meteorological parameters, solar radiation, surface ozone and air ions, as well as Very Low Frequency (VLF, 3–30 kHz) and Low Frequency (LF, 30–300 kHz) signals to detect low-ionospheric plasma perturbations. The observed decrease of global solar and UV-B radiation was 48%, similar to the solar disc coverage. Meteorological parameters showed similar behavior at two measurement sites, with different elevations and different measurement heights. Air temperature change due to solar eclipse was more pronounced at the lower measurement height, showing a decrease of 2.6 °C, with 15-min time delay relative to the eclipse maximum. However, at the other site temperature did not decrease; its morning increase ceased with the start of the eclipse, and continued after the eclipse maximum. Relative humidity at both sites remained almost constant until the eclipse maximum and then decreased as the temperature increased. The wind speed decreased and reached minimum 35 min after the last contact. The eclipse-induced decrease of PBL height was about 200 m, with minimum reached 20 min after the eclipse maximum. Although dependent on UV radiation, surface ozone concentration did not show the expected decrease, possibly due to less significant influence of photochemical reactions at the measurement site and decline of PBL height. Air-ion concentration decreased during the solar eclipse, with minimum almost coinciding with the eclipse maximum. Additionally, the referential Line-of-Sight (LOS) radio link was set in the area of Belgrade, using the carrier frequency of 3 GHz. Perturbation of the receiving signal level (RSL) was observed on March 20, probably induced by the solar eclipse. Eclipse-related perturbations in ionospheric D-region were detected based on the VLF/LF signal variations, as a consequence of Lyα radiation decrease.

1. Introduction

Abrupt change in the incoming solar radiation flux during solar eclipse induces disturbances in different atmospheric layers (Gerasopoulos et al., 2008; Aplin et al., 2016). These disturbances are not necessarily similar to those during sunset/sunrise, because of different time scales and initial conditions. They depend on a number of factors, including the percentage of sun obscuration, latitude, season, time of the day, synoptic conditions, terrain complexity and surface properties. Since solar energy impacts the atmosphere primarily by convection of heat from the ground, lower atmospheric layers are more influenced by changes in solar radiation. The layer of the atmosphere in direct interaction with the surface, thus directly influenced by the Earth's surface forcing, is called the planetary boundary layer (PBL). Since surface is also a source of humidity and pollutants, turbulence within the PBL is responsible for mixing and dispersion of pollutants, while air pollution concentrations in the PBL are generally higher than those in the free troposphere (Stull, 1988).

A number of studies have focused on the effect of solar eclipse on various atmospheric properties, mainly in PBL. Changes in meteorological parameters near the ground level were most extensively investigated, for several eclipse events (Anderson, 1999; Ahrens et al., 2001; Kolarž

* Corresponding author.
E-mail address: luka@ipb.ac.rs (L. Ilić).

https://doi.org/10.1016/j.jastp.2017.10.001
Received 31 March 2017; Received in revised form 16 August 2017; Accepted 3 October 2017
Available online 4 October 2017

et al., 2005; Founda et al., 2007; Nymphas et al., 2009). The studies reported decrease in temperature and wind speed, changes in wind direction and increase in relative humidity, as a result of solar eclipse. The magnitude of these changes varied in different studies. Decrease in height of the PBL during solar eclipse was also observed (Kolev et al., 2005; Amiridis et al., 2007). The PBL quickly responds to surface forcing and its height can range from as low as a few hundred meters to a few kilometers. Diurnal cycle of the PBL height starts with the sunrise by heating of the surface and development of a convective boundary layer (CBL), reaching a steady state in the afternoon. The CBL remains as a residual layer until the development of a new mixing layer on the following day. A region of statically stable layer – the entrainment zone forms at the top of the PBL. It closely follows the PBL development, being shallow in the morning and thickening during the day due to intense turbulence and vigorous convection (Stull, 1988). During a solar eclipse, the change in the incoming radiation is more abrupt and affects the evolution of the PBL (Amiridis et al., 2007; Kolev et al., 2005), thus providing opportunity for investigating mechanisms involved in PBL evolution.

Some studies investigated eclipse-related changes in ozone concentration (Zerefos et al., 2001; Kolev et al., 2005; Zanis et al., 2001, 2007), due to its strong dependence upon the magnitude of UV flux (Bian et al., 2007). Tropospheric ozone (O_3)is the result of chemical reactions, mostly between nitrogen oxides (NOx), carbon monoxide (CO) and volatile organic compounds (VOCs), helped with UV radiation via process of photo-dissociation of O_3. Surface ozone concentrations were reported in literature to decrease during solar eclipse, with exception of unpolluted sites (Zanis et al., 2001, 2007).

Reported observations suggest increase in air ion (Kolarž et al., 2005; Aplin and Harrison, 2003 and references therein) and air radon concentrations (Gaso et al., 1994 and references therein) during solar eclipse, mainly attributed to PBL height decrease. Air ions are natural constituents of the atmosphere produced mostly by cosmic rays (20% of overall ionization) and natural radioactivity from soil (gamma decay of ^{40}K)and the air (^{222}Rn). The first two ionization sources mentioned above are nearly constant in time, and consequently changes of air ion generation areprimarily related to changes in Rn concentration. The background concentration of cluster air ions in lower troposphere vary from a few hundred to a few thousand ions cm^{-1}, with an average near-ground ionization rate of 10 ion pairs $cm^{-3}s^{-1}$. Air ions are neutralized mostly by ion-to-ion recombination and ion-aerosol attachment (Dolezalek, 1974). Their concentration changes diurnally: during the night, when the boundary layer conditions are stable concentrations are high, with maximum at dawn. During the day, with the development of convective boundary layer, air ion concentration decreases with minimum in the afternoon (Blaauboer and Smetsers, 1996). Radon and aerosol-carried Rn progenies are powerful air ionizers (energy of α particle decay is more than 5 MeV, while average ionization energy of air is 34 eV/ion pair) and thus the main source of cluster air ion pair production in the troposphere. Radon exhalation from the ground is determined by concentration of uranium, diffusion coefficients and porosity of soil layers on the way to surface (Ishimori et al., 2013). Average Rn concentration over the continents is 10 Bq m^{-3} (UNSCEAR, 1993).

The solar eclipse also influences ionosphere. In the upper part of this area variations in plasma frequencies are detected (Verhulst et al., 2016). Also, there are detected plasma variations in the lower ionosphere (see e.g. Guha et al., 2010; Maurya et al., 2014). One of the ways to register the variations of solar radiation impact within upper atmosphere is based on technology of radio waves which are reflected in ionosphere during propagation between emitters and receivers. Namely, the signal reflection height in the ionosphere and, consequently, parameters describing signal characteristics (propagation geometry, altitude distributions of refractive index and attenuation) depend on local plasma properties (primarily on electron density) (Bajčetić et al., 2015). Electron density declines during solar eclipse, similarly to sunset, resulting in increase of the reflection height of radio signals reflected on relevant atmospheric layer (Guha et al., 2010), as well as the occurrence of hydrodynamic waves (Nina and Čadež, 2013; Maurya et al., 2014). Because of that, the registered wave variations reflect the non-stationary physical and chemical conditions in the medium, along the considered wave trajectories, in real time. In addition to plasma parameters related to low ionosphere, several parameters describing signal propagation, like distance between transmitter and receiver, influence temporal changes in recorded signal characteristics. Because of that, the electron density decrease (or increase) can result in either increase and decrease of recorded amplitude (Grubor et al., 2008). Thus, only variation from the expected values is important for detection of influences of an event on low ionosphere.

The aim of this paper is to study atmospheric disturbances detected in Belgrade, induced by partial solar eclipse (51% coverage of solar disc) on March 20, 2015. Focusing on troposphere (mainly PBL) and ionosphere (D-region). For that purpose, four experimental setups were used to collect data, including lidar (Light Detection and Ranging) for measurement of PBL height and heights of elevated layers, AWESOME (Atmospheric Weather Electromagnetic System for Observation Modelling and Education) VLF/LF receiver (Cohen et al., 2010) and instruments for measurements solar radiation, meteorological parameters, concentrations of ozone, air ions and radon, and propagation of radio signals in troposphere.

The paper is organized as follows. In Section 2 we describe measurements and methods used in the study, and give overview of background conditions. The results are described in Section 3, and a conclusion of this study is given in Section 4.

2. Measurements and methods

2.1. UVradiation, ozone and air-ion measurements

UV-B erythemal radiation was measured using 501 biometer made by Solar light company, USA. Instrument was set on the roof of the Institute of Physics Belgrade (IPB), so that no obstacles entered the field of view. During the eclipse, data acquisition was set to 10 min. Global Sun radiation was measured by Republic Hydro-meteorological Service in Belgrade using Kipp&Zonen CMP6 pyranometer (http://www.kippzonen.com/Product/12/CMP6-Pyranometer), with 1-min data acquisition. Surface ozone measurements were conducted using Aeroqual monitor, series 500 (http://aeroqual.com/product/series-500-portable-air-pollution-monitor), made in New Zealand. The instrument was placed near UV 501 biometer and acquisition was set to 6 min. Air ions, temperature, pressure and relative humidity were measured using a Cylindrical Detector and Ion Spectrometer CDIS (Kolarž et al., 2011), made at IPB. The CDIS was placed 1 m above grassy surface (where the soil allows the radon exhalation), at IPB (44.86° N, 20.39° E, 89 m a.s.l.). Only positive air ion concentrations were measured since they have lower mobility than negative ions and consequently lower ion-to-aerosol attachment coefficient. Thus, they are less sensitive to air pollution and provide better picture of atmosphere processes. Radon was measured using continual radon measuring instrument RAD7, Durridge company, USA. Quality of continual Rn measurements is related to level of radon concentration and measuring period, i.e. counting events. The instrument was placed next to CDIS at the same level.

2.2. Measurements of meteorological parameters

The meteorological measurements were obtained at two semi-urban sites in Belgrade. One measurement site was located at IPB. At the site, temperature, relative humidity and atmospheric pressure at altitude 1 m above ground were measured. The meteorological measurements were also available from an automatic weather station collocated with a SYNOP station at Košutnjak, Belgrade (WMO no. 13275, 203 m a.s.l.), about 10 km away from the IPB site.

2.3. Detection of PBL height

A variety of methods can be used to quantify the PBL height, depending on available measurements (Emeis et al., 2008). Differences between PBL and free troposphere can be observed using vertical profiles of thermodynamic quantities and wind from radiosounding measurements. Lidar observations, using atmospheric aerosol as a tracer, can be used to determine heights of both PBL and elevated aerosol layers if present in the atmosphere.

In this study radiosounding and lidar measurements were used to determine PBL height. While radiosoudings are regularly available at 00UTC and 12UTC at the WMO station, providing meteorological data on mandatory and significant pressure levels, the advantage of lidar measurements is that they can be performed continuously with high vertical andtemporal resolutions. Data derived from lidarmeasurements can be used for detection and characterization of aerosols and PBL evolution, and allow for the detection of abrupt and smaller scale changes in the layer structure.

The lidar system at IPB, is a bi-axial system with combined elastic and Raman detection designed to perform continuous measurements of suspended aerosol particles in the PBL and the lower free - troposphere. It is based on the third harmonic frequency of a compact, pulsed Nd:YAG laser, emitting pulses of 65 mJ output energy at 355 nm with a 20 Hz repetition rate. The optical receiver is a Cassegrain reflecting telescope with a primary mirror of 250 mm diameter and a focal length of 1,250 mm. Photomultiplier tubes are used to detect elastic backscatter lidar signal at 355 nm and Raman signal at 387 nm. The detectors are operated both in the analog and photon-counting mode and the spatial raw resolution of the detected signals is 7.5 m. Averaging time of the lidar profiles during the March 2015 solar eclipse case was 1 min corresponding to 1,200 laser shots.

Lidar measurements can be used to estimate PBL height using different approaches (Sicard et al., 2006; Baars et al., 2008). In this study, the gradient method was used to determine the position of the strongest gradient of the aerosol vertical distribution, associated with the PBL height (Flamant et al., 1997). The height of a strong negative peak which can be identified as the absolute minimum of the range corrected signal's (RCS) derivative, determines the PBL top height. A strong negative gradient in lidar RCS is a result of decrease in aerosol backscatter due to decrease in aerosol concentration and humidity (Matthias et al., 2004). Our estimate of PBL height is based on lidar measurements at 355 nm. However, when available, measurements at larger wavelengths (i.e. 532 nm and 1,064 nm) are more appropriate for analysis of PBL height due to smaller relative contribution of molecular backscatter compared to 355 nm. Other local minima in the signal derivative, with absolute values above a specified threshold and with transition intervals including a minimum of five points, are associated with elevated aerosol layer top heights in the free troposphere (Flamant et al., 1997).

The Richardson number is used for PBL height estimation from radiosounding measurements. Radiosoundings are performed two times each day, at 00 and 12 UTC, at a weather station (Belgrade Košutnjak, WMO number 13275), 10 km away from the lidar measurement site at 203 m altitude. The Richardson number is defined as (Stull, 1988):

$$R_{ib} = \frac{g[z - z_0][\theta(z) - \theta(z_0)]}{\theta(z)\left[u(z)^2 + v(z)^2\right]} \quad (1)$$

where g is acceleration due to gravity, z_0 is the altitude of the weather station, $\theta(z)$ is the potential temperature and $u(z)$ and $v(z)$ are zonal and meridional components of the wind. The layers in which R_{ib} is above a critical value of 0.21 (Vogelezang and Holtslag, 1996; Menut et al., 1999) are considered to be above the PBL.

Since the data are available at discrete heights, at standard and significant pressure levels, the bulk Richardson number is used (Stull, 1988). Successful estimation of the PBL height from radiosounding measurements from stations in the WMO network, has been previously reported (Jeričević and Grisogono, 2006; Amiridis et al., 2007). Average uncertainty of the PBL height was estimated for March for a 10-year period from 2006 to 2015, from radiosounding profiles retrieved at 12 UTC. Typical resolutions varied from 100 m to 1,000 m, and the uncertainty of PBL height H was estimatedusing the following formula:

$$H = H_{estimated} \pm \frac{\Delta z}{2} \quad (2)$$

where Δz is the measurement resolution (Jeričević and Grisogono, 2006). It was calculated to be 180 m corresponding to the average vertical resolution of 350 m. On the eclipse day, the resolution and the uncertainty were estimated to be 150 m and 80 m, respectively.

2.4. Terrestrial line-of-sight radio communication measurement setup

The referential Line-of-Sight (LOS) radio link was set in the area of Belgrade, using the carrier frequency of 3 GHz, with the purpose of investigating solar eclipse contribution to receiving signal level (RSL) instability.

The transmitter was emitting non-modulated carrier, having the radio frequency (RF) output power level of 0 dBm. LOS link was established at the distance of 70 m. The signal was transmitted using the signal generator with the frequency stability of TCXO $\leq \pm 0.5$ ppm and signal level stability $\leq \pm 0.7$ dB which was housed at constant temperature. Antenna emitted horizontally polarized electromagnetic (EM) wave. The receiving system (Rx) was formed with Tektronix SA2600 spectrum analyser that was programmed to perform 1 kHz width spectral recording into 500 points. In this way, the generated signal spectrum at the receiving side could be reconstructed with an accuracy of 2 Hz, which made it possible to monitor temporal changes in the level of the received signal peak.

The measuring samples of the received signal level were recorded every 45 s equidistantly during continuous operation of the LOS link. On 20 March 2015, we made 480 recordings through 6 h, includingthe solar eclipse period.

2.5. Ionospheric observations

Global experimental setup for the low ionospheric observation is based on continuously emitting and receiving the VLF/LF signals by numerous worldwide-distributed VLF/LF transmitters and receivers, respectively. In this study, we based our analysis on D-region monitoring using the 37.5 kHz LF signal emitted by the NRK transmitter located in Grindavik (Iceland) and received at IPB by the AWESOMEVLF/LF receiver. This transmitter was chosen because the path of this signal passes through an area that was affected by a total eclipse.

2.6. Background conditions

The eclipse on March 20, 2015 started at 8:40 UTC, ended at 10:58 UTC, reaching maximum coverage of 51% at 9:48 UTC. In the days prior to the eclipse, the synoptic conditions were influenced by a cyclone moving to the east, over Balkans, followed by an increase in geopotential. Wind field was characterized by northwesterly flow shifting to northerly. On the day of the eclipse surface conditions were influenced by weak-gradient anticyclonic field. On the previous day, overcast skies with light rain in the evening were reported. From the morning of the March 20 and during the day, the sky was clear. The calm meteorological conditions provided good opportunity to observe possible eclipse-related changes in meteorological parameters near surface.

3. Results

3.1. Global and UV radiation

Primary effect of solar eclipse is reduction of solar radiation reaching the surface. In Fig. 1 diurnal variation of global sun radiation and UV-B erythemalradiation are shown for the day of the solar eclipse, and for three clear days after the eclipse. Solar eclipse on March 20 occurred during morning increase of both global and UV-B radiation due to sun elevation. Their attenuation was 48%, slightly smaller than the obscuration of the solar disc (51%). This difference could be due to diffuse solar irradianceknowing that UV-B radiation is the shortest wavelength reaching the surface and thus most prone to scattering. While the direct solar irradiance is reduced proportionally to the obscuration of solar disc during the eclipse, the diffuse irradiance is less affected due to contribution of multiple scattering from less shadowed part of the sky (Zerefos et al., 2001). They reported that the difference in reduction of diffuse and direct irradiance was more pronounced at shorter wavelengths.

3.2. Meteorological parameters

Meteorological measurements were analyzed to investigate the response of the air temperature, relative humidity and pressure at near-surface level to the eclipse. As mentioned in the previous section, the meteorological measurements were conducted at two locations: at IPB lidar measurement site and at Košutnjakstation, about10 km away. Diurnal cycle of the temperature was interrupted by the eclipse at both measurement sites (Fig. 2). Change in temperature increase rate was observed at both sites, with similar delay after the first contact. Higher temperatures were measured, and temperature decrease was more pronounced at IPB station, probably due to lower altitude and as a result of lower measurement height above ground. At this station, the temperature decreased during the eclipse, by 2.6 °C, at the rate of 0.043 °Cmin^{-1}, reaching minimum about 15 min after the maximum of the eclipse. At Košutnjakstation the temperature was almost constant after the first contact until the maximum of the eclipse, with an increase rate of 0.003 °wCmin^{-1}. After the eclipse maximum, it started increasing with increased downward radiation, at a higher rate of0.03 °C/min.To further investigate the effect of the eclipse on temperature, measurements available from Košutnjakstation on days following the eclipse were used. The rate of temperature change during the eclipse was compared to the rates recorded during the same period of day on three cloud-free days after the eclipse – March 21, 23 and 24. Increasing trend of maximum daily temperature was measured in this period. On the eclipse day, the increase rate from the first contact to the eclipse maximum (0.003 °Cmin^{-1})was very low in comparison to the rates of 0.016 °C min^{-1}, 0.025 °Cmin^{-1} and 0.032 °Cmin^{-1} for the same period on March 21, 23 and 24, respectively. After the eclipse maximum until the end of the eclipse, temperature increase rate of 0.025 °Cmin^{-1}was comparable to the corresponding rates on the three following days. Total increase in temperature during the eclipse was 2.0 °C, while the corresponding measured increase on March 21, 23 and 24, was 2.3 °C, 3.3 °C and 4.0 °C, respectively.

Relative humidity showed decreasing trend, typical for the beginning of the day and morning increase of temperature. During the eclipse, humidity was almost constant until the maximal obscuration of solar disc, and then it decreased by 10% at both locations (IPB and Košutnjak), in consistence with temperature increase. Until the maximal obscuaration, at IPB, the temperature was decreasing while the relative humidity was almost constant. It remains unclear whether its behaviour is an effect of eclipse.

The wind speed measured at the Košutnjak station followed atypical diurnal cycle, until the maximum of the eclipse, when both wind speed and gustiness dropped, and started increasing after the event (Fig. 3). Wind speed decreased from a maximum of 2.7 ms^{-1} to about 1.1 ms^{-1}at the end of the eclipse. The absolute minimum of wind speed and gusts was reached about 35 min after the last contact. Wind direction changed from northerly to northeasterly for the duration of the eclipse.

Pressure drop during the eclipse at Košutnjak station was 0.9 hPa (not shown here), which is most probably the consequence of the temperature

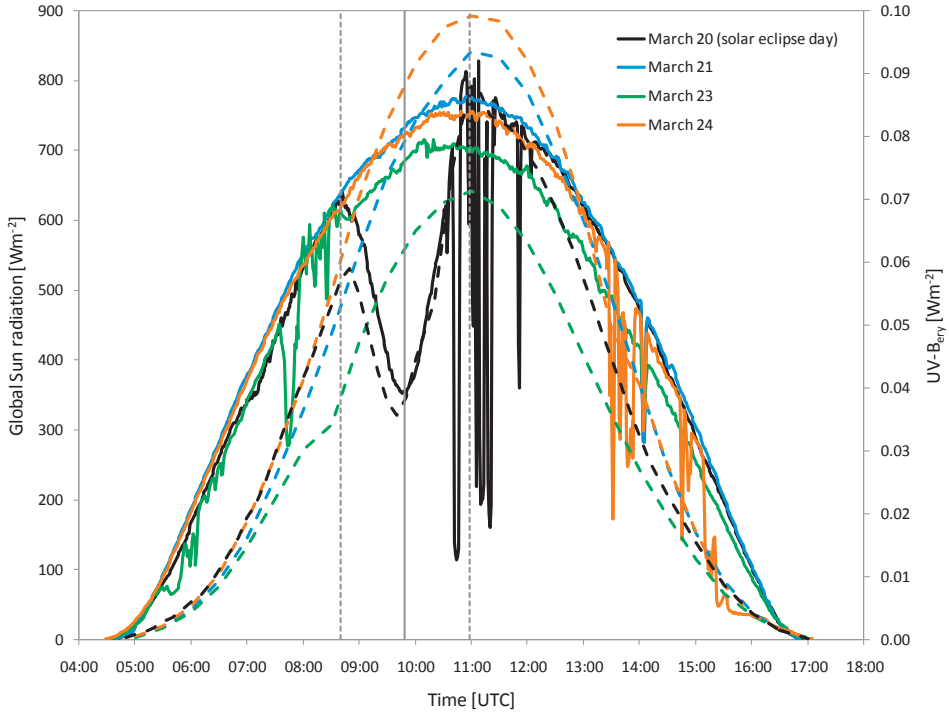

Fig. 1. Global Sun radiation (solid lines) and UV-B erythemal radiation (dashed lines) during partial Solar eclipse (March 20, 2015) and three clear days after the eclipse. Dotted vertical lines indicate beginning, maximum and end of the eclipse.

drop (Fig. 2). The pressure minimum was reached about 30 min after the eclipse maximum. Additional data, from radiosounding, provided information on vertical profiles of meteorological variables 1 h after the event. Up to the top of the PBL, the northerly wind speeds were relatively low, from 2 to 3.5 ms^{-1}. Air in the PBL was not very humid, with relative humidity of 35–60%.

These observed changes are generally in agreement with those reported in previous studies, related to eclipse events with larger obscuration of solar disc. The exception is relative humidity, which was almost constant until the eclipse maximum in this work, while it was reported to increase in previous studies. Anderson (1999) compiled data on near-surface temperature during selected total eclipse events, given in literature. These data showed temperature decrease of 2.0–3.6 °C, with minimal value coinciding with mid-eclipse (in one case), or reached with the time lag of 7–17 min. Foundaet al. (2007) presented observations at several sites in Greece, with different degrees of sun obscuration (74–100%) during solar eclipse in March 2007. Their results showed that temperature (measured at altitudes varying from 1.5 m to 17 m at different sites) decreased by 1.6–2.7 °C (3.9 °C at a site affected by low clouds), reaching minimal value 12–14 min after the mid-eclipse. Following the temperature response, the relative humidity was reported to increase by about 20% (Founda et al., 2007; Kolev et al., 2005). A decline in wind speed, after mid-eclipse, as a result of cooling the boundary layer and reduction of turbulent transport (Girard-Ardhuin et al., 2003) was also reported in literature (Anderson, 1999; Founda et al., 2007).

3.3. PBL evolution assessment from meteorological and lidar measurements

The presence of the residual layer, evolution of the PBL and aerosol layers in the free troposphere during the solar eclipse were observed using lidar measurements in Belgrade. For that purpose, the vertical profiles of the range-corrected analog signal at 355 nm, obtained from 10:15 UTC until 15:25 UTC with temporal resolution of 1 min, were analyzed, using the gradient method. The time series of range corrected signal (RCS) vertical profiles, along with heights of PBL and elevated aerosol layers are presented in Fig. 4.

The eclipse occurred before local noon, during the development of the mixing layer. In the morning, with surface heating, PBL started increasing from 600 m height to about 800 m above ground during the time period of about 2 h until the start of the eclipse at 8:40 UTC. The increase of the PBL height before the eclipse was steady and gradual. During this period, a layer was identified at height of about 1 km. This layer can be identified as the residual layer. With the beginning of the eclipse, the amount of solar radiation reaching the surface started decreasing (Fig. 1). This affected the change in surface temperature (Fig. 2), and therefore convective motion, with the effects diminishing with height. The PBL height decreased by about 200 m during the solar eclipse, reaching minimum 20 min after the maximum of the eclipse. This decrease in PBL height is similar to those reported in previous research (Amiridis et al., 2007; Kolev et al., 2005), for solar eclipse with larger solar disc obscuration. With passing of the eclipse, the PBL started gaining height until reaching the height of about 1700 m around 13 UTC. Stronger variations of PBL height observed after the eclipse can be attributed to stronger convective motions. In first minutes after the eclipse, shallow cumulus clouds formed with their base at the top of the PBL. A peak in PBL height, coinciding with peaks in temperature and wind speed measurements was observed during the later phase of the event. Depth of the entrainment zone followed the development of the PBL. It showed gradual increase before the eclipse, from low values of about 30 m, to variations in height of several tens of meters after the eclipse as a result of strong convective motions.

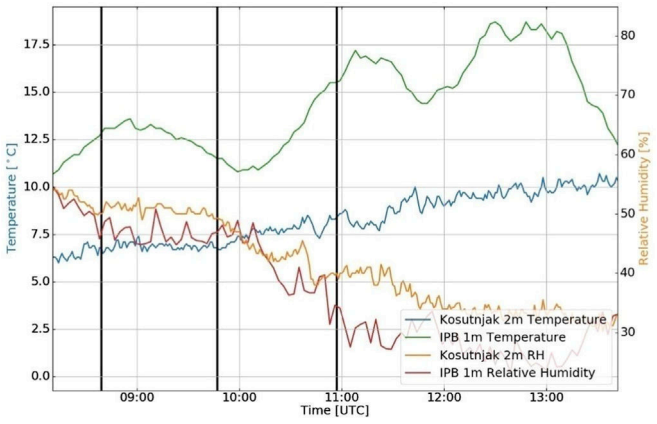

Fig. 2. Temperature and relative humidity. Vertical lines indicate beginning, maximum and end of the eclipse.

The PBL height value calculated as an hourly average around 12 UTC (soon after the end of the eclipse), was 1 500 ± 100 m, in agreement with the one estimated from radiosounding:1 600 ± 80 m.Small differences of results obtained from radiosounding and lidar measurements can be due to local effects at two measurement sites and differences in the methods used. The gradient method uses gradient in lidar RCS due to decrease in aerosol backscatter while the bulk Richardson number approach relies on thermodynamic properties. Different surface properties and elevations of measurement sites influence the heat and momentum fluxes contributing to the PBL development. Lidar is operated on a fixed location during the whole measurement period, providing information on vertical column of air directly above the instrument. Radiosounding profiles are affected by the horizontal drift of the instrument caused by wind and depend on whether the ascent is made in a thermal or between thermals (Stull, 1988). To further estimate impact of eclipse on PBL height we compared these values with the PBL heights calculated for March for a 10-year period from 2006 to 2015 from the radiosounding profiles taken at 12 UTC (excluding the profile on the day of the eclipse). The values estimated both from lidar (around 12 UTC) and radiosounding measurements made on the day of the eclipse fall within the inter-quartile range of the values for the 10-year reference period (Fig. 4).

The lidar measurements during solar eclipse also showed presence of aerosol layers in free troposphere, at altitudes up to 4 km.

3.4. Ozone and air-ion concentrations

Surface ozone measurements showed no significant decrease, as opposed to most other measured parameters, possibly indicating less significant influence of photochemical reactions at the IPB semi-urban measurement site (see Fig. 5). While a decrease of surface ozone concentration during solar eclipse is expected, this effect could be missing in less polluted areas, or it could be masked by air transport or decline of PBL height (Zanis et al., 2001, 2007). For an urban station in Thessaloniki, Zanis et al. (2001) reported that surface ozone concentration decreased by 10–15 ppbv during the solar eclipse in August 1999 (maximum sun obscuration 90%), with a half-hour delay in starting time of the decrease after the first contact. However, they did not observe any effect on surface ozone in an elevated rural station at Hohenpeissenberg (99.4% sun coverage). Measurements during the solar eclipse in March 2006, conducted in Greece, showed decrease of 5–10 ppb surface ozone in an urban site in Thessaloniki (about 70% sun obscuration), while no effect was observed in relatively unpolluted sites in Finokalia and Kastelorizo, with 82% and 86% solar obscuration, respectively (Zanis et al., 2007). In our study, the measurements were taken at semi-urban site, during solar eclipse event with 51% sun obscuration. It is also noteworthy that measurements conducted for few other days, after the solar eclipse, in the present study showed high time lag of ozone concentration peaks compared to UV radiation peak. This was also reported in Tie et al. (2007) and Bian et al. (2007).

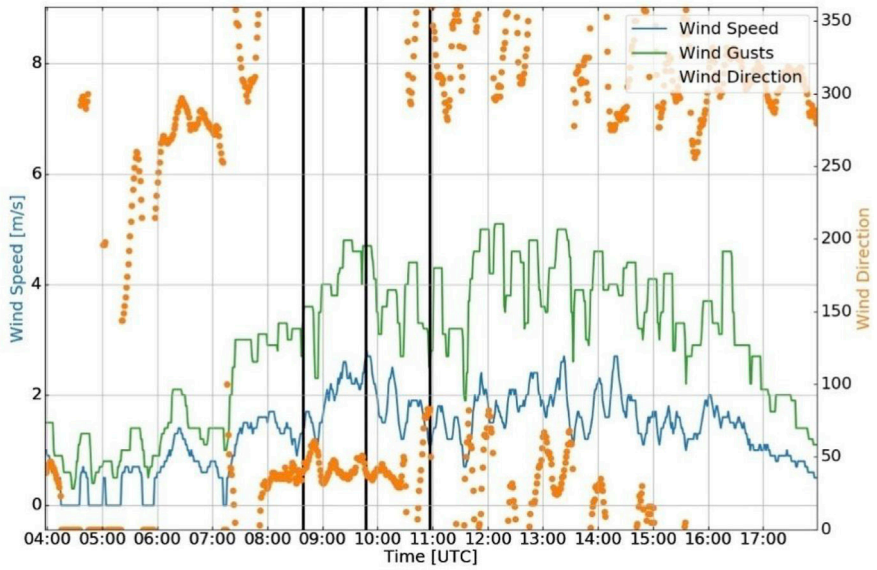

Fig. 3. Wind speed, gusts and direction. Vertical lines indicate beginning, maximum and end of the eclipse.

Radon concentrations measured during the eclipse (not shown here) were in the range between 0 and 15 Bq m^{-3} which is typical background for this part of the day. As shown in Fig. 6, air ion concentration decreased during the course of the day. The decrease was more intensive during the eclipse. After the eclipse, air ion concentration returned to its usual diurnal path to afternoon minimum. This could be explained by decrease of diffusion processes that are responsible for radon exhalation from the soil, as a result of cease of heating the surface during the eclipse. Differences were noted in air ion change during the eclipse in 1999 (97.7% sun obscuration), described in Kolarž et al. (2005) and that described in this study (51% sun obscuration).

3.5. Line-of-Sight radio communication receiving signal change

The observed RSL change during the time of solar eclipse was compared with the RSL change in few following days. The usual change of RSL in morning hours presented in Bajčetić et al. (2013) was confirmed during regular days, while, the pattern of signal level variation was quite different during the solar eclipse (Fig. 7, left panel).

Additionally, the observed meteorological variables were used to calculate the value of the air refractivity parameter (R) using (3), with the aim of the correlation between variation of that parameter and microwave RSL change (Fig. 7, right panel).

$$R = 77,6\frac{P}{T} + 3,73\cdot 10^5\frac{P_{vp}}{T^2}. \quad (3)$$

R is the value which describes the overall influence of the tropospheric medium on the radio wave propagation and depends on relative air pressure P, absolute temperature T and partially on water vapour pressure P_{vp} (Debye, 1957; Falodun and Ajewole, 2006).

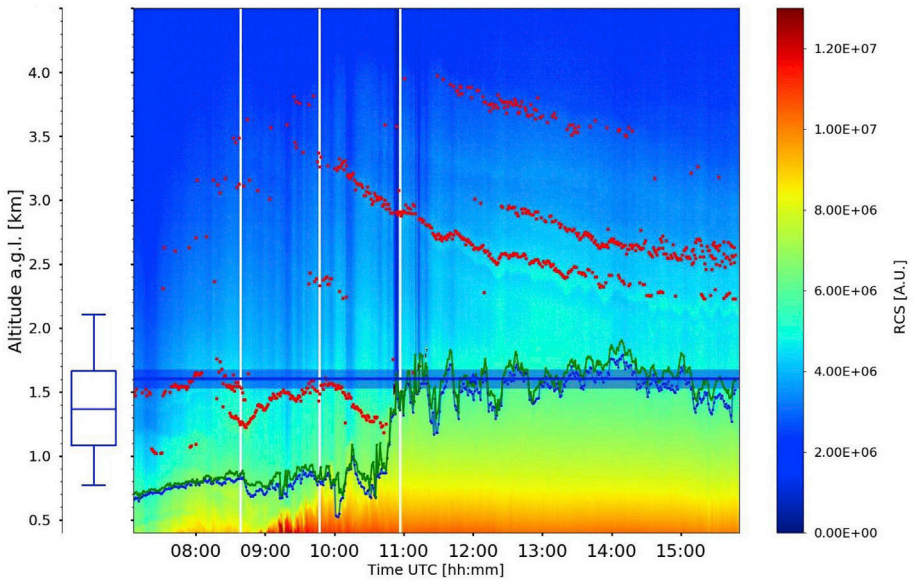

Fig. 4. Temporal evolution of PBL (blue line) and elevated aerosol layers (red dots). Colormaps represent the lidar RCS at 355 nm on March 20, 2015. White vertical lines indicate beginning, maximum and end of the eclipse. Box plot shows the median, first and third quartiles and 5th and 95th percentiles of PBL heights in March for period 2006–2015. (For interpretation of the references to colour in this figure legend, the reader is referred to the web version of this article.)

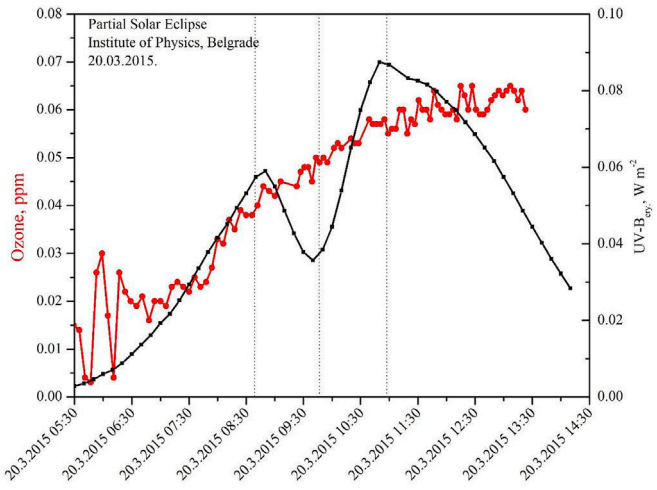

Fig. 5. Ozone and UV-B erythemal radiation during partial solar eclipse. Dotted vertical lines indicate beginning, maximum and end of the eclipse.

We normalized the measured values R_{xi} (i = 1,…, 480) of the air refractivity parameterto its mean value during the related day ($\overline{R}_x$), using Eq.2measured values R_{xi} of the air refractivity parameter, in order to emphasize the level of variation.

$$RSL = 100 \cdot \frac{R_{xi} - \overline{R}_x}{|\overline{R}_x|}. \quad (4)$$

Following the presented data in Fig. 8, it can be seen that there was meaningful correlation between RSL and R during the days after the solar eclipse, while their values change fairly independently on the day of the solar eclipse.

Analysing data presented in Fig. 8, it can be seen that before the period of solar eclipse, the disturbance manifested through the unusual *R* constant value until 08:40 is well correlated with the constant value of *RSL*. At the moment of solar eclipse maximum, the considerable *R* disturbance can be noticed, while this phenomenon does not reflect to the *RSL*. From 10:00, until the end of the solar eclipse, value of *R* varied within expected usual values, however *RSL* changed unusually.

This unusual RSL variation was possibly triggered by the solar eclipse event. In ordinary periods of measurements, the relative air pressure, absolute temperature and partially the pressure of the water vapour directly influence the permittivity of the air, causing the refraction of the electromagnetic wave, so the effects are noticeable as the RSL variation. However, during a solar eclipse event, it is not possible to consequently relate RSL and R. Considering the absolute amplitude variation of RSL, which was in the domain of 2,5 dB for the presented time periods, the sudden not so intense air permittivity perturbation within the area where LOS link was established did not have direct influence on the radio propagation at 3 GHz frequency. While RSLwas evidently slightly perturbedduring solar eclipse, there is not clear evidence that this perturbation is related to solar eclipse. The observed phenomena are not well presented in the literature for this particular scenario, and will be a subject of future analyses.

3.6. *Effects on the ionosphere and LF radio signal propagation*

The ionospheric perturbations were detected as variations of recorded NRK signal from Iceland. Generally, the temporal evolution of recorded signal can be used for detection of low ionospheric plasma perturbations; these changes in medium through which signal propagates affect wave reflection height, and consequently, propagation geometry and attenuation, resulting in variations of recorded signal characteristics.

The shapes of the temporal change depend on numerous parameters. Namely, in addition to periodic and sudden variations in the ionospheric plasma conditions, characteristics of signals like mutual locations of transmitter and receiver, power of transmitted signal, and geographical area through which the signal propagates, affect the recorded signal properties. For these reasons the dependencies between the ionospheric changes of electron density induced by radiation increase and VLF/LF signal amplitude are not monotonous, e.g. growth in the electron density does not necessarily cause amplification of recorded signal amplitudes (for detailed explanation see Nina et al., 2017). Thus, for detection of some sudden perturbationit is sufficient toobservechanges in temporal

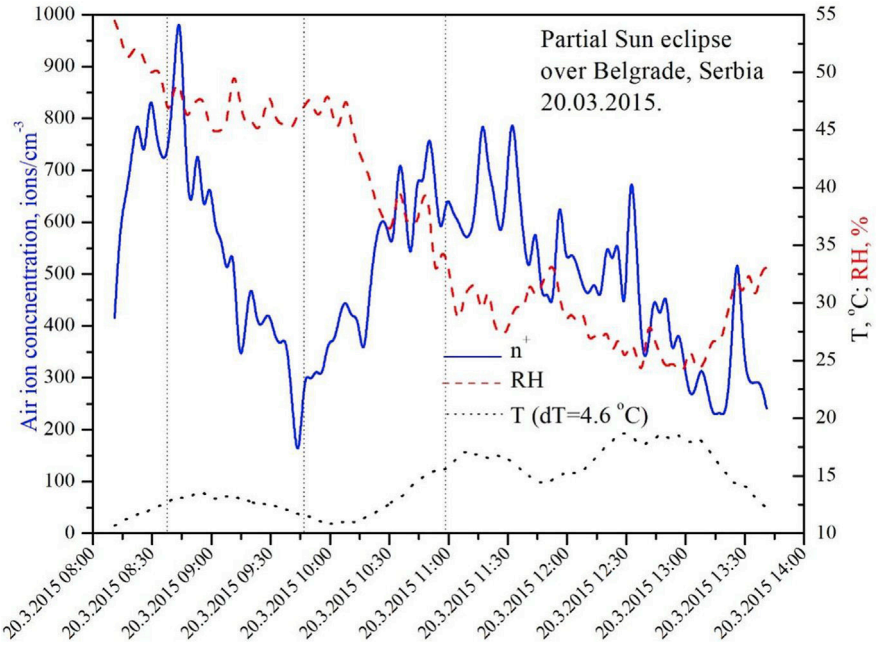

Fig. 6. Air ion concentration, temperature and relative humidity during partial solar eclipse. Dotted vertical lines indicate beginning, maximum and end of the eclipse.

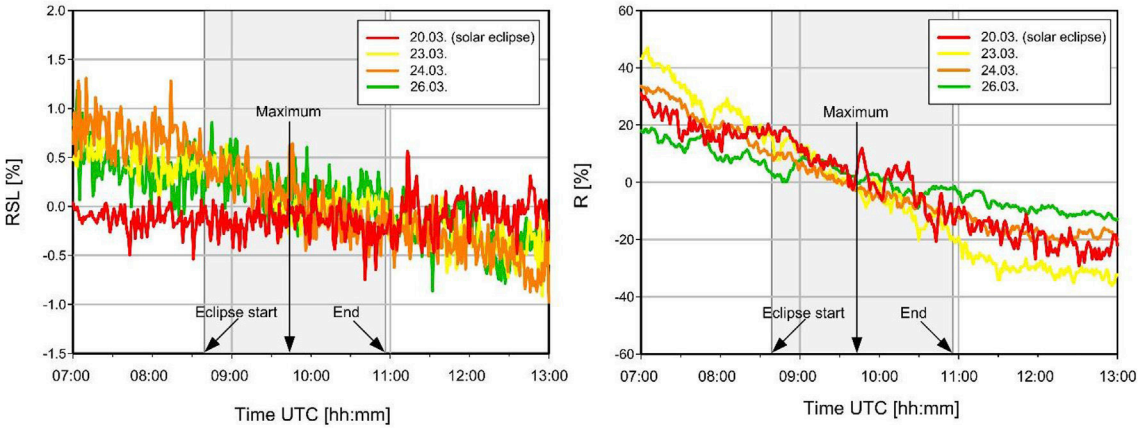

Fig. 7. Receiving signal level (*RSL*) and refractivity (R) variation. Shaded domains represent the time period when eclipse occurred.

evolution of signal characteristics.

Fig. 9 shows temporal variations of amplitude difference from its initial considered values, recorded by the AWESOME system at the Belgrade station on March 20, 2015 when solar eclipse occurred, and three days after that. The additional days are shown to visualize amplitude variation in solar eclipse period with respect to its shapes in other relevant periods without influence of the eclipse. The reason for choosing these particular days was relatively quiet conditions without significant traveling ionospheric disturbance resulting from atmospheric lightnings, and solar flares among other events. While amplitude variations are pronounced during the solar eclipse, they are practically within noise domains on the other three days. In the first period, a decrease in amplitude was observed, with the minimum occurring before the eclipse maximum. Further, the amplitude increased, exceeded the amplitude values during the first contact and reached the larger value approximately coincidently with the eclipse maximum time (indicated by a vertical line). Finally, it returned to the expected values, which are around initial values (this can be concluded from the three referent signals).

As explained in Section 1, electron density variation is most important for changes of plasma parameters which influence signal propagation. Its time variations depend on different electron gain and loss processes. The constituents of the low ionosphere can be ionized by γ, X and a part of UV photons. The most important solar influences on the ionization processes in the D-region in absence of large radiation increase, primarily as consequence of solar X-flares (Nina et al., 2012a,b) is coming from the solar Lyα line (121.6 nm) radiation (Swamy, 1991) whose presence is periodically intensified during the day. Bearing in mind that satellites did not register significant increase of intensity of X radiation, we can conclude that the signal variations are a consequence of Lyα radiation decrease. http://en.wikipedia.org/wiki/Solar_eclipse.

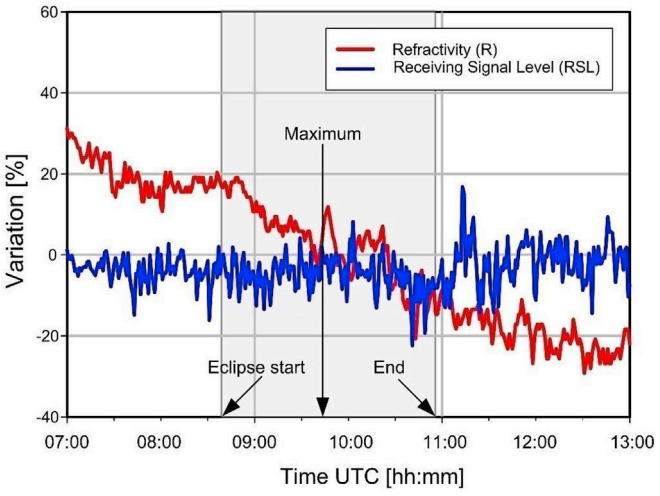

Fig. 8. *RSL* and R variation during solar eclipse. Shaded domains represent the time period when eclipse occurred.

4. Conclusions

Changes in atmospheric properties were observed during a partial solar eclipse (51%) on March 20, 2015 in Belgrade. For that purpose, four experimental setups were used to collect data, including lidar to derive PBL height and heights of elevated layers, AWESOME VLF/LF receiver (Cohen et al., 2010) and instruments for measurements of solar radiation, meteorological parameters, concentrations of ozone, air ions and radon and propagation of radio signals in troposphere. Although the solar eclipse was only partial, its influence on atmospheric properties in troposphere and ionosphere was noticeable. The detected changes in atmospheric parameters were generally similar, but weaker in intensity, to those reported in literature for solar eclipse events with larger obscuration of solar disc.

In troposphere, the influence of the eclipse was observed in meteorological surface parameters, and it was evident up to the top of the PBL. Eclipse-induced decrease in PBL height was 200 m, comparable to that reported in literature, with minimal value occurring 20 min after the eclipse maximum. The PBL height determined from 12 UTC radiosounding measurements (soon after the eclipse), showed that it was within the usual values for this location at that time of year. The meteorological parameters showed similar behavior at two measurement sites Košutnjak and IPB, respectively. The temperature change was more pronounced and abrupt at the –IPB station, probably due to lower measurement height, where it decreased by 2.6 °C, reaching minimum 15 min after the eclipse maximum. This temperature change is similar to those reported in literature for solar eclipse with larger obscuration of solar disc. At the Košutnjakstation the temperature was almost constant, until the eclipse maximum. Relative humidity was almost constant at both sites from the first contact until the eclipse maximum, as opposed to the increase reported in literature. The diurnal cycle then continued, with the increase in temperature and decrease in relative humidity at both sites. The 10-m wind speed and gusts decreased, reaching a minimum about 30 min after the eclipse. The wind direction changed from northerly to northeasterly for the duration of the event. Decrease of PBL height and the entrainment zone thickness were also observed during the eclipse, as a result of diminished surface heating. Ozone concentrations showed no decrease, as opposed to most results reported in literature, except for those reported for rural measurement sites. The possible reasons are less significant influence of photochemical reactions, decrease in PBL height or advection by changing wind during the event. Measured

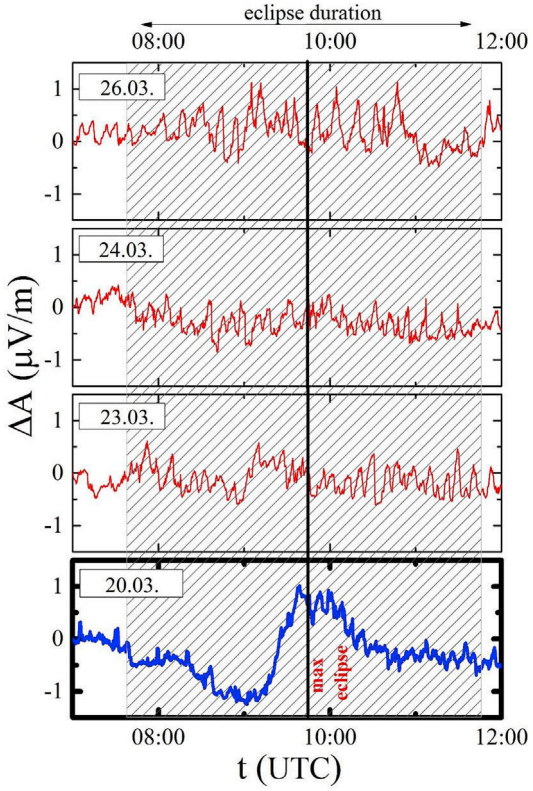

Fig. 9. The variations of amplitude difference from its initial considered values against the universal time (UT), recorded by the AWESOME system at the Belgrade station on March 20, 2015 when solar eclipseoccurred (lower panel) and three days after that (top panels). Shaded domains represent the time period when eclipse occurred (here we consider a whole period of eclipse because of long signal propagation path from Iceland to Serbia).

radon concentrations were typically low for this time of the day, while the air ion concentration sharply decreased.

The referential Line-of-Sight (LOS) radio link was set in the area of Belgrade, in order to investigate influence of the event on RSL instability. During the solar eclipse, an unusual pattern of the signal level variation was observed and different relationship between the RSL and the air refractivity parameter (R). Further analysis is needed to clearly relate the perturbation with solar eclipse which affected the atmospheric variables and therefore R.

Impact of the solar eclipse on the ionosphere was registered through changes of characteristics of radio waves which are reflected in ionosphere. The amplitude variations, were pronounced during the solar eclipse, and were at the expected values on the days after the event. Since satellite measurements did not show significant increase of intensity of X radiation, it was concluded that the signal variations are consequence of Lyα radiation decrease.

Acknowledgements

This research was realized as a part of projects no. III43007, no. III41011, no. III44002, no. 176002, no. P171020, no. III45003 financed by the Ministry of Education, Science and Technological Development of the Republic of Serbia within the framework of integrated and interdisciplinary research for the period 2011–2017. Also, this study is made within the COST project TD1403 and VarSITY project.

References

Ahrens, D., Moses, G.I., Lutz, J., Andreas, M., Helmut, M., 2001. Impacts of the solar eclipse of 11 August, 1999 on routinely recorded meteorological and air quality data in South-West Germany. Meteorol. Z. 10 (3), 215–223.

Amiridis, V., Melas, D., Balis, D.S., Papayannis, A., Founda, D., Katragkou, E., Giannakaki, E., Mamouri, R.E., Gerasopoulos, E., Zerefos, C., 2007. Aerosol Lidar observations and model calculations of the planetary boundary layer evolution over Greece, during the March 2006 total solar eclipse. Atmos. Chem. Phys. 7, 6181–6189. https://doi.org/10.5194/acp-7-6181-2007.

Anderson, J., 1999. Meteorological changes during a solar eclipse. Weather 54 (7), 207–215.

Aplin, K.L., Harrison, R.G., 2003. Meteorological effects of the eclipse of 11 August 1999 in cloudy and clear conditions. Proc. R. Soc. Lond. A 459, 353–371.

Aplin, K.L., Scott, C.J., Gray, S.L., 2016. Atmospheric changes from solar eclipses. Philosophycal Trans. R. Soc. A 374, 20150217.

Baars, H., Ansmann, A., Engelmann, R., Althausen, D., 2008. Continuous monitoring of the boundary-layer top with lidar. Atmos. Chem. Phys. 8, 7281–7296. https://doi.org/10.5194/acp-8-7281-2008.

Bajčetić, J., Andrić, M., Todorović, B., Pavlović, B., Suša, V., 2013. The correlation of geomagnetic component disturbances and 5 GHz LOS received signal daily variation. Microw. Rev. 19 (1).

Bajčetić, J.B., Nina, A., Čadež, V., Todorović, B.M., 2015. Ionospheric D-region temperature relaxation and its influences on radio signal propagation after solar X-flares occurrence. Therm. Sci. 19 (Suppl. 2), S299–S309.

Bian, H., Han, S., Tie, X., Sun, M., Liu, A., 2007. Evidence of impact of aerosols on surface ozone concentration in Tianjin, China. Atmos. Environ. 41, 4672–4681.

Blaauboer, R.O., Smetsers, R.C.G.M., 1996. Outdoor concentrations of the equilibrium-equivalent decay products of ^{222}Rn in The Netherlands and the effect of meteorological variables. Radiat. Prot. Dosim. 69, 7–18.

Cohen, M.B., Inan, U.S., Paschal, E.W., 2010. Sensitive broadband ELF/VLF radio reception with the AWESOME instrument. IEEE Trans. Geosci. Remote. 48, 3–17.

Debye, P., 1957. Polar Molecules. Dover Publications, New York.

Dolezalek, H., 1974. Electrical Processes in Atmospheres, Springer Verlag, Electrical Processes in Atmospheres. Springer Verlag.

Emeis, S., Schafer, K., Munkel, C., 2008. Surface-based remote sensing of the mixing-layer height – A review. Meteorol. Z. 17 (5), 621–630.

Falodun, S.E., Ajewole, M.O., 2006. Radio refractive index in the lowest 100-m layer of the troposphere in Akure, South Western Nigeria. J. Atmos. Sol.-Terr. Phys 236–243.

Flamant, C., Pelon, J., Flamant, P.H., Durand, P., 1997. Lidar determination of the entrainement zone thickness at the top of the unstable marine atmospheric boundary-layer. Boundary-Layer Meteorol. 83, 247–284.

Founda, D., Melas, D., Lykoudis, S., Lisaridis, I., Gerasopoulos, E., Kouvarakis, G., Petrakis, M., Zerefos, C., 2007. The effect of the total solar eclipse of 29 March 2006 on meteorological variables in Greece. Atmos. Chem. Phys. 7, 5543–5553. https://doi.org/10.5194/acp-7-5543-2007.

Gaso, M.I., Cervantes, M.L., Segovia, N., Espindola, V.H., 1994. Atmospheric radon concentration levels. Radiat. Meas. 23, 225–230.

Gerasopoulos, E., Zerefos, C.S., Tsagouri, I., Founda, D., Amiridis, V., Bais, A.F., Belehaki, A., Christou, N., Economou, G., Kanakidou, M., Karamanos, A., Petrakis, M., Zanis, P., 2008. The total solar eclipse of March 2006: overview. Atmos. Chem. Phys. 8, 5205–5220.

Girard-Ardhuin, F., Bénech, B., Campistron, B., Dessens, J., Jacoby-Koaly, S., 2003. Remote sensing and surface observations of the response of the atmospheric boundary layer to a solar eclipse. Boundary-Layer Meteorol. 106, 93–115.

Grubor, D.P., Šulić, D.M., Žigman, V., 2008. Classification of X-ray solar flares regarding their effects on the lower ionosphere electron density profile. Ann. Geophys. 26 (7), 1731–1740.

Guha, A., De, B.K., Roy, R., Choudhury, A., 2010. Response of the equatorial lower ionosphere to the total solar eclipse of 22 July 2009 during sunrise transition period studied using VLF signal. J. Geophys. Res. 115, A11302. https://doi.org/10.1029/2009JA015101.

Ishimori, Y., Lange, K., Martin, P., Mayya, Y.S., Phaneuf, M., 2013. Measurement and Calculation of Radon Releases from NORM Residues. International Atomic Energy Agency, Vienna.

Jeričević, A., Grisogono, B., 2006. The critical bulk richardson number in urban areas: verification and application in a numerical weather prediction model. Tellus A 58, 19–27. https://doi.org/10.1111/j.1600-0870.2006.00153.x.

Kolarž, P., Šekarić, J., Marinković, B.P., Filipović, D.M., 2005. Correlation between some of the meteorological parameters measured during the partial solar eclipse, 11 August, 1999. J. Atmos. Sol. Terr. Phys. 67, 1357–1364.

Kolarž, P., Miljković, B., Ćurguz, Z., 2011. Air-ion counter and mobility spectrometer. Nucl. Instrum. Methods Phys. Res. B 279, 219–222.

Kolev, N., Tatarov, B., Grigorieva, V., Donev, E., Simenonov, P., Umlensky, V., Kaprielov, B., Kolev, I., 2005. Aerosol Lidar and in situ ozone observations of the planetary boundary layer over Bulgaria during the solar eclipse of 11 August 1999. Int. J. Remote Sens. 26, 3567–3584.

Matthias, V., Balis, D., Bosenberg, J., Eixmann, R., Iarlori, M., Komguem, L., Mattis, I., Papayannis, A., Pappalardo, G., Perrone, M.R., Wang, X., 2004. Vertical aerosol distribution over Europe: statistical analysis of Raman lidar data from 10 European aerosol research lidar network (EARLINET) stations. J. Geophys. Res. 109, D18201. https://doi.org/10.1029/2004JD004638.

Maurya, Ajeet K., Phanikumar, D.V., Rajesh, Singh, Sushil, Kumar, Veenadhari, B., Kwak, Y.-S., Abhikesh, Kumar, Singh Abhay, K., Niranjan, Kumar K., 2014. Low-mid latitude D region ionospheric perturbations associated with 22 July 2009 total solar eclipse: wave-like signatures inferred from VLF observations. J. Geophys. Res. Space Phys. 119 (10), 8512–8523.

Menut, L., Flamant, C., Pelon, J., Flamant, P.H., 1999. Evidence of interaction between synoptic and local scales in the surface layer over the Paris area. Bound. Layer. Meteorol. 93, 269–286. https://doi.org/10.1023/A:1002013631786.

Nina, A., Čadež, V.M., 2013. Detection of acoustic-gravity waves in lower ionosphere by VLF radio waves. Geophys. Res. Lett. 4018, 4803–4807.

Nina, A., Čadež, V., Srećković, V., Šulić, D., 2012a. Altitude distribution of electron concentration in ionospheric D-region in presence of time-varying solar radiation flux. Nucl. Instrum. Methods. B 279, 110–113.

Nina, A., Čadež, V., Šulić, D., Srećković, V., Žigman, V., 2012b. Effective electron recombination coefficient in ionospheric D-region during the relaxation regime after solar flare from February 18, 2011. Nucl. Instrum. Methods. B 279, 106–109.

Nina, A., Čadež, V.M., Popović, Č.L., Srećković, A.V., 2017. Diagnostics of plasma in the ionospheric D-region: detection and study of different ionospheric disturbance types. Eur. Phys. J. D 71 (7). https://doi.org/10.1140/epjd/e2017-70747-0, 189, 1-12.

Nymphas, E.F., Adeniyi, M.O., Ayoola, M.A., Oladiran, E.O., 2009. Micrometeorological measurements in Nigeria during the total solar eclipse of 29 March, 2006. J. Atmos. Sol. Terr. Phys. 71 (12), 1245–1253.

Sicard, M., Pérez, C., Rocadenbosch, F., Baldasano, J.M., García-Vizcaino, D., 2006. Mixed-layer depth determination in the Barcelona Coastal area from regular lidar measurements: methods, results and limitations. Bound. Layer Meteorol. 119 (1), 135–157. https://doi.org/10.1007/s10546-005-9005-9.

Stull, R.B., 1988. An Introduction to Boundary Layer Meteorology. Kluwer Acad., Dordrecht, The Netherlands.

Swamy, A.B., 1991. A new technique for estimating D-region effective recombination coefficients under different solar flare conditions. Astrophys. Space Sci. 185 (1), 153–164.

Tie, X., Madronich, S., Li, G.H., Ying, Z.M., Zhang, R., Garcia, A., Lee-Taylor, J., Liu, Y., 2007. Characterizations of chemical oxidants in Mexico City: a regional chemical/dynamical model (WRF-Chem) study. Atmos. Environ. 41, 1989–2008.

United Nations Scientific Committee on the Effects of Atomic Radiation (UNSCEAR), 1993. Report to the General Assembly, with Scientific Annexes. New York.

Verhulst, T.G.W., Sapundjiev, D., Stankov, S.M., 2016. High-resolution ionospheric observations and modeling over Belgium during the solar eclipse of 20 March 2015 including first results of ionospheric tilt and plasma drift measurements. Adv. Space Res. 57 (No.11), 2407–2419. https://doi.org/10.1016/j.asr.2016.03.009.

Vogelezang, D.H.P., Holtslag, A.A.M., 1996. Evolution and model impacts of alternative boundary layer formulations. Bound. Layer. Meteorol. 81, 245–269. https://doi.org/10.1007/BF02430331.

Zanis, P., Zerefos, C.S., Gilge, S., Melas, D., Balis, D., Ziomas, I., Gerasopoulos, E., Tzoumaka, P., Kaminski, U., Fricke, W., 2001. Comparison of measured and modeled surface ozone concentrations at two different sites in Europe during the solar eclipse on August 11, 1999. Atmos. Environ. 35, 4663–4673.

Zanis, P., Katragkou, E., Kanakidou, M., Psiloglou, B., Karathanasis, S., Vrekoussis, M., Gerasopoulos, E., Lysaridis, I., Markakis, K., Poupkou, A., Amiridis, V., Melas, D., Mihalopoulos, N., Zerefos, C., 2007. Effects on surface atmospheric photo-oxidants over Greece during the total solar eclipse event of 29 March 2006. Atmos. Chem. Phys. Discuss. 7, 11399–11428.

Zerefos, C.S., Balis, D.S., Zanis, P., Meleti, C., Bais, A.F., Tourpali, K., Melas, D., Ziomas, I., Galani, E., Kourtidis, K., Papayannis, A., Gogosheva, Z., 2001. Changes in surface UV solar irradiance and ozone over the Balkans during the eclipse of 11 August 1999. Adv. Space Res. 27 (12), 1955–1963.

applied sciences

MDPI

Article

Novel Modelling Approach for Obtaining the Parameters of Low Ionosphere under Extreme Radiation in X-Spectral Range

Vladimir A. Srećković [1,*], Desanka M. Šulić [2], Veljko Vujčić [3], Zoran R. Mijić [1] and Ljubinko M. Ignjatović [1]

[1] Institute of Physics Belgrade, University of Belgrade, Pregrevica 118, 11080 Belgrade, Serbia; zoran.mijic@ipb.ac.rs (Z.R.M.); ljuba@ipb.ac.rs (L.M.I.)
[2] Faculty of Ecology and Environmental Protection, University Union—Nikola Tesla, 11000 Belgrade, Serbia; dsulic@unionnikolatesla.edu.rs
[3] Astronomical Observatory, Volgina 7, 11060 Belgrade, Serbia; veljko@aob.rs
* Correspondence: vlada@ipb.ac.rs; Tel.: +381-(0)11-37-13-000

Abstract: Strong radiation from solar X-ray flares can produce increased ionization in the terrestrial D-region and change its structure. Moreover, extreme solar radiation in X-spectral range can create sudden ionospheric disturbances and can consequently affect devices on the terrain as well as signals from satellites and presumably cause numerous uncontrollable catastrophic events. One of the techniques for detection and analysis of solar flares is studying the variations in time of specific spectral lines. The aim of this work is to present our study of solar X-ray flare effects on D-region using very low-frequency radio signal measurements over a long path in parallel with the analysis of X-spectral radiation, and to obtain the atmospheric parameters (sharpness, reflection height, time delay). We introduce a novel modelling approach and give D-region coefficients needed for modelling this medium, as well as a simple expression for electron density of lower ionosphere plasmas. We provide the analysis and software on GitHub.

Keywords: solar radiation; sun activity; disturbances; radio spectra; X-spectral domain; Lyman-alpha

Citation: Srećković, V.A.; Šulić, D.M.; Vujčić, V.; Mijić, Z.R.; Ignjatović, L.M. Novel Modelling Approach for Obtaining the Parameters of Low Ionosphere under Extreme Radiation in X-Spectral Range. *Appl. Sci.* **2021**, *11*, 11574. https://doi.org/10.3390/app112311574

Academic Editor: Harry D. Kambezidis

Received: 20 October 2021
Accepted: 1 December 2021
Published: 6 December 2021

1. Introduction

Solar flares (SFs) are giant eruptions on the surface of the Sun [1,2] that release huge amounts of electromagnetic energy over the whole electromagnetic spectrum [3–7]. Levels of photoionization processes in the ionosphere depend on plasma composition along with radiation spectral ranges at specific altitudes [8]. Information on certain solar spectral lines could be of importance in research of solar flares [9,10]. The enhanced Extreme Ultraviolet (EUV) radiation is absorbed at higher terrestrial altitudes additionally ionizing E and F regions of the ionosphere [11]. In addition, Lyman-alpha and X-rays penetrate more deeply into the ionosphere, reaching the D-region and causing enhanced ionization and absorption of electromagnetic (EM) waves there [12–14]. Solar flares can be classified into different classes based on their peak emission in the X-ray 0.1–0.8 nm spectral range as B ($\geq 10^{-7}$ Wm^{-2}), C ($\geq 10^{-6}$ Wm^{-2}), M ($\geq 10^{-5}$ Wm^{-2}), and X ($\geq 10^{-4}$ Wm^{-2}) classes [15–17].

The abrupt increase in X-radiation and EUV emission following solar flares causes additional ionization and increased absorption of EM waves in the sunlit part of the Earth's ionosphere. At the time of SFs and consequently during sudden ionospheric disturbances (SIDs), the gain of the atmosphere electron density at all heights is noticeable [18,19]. As a consequence of radiation influence, SFs create SIDs and induce disturbance in the monitored amplitude and phase of Very Low-Frequency (VLF in narrow band 3–30 kHz) radio signals, primarily in the D layer, which is located between the Earth's lower atmosphere, which has dense air, and its strongly conducting ionosphere [20,21]. These events of X-ray SFs have been monitored by Geostationary Operational Environmental Satellite (GOES) [15].

In this paper we will focus on the VLF technique—on amplitude and phase signals of worldwide transmitters of signals monitored by BEL VLF system (Belgrade, Serbia) [22]. VLF signals from the emitters located all over the world are continuously recorded by the BEL system. Events of X-ray SFs monitored by GOES satellites are further identified using a radio station's system of receivers. For these events, VLF wave enhancements are measured and analysed for the daytime atmosphere. In continuation of our previous research, the aim of this contribution is to present our study of solar X-ray flare effects and to obtain the daytime atmospheric parameters and ionization rate induced by this extreme radiation, and to provide a simple equation for altitude-dependent electron density of D-region plasma which depends on X-ray spectral intensity and sluggishness of the medium. Finally, we discuss how the approximately obtained altitude-dependent electron density relies on the shape of X-ray flux. The python scripts for calculating ionosphere parameters can be found on GitHub: https://github.com/sambolino/flarED (accessed on 17 October 2021).

The text is organized as follows: Section 2 briefly presents methods for observing the D-region and introduces a methodology. Section 3 provides the details of numerical results, analyses, and introduces a simple expression of electron density of the D-region. In Section 4 the results are discussed together with further directions of research.

2. SFs Impact

We have studied the VLF amplitude (A) and phase (P), acquired by recording VLF radio signals broadcast by NAA transmitter at Maine, USA (44.63° N, 67.28° W) during solar-induced SIDs. The data were recorded by Belgrade VLF system (44.85° N, 20.38° E). The BEL stations can synchronously record several radio signals broadcast by different transmitters. The technicalities and description of the BEL VLF system are presented in [22]. The NAA-BEL path is sufficiently long (6540 km) and correctly oriented west–east.

Here, we present the study of SIDs induced by the large SFs of solar cycles 24 and 25. The acquisition and research of VLF signals has been carried out together with the investigation of the corresponding X-ray fluxes obtained from GOES. In this research, the registered data of incoming solar radiation X-ray flux in the XRS spectral range of 0.1–0.8 nm are of primary interest.

2.1. Monitoring SF

We have studied the amplitude and phase data, obtained by monitoring VLF radio signals emitted by NAA/24.00 kHz transmitter during solar-induced SIDs. During SIDs, a regular method for signal examination and the determination of ionospheric parameters rely on the comparison between the registered variation of amplitude and phase and the matching values acquired with simulations by the Long-Wave Propagation Capability (LWPC) numerical software package [23,24], as explained in [20,25,26].

As an instructive example of a monitored active day, we present 7 September 2017 (see Figure 1). Three M-class solar flares erupted from sunspot AR2673 of magnitudes M2.4, M1.5, and M7.3, followed by a huge X1.3-class SF. Energy and particulates hurled at the Earth while the proton flux velocity was two times greater than normal. The aurora borealis was also seen.

In Figure 1 we present measured amplitude (lower panel) and phase (upper panel) for NAA/24.00 kHz signal on high solar activity during M1.5 ($I_x = 1.5 \times 10^{-5}$, Wm^{-2} at peak time, 09:54 UT), M7.3 (10:15 UT), C3 (12:14 UT) and X1.3 (14:36 UT) events on 7 September 2017 as a function of time. There were visible changes in the VLF daily signal during the C, M and X flares (see signal peaks on panels). From Figure 1, one can see that these VLF and GOES peaks during the daytime happened almost simultaneously (with a time delay of the order of minutes).

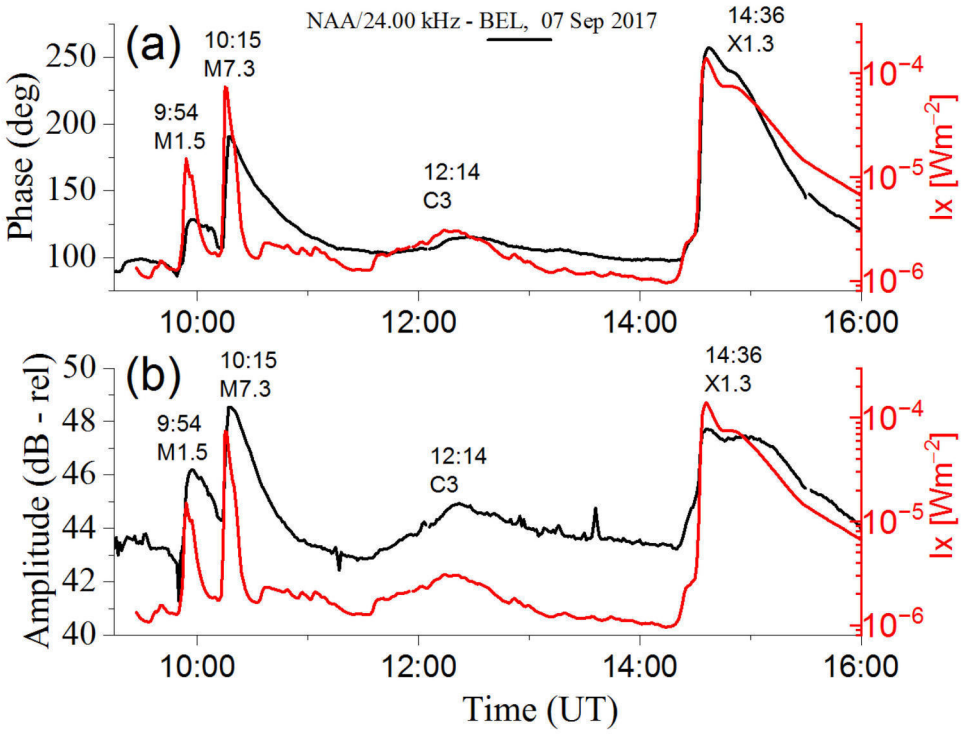

Figure 1. Time variation of X-ray irradiance on the right axes, NAA/24.00 kHz signal phase (**a**) and amplitude (**b**) during M1.5 (09:54 UT), M7.3 (10:15 UT), C3 (12:14 UT) and X1.3 (14:36 UT) events on 7 September 2017.

In this work we have calculated the amplitude increase ΔA_{rec}, defined as the difference between the maximum amplitude $A_{\max}$ registered during the flare and the regular amplitude during quiet condition A_{quiet} as:

$$\Delta A_{rec} = A_{\max} - A_{quiet} \quad (1)$$

In the same way, phase delay increase ΔP_{rec} has been calculated as:

$$\Delta P_{rec} = P_{\max} - P_{quiet} \quad (2)$$

The time delay Δt can be defined as: $\Delta t = t_{\mathrm{Amax}} - t_{\mathrm{Imax}}$ where t_{Amax} is the time of maximum of VLF amplitude $A_{\max}$ and t_{Imax} is time of maximum of X-ray irradiance $I_{\max}$ [20]. The time delay is nearly similar to the D-region sluggishness [13] and is an important quantity that can be used to study the ionospheric response to the flares [27]. The quantity Δt depends on flare intensity and other factors, and usually takes values of about a few minutes [16,27].

For the representative quiet days, i.e., conditions, we have chosen the days under low solar activity. The conditions were that the daylight maximum of X-ray flux had to be lower than 10^{-6} Wm^{-2} in the 0.1–0.8 nm XL band.

2.2. Used Numerical Methods

2.2.1. Two-Component Exponential Model and Simulations

The daytime two-parameter exponential profile of electron density can be used for VLF modelling [28] and is given by:

$$N_e(h, H', \beta) = 1.43{\cdot}10^{13} \exp(-0.15{\cdot}H') \exp[(\beta - 0.15){\cdot}(h - H')] \ [\mathrm{m}^{-3}]. \quad (3)$$

Here, β in km^{-1} is a time-dependent parameter of sharpness, H' is a reflection height in km, and h is the height in kilometres above surface.

During SIDs, a regular method for the obtaining of ionospheric parameters is based on comparison of the registered variation of amplitude and phase (Equations (1) and (2)) with the equal values obtained in computation by the LWPC software [23] as interpreted in [20,25,26]. N_e can be obtained from the measured amplitude and phase changes by a trial-and-error method where density profile is modified until the LWPC computed amplitude and phase match with monitored data (see, e.g., [22]). Thus, the obtained parameters β and H' can be applied for further calculation and simulations (Equation (3), etc.).

2.2.2. FlarED' Method

In [29], i.e., GitHub: https://github.com/sambolino/flarED (accessed on 17 October 2021), the database is created with SID VLF data (ΔA_{rec}, ΔP_{rec}) parameters, sharpness β and reflection height H' for different values of I_x, i.e., different classes of solar flares (during the period of ascending phase and maximum of the solar cycle 24 and 25). Solar flares are monitored and analysed by VLF technique and ΔA_{rec}, ΔP_{rec} while parameters β and H' in database are obtained by the method described in [20]. The python scripts for calculating ionosphere parameters can be found https://github.com/sambolino/flarED (accessed on 19 September 2021). For the input values of solar X-ray flux, parameters β and H' can be evaluated and altitude values of electron density for the low terrestrial ionosphere can be calculated. Users can easily calculate time series and hight profile of electron density. The results, i.e., data, can be plotted and exported in csv.

2.2.3. Approximate Analytic Expression

In order to create an easier and more adequate use of results and data, we give an electron density specially modified simple logarithmic second-degree polynomial expression, with height-dependent coefficients taking into account the delay time of the ionosphere response. The python scripts for calculating electron density by this specially modified expression can be found at https://github.com/sambolino/flarED (accessed on 10 October 2021). Additionally, for details see Section 3.2.

3. Results and Discussion

3.1. Analyses of SF Events

An example of flare-induced phase and amplitude perturbations, measured for the NAA/24.00 kHz signal on an active day of 10 May 2013, is given in Figure 2 (red lines on both panels). The unperturbed daytime values of phase and amplitude were measured on 9 May 2013 (black lines on both panels in Figure 2). There were visible changes in the VLF daily signal during the duration of M1.3 SF (peak time, 12:56 UT) and C2.5 SF (peak time, 14:37 UT).

One can see visible variations in amplitude and phase. SID VLF changes at the time of the maximum of SF of M1.3 and C2.5 SF classes are ΔA = 4.2 dB, ΔP = 68.19 deg and ΔA = 1.06 dB, ΔP = 19.20 deg, respectively (see Table 1 and Figure 3c,d). It can be seen that during SF class C, amplitude and phase disturbances are not well defined, but are still noticeable.

Figure 3 shows simultaneous variations of the sharpness β, effective reflection height H', amplitude and phase (recorded and simulated), electron density at reference height (74 km) and X-ray flux, during the occurrence of two successive flares on 10 May 2013 from Figure 3a–e, respectively.

For the period around SFs on 10 May 2013, we have calculated the time-dependent H' and β parameters as shown in Figure 3a,b. During M1.3- and C2.5-class SFs on 10 May 2013, the change of H' with time has normal behaviour. After the start of the SFs it falls to a minimum, and after X-ray peak it keeps growing to a preflare value. Sharpness behaviour is connected with form of registered increase of VLF amplitude, i.e., β rises sharply to a maximum, and after the peak of X-ray flux it drops to a preflare value. At 12:56 UT, i.e.,

at peak time of the M1.3-class SF, with $I_x = 1.36 \cdot 10^{-5}$ Wm^{-2}, H' decreases to a value of 67 km and the β rises to 0.41 km^{-1}. At C2.5-class SF peak time (14:37 UT) with $I_x = 2.59 \cdot 10^{-6}$ Wm^{-2} the H' decreases to 72 km and the β increase to 0.32 km^{-1}. It can be noted that the reflection height and the sharpness are in correlation with X-ray flux shape.

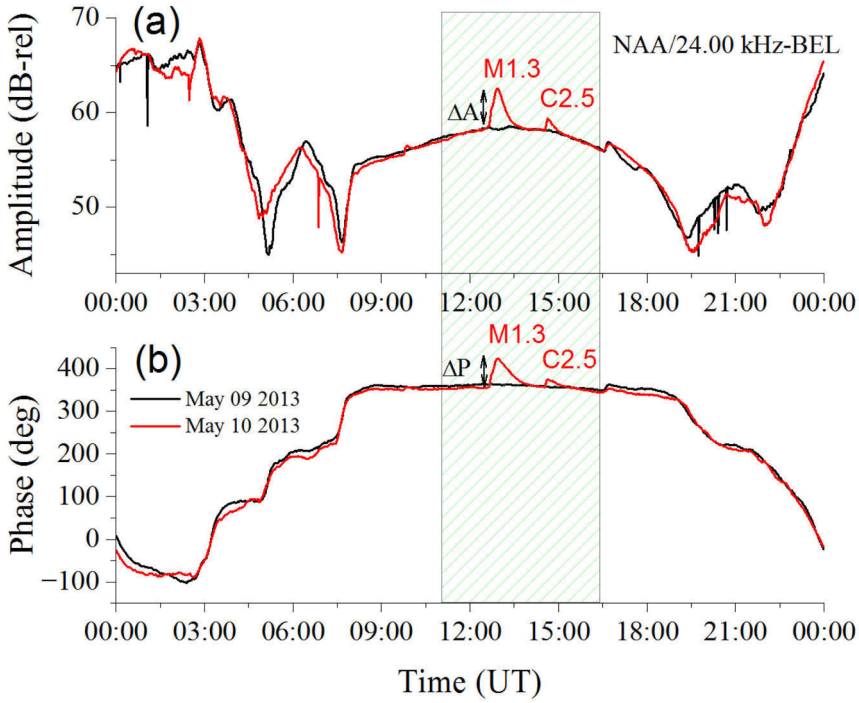

Figure 2. Measured variation of amplitude (**a**) and phase (**b**) on NAA signals for 9 May 2013 (quiet day) and 10 May 2013 with noticeable SF events.

Table 1. The data on SFs, amplitude and phase perturbations of VLF signals caused by different events analysed in this study.

	SF Tim			SID VLF Signatures			SF Data	
SF (Class, Date)	**Start [UT]**	**Peak [UT]**	**End [UT]**	**ΔA [dB]**	**ΔP [deg]**	**Δt [min]**	**I_x max XL [Wm^{-2}]**	**Active Region**
M1.3 10.05.2013	12:37	12:56	13:04	4.20	68.19	0	1.36×10^{-5}	1745
C2.5 10.05.2013	14:30	14:37	14:42	1.06	19.20	1	2.59×10^{-6}	1745
M1.8 12.06.2014	09:23	09:37	09:42	4.50	51.47	4	1.81×10^{-5}	2085
M2.7 12.06.2014	10:14	10:21	10:27	5.72	83.01	2	2.74×10^{-5}	2087
X1.0 11.06.2014	08:59	09:06	09:10	5.54	90.45	3	1.00×10^{-4}	2087
X1.3 07.09.2017	14:20	14:36	14:55	4.50	159	1	1.39×10^{-4}	2673

Figure 4 shows the height profile, i.e., vertical electron-density profile before, after and during the M1.3- and C2.5-class solar flares that occurred on 10 May 2013. Electron-density altitude profile changes describe the variation of ionization at the D layer due to SF events and are relevant for mapping the low ionosphere [30,31] and moreover are important for checking the validity of the method and results [32] as shown in many examples. For unperturbed (preflare) ionospheric conditions (blue line) and post flare, there is a moderate increment in N_e (from $2.8 \cdot 10^7$ m^{-3} at h = 60 km height, to $6.7 \cdot 10^8$ m^{-3} at the upper part of

this region, i.e., at h = 80 km). These lines have almost the same behaviour. Completely different slope and behaviour have black and dashed dotted–dotted pink lines at peak times of M- and C-class SFs with increment from ~$7{\cdot}10^7$ m^{-3} at 60 km height to $1.6{\cdot}10^{10}$ m^{-3} and $4{\cdot}10^9$ m^{-3}, respectively. It can be noted that the electron density profiles moved to higher electron densities with different slopes when compared to the density profile of the preflare ionospheric condition. These changes in altitude profile of electron density are important for the nature of VLF propagation.

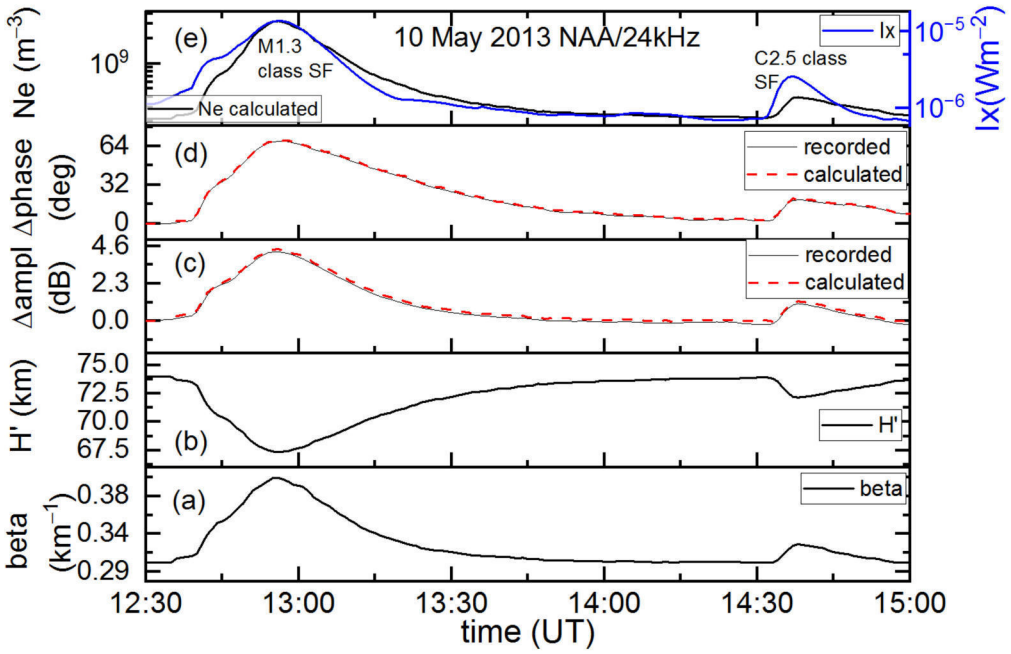

Figure 3. Simultaneous variations of the sharpness β (**a**), effective reflection height H' (**b**), VLF amplitude (**c**) and phase (**d**) excess recorded and simulated, electron density at reference height (**e**) and X-ray flux (on the right axis (**e**)) during the occurrence of two successive SFs on 10 May 2013.

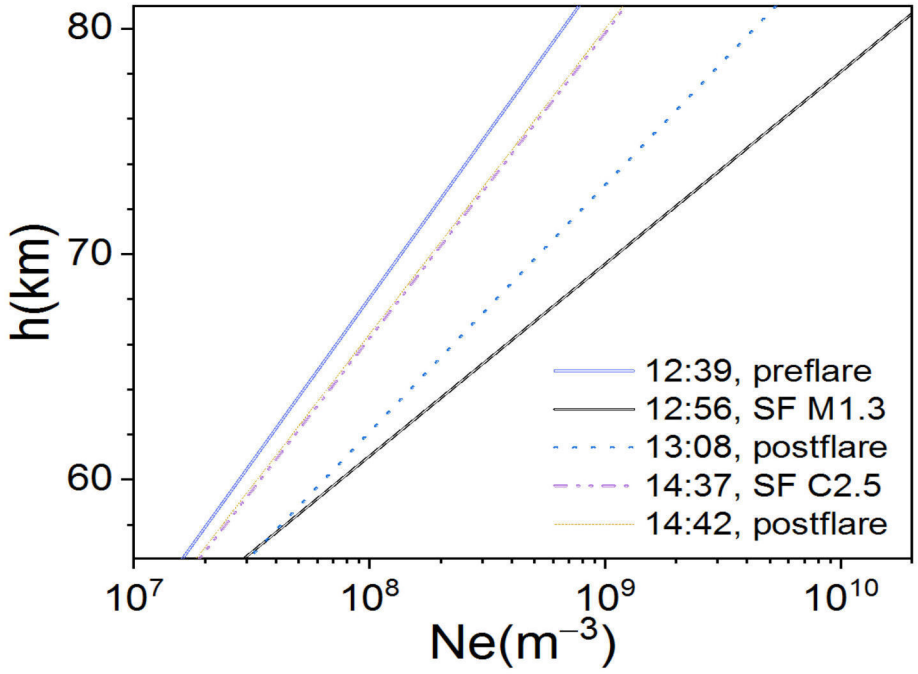

Figure 4. The altitude profile of electron density during two successive SFs on 10 May 2013.

X-ray flux, amplitude, and phase of NAA/24.00 kHz radio signal as a function of UT during strong M-class successive SF on 12 June 2014 is presented in Figure 5. The lower panel shows perturbation of amplitude and X-ray flux, and in the upper panel perturbation of phase and X-ray flux is presented. We analysed two successive M-class solar flares (M1.8 with peak time 09:37 UT and M2.7 with peak time 10:21 UT). There were visible changes in the VLF daily signal during the duration of M1.8 SF and M2.7 SF. SID amplitude and phase changes at the peak time of SF of M1.8 and M2.7 SF classes are ΔA = 4.5 dB, ΔP = 51.47 deg and ΔA = 5.72 dB, ΔP = 83.01 deg, respectively (see Table 1 and Figure 6c,d).

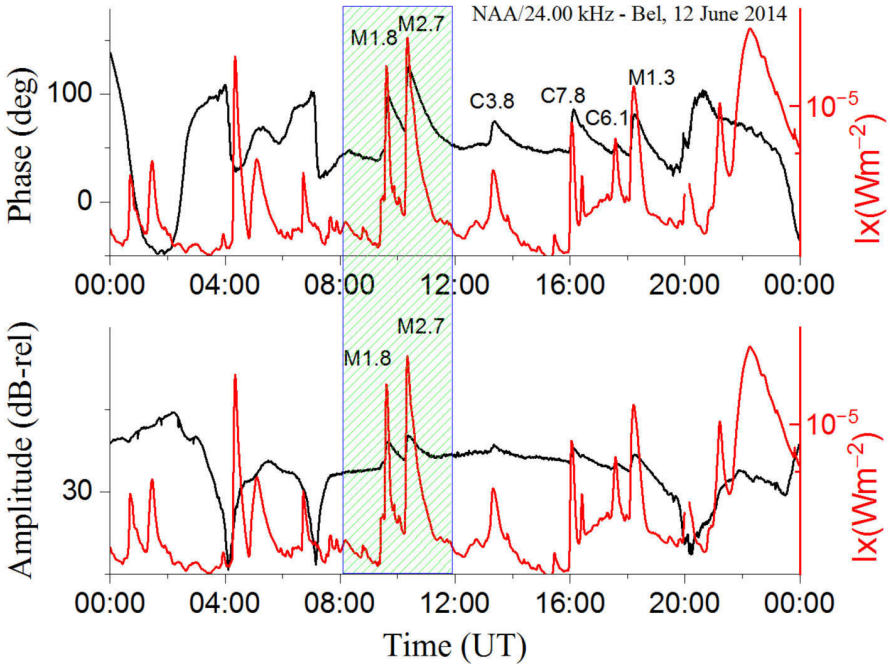

Figure 5. X-ray flux, amplitude, and phase of NAA signal during strong successive flares on 12 June 2014. (Lower panel) Amplitude and X-ray flux variation; (Upper panel) phase and X-ray flux variation.

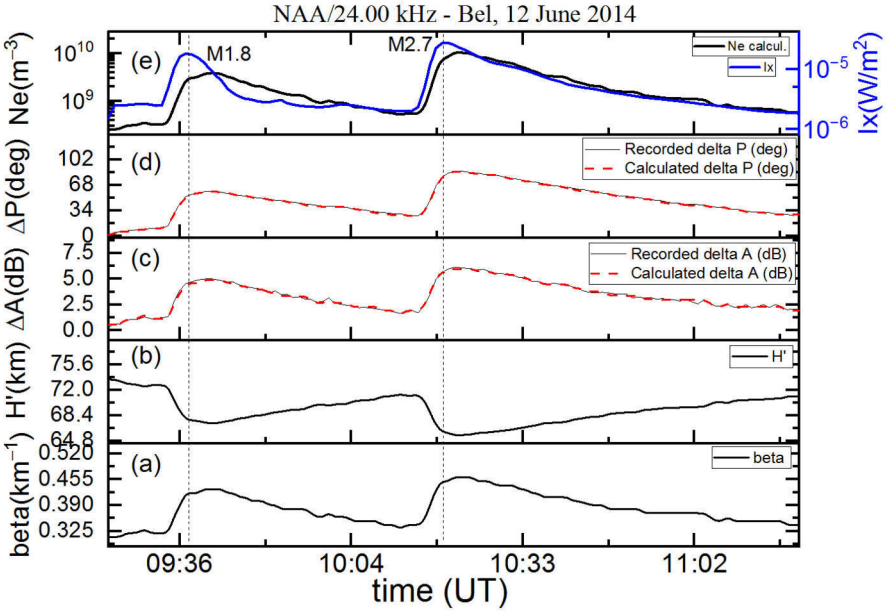

Figure 6. Variations of the sharpness β (**a**), effective reflection height H' (**b**), VLF amplitude (**c**) and phase (**d**) recorded and simulated, reference height electron density (**e**) and X-ray flux (on the right axis (**e**)), during the occurrence of two successive M-class SFs on 12 June 2014.

Sharpness β, effective reflection height H', amplitude and phase of VLF signals (recorded and simulated), electron density at reference height, and X-ray flux during the presence of two M flares on 12 June 2014 are presented in Figure 6 on the upper to lower panels, respectively.

For the period around SF on 12 June 2014, we have calculated the time-dependent effective reflection height and sharpness as shown in Figure 6b,a. Generally, as in previous example, the shape of H' and β are in correlation with solar X-ray flux. During occurrences of M1.8- and M2.7-class SFs on 12 June 2014, the changes of H' during time have a normal nature. H' lowers in intensity to a minimum after SFs beginning and it rises to a preflare value after X-ray flux peaks. The structure of β is correlated with the amplitude shape. At the time of this SF, it rose quickly to a maximum after the SF peak time and then collapsed to preflare size. At peak time of the M1.8-class SF, (I_x = 1.81·10^{-5} Wm^{-2}), H' lowers to a value of 67 km and β rises to 0.42 km^{-1}. At peak time 10:21 UT during M2.7-class SF with flux I_x = 2.7·10^{-5} Wm^{-2}, the H' decreases to 65 km and the sharpness increases to 0.46 km^{-1}.

The N_e at reference height is also in correlation with the intensity and shape of X-ray flux during the analysed time period (see Figure 6e).

Figure 7 presents the values of simulated amplitude and phase of the NAA signal along the GCP distance, obtained for quiet and disturbed ionospheric state during SFs on 12 June 2014. The simulations of propagation were performed using LWPC code. Amplitude and phase values of NAA signal proportionally increase with increasing X-ray intensity along the whole path. During the initial and main phase of the SID event, the signal variations are more frequent. SID events in the D-region are most noticeable as changes in the phase of VLF radio signals.

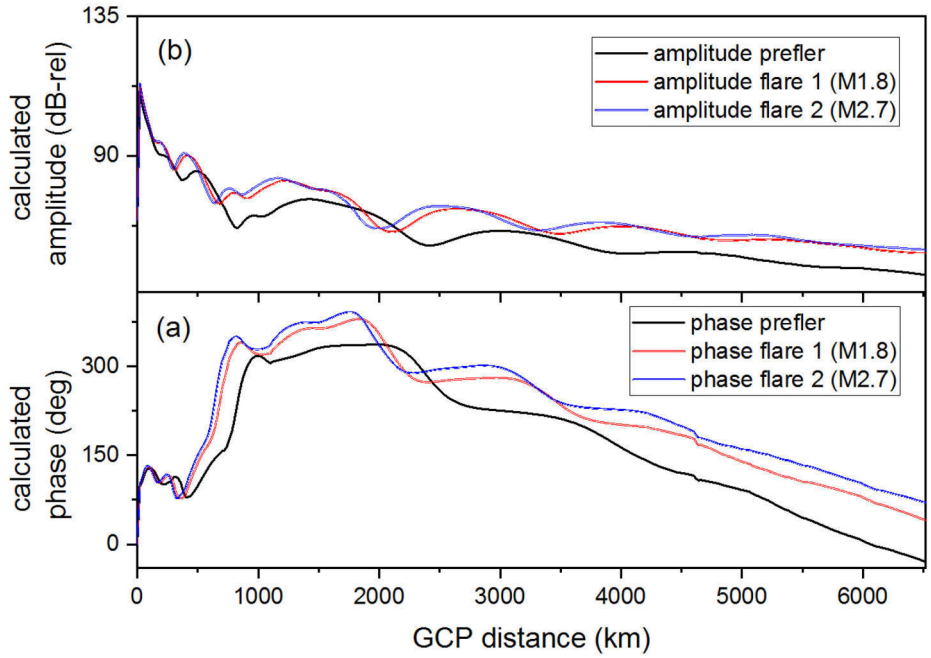

Figure 7. The phase (**a**) and amplitude (**b**) of the NAA/24.0 kHz signal along the GCP distance from Maine, USA, to BEL VLF station, Belgrade, obtained for quiet and disturbed ionospheric state during SFs on 12 June 2014.

The height profile, i.e., vertical N_e density profile before, after and during the M1.8- and M2.7-class solar flares on 12 June 2014 are shown in Figure 8. For unperturbed (preflare) conditions (black dashed line), one can see a slow increment of N_e (from 3.2·10^7 m^{-3} at 60 km height, to about 9.7·10^8 m^{-3} at 80 km height). Different slopes have a pink line and dashed red lines (at peak times of M-class SFs), with an increment from ~6·10^7 m^{-3} and ~1.2·10^8 m^{-3} at 60 km height to 1.45·10^{10} m^{-3} and 5·10^{10} m^{-3} at 80 km height, respectively.

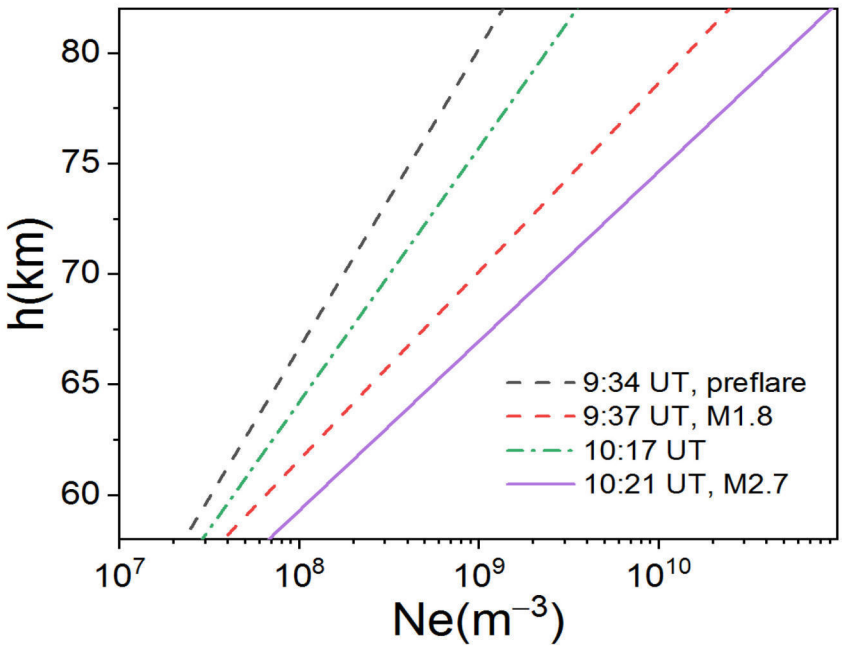

Figure 8. The altitude profile of electron density during two successive M-class SFs on 12 June 2014.

Strong SF: In order to cover the whole I_x spectral range needed for further analysis, we studied X-class solar flares with flux $\geq 10^{-4}$ Wm^{-2}. Figure 9 presents the values of the monitored and simulated excess of amplitude and phase of the NAA signal simultaneously with X-ray flux during SF on 11 June 2014. Measured and simulated signal values are in good agreement, i.e., almost identical. Barely visible differences are at the right corner of the figure, i.e., during relaxation time and the end of SF.

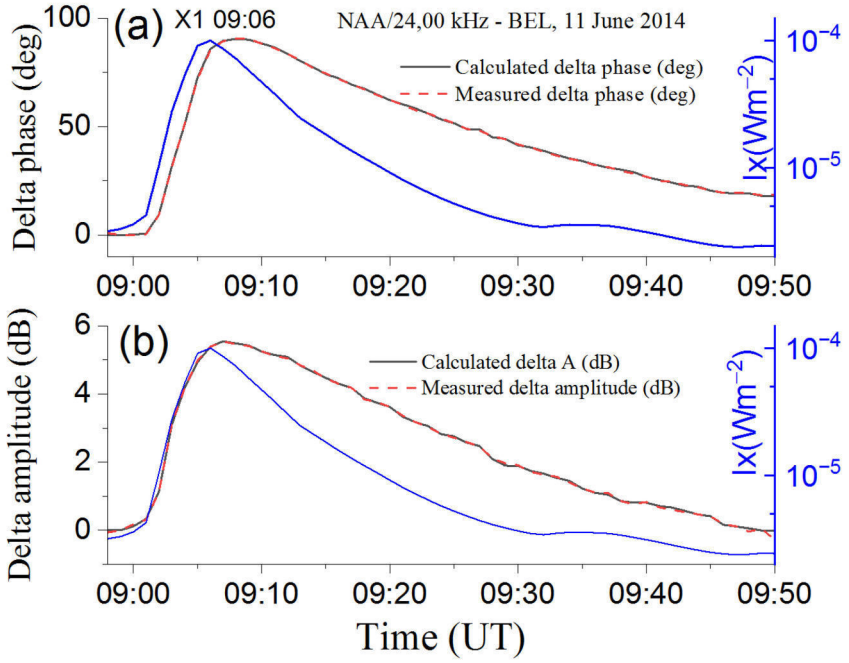

Figure 9. Time variation of X-ray irradiance (on the right axes), NAA/24.00 kHz signal phase (**a**) and amplitude (**b**) enhancement during M1.0 (09:06 UT) events on 11 June 2014.

Additionally, amplitude and phase values of NAA signal proportionally increase with increasing X-ray intensity, and during relaxation time (right wings of signal) amplitude

values decrease more slowly than the flux due to ionosphere sluggishness. For the period around SF on 11 June 2014, we have calculated the quantities needed for modelling such as the effective reflection height H' and the sharpness β, as shown in lower panels of Figure 10. One can see that the time profile, i.e., shape of reflection height and the sharpness are in correlation with X-ray flux. More precisely, β has almost the same form as I_x but shifted by Δt, while H' has a reverse shape.

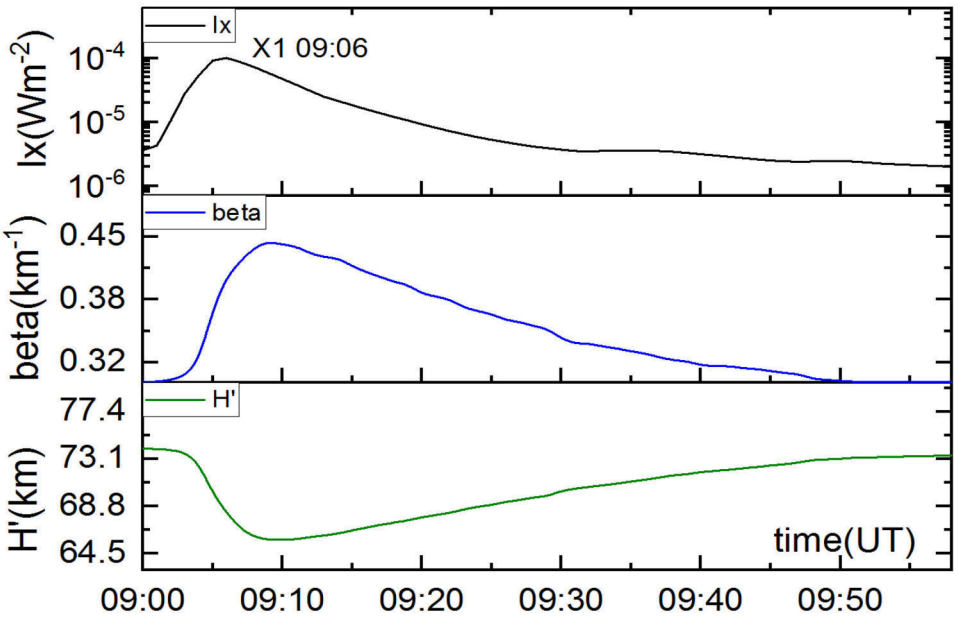

Figure 10. Variations in the effective reflection height H', sharpness β and X-ray irradiance during the occurrence of SF on 11 June 2014 are shown in panels from lower to upper, respectively.

3.2. Approximative Expressions and Simulations

Nowadays, more complicated methods and formulas exist and can be used in this field of science [27,33,34]. They are mostly related to calm conditions in the ionosphere, but still they are also used for perturbed conditions. However, the question arises of how easy some of them are for use and whether they are applicable when speed of analysis and obtaining products are important. The idea is to make the formula easy to use as well as to enable rapid calculations and analysis, such as for example the IRI model—the international standard empirical model for the terrestrial ionosphere [35,36].

In order to create an easier and more adequate use of the results and data, here we introduce the electron-density expression:

$$\log Ne(h, Ix(t), t + \Delta t) = \begin{cases} \sum_{i=0}^{2} a_i(h) \cdot (\log(I_x^{\max}))^i, \quad t \le t_{Ix^{\max}} \quad \text{a)} \\ y0 + (2 * A/pi) * (w/(4 * (t - xc)^2 + w^2)), \quad t > t_{Ix^{\max}} \quad \text{b)} \end{cases} \tag{4}$$

where, t_{Imax} is time of maximum of X-ray flux (Wm^{-2}) and h is height (km), Δt is time delay defined earlier in the text and $a_i(h)$ represents height-dependent dimensionless coefficients. Here, $y0 + (2 * A/pi) * (w/(4 * (t - xc)^2 + w^2))$ is Lorentzian function. Equation (4) gives more than satisfactory results when simplified (which was our intention to make it easy to use), i.e., when (4a) is valid for the whole time interval. Consequently, instead of whole Equation (4) we can use a simple logarithmic second-degree polynomial expression for theentire time interval, with height-dependent coefficients:

$$\log Ne(h, Ix(t), t + \Delta t) = \sum_{i=0}^{2} a_i(h) \cdot (\log(I_x^{\max}))^i \tag{5}$$

Height-dependent coefficients $a_i(h)$ can be found in the Github project. Compared to paper [37], here for the first time we introduce Δt and improve the expression by taking into account the delay time of the ionosphere response, making it more physical.

Time delay Δt in min can be presented (we use it further in the investigation) by linear dependence on the logarithm of X-ray flux (see, e.g., Figure 11)

$$\Delta t = \sum_{i=0}^{1} c_i \cdot (\log(I_x^{\max}))^i \text{ [min]} \quad (6)$$

where dimensionless quantities take values $c_0 = 0.45385$ and $c_1 = -0.44863$ and $I_x{}^{\max}$ is X-ray flux at peak time in [Wm^{-2}]. Further in the investigation we will use expression (6), which can be additionally corrected by inserting various influences. Of course, a more sophisticated formula might have been developed, but such precision was unnecessary since the values of the D-region parameters are known to fluctuate by an order of magnitude. The goal was to make the formula simple to use while also allowing for quick calculations and analysis.

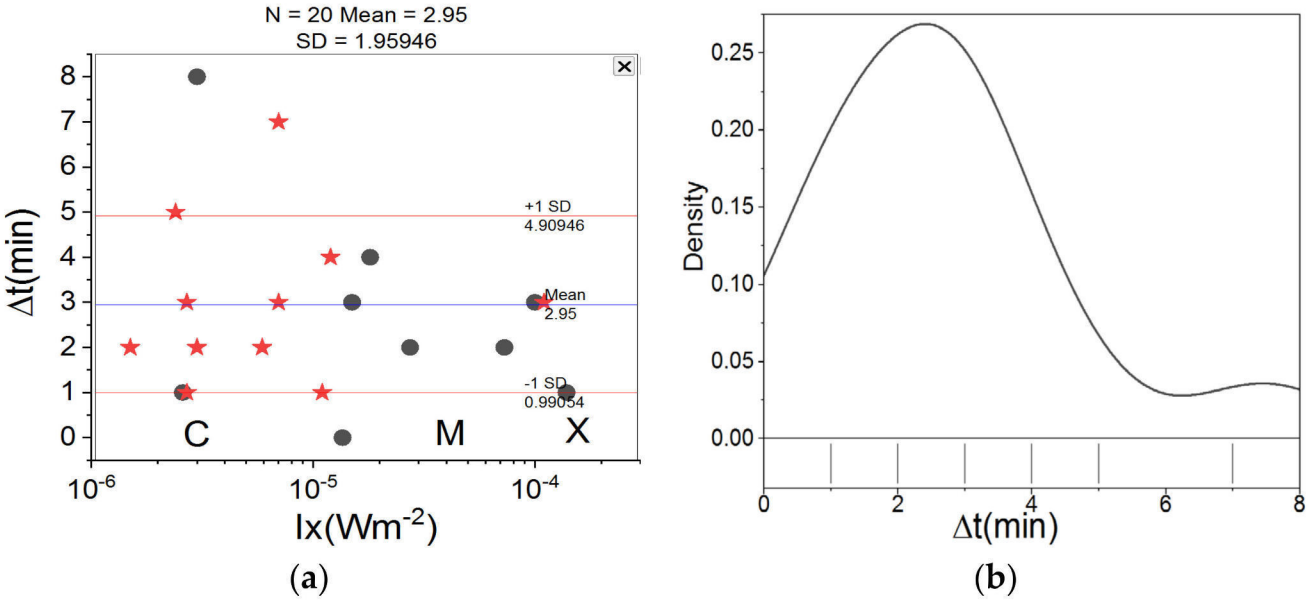

Figure 11. (**a**) The time delay Δt between the VLF amplitude max and the peak of SF X-ray flux as a function of peak flux (black circles are data from present investigation, red stars data from [27]; (**b**) Distribution of Δt data points (a rug plot).

In Figure 11a, we present values of obtained time delay Δt between the X-ray flux and the VLF amplitude as a function of peak flux. Black circles are data from present work and red stars are data from [27], obtained under the same conditions, i.e., with the same equipment and for the same transmitter–receiver path. Additionally, in Figure 11b we provide the distribution of Δt data points—a rug plot. The time delay between the X-ray flux and the VLF amplitude maximum Δt has a mean value of about 3 min. For C-class SFs, Δt is more scattered and has the highest variation, and for the larger values of flux I_x (M- and X-class SFs), the increase is the smallest.

From Figure 6 of the paper by Hayes et al. [38], one can see that presented data are scattered, even more so than in our case, with Δt up to 10 min and with a mean value of about two minutes, which is in accordance with our results. From Figure 11b (see rug plot), we certainly have the largest grouping between 1–4 min, which is also the case with the results of Hayes et al. [38] i.e., the results are in accordance. Certainly, there are other results in the literature such as from the paper of Basak & Chakrabarti [39], but our results and also the recent findings of Hayes et al. [38] differ from findings of Basak & Chakrabarti, which surely does not affect the main goal of the present work.

The conclusion is that the maximum of the signal, and consequently the electron density, is shifted by an average value of three minutes in relation to the maximum of the flux during the flare event due to ionosphere sluggishness. In addition, detailed statistics could have been performed but the main goal was to obtain a useful and easy to use expression for N_e.

Variation in X-ray flux (upper panel), measured by GOES-15, and N_e (h = 74 km) as a function of UT during two successive flares on 12 June 2014 (lower panel) are presented in Figure 12. The red line in the lower panel shows results acquired by approximative Equation (5). The circles present values of electron density N_e obtained in this research by the method mentioned above using Equation (3). One can see that the results are in good agreement except the post-flare wings (N_e shape is more stretched). It can be noted that due to the sluggishness of the ionosphere, the shape of electron density over time does not totally follow the solar flux shape and it returns more slowly (post-flare wings) to a calm state due to the D-region relaxation time.

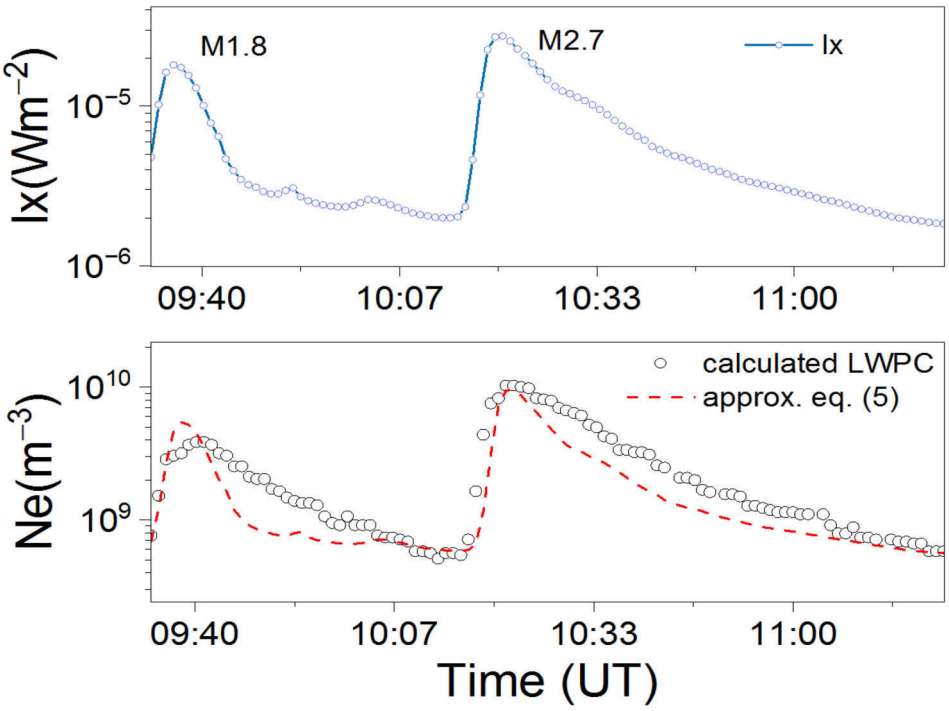

Figure 12. X-ray flux from GOES-15, and N_e (h = 74 km) as a function of UT during two M-class SFs on 12 June 2014. The dashed red line shows results acquired by approximative Equation (5). N_e obtained by the above-mentioned method is presented by circles.

In [29], the database contains parameters β and H' for different values of I_x, i.e., different classes of solar flares (during the period of ascending phase and maximum of the solar cycle 24 and 25). Solar flares are monitored and analysed by VLF technique and parameters β and H' in database are obtained by method described in [20]. In https://github.com/sambolino/flarED (accessed on 19 September 2021) [29] for the input values of solar X-ray flux, Wait's parameters β and H' can be evaluated and altitude values of electron density for the low terrestrial ionosphere can be calculated.

Figure 13 presents a scatter plot of a pair of D-region parameters, H' and β, for SID cases analysed in this study together with data obtained using methods from [29]. Calculated parameters H' and β are in the range of 60–74 km and 0.30–0.60 km^{-1}, respectively. Black circles represent data from present work and red circles are related to the data obtained using the flared method (see Section 2.2.2). In the bottom right corner (for M- and X-classes of SF) data are more scattered.

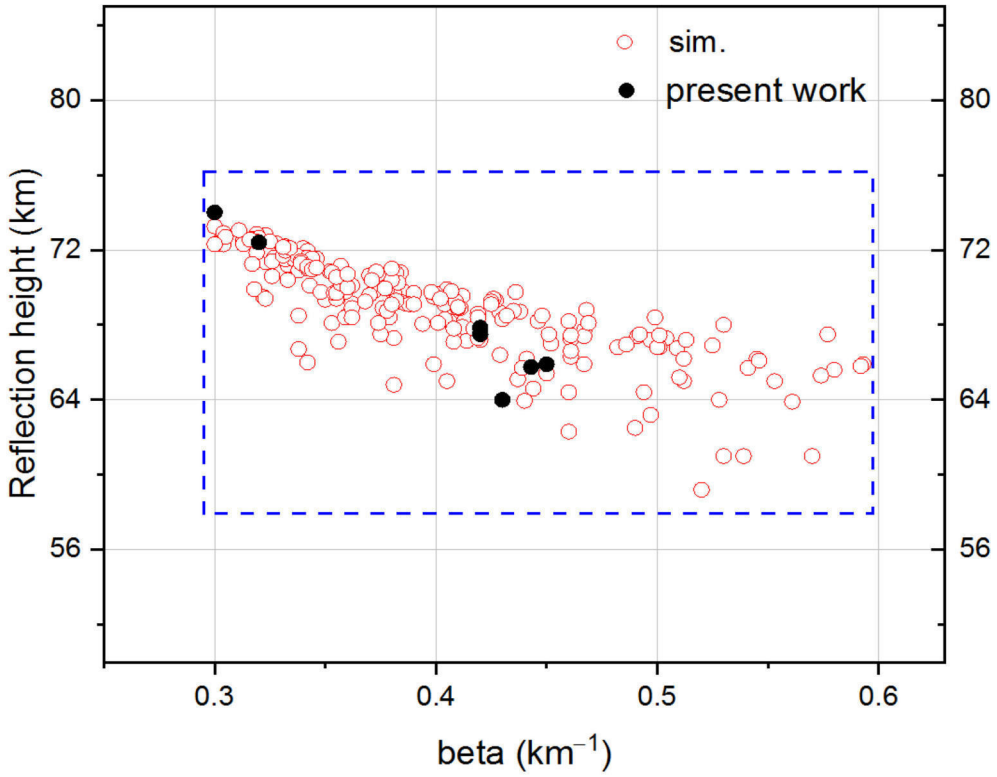

Figure 13. A scatter plot of a pair of D-region parameters, i.e., H' versus β, is shown for SID cases analysed in this study using LWPC and two-component exponential model together with ones obtained using flared method from Github project [29].

3.3. Comparison of Results

In Figure 14, we present the results from this investigation, i.e., paper (using three methods from Sections 2.2.1–2.2.3), which are either simulated, calculated, approximated or the data obtained from literature [16,37,40–42], for electron density N_e at reference height as a function of X-ray flux. The area of importance is between the two red lines. It can be noticed that the results differ from each other in some cases by an order of magnitude or more. Although the data are scattered, especially for stronger flares (right side of the graph), they still tend to increase with the intensity of the X-ray radiation. As noted, our results were acquired on the basis of analysis of SID events on NAA/24.00 kHz signal and using methods described in the text. Electron density at reference height h = 74 km changed from $N_e = 2.16 \times 10^8$ m^{-3} to $N_e > 10^{11}$ m^{-3}. Additionally, we compared data with the N_e data obtained using approximate Equation (5) (plus sign in Figure 14) and simulations (black star) using the flared method. The results are in fair agreement with previous studies. We can conclude that measurements over a long path give slightly higher slope, i.e., lower values of electron density than expected, but are quite satisfactory. This is important because most results concerning investigation in the D-region are scattered and vary in order of magnitude and we need to take into account all the data and correct the existing ones. During SIDs the time profile of electron density follows the solar X-ray flux variation.

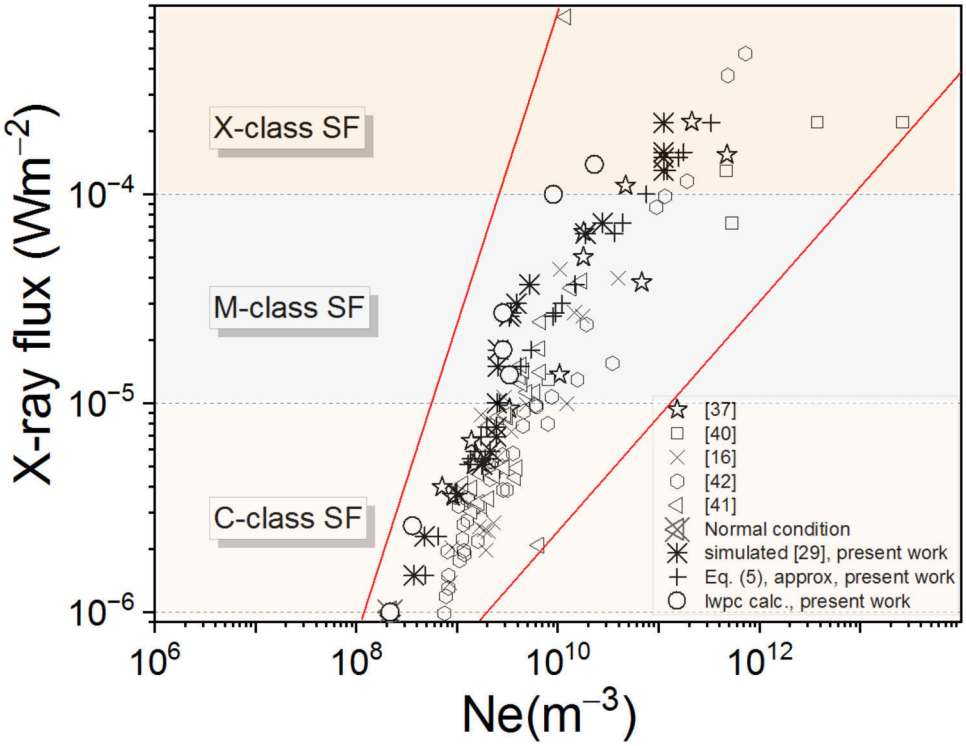

Figure 14. Electron-density data (calculated, simulated and approximated) at reference height h = 74 km and maximum of I_x flux during occurrence of different class SFs. The data are compared with results from [16,37,40–42]. Area of importance is between the two red lines.

4. Conclusions and Perspectives

In this paper we analysed SF events with extreme radiation in the X-spectral range. The perturbed VLF data were collected by monitoring the NAA/24.00 kHz VLF signal (transmitted in Maine, USA and then received in Belgrade, with GCP = 6540 km) and used together with GOES satellite data. The magnitude of impact of SFs on D-region and the consequences of these explosive events were analysed using measurements over a long path. The amplitude and phase data and ionosphere parameters during the enhancements of radiation due to the SF obtained in our study, are presented.

The GCP from the NAA transmitter to the Belgrade receiver is about 6540 km long and characterized as a long, dominantly sea path, and we studied cases when it is entirely sunlit. The data obtained here demonstrate the advantages of using these long-path measurements due to stable form of phase and amplitude variation caused by SID in contrast to the VLF perturbations on the short path which display more complexity and oscillations, including decreases and increases depending on the flare intensity. This is very important during the modelling process.

Furthermore, we conclude that the intensity of amplitude and phase perturbations on VLF kHz signal over a long path is in correlation with the size and shape of X-ray flux. This is in line with previous studies. The most effective influence on the enhancement of the ionization rate in the D-region during the observed SFs is due to the increased intensity of spectral lines in the X-ray spectra. Moreover, X-ray SFs with larger line intensities produce a larger increase in electron density. The computation was applied, and we obtained coefficients, i.e., sharpness, reflection height, and time delay needed for modelling this medium under increased radiation in the X-spectral range. One can notice that the intensified solar radiation in the X-spectral range changes D-region parameters and conducts an enhanced production rate, consequently deforming the VLF signal. The dependence of electron density on X-ray flux has slightly lower slope but is in fair agreement with previous studies.

The present manuscript offers an extension of the electron-density modeling in the daytime, SF-perturbed D-region of the ionosphere already introduced in [37]. In particular, the extension includes time delays from ionospheric sluggishness in N_e modeling, making use of data over a long GC path that ensures enhanced stability of SID-induced variations in phase and amplitude shape. The construction of the associated flarED GitHub project is designed to be easily applicable.

Moreover, we introduce novel methods and provide a simple, modified expression for N_e as a function of I_x, valid for unperturbed and perturbed conditions. We develop the expression by taking into account the delay time of the ionosphere response, making it more physical. The analysis and software are provided on GitHub under the MIT license.

In addition, the observed increase in the atmospheric aerosol number density after the event of SFs in February and March 2011, as well as high-level cloud formation in the upper atmosphere, reveal the importance of further investigation of SF and possible influence on particle-electrification mechanisms [43–45]. Recent studies [46] have introduced reconsideration of atmospheric aerosol–electricity interactions, which could improve theoretical understanding and simulations of the aerosol lifecycle, opening new horizons for weather and climate science. Future research will focus on a multidiscipline approach, investigating solar–geomagnetic activity effects on aerosol particles and on radiative transfer.

Author Contributions: Conceptualization, V.A.S. and D.M.Š.; writing—original draft preparation, V.A.S., Z.R.M.; writing—review and editing, V.A.S., D.M.Š., V.V., Z.R.M.; supervision, L.M.I. All authors have read and agreed to the published version of the manuscript.

Funding: This work was funded by the Institute of Physics Belgrade and University Union—Nikola Tesla Belgrade, through a grant by the Ministry of Education and Science of the Republic of Serbia. This article/publication is based upon work from COST Action CA17126—Towards understanding and modelling intense electronic excitation (TUMIEE), supported by COST (European Cooperation in Science and Technology).

Institutional Review Board Statement: Not applicable.

Informed Consent Statement: Not applicable.

Data Availability Statement: New dataset from this study is publicly available as well as python functions for calculating ionosphere parameters on GitHub: https://github.com/sambolino/flarED (accessed on 10 October 2021). Publicly available datasets were analysed in this study and can be found at https://satdat.ngdc.noaa.gov/sem/goes/data/avg (accessed on 2 September 2021).

Acknowledgments: We would like to express our appreciation to Ognyan Kounchev and Magdalena Christova for the shown attention to this paper and for a fruitful dialogue.

Conflicts of Interest: The authors declare no conflict of interest. The funders had no role in the design of the study; in the collection, analyses, or interpretation of data; in the writing of the manuscript, or in the decision to publish the results.

References

1. Bothmer, V.; Daglis, I.A. *Space Weather: Physics and Effects*; Springer Science & Business Media: Berlin/Heidelberg, Germany, 2007.
2. Smith, H.J.; Smith, E.V.P. *Solar Flares*; Macmillan: New York, NY, USA, 1963.
3. Davidson, B. *Weatherman's Guide to the Sun*, 3rd ed.; Space Weather News, LLC.: New York, NY, USA, 2020.
4. Doschek, G.; Meekins, J.; Cowan, R.D. Spectra of solar flares from 8.5 Å to 16 Å. *Sol. Phys.* **1973**, *29*, 125–141. [CrossRef]
5. Tandberg-Hanssen, E.; Emslie, A.G. *The Physics of Solar Flares*; Cambridge University Press: Cambridge, UK, 2009.
6. Reames, D.V.; Murdin, P. Solar Wind: Energetic Particles. *Encycl. Astron. Astrophys.* **2002**, *2312*, 1–122.
7. Tandon, J.; Deshpande, S.; Bhatia, V. Electromagnetic radiation from solar flares. *Nature* **1968**, *220*, 1213–1214. [CrossRef]
8. Brasseur, G.P.; Solomon, S. Composition and chemistry. In *Aeronomy of the Middle Atmosphere: Chemistry and Physics of the Stratosphere and Mesosphere*; Springer: Berlin/Heidelberg, Germany, 2005; pp. 265–442.
9. Nina, A.; Čadež, V.; Srećković, V.; Šulić, D. The influence of solar spectral lines on electron concentration in terrestrial ionosphere. *Open Astron.* **2011**, *20*, 609–612. [CrossRef]
10. Valnicek, B.; Ranzinger, P. X-ray emission and D-region "sluggishness". *Bull. Astron. Inst. Czechoslov.* **1972**, *23*, 318.
11. Bain, W.C.; Hammond, E. Ionospheric solar flare effect observations. *J. Atmos. Sol. Terr. Phys.* **1975**, *37*, 573–574. [CrossRef]

12. Brasseur, G.P.; Solomon, S. Radiation. In *Aeronomy of the Middle Atmosphere: Chemistry and Physics of the Stratosphere and Mesosphere*; Springer: Berlin/Heidelberg, Germany, 2005; pp. 151–264.
13. Mitra, A.P. *Ionospheric Effects of Solar Flares*; Springer: Berlin/Heidelberg, The Netherlands, 1974. [CrossRef]
14. Nicolet, M.; Swider, W., Jr. Ionospheric conditions. *Planet. Space Sci.* **1963**, *11*, 1459–1482. [CrossRef]
15. Garcia, H.A. Temperature and emission measure from GOES soft X-ray measurements. *Sol. Phys.* **1994**, *154*, 275–308. [CrossRef]
16. Grubor, D.; Šulić, D.; Žigman, V. Classification of X-ray solar flares regarding their effects on the lower ionosphere electron density profile. *Ann. Geophys.* **2008**, *26*, 1731–1740. [CrossRef]
17. Wang, X.; Chen, Y.; Toth, G.; Manchester, W.B.; Gombosi, T.I.; Hero, A.O.; Jiao, Z.; Sun, H.; Jin, M.; Liu, Y. Predicting solar flares with machine learning: Investigating solar cycle dependence. *Astrophys. J.* **2020**, *895*, 3. [CrossRef]
18. Kelley, M.C. *The Earth's Ionosphere: Plasma Physics and Electrodynamics, ser. International Geophysics*, 2nd ed.; Academic Press: Cambridge, MA, USA, 2009.
19. Wah, W.P.; Abdullah, M.; Hasbi, A.M.; Bahari, S.A. Development of a VLF receiver system for sudden ionospheric disturbances (SID) detection. In Proceedings of the 2012 IEEE Asia-Pacific Conference on Applied Electromagnetics (APACE), Melaka, Malaysia, 11–13 December; pp. 98–103.
20. Šulić, D.; Srećković, V.; Mihajlov, A. A study of VLF signals variations associated with the changes of ionization level in the D-region in consequence of solar conditions. *Adv. Space Res.* **2016**, *57*, 1029–1043. [CrossRef]
21. Volland, H. On the solar flare effect of vlf-waves in the lower ionosphere. *J. Atmos. Sol.-Terr. Phys.* **1964**, *26*, 695–709. [CrossRef]
22. Šulić, D.; Srećković, V. A comparative study of measured amplitude and phase perturbations of VLF and LF radio signals induced by solar flares. *Serb. Astron. J.* **2014**, *188*, 45–54. [CrossRef]
23. Ferguson, A.J. *Computer Programs for Assessment of Long-Wavelength Radio Communications, Version 2.0: User's Guide and Source Files*; Space and Naval Warfare Systems Center: San Diego, CA, USA, 1998.
24. LWPC. Computer Programs for Assessment of Long-Wavelength Radio Communications, V2.1. 2018. Available online: https://github.com/space-physics/LWPC (accessed on 30 June 2021).
25. Nina, A.; Čadež, V.; Srećković, V.; Šulić, D. Altitude distribution of electron concentration in ionospheric D-region in presence of time-varying solar radiation flux. *Nucl. Instrum. Methods Phys. Res. B* **2012**, *279*, 110–113. [CrossRef]
26. Nina, A.; Čadež, V.; Šulić, D.; Srećković, V.; Žigman, V. Effective electron recombination coefficient in ionospheric D-region during the relaxation regime after solar flare from February 18, 2011. *Nucl. Instrum. Methods Phys. Res. B* **2012**, *279*, 106–109. [CrossRef]
27. Žigman, V.; Grubor, D.; Šulić, D. D-region electron density evaluated from VLF amplitude time delay during X-ray solar flares. *J. Atmos. Sol.-Terr. Phys.* **2007**, *69*, 775–792. [CrossRef]
28. Wait, J.R.; Spies, K.P. *Characteristics of the Earth-Ionosphere Waveguide for VLF Radio Waves, Technical Note 300*; US Department of Commerce, National Bureau of Standards: Boulder, CO, USA, 1964.
29. Vujčić, V.; Srećković, V.A. flarED Flare Electron Density. Available online: https://github.com/sambolino/flarED (accessed on 19 September 2021).
30. Da Silva, C.L.; Salazar, S.D.; Brum, C.G.; Terra, P. Survey of electron density changes in the daytime ionosphere over the Arecibo observatory due to lightning and solar flares. *Sci. Rep.* **2021**, *11*, 1–12. [CrossRef]
31. Kolarski, A.; Grubor, D. Sensing the Earth's low ionosphere during solar flares using VLF signals and goes solar X-ray data. *Adv. Space Res.* **2014**, *53*, 1595–1602. [CrossRef]
32. Kolarski, A.; Grubor, D. Comparative analysis of VLF signal variation along trajectory induced by X-ray solar flares. *J. Astrophys. Astron.* **2015**, *36*, 565–579. [CrossRef]
33. Nina, A.; Nico, G.; Mitrović, S.T.; Čadež, V.M.; Milošević, I.R.; Radovanović, M.; Popović, L.Č. Quiet Ionospheric D-Region (QIonDR) Model Based on VLF/LF Observations. *Remote Sens.* **2021**, *13*, 483. [CrossRef]
34. Palit, S.; Basak, T.; Mondal, S.; Pal, S.; Chakrabarti, S. Modeling of very low frequency (VLF) radio wave signal profile due to solar flares using the GEANT4 Monte Carlo simulation coupled with ionospheric chemistry. *Atmos. Chem. Phys.* **2013**, *13*, 9159–9168. [CrossRef]
35. Sezen, U.; Gulyaeva, T.L.; Arikan, F. Online international reference ionosphere extended to plasmasphere (IRI-Plas) model. In Proceedings of the 2017 XXXIInd General Assembly and Scientific Symposium of the International Union of Radio Science (URSI GASS), Montreal, QC, Canada, 19–26 August 2017; pp. 1–4.
36. Bilitza, D.; Altadill, D.; Truhlik, V.; Shubin, V.; Galkin, I.; Reinisch, B.; Huang, X. International Reference Ionosphere 2016: From Ionospheric Climate to Real-Time Weather Predictions. *Space Weather.* **2017**, *15*, 418–429. [CrossRef]
37. Srećković, V.A.; Šulić, D.M.; Ignjatović, L.; Vujčić, V. Low Ionosphere under Influence of Strong Solar Radiation: Diagnostics and Modeling. *Appl. Sci.* **2021**, *11*, 7194. [CrossRef]
38. Hayes, L.A.; O'Hara, O.S.; Murray, S.A.; Gallagher, P.T. Solar Flare Effects on the Earth's Lower Ionosphere. *Sol. Phys.* **2021**, *296*, 1–17. [CrossRef]
39. Basak, T.; Chakrabarti, S.K. Effective recombination coefficient and solar zenith angle effects on low-latitude D-region ionosphere evaluated from VLF signal amplitude and its time delay during X-ray solar flares. *Astrophys. Space Sci.* **2013**, *348*, 315–326. [CrossRef]
40. Gavrilov, B.; Ermak, V.; Lyakhov, A.; Poklad, Y.V.; Rybakov, V.; Ryakhovsky, I. Reconstruction of the Parameters of the Lower Midlatitude Ionosphere in M-and X-Class Solar Flares. *Geomagn. Aeron.* **2020**, *60*, 747–753. [CrossRef]

41. Pandey, U.; Singh, B.; Singh, O.; Saraswat, V. Solar flare induced ionospheric D-region perturbation as observed at a low latitude station Agra, India. *Astrophys. Space Sci.* **2015**, *357*, 1–11. [CrossRef]
42. Thomson, N.R.; Clilverd, M.A. Solar flare induced ionospheric D-region enhancements from VLF amplitude observations. *J. Atmos. Sol.-Terr. Phys.* **2001**, *63*, 1729–1737. [CrossRef]
43. Avakyan, S. Supramolecular physics of the solar-troposphere links: Control of the cloud cover by solar flares and geomagnetic storms. In Proceedings of the 11th Intl School and Conference "Problems of Geocosmos", St. Petersburg, Russia, 3–7 October 2016; pp. 187–191.
44. Goncharenko, Y.V.; Kivva, F. Evaluation of Size of the Atmospheric Aerosol Particles in the Reflecting Layers Occurring after Intense Solar Flares. *Telecommun. Radio Eng.* **2003**, *59*, 1–6.
45. McGrath-Spangler, E.L.; Denning, A.S. Global seasonal variations of midday planetary boundary layer depth from CALIPSO space-borne LIDAR. *J. Geophys. Res.* **2013**, *118*, 1226–1233. [CrossRef]
46. Mallios, S.A.; Daskalopoulou, V.; Amiridis, V. Orientation of non spherical prolate dust particles moving vertically in the Earth's atmosphere. *J. Aerosol. Sci.* **2021**, *151*, 105657. [CrossRef]

applied sciences

MDPI

Article

Response of the Earth's Lower Ionosphere to Solar Flares and Lightning-Induced Electron Precipitation Events by Analysis of VLF Signals: Similarities and Differences

Aleksandra Kolarski [1], Vladimir A. Srećković [2] and Zoran R. Mijić [2,*]

[1] Technical Faculty Mihajlo Pupin, University of Novi Sad, Đure Đakovića bb, 23000 Zrenjanin, Serbia; aleksandra.kolarski@tfzr.rs
[2] Institute of Physics Belgrade, University of Belgrade, Pregrevica 118, 11080 Belgrade, Serbia; vlada@ipb.ac.rs
* Correspondence: zoran.mijic@ipb.ac.rs

Abstract: The lower ionosphere influences the propagation of electromagnetic (EM) waves, satellite and also terrestrial (anthropic) signals at the time of intense perturbations and disturbances. Therefore, data and modelling of the perturbed lower ionosphere are crucial in various technological areas. An analysis of the lower ionospheric response induced by sudden events during daytime-solar flares and during night-time-lightning-induced electron precipitation was carried out. A case study of the solar flare event recorded on 7 September 2017 and lightning-induced electron precipitation event recorded on 16 November 2004 were used in this work. Sudden events induced changes in the ionosphere and, consequently, the electron density height profile. All data are recorded by Belgrade (BEL) radio station system and the model computation is used to obtain the ionospheric parameters induced by these sudden events. According to perturbed conditions, variation of estimated parameters, sharpness and reflection height differ for analysed cases. Data and results are useful for Earth observation, telecommunication and other applications in modern society.

Keywords: atmosphere; radio signal; disturbances; data; modelling

Citation: Kolarski, A.; Srećković, V.A.; Mijić, Z.R. Response of the Earth's Lower Ionosphere to Solar Flares and Lightning-Induced Electron Precipitation Events by Analysis of VLF Signals: Similarities and Differences. *Appl. Sci.* **2022**, *12*, 582. https://doi.org/10.3390/app12020582

Academic Editor: Amalia Miliou

Received: 25 November 2021
Accepted: 5 January 2022
Published: 7 January 2022

1. Introduction

The ionosphere, as a huge layer of the atmosphere, has physical and chemical properties that depend on the incident radiation and local energetic processes [1,2]. In particular, the lower ionospheric region and the fluctuations of its parameters are very important for human life and many activities on Earth and require continuous measurements, observations and available information [3].

In-situ observations of the lower ionospheric layers are difficult and expensive and, consequently, remote sensing measurements are mainly used for investigating this region [4,5]. High-energy events, triggered from an external source or inside the atmosphere, can induce ionospheric disturbances and as a consequence affect all processes within [6].

For example, during solar flares (SFs) the increase in the ionospheric electron concentration at all altitudes is noticeable. Solar flares are giant explosions on the surface of the Sun when a huge amount of electromagnetic energy is released across the entire electromagnetic spectrum [7]. The enhanced extreme ultraviolet (EUV) radiation is absorbed at higher altitudes ionizing the E (90–150 km above Earth's surface during daytime conditions) and F (160–400 km, same) regions of the ionosphere (see e.g., [8]). During SFs, electromagnetic radiation within soft X-rays in a wavelength range of 0.1–0.8 nm, significantly oversteps the ionization of the Lyman-a spectral line 121.6 nm and cosmic rays, becoming a major source of ionization at a range of altitudes corresponding to the D region (50–90 km, same), causing enhanced ionization and absorption of the EM waves that propagate within the Earth-ionosphere waveguide [9,10]. As a result of radiation effects,

the solar induced ionospheric disturbances and plasma irregularities cause perturbations in the amplitude and phase of radio signals.

Furthermore, some processes create localised areas of increased electron density in the low ionosphere and thus change its properties. Radio waves, generated by atmospheric discharge and propagating along geomagnetic field lines into the plasmasphere, get into transversal cyclotron resonance with energetic electron beams (30–300 keV) moving in the opposite direction. As a consequence of such interaction, electron precipitation into the atmosphere takes place. Electron precipitation produces localised areas of increased electron density in the low ionosphere (on heights corresponding to D–region heights of 50–90 km [11–13]), known as localised ionization enhancement (LIE) [14]. Perturbations in very low frequency (VLF) propagation, known as trimpi events, can be explained by formation of such areas. Classic trimpi events [15] are phase delay and/or amplitude perturbations of VLF signals propagating in the Earth-ionosphere waveguide. Whistlers occur about one second after a corresponding atmospheric discharge and propagate in the magnetosphere along geomagnetic field lines [16]. Electron precipitation, caused by ducted whistlers, is explained in [17]. Since disturbances of VLF signals are a consequence of electron precipitation caused by atmospheric discharges, they are named as lightning-induced electron precipitation events (LEP). In addition to the above-mentioned phenomena, which can be detected as disturbances in VLF propagation, there are a number of other phenomena which can be optically detected in areas above thunderclouds. The formation of ducts of enhanced electroconductivity between thunderclouds and the ionosphere is connected with such phenomena [18–20]. Trimpi perturbations can be simultaneously monitored on multiple adjacent traces of VLF signals. Based on adjacent VLF signals recordings comparison, LIE dimensions and spatial position can be estimated by numerical modelling, depending on the transmitter frequency, VLF signal great circle path (GCP) length and position of LIE in relation to the VLF signal path.

Disturbances in propagation of VLF radio signals at the Belgrade station BEL (located at the Institute of Physics Belgrade (44.85° N, 20.38° E), Serbia) were observed and the model computation is used to obtain the atmosphere parameters induced by these sudden events. According to perturbed conditions, variation of estimated parameters, sharpness and reflection height differ for the analysed cases.

2. Methods

For the examination of the ionospheric composition, altitudes, locations and other properties, experts usually make use of satellites equipped with suitable sensors, GPS, sonde, radars, various optical instruments, or balloons, rocket probes, etc. A widely used technique for remote sensing of the Earth's ionosphere exploits radio signals (e.g., [21–24]), and for altitude range that corresponds to the ionospheric lowest layer, i.e., the D region, VLF radio signal range is preferred (e.g., [25–30]). Remote sensing of the lower ionosphere by utilisation of radio signals in the VLF range is based on the hop wave theory (see, e.g., [31–34]). These techniques are successfully used for exploration of Earth's lower ionosphere's response to a number of processes, with their origin from extra-terrestrial to terrestrial environments (e.g., [35–41]).

The methodology used and results of mid-latitude lower ionosphere diagnostic obtained by this technique, based on VLF radio signals recorded at the Belgrade receiver site, in cases of regular and irregular solar-terrestrial conditions, can be found in, e.g., [23,37,39,42–50]. In our study, at the ionosphere altitudes 50–90 km (D region), measurements rely on radio wave propagation technique, i.e., monitoring of phase and amplitude of VLF radio signals. For this reason, the perturbation of VLF phase delay and amplitude was estimated as a difference between values of the perturbed signal induced by external disturbance and signal in the normal unperturbed conditions. The details are described in the next section.

Used Numerical Model

A standard technique for retrieving ionospheric parameters during sudden ionospheric disturbances (SIDs) is based on comparing the registered amplitude and phase changes with the equal values computed by Long Wavelength Propagation Capability (LWPC) software [51], as interpreted in [9,10]. To determine electron density from recorded amplitude and phase variations, a trial and error procedure can be utilized, with the density profile being changed until the LWPC predicted amplitude and phase matched the monitored data (see, e.g., [42]). As a result, the calculated beta and H' values can be employed in subsequent computations and simulations (e.g., electron gain and electron loss processes coefficient, etc.).

3. Results

3.1. Lower Ionosphere during SF Event

The monitoring and investigation of VLF data has been carried out simultaneously with the examination of the correlative incoming solar X-ray fluxes collected from the Geostationary Operational Environmental Satellite (GOES).

In the presence of SIDs, a standard numerical procedure for the estimation of plasma parameters is based on comparison of the recorded changes of amplitude and phase with the matching values acquired in simulations by the LWPC numerical software package as explained in [9,44,46,47].

We studied data for 7 September 2017, as an example of a day with strong X1.3 class SFs that caused SID and seriously affected the VLF signal. It should be noted that the development to the flux of X-ray lasted almost one hour.

The monitored and simulated changes of amplitude (ΔA) and phase delay (ΔP) compared to normal day-time levels for a signal emitted on frequency 24 kHz from Cutler (44.65° N, 67.30° W), ME, USA, with codename NAA measured at the BEL site is presented in Figure 1. Besides the good agreement between simulated and monitored data, X-ray flux peak and VLF signal perturbation happened synchronously i.e., energetic radiation perturbed the ionosphere which, in turn, caused the activation of disturbances in radio signal.

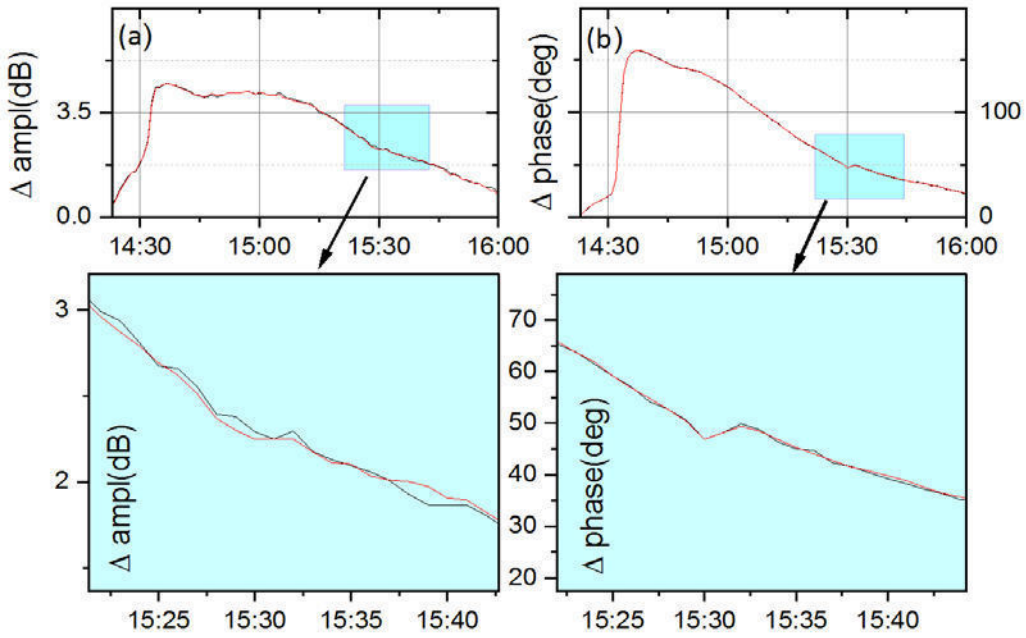

Figure 1. Measured and simulated amplitude (**a**), and phase delay (**b**) excesses of NAA radio signal during X1.3 class SF on 7 September 2017.

Figure 2 presents obtained values of effective reflection height H' and the sharpness β during almost two hours, i.e., during occurrences of SFs on 7 September 2017. During X1.3 class SFs, the shape of reflection height is in anticorrelation and the sharpness is in correlation with X-ray flux.

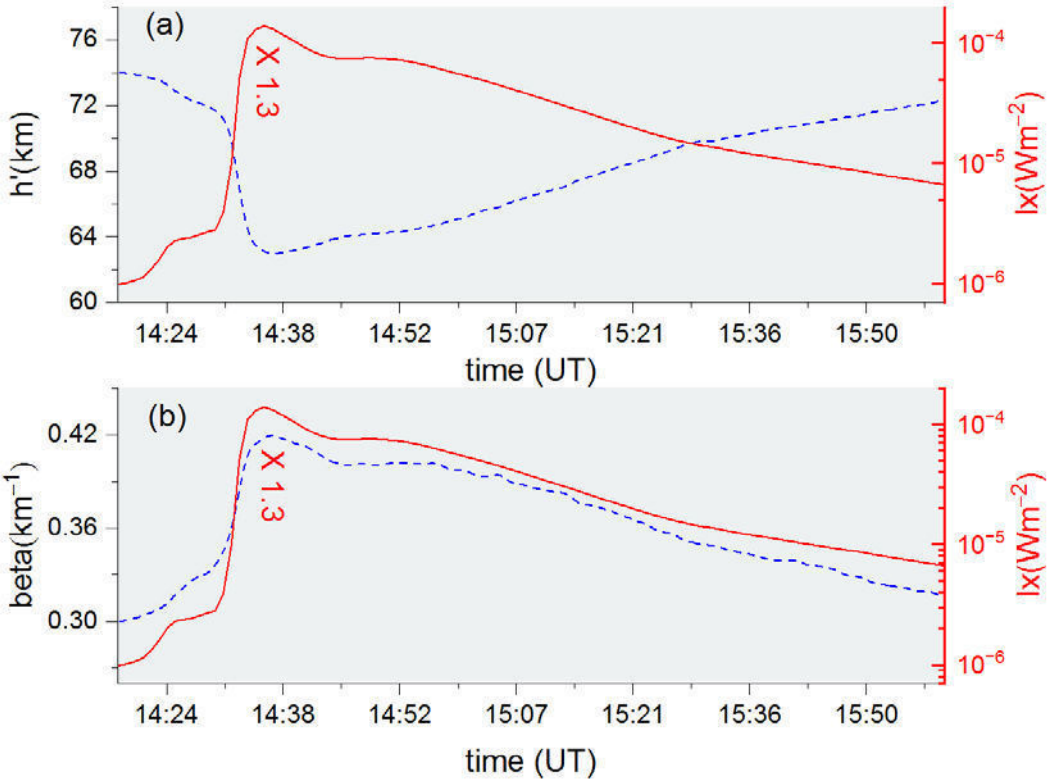

Figure 2. Parameters H' (**a**), and β (**b**) and X-ray flux (right axis) during occurrence of X1.3 class SF on 7 September 2017.

The change of the reflection height is a normal behaviour, i.e., after the beginning of SFs the reflection height decreases to a minimum and after peaks of X-ray flux it rises to the preflare value (see Figure 2a). The shape of sharpness is correlated with the shape of recorded X-ray flux increase. During the X1.3 SF, the sharpness increases to a maximum and after the SF peak (14:36 UT) it decreases to the pre-flare value (Figure 2b). At peak time (14:36 UT), the X-ray flux is $Ix = 1.3 \times 10^{-4}$ Wm^{-2}, and the H' lowers by 13 km to a value H' ~63 km. The sharpness values increase to 0.42 km^{-1} at peak time 14:36 UT on 7 September 2017.

Electron density profile changes can demonstrate the variation in distribution of ionization at the D-layer due to SFs. Figure 3a presents the simultaneous change of X-ray flux, and the corresponding *Ne* (Figure 3b) obtained at reference height 74 km versus UT during occurrence of X1.3 class SF on 7 September 2017. It can be seen that the electron density is in correlation with X-ray flux and, *Ne* increased by almost two orders of magnitude during the X1.3 class SF.

The current study is important because most results concerning investigation in the D-region are scattered and vary in order of magnitude (see [9,23,52,53]), thus it is necessary to take into account all the data and correct the existing data. Sudden events induce changes in the ionosphere and, consequently, the electron density height profile. It is useful to obtain new results by analysing the similarities and differences, especially for case studies, i.e., when solar flares last significantly longer and perturb the ionosphere in a specific way. An additional aim is the simultaneous analysis of the lower ionospheric response and electron density height profile variations in the lower ionosphere induced by sudden events during daytime solar flares and during night-time lightning-induced electron precipitation.

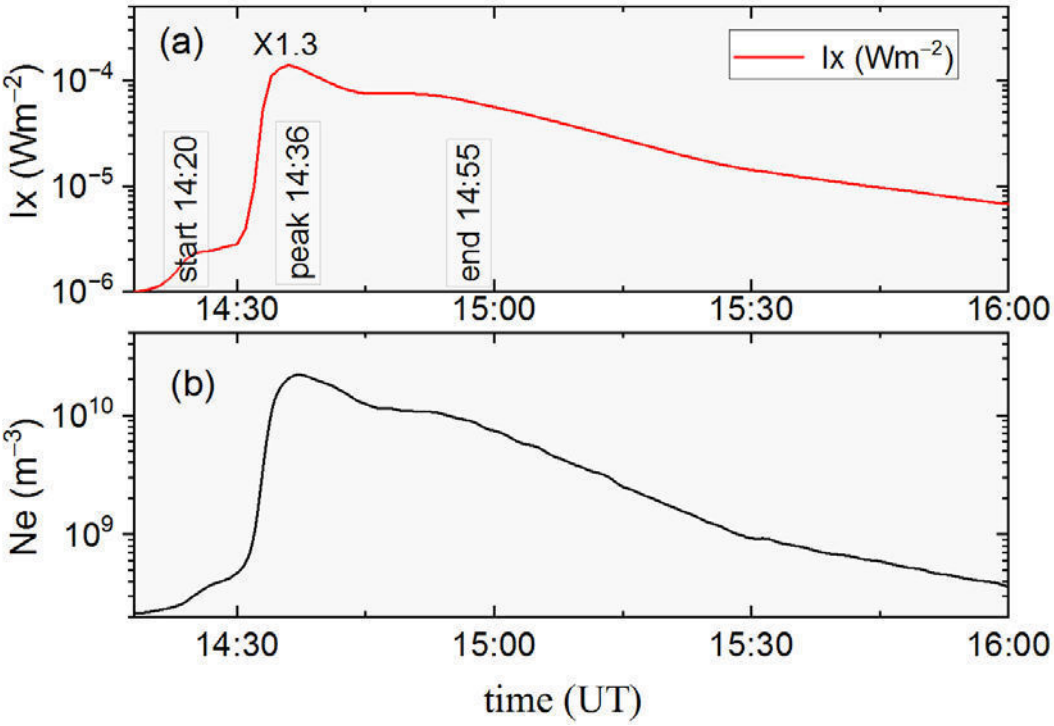

Figure 3. X-ray flux measured by the GOES satellite (**a**), and evaluated electron density profiles (**b**) during occurrence of X1.3 class SF on 7 September 2017.

3.2. Signal Propagation Parameters during LEP Event

Lightning-induced electron precipitation, i.e., LEP, is triggered by an extremely low frequency (VLF and ELF) portion of EM energy released by lightning discharges that manage to reach the Earth's magnetosphere and by propagating as whistler mode wave interactions with electrons from radiation belts forcing them to precipitate to lower altitudes of 60–120 km, causing an increase in electron density. Such localised and transient electron density enhancements in the D-region altitude range can produce significant amplitude and phase delay perturbations on narrowband VLF signals (with change in amplitude level up to 6 dB and in phase delay of about 20 degrees, typically with rise times up to 1 s and signal decay below 100 s) propagating through or near-by the disturbed region (e.g., [18,48,54] and references therein). An LEP event occurred on 16 November 2004 and its impact on VLF signal traces NAA/24.0 kHz and GQD/22.1 kHz (signal with codename GQD emitted from Anthorn (52.40° N, 1.20° W), GB) was selected for analysis. The presented LEP event is one of the typical LEPs recorded by the Belgrade VLF station, from those during the period 2008–2010 [48,55], similar in absolute perturbation amplitude change of up to 5 dB and phase delay of up to a few tens of degrees with maximal duration of up to two minutes. Amplitude (solid lines) and phase delay (dotted lines) registrations, with resolution 0.1 s on NAA and GQD signals, before, during and after the LEP event occurred on 16 November 2004 and are presented in Figure 4a,b, respectively. Moments at which amplitude and phase delay values for unperturbed (regular) and perturbed (irregular) ionospheric conditions in waveguide were read, are marked with red and blue arrows.

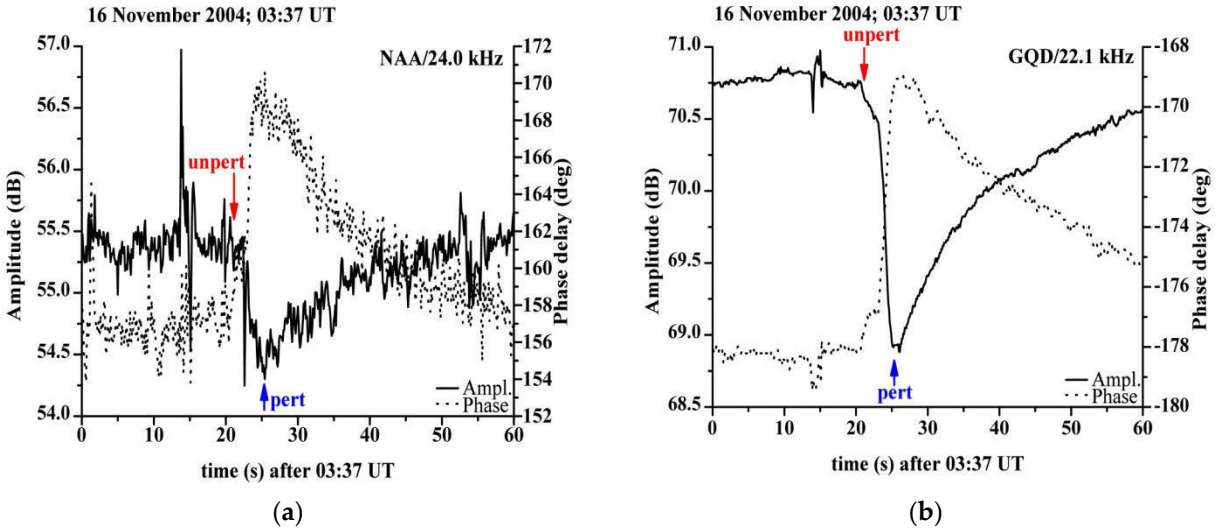

Figure 4. Amplitude (solid lines) and phase delay (dotted lines) time evolution before and during the LEP event occurred on 16 November 2004 on considered VLF signal traces: (**a**) NAA/24.0 kHz and (**b**) GQD/22.1 kHz.

3.3. Modelling and Simulation during LEP Event

NAA/24 kHz signal propagates along W–E direction and has a long (GCP distance D = 6540 km) and mostly oversea path, while GQD/22.1 kHz signal propagates along a short (GCP distance D = 1980 km) and mostly overland path (Figure 5). Disturbance occurred on both analysed signal traces, so it is reasonable to assume that ionospheric irregularity caused by an LEP event was located in the vicinity of the Belgrade receiver site. That is why, both for unperturbed and perturbed ionospheric conditions, the VLF propagation conditions were modelled only in that section of waveguide which is just a few hundred km away from the Belgrade receiver site (44.85° N, 20.38° E).

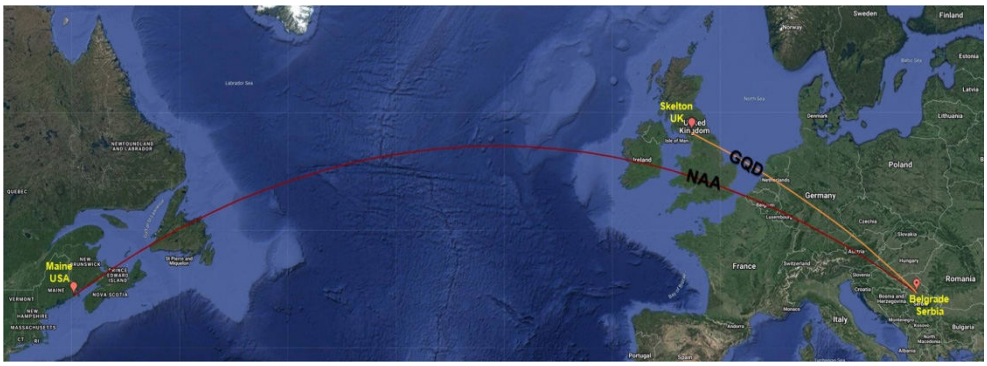

Figure 5. Possible paths for considered NAA/24.0 kHz (red) and GQD/22.1 kHz (yellow) VLF signals emitted towards Belgrade (Serbia) from Maine (USA) and Skelton (UK).

By means of Long Wavelength Propagation Capability computer program (LWPCv21) [51], the propagation paths of NAA/24.0 kHz and GQD/22.1 kHz signals were simulated and modelled. Best fitting pairs of parameters sharpness β (km^{-1}) and reflection height H' (km) were estimated in order to obtain values as close as possible to real measured values of the signals' phase delay (deg) and amplitude (dB) at the place of the receiver in Belgrade, for both cases of regular and disturbed ionospheric conditions in observed sections of waveguides. The estimated amplitude and phase delay values obtained by the LWPCv21 program are in good agreement with real measured values at

the Belgrade receiver site (Table 1: first and third rows indicate unperturbed VLF signal values, while the second and fourth rows indicate the perturbed ones).

Table 1. Measured and estimated amplitude and phase delay values of NAA and GQD signals during the LEP event that occurred on 16 November 2004.

VLF Signal	Time UT 0337 UT +	Measured Values				LWPC Simulation			
		A **(dB)**	**Δ*A*** **(dB)**	***P*** **(°)**	**Δ*P*** **(°)**	***A*** **(dB)**	**Δ*A*** **(dB)**	***P*** **(°)**	**Δ*P*** **(°)**
NAA/24.0 kHz unperturbed values	20.16 s	55.42	0	157.08	0	55.63	0	173.18	0
NAA/24.0 kHz perturbed values	25.54 s	54.37	−1.05	170.03	12.95	54.62	−1.01	195.02	21.84
GQD/22.1 kHz unperturbed values	20.16 s	70.70	0	−178.05	0	70.40	0	−214.88	0
GQD/22.1 kHz perturbed values	25.54 s	68.96	−1.74	−169.05	9	68.65	−1.75	−209.22	5.66

The amplitude change ΔA (dB), was obtained as the difference between the maximum value of the amplitude during the perturbation and the value of the amplitude in undisturbed signal. The phase delay change ΔP (°) was obtained as the difference between the phase delay value that corresponds in time to the maximum value of the amplitude during the perturbation and phase delay value in the undisturbed signal interval that corresponds in time to the amplitude value chosen as unperturbed.

The model for the propagation of VLF signals within the Earth-ionosphere waveguide is defined by pairs of parameters (β, H') and analytically described by equations for the calculation of the electron density height profile $N_e(z)$ (m^{-3}) during daytime ionospheric conditions is given in [56]. The procedure for the computation of the electron density height profile is based on the equation for determining the electron density $N_e(z)$ (m^{-3}) within the Earth-ionosphere waveguide during night-time conditions [14], where the electron density was calculated as a function of a certain pair of parameters β and H', at the height z (km), based on the equation adapted for the nocturnal ionosphere [14]. Electron density height profile $N_e(z)$ (m^{-3}), for given parameters β and H', was calculated using the expression for the night-time ionosphere given by [14]:

$$N_e(z, H', \beta) = 1.86 \times 10^{11} \cdot e^{-0.15 \cdot z} \cdot 78.57 \cdot e^{\beta (z - H')}, \quad (m^{-3}) \tag{1}$$

Parameter β, for night-time ionospheric conditions, is in the range 0.47–0.50 km^{-1}, while parameter H' is in the range 50–87 km. Electron density was calculated at the reflection height, when $z = H'$, and in that case (1) takes the form:

$$N_e(z) = 146.1402 \times 10^{11} \cdot e^{-0.15 \cdot z}, \quad (m^{-3}) \tag{2}$$

For modelling of parameters β and H', the LWPC software was used. Detailed methodology, related to utilisation of LWPC software and VLF signal propagation modelling for different cases, can be found in [14,29,56,57]. Here, the procedure for modelling parameters β and H' is only outlined. The basic parameters of the propagation medium, the sharpness of the upper boundary of the Earth-ionosphere waveguide β and the height of the signal's reflection H' are related to the electron density $N_e(z)$ within the waveguide. Each change in the electron density in the waveguide changes the propagation parameters, amplitude and phase delay of the VLF signal. According to the LWPM model, for regular night-time conditions in the ionosphere, the program code takes the parameter β as 0.40 km^{-1} and the parameter H' as 87 km. However, to model the values of the amplitude and phase delay of the VLF signal, in each individual case, it is necessary to independently determine the appropriate parameter pairs (β, H') as input parameters, so that the simulated values of the amplitude and phase delay obtained as output by the computation, correspond to

the measured values of the amplitude and phase delay as close as possible, as the best fitting pair.

The procedure itself consists of numerous trials, in which parameter pairs (β, H') are manually defined as input parameters and the program gives calculated amplitude and phase delay as the output values. Program output is dependent on numerous factors (such as signal frequency, bearing angle, receiver and transmitter locations, observed date and time, solar zenith angle, geomagnetic dip and electro-conductivity of lower waveguide boundary) that are imbedded as background data in calculations.

During night-time ionospheric VLF transmission, signal's amplitude is more stable than phase delay. During modelling, we focused on providing (β, H') parameter pairs to obtain a really good agreement for relative amplitude change ΔA (dB) for both analysed signals, while still obtaining a relatively good agreement for relative change in phase delay ΔP (°). Simulated amplitude and phase delay values for NAA/24.0 kHz and GQD/22.1 kHz along GCP path, for the unperturbed (red) and perturbed (blue) state in waveguides on 16 November 2004, are presented in Figures 6 and 7, respectively. Areas of amplitude and phase delay changing near the Belgrade receiver site are framed and as zoomed in panels presented on the right.

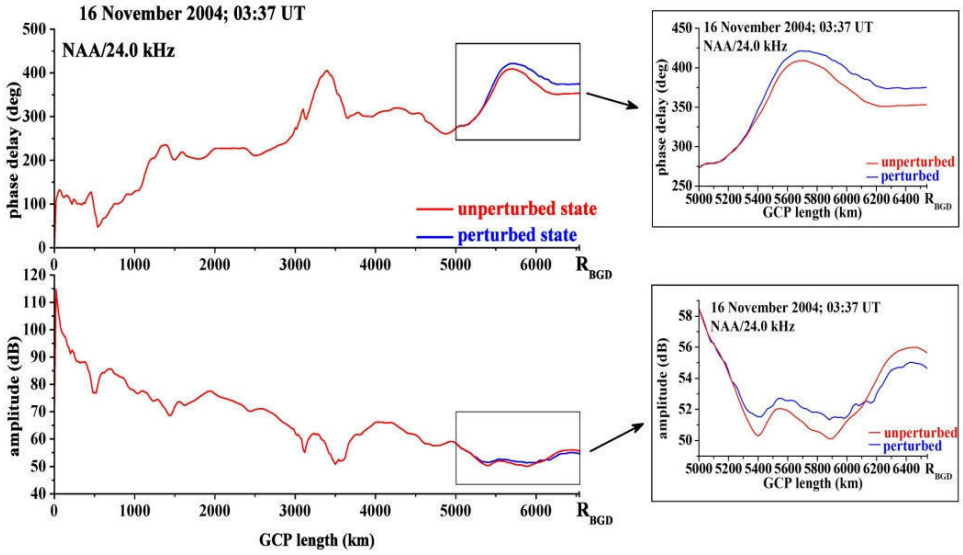

Figure 6. Simulated amplitude and phase delay along GCP path towards the Belgrade receiver, for unperturbed (red) and perturbed (blue) ionospheric states for NAA/24.0 kHz VLF signal waveguides, on 16 November 2004.

Parameters β and H' changing along GCP path, for NAA/24.0 kHz (dashed lines) and GQD/22.1 kHz (dotted lines) VLF signal waveguides, for unperturbed (red) and perturbed (blue) ionospheric states, on 16 November 2004, are presented in Figure 8a,b, respectively (for waveguide sections of 1980 km along GCPs looking towards the Belgrade receiver; direction of view on x axis is presented by black arrows, pointing from left to right at the bottom scale when looking from transmitter T towards receiver R and pointing from left to right at the upper scale if looking from receiver R towards transmitter T). Using the expression (1), for given parameter pairs (β, H'), electron density height profile $N_e(z)$ within ionospheric irregularity, in perturbed section of waveguide, for both analysed VLF signals, was calculated. Irregularity modelling indicates that both VLF signal traces, in some part of the waveguide, encounter an area of enhanced electron density. Electron density changing along GCP path, for NAA/24.0 kHz (dashed line) and GQD/22.1 kHz (dotted line) VLF signal waveguides, for unperturbed (red) and perturbed (blue) ionospheric states on 16 November 2004, are presented on Figure 9 (in length of 1980 km, as looking from Belgrade towards both transmitters). Electron densities along GCPs for unperturbed state (Figure 9—red) were calculated based on modelled parameter pairs

(β, H') posted as unperturbed for all characteristic altitudes (Figure 8—red), where parameters β and H' undergo changes due to signal propagation within the unperturbed waveguide. Electron densities along GCPs for perturbed state (Figure 9—blue) were calculated based on modelled parameter pairs (β, H') for all characteristic altitudes (Figure 8—blue), where parameters undergo changes due to present irregularity and deviated from their posted unperturbed values.

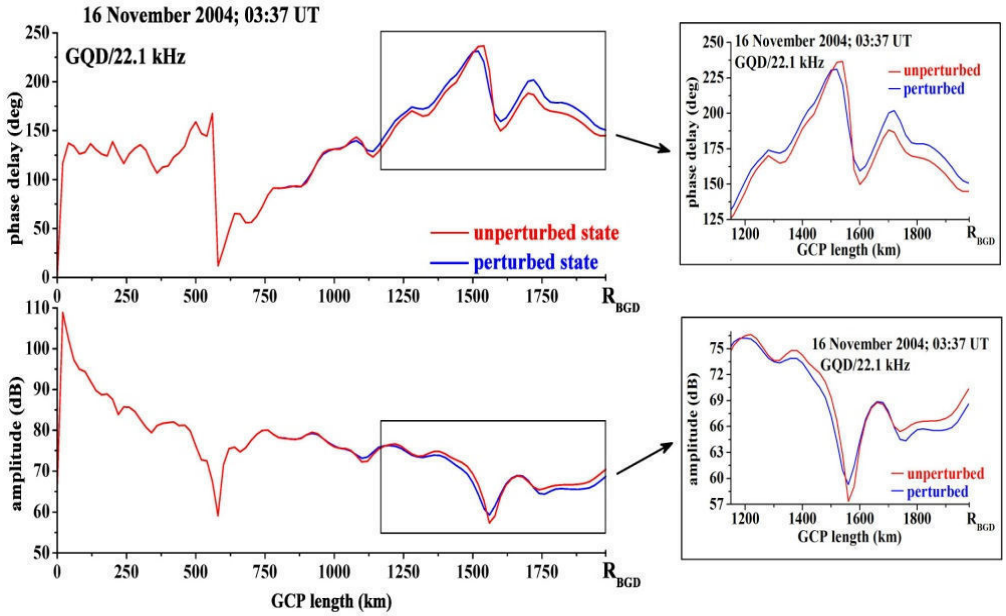

Figure 7. Simulated amplitude and phase delay along GCP path towards the Belgrade receiver, for unperturbed (red) and perturbed (blue) ionospheric states for GQD/22.1 kHz VLF signal waveguides, on 16 November 2004.

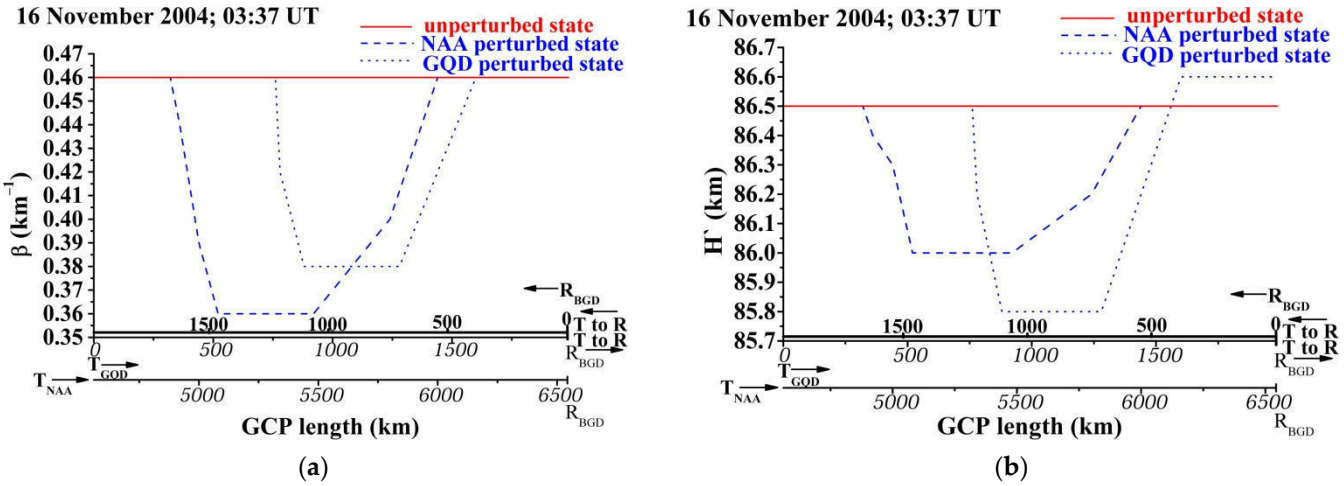

Figure 8. Parameter β and H' changing along GCP path towards the Belgrade receiver, for considered VLF signal waveguides (NAA in dashed lines and GQD in dotted lines), for unperturbed (red) and perturbed (blue) ionospheric states, on 16 November 2004 (R is for receiver, T is for transmitter, black arrows on x axis point the direction of view): (**a**) parameter β and (**b**) parameter H'.

Transmission in entirely nocturnal unperturbed ionospheric conditions, in the case of short GCPs is described by LWPC program usually with only one parameter pair (β, H'), while in the case of moderate GCPs usually with several parameter pairs (β, H'), along the entire path. It should be noted, that in this case, the unperturbed conditions were also modelled in order to provide the best possible match with real measured data. As

already mentioned, since the perturbation was recorded on both monitored signals, in order to provide the best possible match with real measured data, in cases of perturbed conditions, sections of paths of several hundred km away from Belgrade towards transmitters, were modelled.

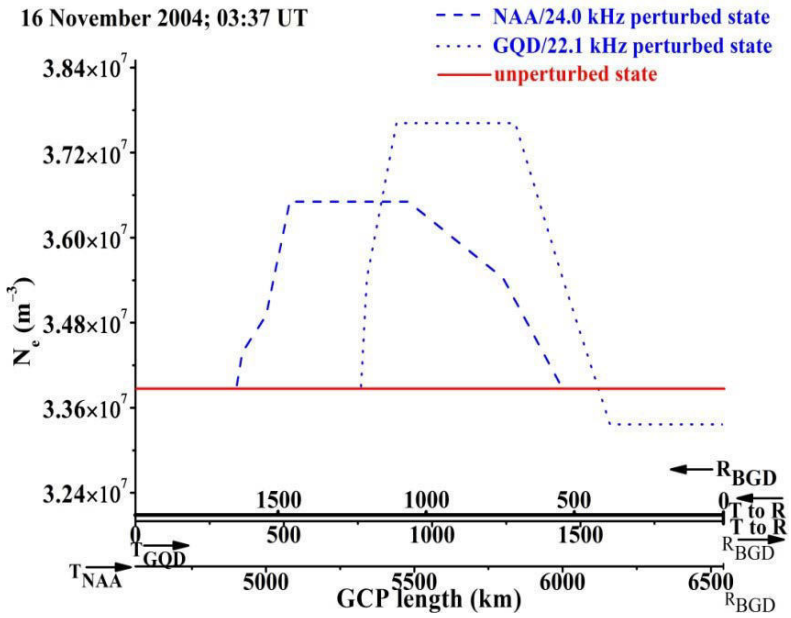

Figure 9. Electron density changing along GCP path towards the Belgrade receiver, for considered VLF signal waveguides (NAA/24.0 kHz in dashed line and GQD/22.1 kHz in dotted line), for unperturbed (red) and perturbed (blue) ionospheric states, on 16 November 2004 (R is for receiver, T is for transmitter, black arrows on x axis point the direction of view).

On the NAA signal trace section, where ionospheric irregularity occurs, the calculated maximum value of electron density is 3.65 × 10^7 m^{-3}, while in unperturbed ionospheric conditions, on the same NAA signal path section, it is 3.39 × 10^7 m^{-3}. On the GQD signal trace section, where ionospheric irregularity occurs, the calculated maximum value of electron density is 3.76 × 10^7 m^{-3}, while in unperturbed ionospheric conditions, on same GQD signal path section, it is 3.39 × 10^7 m^{-3}. In Figure 9, the electron density height profiles in the altitude range 60–90 km, for unperturbed and perturbed conditions due to the analysed LEP event were calculated at the reflection heights in the case of both monitored VLF signals (altitude 86 km for NAA and 85.8 km for GQD in Figure 8b), in the area of the most prominent electron density change along GCPs (e.g., at about 5300 km in the case of NAA and 1100 km in the case of the GQD signal looking from the transmitter towards the Belgrade receiver, i.e., at the approximate location of about 1100 km looking from Belgrade towards both transmitters) are given. Electron density $N_e(z)$ height profiles for GQD (at reflection height 85.8 km) and NAA (at reflection height 86 km) signals, calculated for the altitude range 60–90 km, for 16 November 2004, are given in Figure 10.

In order to create an easier and more convenient use of results presented in the analysis conducted in this paper, an expression for electron density $Ne(z)$ at reflection height is introduced in the form of a polynomial function as given in the equation below:

$$\log Ne(z, H', \beta) = \sum_{i=0}^{1} a_i \cdot z^i, \quad (3)$$

where z is height in km, and dimensionless quantities take values of $a_0 = -5.88339$ and $a_1 = 0.15635$.

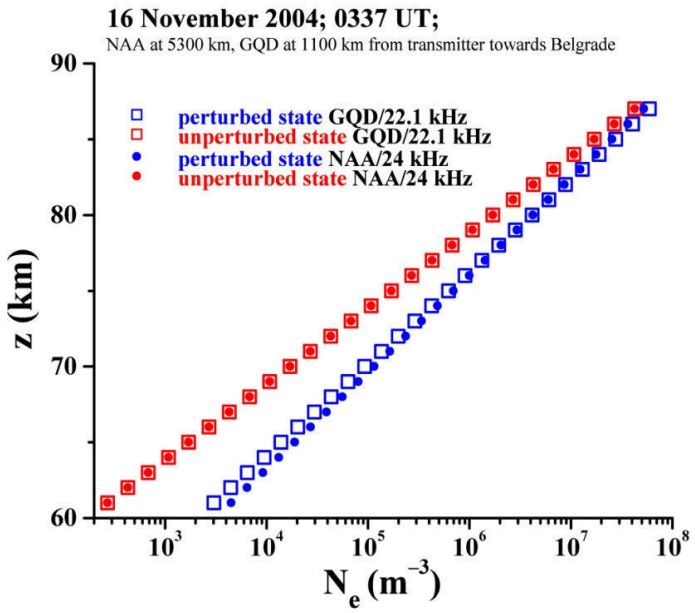

Figure 10. Electron density $N_e(z)$ height profiles for GQD (at reflection height 85.8 km) and NAA (at reflection height 86 km) signals, calculated for altitude range 60–90 km, for 16 November 2004, at 03:37 UT, in the area of the most prominent electron density change along GCPs at a location approximately 1100 km looking from Belgrade towards both transmitters. The unperturbed state for GQD signal is given in red hollow squares, the perturbed state for GQD signal is given in blue hollow squares, unperturbed state for NAA signal is given in red solid circles and perturbed state for NAA signal is given in blue solid circles.

3.4. Analysis of the LEP Event

In perturbed ionospheric conditions at the Belgrade receiver site (44.85° N, 20.38° E), an increase in phase delay and decrease in amplitude for both analysed VLF signals, are registered (Figures 4 and 10). Such behaviour can be explained by lowering the VLF signal reflection height (delay in the phase is less) and, respectively, by reducing the sharpness of the ionized environment lower edge. In perturbed waveguides, modal minima are mitigated compared to the unperturbed ionospheric state. In the perturbed NAA waveguide, reflection height decreased from 86.5 km (characteristic value for normal unperturbed night-time ionospheric conditions) to 86 km, while reflection edge sharpness decreased from 0.46 km^{-1} (characteristic value for normal unperturbed night-time ionospheric conditions) to 0.36 km^{-1}, which is a value characteristic for daytime ionospheric conditions. Changes in GQD propagation are similar: in perturbed waveguide, reflection height decreased from 86.5 km to 85.8 km, while reflection edge sharpness decreased from 0.46 km^{-1} to 0.38 km^{-1} (value characteristic for daytime ionospheric conditions). A less sharp lower edge of the ionized environment enables the VLF signal to penetrate into the ionized environment, and at the same time, VLF signal deviant energy absorption takes place. It is well known that β is a function of ω. After an LEP event, an NAA signal pair (β/H') have values (0.46 km^{-1}/86.5 km) and GQD have values (0.46 km^{-1}/86.6 km), so it can be said that the ionosphere is fully recovered. Same ionospheric conditions ((β/H') have values of 0.46 km^{-1}/86.5 km) that apply for areas outside of the irregularity, too. Obtained values of (β/H') pairs are in agreement with [48], who reported β in the range 0.48–0.5 km^{-1} and H' in the range 85.3–87 km for cases of short signals with a mid-latitudinal transmission, also with [57] who reported β in the range 0.46–0.5 km^{-1} and H' in the range 84–87 km for cases of short and moderate length signals in most cases with mid-latitudinal transmission, and [54], who reported β in the range 0.307–0.42 km^{-1} and H' in the range 80.3–87 km for cases of short length signals in most cases with mid-latitudinal transmission. An obtained relative change in reflection height during analysed perturbation of 0.5 km and

0.7 km in cases of NAA and GQD signals, respectively, are in agreement with the results reported by [54,55] who reported ranges of 7–10 km and 3.7–6.7 km, respectively. Measured and simulated relative change in amplitude and phase delay values (Table 1) are in line with [18] and reference therein, an amplitude difference ~6 dB and ~20 deg of phase shift and [48,54] who reported relative measured and modelled amplitude and phase change of 1.4 and 1.5 dB and 9 and 8 deg and up to 2.01 and 1.74 dB and 3.63 and 3.15 deg, respectively. Calculated maximum electron density values (for NAA signal $N_{e\ pert}$ (86.5 km) = 3.65×10^7 m^{-3} and $N_{e\ unpert}$ (86 km) = 3.39×10^7 m^{-3} and for GQD signal $N_{e\ pert}$ (86.5 km) = 3.76×10^7 m^{-3} and $N_{e\ unpert}$ (85.8 km) = 3.39×10^7 m^{-3}) are in agreement with [48] who reported $N_{e\ unpert}$ (87 km) = 3.14×10^7 m^{-3} and $N_{e\ pert}$ (85.3 km) = 3.67×10^7 m^{-3}, while [54] reported higher values and a steeper slope (variation of $N_{e\ pert}$ (84 km) from ambient $N_{e\ unpert}$ (84 km) reported 1.519×10^8 and 0.607×10^8 m^{-3}, respectively). The errors, introduced by the technique used, place the uncertainty of the results between 10% and 25% (see, e.g., [23]). More precisely we estimate that the total error, i.e., noise error and the calibration error is ~5% in amplitude and phase delay, which is in agreement with [58]. Moreover, the absolute amplitude variation between the recorded values and the signal amplitude and phase values acquired using LWPC is usually 10–20% which gives uncertainty of the results between 10% and 25%. Electron densities and ionospheric parameters obtained by different models and techniques [23,30,47,59] vary by about one order of magnitude (factor 10). Electron density ratios related to flare Ixmax given in [60] are within one order of magnitude and for unperturbed flare conditions given in [61] are smaller. Results obtained by VLF technique and LWPCV2.1 software are satisfactory for conducted qualitative analysis presented in this work.

By NAA signal trace modelling, it was found that ionospheric irregularity related to LIE outreach from 4920 km to 5800 km when looking along the GCP path from transmitter to receiver, thus, LIE extent is 880 km, with corresponding coordinates (0.7° E, 51.5° N) and (12° E, 48.3° N). By GQD signal trace modelling, ionospheric irregularity outreach was found from 780 km to 1440 km when looking along the GCP path from transmitter to receiver, thus, LIE extent is 660 km, with corresponding coordinates (7.4° E, 51.4° N) and (14.9° E, 48° N). Modelled LIE extent for both cases is in agreement with [54,57] who reported precipitation patches estimated as at least 1500 × 600 km and spatial extent of disturbance as 728 km, respectively. Assumed geographical position of modelled irregularity in NAA and GQD waveguides, i.e., electron density increases in D–region due to energetic electron precipitation (see Figure 9), is presented by a blue oval in Figure 11, indicating that energetic electron precipitation took place over central Europe.

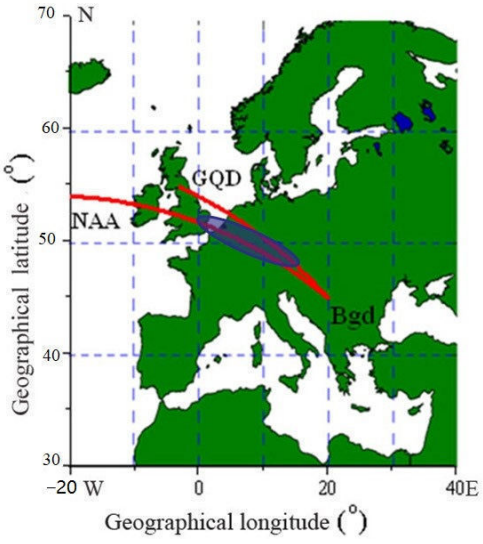

Figure 11. Geographical position of modelled LIE (blue oval) related to energetic electron precipitation on 16 November 2004.

4. Conclusions and Perspectives

Ionospheric conditions highly differ depending on the time of day when sudden disturbances occur, with a transition period between stable daytime and stable night-time ionospheric conditions, i.e., during dawn and sunset being especially challenging for modelling. Regular night-time ionospheric conditions are described with parameter pairs (β, H') within a range of values, that is 0.47–0.50 km^{-1} and 50–87 km, respectively, while in unperturbed daytime ionospheric conditions, this pair is defined only by one pair (0.3 km^{-1}, 74 km). In the case of perturbation presence, ionospheric conditions are changed affecting VLF transmission within the Earth-ionosphere waveguide, inducing signal's amplitude and phase delay to deviate from their regular values. In such disturbed environment, parameter pairs (β, H') also deviate from their regular values, depicting the change in electron density that takes place, following the causative agent's behaviour. In the case of the examined LEP event example, parameter pairs (β, H') changed according to perturbed nocturnal waveguides. Specifically, in the case of the NAA signal parameter, H' went through a decrease from 86.5 km (characteristic value for normal unperturbed night-time ionospheric conditions in pre-LEP state) to 86 km at LEP's peak and returned to its regular value of 86.5 km in post-LEP conditions, while parameter reflection edge sharpness β decreased from 0.46 km^{-1} (characteristic value for normal unperturbed night-time ionospheric conditions before LEP occurrence) to 0.36 km^{-1} at LEP's peak, which is the value characteristic for daytime ionospheric conditions and returned to 0.46 km^{-1}, its regular value after the influence of the LEP event. Similar behaviour is also present in the case of GQD trace, where parameter H' went through a decrease from 86.5 km to 85.8 km at LEP's peak and returned to 86.6 km, while reflection edge sharpness β decreased from 0.46 km^{-1} to 0.38 km^{-1} and returned to 0.46 km^{-1}. It can be concluded that after the influence of the analysed LEP event, the ionosphere is fully recovered in both waveguides, still remaining slightly higher, reflecting the edge height in the case of the GQD signal. Electron density change is one order of magnitude below regular values.

Regarding measured ΔA (dB) and ΔP (°), in the case of the LEP event, they are in a range of -1 to -2 dB and +9 to +13° (where the minus sign denotes decrease and plus sign increase in signal values compared to pre-LEP state). In the case of mid- and strong flare events, ΔA (dB) and ΔP (°) are usually of higher values [38,62,63], and especially in X-class flare events such as the one analysed here, where they took values of about +4 dB and +159°, respectively. At the maximum X-ray irradiance during X1.3 class flare event that occurred on 7 September 2017, as the response within lower ionosphere, the reflecting edge height decreased by 13 km to the height 63 km, and the reflection edge sharpness increased to the value 0.42 km^{-1}, while the induced electron density increase reached almost two orders of magnitude compared to the regular value. The analysed flare event lasted for almost two hours, while it took much longer for the lower ionosphere to fully recover.

Data related to the ionospheric research and the results obtained are of great use for various Earth observations and especially for telecommunications, while they also can be significant to other applications in modern society. Modelling ionospheric parameters is crucial for validation of proposed models. Results presented in this paper are related to modelling the plasma response of the ionospheric lowest region, to some high energy events, as recorded by radio signals. The presented results are important for the modelling of this region but also useful for future atmospheric aerosol–electricity interactions research in climate science. Monitoring and observing ionospheric characteristics related to the mid-latitude European ionosphere using VLF signals is particularly important, especially bearing in mind that beside the Hungarian system, this is the only available source of such data [64]. The computational results can differ by a factor of ten depending on which method is used, thus it is important to present new modelling results and make comparisons to the results obtained by the same or similar technique. The findings are significant in light of possible future collaboration on VLF studies in this part of Europe.

Author Contributions: Conceptualization, A.K.; writing—original draft preparation, A.K.; writing—review and editing A.K., V.A.S. and Z.R.M. The authors had full access to the data and take responsibility for their integrity. All authors have read and agreed to the published version of the manuscript.

Funding: This work was funded by the Institute of Physics Belgrade through a grant by the Ministry of Education, Science, and Technological Development of the Republic of Serbia. This article/publication is based upon work from COST Action CA17126—Towards understanding and modelling intense electronic excitation (TUMIEE), supported by COST (European Cooperation in Science and Technology).

Institutional Review Board Statement: Not applicable.

Informed Consent Statement: Not applicable.

Data Availability Statement: VLF data recorded at the Institute of Physics, University of Belgrade, Belgrade, Serbia can be obtained upon a request. Please contact V.A.S.

Acknowledgments: Authors thank D. Šulić for instrumental set-up and useful discussions.

Conflicts of Interest: The authors declare no conflict of interest. The funders had no role in the design of the study; in the collection, analyses, or interpretation of data; in the writing of the manuscript, or in the decision to publish the results.

References

1. Kelley, M.C. *The Earth's Ionosphere: Plasma Physics and Electrodynamics*; Academic Press: Oxford, UK, 2009.
2. Rycroft, M.J. Electrical processes coupling the atmosphere and ionosphere: An overview. *J. Atmos. Sol. Terr. Phys.* **2006**, *68*, 445–456. [CrossRef]
3. Kourtidis, K.; André, K.S.; Karagioras, A.; Nita, I.-A.; Sátori, G.; Bór, J.; Kastelis, N. The influence of circulation weather types on the exposure of the biosphere to atmospheric electric fields. *Int. J. Biometeorol.* **2021**, *65*, 93–105. [CrossRef]
4. Cummer, S.A.; Inan, U.S. Ionospheric E region remote sensing with ELF radio atmospherics. *Radio Sci.* **2000**, *35*, 1437–1444. [CrossRef]
5. Mannucci, A.J.; Hajj, G.A.; Iijima, B.A.; Komjathy, A.; Meehan, T.K.; Pi, X.Q.; Srinivasan, J.; Tsurutani, B.T.; Wilson, B.; Zhang, L.D. GPS-based remote sensing of the geospace environment: Horizontal and vertical structure of the ionosphere and plasmasphere. In Proceedings of the Instruments, Science, and Methods for Geospace and Planetary Remote Sensing, Honolulu, HI, USA, 30 December 2004; pp. 1–13.
6. Goodman, J.M. *Space Weather & Telecommunications*; Springer: New York, NY, USA, 2005; Volume 382.
7. Tandberg-Hanssen, E.; Emslie, A.G. *The Physics of Solar Flares*; Cambridge University Press: Cambridge, UK, 1988; Volume 14.
8. Berényi, K.; Barta, V.; Kis, Á. Midlatitude ionospheric F2-layer response to eruptive solar events-caused geomagnetic disturbances over Hungary during the maximum of the solar cycle 24: A case study. *Adv. Space Res.* **2018**, *61*, 1230–1243. [CrossRef]
9. Šulić, D.; Srećković, V.; Mihajlov, A. A study of VLF signals variations associated with the changes of ionization level in the D-region in consequence of solar conditions. *Adv. Space Res.* **2016**, *57*, 1029–1043. [CrossRef]
10. Šulić, D.; Srećković, V. A comparative study of measured amplitude and phase perturbations of VLF and LF radio signals induced by solar flares. *Serb. Astron. J.* **2014**, *188*, 45–54. [CrossRef]
11. Reid, G.C. *Ion Chemistry in the D Region*; Academic Press: Cambridge, MA, USA, 1976; Volume 12, pp. 375–413.
12. Brasseur, G.P.; Solomon, S. *Aeronomy of the Middle Atmosphere: Chemistry and Physics of the Stratosphere and Mesosphere*; Springer Science & Business Media: Dordrecht, The Netherlands, 2006; Volume 32.
13. Nicolet, M.; Aikin, A. The formation of the D region of the ionosphere. *J. Geophys. Res.* **1960**, *65*, 1469–1483. [CrossRef]
14. Nunn, D. On the numerical modelling of the VLF Trimpi effect. *J. Atmos. Sol. Terr. Phys.* **1997**, *59*, 537–560. [CrossRef]
15. Helliwell, R.; Katsufrakis, J.; Trimpi, M. Whistler-Induced Amplitude Perturbations in VLF Propagation. *J. Geophys. Res.* **1973**, *78*, 4679–4688. [CrossRef]
16. Helliwell, R.A. *Whistlers and Related Ionospheric Phenomena*; Stanford University Press Stanford: Palo Alto, CA, USA, 1965; Volume 50.
17. Strangeways, H. *Lightning, Trimpis and Sprites*; Oxford University Press: Oxford, UK, 1996; Volume 1993, pp. 741–780.
18. Silber, I.; Price, C. On the use of VLF narrowband measurements to study the lower ionosphere and the mesosphere–lower thermosphere. *Surv. Geophys.* **2017**, *38*, 407–441. [CrossRef]
19. Trichtchenko, L.; Zhukov, A.; Van der Linden, R.; Stankov, S.; Jakowski, N.; Stanisławska, I.; Juchnikowski, G.; Wilkinson, P.; Patterson, G.; Thomson, A. November 2004 space weather events: Real-time observations and forecasts. *Space Weather* **2007**, *5*, 1–17. [CrossRef]
20. Rodger, C.J. Subionospheric VLF perturbations associated with lightning discharges. *J. Atmos. Sol. Terr. Phys.* **2003**, *65*, 591–606. [CrossRef]

21. Belenkiy, M.; Orlov, A.; Petrova, G.; Uvarov, A. Modeling of the electron density profile of the lower ionosphere (45–75 km) for sudden ionospheric disturbance conditions based on the data on sudden phase anomalies of VLF signals. *Int. J. Geomag. Aeron.* **2006**, *6*, GI3007. [CrossRef]
22. McKinnell, L.-A.; Friedrich, M. A neural network-based ionospheric model for the auroral zone. *J. Atmos. Sol. Terr. Phys.* **2007**, *69*, 1459–1470. [CrossRef]
23. Žigman, V.; Grubor, D.; Šulić, D. D-region electron density evaluated from VLF amplitude time delay during X-ray solar flares. *J. Atmos. Sol. Terr. Phys.* **2007**, *69*, 775–792. [CrossRef]
24. Chakrabarti, S.; Pal, S.; Sasmal, S.; Mondal, S.; Ray, S.; Basak, T.; Maji, S.; Khadka, B.; Bhowmick, D.; Chowdhury, A. VLF campaign during the total eclipse of July 22nd, 2009: Observational results and interpretations. *J. Atmos. Sol. Terr. Phys.* **2012**, *86*, 65–70. [CrossRef]
25. Thomson, N.R.; Rodger, C.J.; Clilverd, M.A. Daytime D region parameters from long-path VLF phase and amplitude. *J. Geophys. Res.* **2011**, *116*, 1–12.
26. McRae, W.M.; Thomson, N.R. VLF phase and amplitude: Daytime ionospheric parameters. *J. Atmos. Sol. Terr. Phys.* **2000**, *62*, 609–618. [CrossRef]
27. McRae, W.M.; Thomson, N.R. Solar flare induced ionospheric D-region enhancements from VLF phase and amplitude observations. *J. Atmos. Sol. Terr. Phys.* **2004**, *66*, 77–87. [CrossRef]
28. Thomson, N.R.; Rodger, C.J.; Clilverd, M.A. Large solar flares and their ionospheric D region enhancements. *J. Geophys. Res.* **2005**, *110*, 1–10.
29. Thomson, N.R.; Clilverd, M.A.; McRae, W.M. Nighttime ionospheric D region parameters from VLF phase and amplitude. *J. Geophys. Res.* **2007**, *112*, 1–14.
30. Basak, T.; Chakrabarti, S.K. Effective recombination coefficient and solar zenith angle effects on low-latitude D-region ionosphere evaluated from VLF signal amplitude and its time delay during X-ray solar flares. *Astrophys. Space. Sci.* **2013**, *348*, 315–326. [CrossRef]
31. Budden, K. *Radio Waves in the Ionosphere*; Cambridge Univ. Press: Cambridge, UK, 1961.
32. Budden, K.G. *The Wave-Guide Mode Theory of Wave Propagation*; Logos Press: London, UK, 1961.
33. Wait, J.R. *Electromagnetic Waves in Stratified Media*; Pergamon Press: Oxford, UK, 1970; Volume 3.
34. Mitra, A.P. *Ionospheric Effects of Solar Flares*; Springer: Berlin/Heidelberg, The Netherlands, 1974; Volume 46.
35. Balan, N.; Alleyne, H.; Walker, S.; Reme, H.; McCrea, I.; Aylward, A. Magnetosphere–ionosphere coupling during the CME events of 07–12 November 2004. *J. Atmos. Sol. Terr. Phys.* **2008**, *70*, 2101–2111. [CrossRef]
36. Inan, U.S.; Lehtinen, N.G.; Moore, R.; Hurley, K.; Boggs, S.; Smith, D.; Fishman, G. Massive disturbance of the daytime lower ionosphere by the giant γ-ray flare from magnetar SGR 1806–20. *Geophys. Res. Lett.* **2007**, *34*, 8103–8108. [CrossRef]
37. Žigman, V.; Kudela, K.; Grubor, D. Response of the Earth's lower ionosphere to the ground level enhancement event of December 13, 2006. *Adv. Space Res.* **2014**, *53*, 763–775. [CrossRef]
38. Srećković, V.A.; Šulić, D.M.; Ignjatović, L.; Vujčić, V. Low Ionosphere under Influence of Strong Solar Radiation: Diagnostics and Modeling. *Appl.Sci.* **2021**, *11*, 7194. [CrossRef]
39. Nina, A.; Srećković, V.; Radovanović, M. Multidisciplinarity in research of extreme solar energy influences on natural disasters. *Sustainability* **2019**, *11*, 974. [CrossRef]
40. Cannon, P.; Angling, M.; Barclay, L.; Curry, C.; Dyer, C.; Edwards, R.; Greene, G.; Hapgood, M.; Horne, R.B.; Jackson, D. *Extreme Space Weather: Impacts on Engineered Systems and Infrastructure*; Royal Academy of Engineering: Carlton House Terrace, London, 2013.
41. McMorrow, D. *Impacts of Severe Space Weather on the Electric Grid*; JASON: McLean, VA, USA, 2011; pp. 22102–27508.
42. Kolarski, A.; Grubor, D. Sensing the Earth's low ionosphere during solar flares using VLF signals and goes solar X-ray data. *Adv. Space Res.* **2014**, *53*, 1595–1602. [CrossRef]
43. Kolarski, A.; Grubor, D. Comparative analysis of VLF signal variation along trajectory induced by X-ray solar flares. *J. Astrophys. Astr.* **2015**, *36*, 565–579. [CrossRef]
44. Kolarski, A.; Grubor, D.; Šulić, D. Diagnostics Of The Solar X-Flare Impact On Lower Ionosphere Through The Vlf-Naa Signal Recordings. *Open Astron.* **2011**, *20*, 591–595. [CrossRef]
45. Nina, A.; Čadež, V.; Srećković, V.; Šulić, D. The influence of solar spectral lines on electron concentration in terrestrial ionosphere. *Open Astron.* **2011**, *20*, 609–612. [CrossRef]
46. Nina, A.; Čadež, V.; Srećković, V.; Šulić, D. Altitude distribution of electron concentration in ionospheric D-region in presence of time-varying solar radiation flux. *Nucl. Instrum. Meth. B* **2012**, *279*, 110–113. [CrossRef]
47. Nina, A.; Čadež, V.; Šulić, D.; Srećković, V.; Žigman, V. Effective electron recombination coefficient in ionospheric D-region during the relaxation regime after solar flare from 18 February 2011. *Nucl. Instrum. Meth. B* **2012**, *279*, 106–109. [CrossRef]
48. Šulić, D.; Nina, A.; Srećković, V. Numerical Simulations Of The Effect Of Localised Ionospheric Perturbations On Subionospheric VLF Propagation. *arXiv* **2014**, arXiv:1405.3783.
49. Nina, A.; Čadež, V.M.; Popović, L.Č.; Srećković, V.A. Diagnostics of plasma in the ionospheric D-region: Detection and study of different ionospheric disturbance types. *Eur. Phys. J. D* **2017**, *71*, 189. [CrossRef]
50. Nina, A.; Simić, S.; Srećković, V.A.; Popović, L.Č. Detection of short-term response of the low ionosphere on gamma ray bursts. *Geophys. Res. Lett.* **2015**, *42*, 8250–8261. [CrossRef]

51. Ferguson, J. *Computer Programs for Assessment of Long-Wavelength Radio Communications, Version 2.0: User's Guide and Source Files*; Space and Naval Warfare Systems Center: San Diego, CA, USA, 1998.
52. Gavrilov, B.; Ermak, V.; Lyakhov, A.; Poklad, Y.V.; Rybakov, V.; Ryakhovsky, I. Reconstruction of the Parameters of the Lower Midlatitude Ionosphere in M-and X-Class Solar Flares. *Geomagn. Aeron.* **2020**, *60*, 747–753. [CrossRef]
53. Kumar, A.; Kumar, S. Solar flare effects on D-region ionosphere using VLF measurements during low-and high-solar activity phases of solar cycle 24. *Earth Planets Space* **2018**, *70*, 29. [CrossRef]
54. Kerrache, F.; Nait Amor, S.; Kumar, S. Ionospheric D region disturbances due to FAC and LEP associated with three severe Geomagnetic Storms as observed by VLF Signals. *J. Geophys. Res.* **2021**, *126*, e2020JA027838. [CrossRef]
55. Šulić, D.; Žigman, V.; Nina, A. Study of the observed amplitude and phase perturbations on VLF signals from lighting induced electron precipitation and reconstruction of D-region electron density height profile. In Proceedings of the 4rd VERSIM Workshop 2010, Prague, Czech Republic, 13–17 September 2010.
56. Wait, J.R.; Spies, K.P. *Characteristics of the Earth-Ionosphere Waveguide for VLF Radio Waves*; US Department of Commerce, National Bureau of Standards: Boulder, CO, USA, 1964; Volume 13.
57. Clilverd, M.A.; Nunn, D.; Lev-Tov, S.J.; Inan, U.S.; Dowden, R.L.; Rodger, C.J.; Smith, A.J. Determining the size of lightning-induced electron precipitation patches. *J. Geophys. Res.* **2002**, *107*, SIA 10–SIA 11. [CrossRef]
58. Bainbridge, G.; Inan, U.S. Ionospheric D region electron density profiles derived from the measured interference pattern of VLF waveguide modes. *Radio Sci.* **2003**, *38*, 16-11–16-21. [CrossRef]
59. Palit, S.; Basak, T.; Mondal, S.; Pal, S.; Chakrabarti, S. Modeling of very low frequency (VLF) radio wave signal profile due to solar flares using the GEANT4 Monte Carlo simulation coupled with ionospheric chemistry. *Atmos. Chem. Phys.* **2013**, *13*, 9159–9168. [CrossRef]
60. Grubor, D.; Šulić, D.; Žigman, V. Classification of X-ray solar flares regarding their effects on the lower ionosphere electron density profile. *Ann. Geophys.* **2008**, *26*, 1731–1740. [CrossRef]
61. Nina, A.; Čadež, V.M. Electron production by solar Ly-α line radiation in the ionospheric D-region. *Adv. Space Res.* **2014**, *54*, 1276–1284. [CrossRef]
62. Bouderba, Y.; NaitAmor, S.; Tribeche, M. Study of the solar flares effect on VLF radio signal propagating along NRK-ALG path using LWPC code. *J. Geophys. Res.* **2016**, *121*, 6799–6807. [CrossRef]
63. Feng, J.; Han, B.; Gao, F.; Zhang, T.; Zhao, Z. Analysis of Global Ionospheric Response to Solar Flares Based on Total Electron Content and Very Low Frequency Signals. *IEEE Access* **2021**, *9*, 57618–57631. [CrossRef]
64. Barta, V.; Haldoupis, C.; Sátori, G.; Buresova, D.; Chum, J.; Pozoga, M.; Berényi, K.A.; Bór, J.; Popek, M.; Kis, Á. Searching for effects caused by thunderstorms in midlatitude sporadic E layers. *J. Atmos. Sol. Terr. Phys.* **2017**, *161*, 150–159. [CrossRef]

University of Belgrade
Technical Faculty in Bor and
Mining and Metallurgy Institute Bor

49th International October Conference on Mining and Metallurgy

PROCEEDINGS

Editors:
Nada Štrbac
Ivana Marković
Ljubiša Balanović

Bor Lake, Serbia
October 18-21, 2017

IOC 2017
International October Conference

PROCEEDINGS,
49th INTERNATIONAL OCTOBER CONFERNCE
on Mining and Metallurgy

Editors:
Prof. dr Nada Štrbac
Doc. dr Ivana Marković
Doc. dr Ljubiša Balanović
University of Belgrade, Technical Faculty in Bor

Technical Editor:
M. Sc. Uroš Stamenković
University of Belgrade, Technical Faculty in Bor

Publisher: University of Belgrade, Technical Faculty in Bor
For the publisher: Dean Prof. dr Nada Štrbac
Circulation: 200 copies

Printed by "Happy trend DOO", Zaječar, 2017

ISBN 978-86-6305-066-2

CIP - Каталогизација у публикацији - Народна библиотека Србије, Београд

622(082)
669(082)

INTERNATIONAL October Conference on Mining and Metallurgy (49 ; 2017 ; Bor Lake)
Proceedings / 49th International October Conference on Mining and Metallurgy - IOC 2017,
Bor Lake, Serbia, October 18-21, 2017;
[organized by] University of Belgrade, Technical Faculty Bor and Mining and Metallurgy Institute Bor;
editors Nada Štrbac, Ivana Marković, Ljubiša Balanović. - Bor : University of Belgrade, Technical Faculty,
2017 (Zaječar : Happy trend). - XXIII, 664 str. : ilustr. ; 25 cm

Tiraž 200. - Bibliografija uz svaki rad. - Registar.

ISBN 978-86-6305-066-2

a) Рударство - Зборници b) Металургија - Зборници

COBISS.SR-ID 246349324

Bor Lake, Serbia, October 18-21, 2017

SCIENTIFIC COMMITTEE

Prof. dr Nada Štrbac (Serbia) - president
Prof. dr Radoje Pantović (Serbia) - vice-president
Prof. dr Grozdanka Bogdanović (Serbia)- vice-president
Prof. dr Dragoslav Gusković (Serbia) - vice-president
Prof. dr Aleksandar Dimitrov (Macedonia)
Dr Ana Kostov (Serbia)
Dr Andrei Rotaru (Romania)
Prof. dr Anđelka Mihajlov (Serbia)
Prof. dr Batrić Pešić (USA)
Prof. dr Boštjan Markoli (Slovenia)
Prof. dr Boyan Boyanov (Bulgaria)
Prof. dr Branka Jordović (Serbia)
Prof. dr Carl Heinz Spitzer (Germany)
Prof. dr Costas Matis (Greece)
Prof. dr Dejan Tanikić (Serbia)
Prof. dr Desimir Marković (Serbia)
Prof. dr Dimitris Panias (Greece)
Prof. dr Dimitriu Sorin (Romania)
Prof. dr Dragan Manasijević (Serbia)
Prof. dr Duško Minić (Serbia)
Prof. dr Endre Romhanji (Serbia)
Prof. dr Fathi Habashi (Canada)
Prof. dr Guven Onal (Turkey)
Prof. dr György Kaptay (Hungary)
Prof. dr Heikki Jalkanen (Finland)
Prof. dr Iwao Katayama (Japan)
Prof. dr Jakob Lamut (Slovenia)
Prof. dr Jelena Penavin Škundrić (B&H)
Prof. dr Jožef Medved (Slovenia)
Prof. dr Karlo Raić (Serbia)
Prof. dr Kemal Delijić (Montenegro)
Prof. dr Krzystof Fitzner (Poland)
Prof. dr Luis Filipe Malheiros (Portugal)
Dr Magnus Ericsson (Sweden)
Prof. dr Milan Antonijević (Serbia)
Prof. dr Milan Trumić (Serbia)
Prof. dr Mile Dimitrijević (Serbia)
Prof. dr Mirjana Rajčić Vujasinović (Serbia)
Prof. dr Mirko Gojić (Croatia)
Dr Mile Bugarin (Serbia)
Dr Milenko Ljubojev (Serbia)
Dr Mirjam Jan-Blažić (Slovenia)
Dr Miroslav Sokić (Serbia)
Prof. dr Mirsada Oruč (B&H)
Dr Nadežda Talijan (Serbia)
Prof. dr Nenad Radović (Serbia)
Prof. dr Nenad Vušović (Serbia)
Prof. dr Nobuyuki Masuda (Japan)
Prof. dr Onuralp Yucel (Turkey)
Prof. dr Petr M. Solozhenkin (Russia)
Prof. dr Rodoljub Stanojlović (Serbia)
Prof. dr Sanda Krausz (Romania)
Prof. dr Seshadri Seetharaman (Sweden)
Dr Slavomir Hredzak (Slovakia)
Prof. dr Snežana Šerbula (Serbia)
Prof. dr Stoyan Groudev (Bulgaria)
Prof. dr Sulejman Muhamedagić (B&H)
Prof. dr Svetlana Ivanov (Serbia)
Dr Srećko Stopić (Germany)
Prof. dr Tamara Holjevac Grgurić (Croatia)
Prof. dr Tatjana Volkov-Husović (Serbia)
Prof. dr Tomaš Havlik (Slovakia)
Prof. dr Velizar Stanković (Serbia)
Prof. dr Velimir Radmilović (USA)
Prof. dr Vitomir Milić (Serbia)
Dr Vladan Ćosović (Serbia)
Prof. dr Vladimir Krstić (Canada)
Prof. dr Vladislav Kecojević (USA)
Prof. dr Vlastimir Trujić (Serbia)
Prof. dr Yong Du (China)
Prof. dr Zoran Marković (Serbia)
Prof. dr Žarko Radović (Montenegro)
Prof. dr Željko Kamberović (Serbia)
Prof. dr Živan Živković (Serbia)
Dr Walter Valery (Australia)
Dr Zvonko Gulišija (Serbia)

ORGANIZING COMMITTEE

Doc. dr Ivana Marković - president
Doc. dr Ljubiša Balanović - vice-president
Doc. dr Saša Stojadinović - vice-president
Prof. dr Svetlana Ivanov
Prof. dr Dragan Manasijević
Prof. dr Snežana Urošević
Dr Ana Kostov (IRM Bor)
Doc. dr Vesna Grekulović
Doc. dr Aleksandra Mitovski
Doc. dr Dejan Petrović
Doc. dr Milan Gorgievski
Doc. dr Ana Simonović
Doc.dr Tanja Kalinović
Doc.dr Marija Petrović Mihajlović
M.Sc. Uroš Stamenković
M.Sc. Oliver Marković
Slavica Stevanović, prof. engl.
Sandra Vasković, prof. engl.
Predrag Stolić, dipl. ing.
Dr Ana Radojević
M.Sc. Jelena Milosavljević

Marko Pavlović, Ljubiša Andrić, Dragan Radulović, Zoran Čeganjac *(Serbia)*
The influence of mechanical activation of talc- filler on the quality of the refractory coatings 53

Vesna Angelevska, Vasko Stojanovski, Cvete Dimitrieska, Sevde Stavreva *(Macedonia)*
Metodology for measuring of the transfer conveyor BRs 5500 load coordinates 57

Vasko Stojanovski, Vesna Angelevska, Cvete Dimitrieska, Sevde Stavreva *(Macedonia)*
Stability of transfer conveyor BRs 5500 after reconstruction 61

Zoran Mijić, Luka Ilić, Maja Kuzmanoski *(Serbia)*
Raman lidar for atmospheric aerosol profiling in Serbia 65

Zoran Mijić, Mirjana Perišić, Luka Ilić, Andreja Stojić, Maja Kuzmanoski *(Serbia)*
Air mass transport over Balkans region identified by atmospheric modeling and aerosol lidar technique 69

Alexander Udovsky, Dmitry Vasilyev *(Russia)*
Manifestation of ferro-, anti-ferro and paramagnetic phase diagram as specific heat singularities of Fe-Cr alloys 73

Alexander Udovsky, Mikhail Kupavtsev, Dmitry Vasilyev *(Russia)*
Application of a three-sublattice model for consistent calculations of the structural and thermodynamic properties of the σ-phase of Fe-Cr and Fe-V alloys for T=0K 77

Krsto Mijanović *(Bosnia and Herzegovina)*
Enhancement parameters workability with changes tribological characteristics of tools 81

Alina Badulescu, Daniel Badulescu *(Romania)*
Privatization and corporate governance in the metallurgical industry of cee economies: a review 85

Kemal Arslan, Kaan Soysal, Ömer Faruk Murathan *(Turkey)*
Surface characterization of boron nitride nanotubes (BNNT) 89

Georgi Patronov, Irena Kostova *(Bulgaria)*
Influence of rare earth dopants on zinc borophosphate materials 93

Alexander Udovsky *(Russia)*
Magnetism and size factor as main reasons of the birth of segregation at grain boundaries in bcc- Fe - Me alloys 97

Victor Grafutin, Irene Evstyukhina, Vladimir Kolotushkin, Victor Miloserdin, Andrew Mischenko, Serge Rudakov, Antony Sharapov, Alexander Udovsky, Yury Funtikov *(Russia)*
Investigations of short-range order and defects in iron- chromium alloys by nuclear physics methods 102

Ivan Saenko, Alexander Udovsky, Olga Fabrichnaya *(Russia, Germany)*
Experimental investigation of the Fe_2O_3–Y_2O_3 system and thermodynamic calculations 106

Erduan Mehmed, Vladislava Stefanova, Nadezhda Kazakova *(Bulgaria)*
Effect of impurities Co, Sb and Ge on current efficiency and energy consumption during zinc electrowinning 110

Can Çivi, Tuğçe Yağci, Enver Atik *(Turkey)*
Induction sintering of different shaped powder metal parts 114

RAMAN LIDAR FOR ATMOSPHERIC AEROSOL PROFILING IN SERBIA

Zoran Mijić, Luka Ilić, Maja Kuzmanoski

Institute of Physics Belgrade, University of Belgrade, Pregrevica 118, 11080 Belgrade, Serbia

Abstract

Due to the large variability in space and time atmospheric aerosols are considered one of the major uncertainties in climate forcing and atmospheric processes affecting human health and environment. An advanced laser remote sensing technique – lidar is the most appropriate tool for providing range-resolved aerosol vertical distribution. Lidar measurements of aerosol optical properties with high spatial and temporal resolution give detailed information on the occurrence and development of aerosol structures. The characteristics of Raman lidar system at the Institute of Physics Belgrade and its potential for investigation of tropospheric aerosols will be discussed. Lidar case study measurements together with methodology for aerosol layer identification is presented.

***Keywords**: remote sensing, Raman lidar, aerosol vertical distribution*

1. INTRODUCTION

Atmospheric aerosols influence the energy balance of the Earth, the water cycle and atmospheric chemistry, playing a crucial role in climate change and air quality. Due to their short lifetime and the large variability in space and time, atmospheric aerosols are considered one of the major uncertainties in climate forcing and atmospheric processes [1]. For radiative studies, it is necessary to measure aerosol optical properties, size, morphology and composition as a function of time and space, with a high resolution in both domains to account for the large variability. Lidar (Light Detection And Ranging), an active remote sensing technique, represents the optimal tool to provide range-resolved aerosol optical parameters. The first observational lidar stations network called EARLINET (the European Aerosol Research Lidar Network) [2] was founded in 2000 to provide the long-term measurement series needed to build a climatology of aerosol optical properties at the continental scale. The main objectives of EARLINET are the establishment of a comprehensive and quantitative statistical data base of the horizontal and vertical distribution of aerosols on the European scale using a network of advanced laser remote sensing stations, and the use of these data for studies related to the impact of aerosols on a variety of environmental problems. The developments for the quality assurance strategy, the optimization of instruments and data processing, and the dissemination of data have contributed to a significant improvement of the network towards a more sustainable observing system. Several lidar techniques are suitable for aerosol studies and in the last ten years rapid progress in laser technology, measurement techniques, and data acquisition systems has contributed to a much wider use of these techniques for aerosol remote monitoring. In this paper the characteristics of Raman lidar system at the Institute of Physics Belgrade (IPB), the EARLINET joining lidar station, is presented together with several quality tests in order to assess the performance of a lidar system. Case study measurement together with gradient method used to determine heights of both planetary boundary layer (PBL) and elevated aerosol layers is discussed.

2. EXPERIMENTAL

Atmospheric probing by lidar is able to obtain time dependent three dimensional pictures of aerosol distributions. Typical lidar system can be divided into the three main components, transmitter, receiving and data acquisition unit (Figure 1-left panel). Raman lidar system at the IPB (44.860 N, 20.390 E) is bi-axial lidar system with combined elastic and Raman detection designed to perform continuous measurements of aerosols in the planetary boundary layer and the lower free troposphere (Figure 1-right panel). Transmitter unit is based on the third harmonic frequency of a water cooled, pulsed Nd:YAG laser, emitting pulses of 65 mJ output energy at 355 nm with a 20 Hz repetition rate. In order to improve the maximum range and the precision of the system the beam expander is used to reduce the laser beam divergence expanding the beam's diameter by 3 times. The optical receiving unit consists of two sub-units, a receiving telescope and wavelength separation unit. The optical receiver is a Cassegrain reflecting telescope with a primary mirror of 250 mm diameter and a focal length of 1250 mm. Photomultiplier tubes are used to detect elastic backscatter lidar signal at 355 nm and Raman signal at 387 nm (Nitrogen vibrational scattering). The detectors are operated both in the analog and photon-counting mode and the spatial raw resolution of the detected signals is 7.5 m. Averaging time of the lidar profiles is of the order of 1 min corresponding to 1200 laser shots. The Licel transient recorder is comprised of a fast transient digitizer with on board signal averaging, a discriminator for single photon detection and a multichannel scaler combined with preamplifiers for both systems. For analog detection, the signal is amplified according to the input range selected and digitized by a 12-Bit-20 MHz A/D converter. At the same time the signal part in the high frequency domain is amplified and a 250 MHz fast discriminator detects single photon events above the selected threshold voltage.

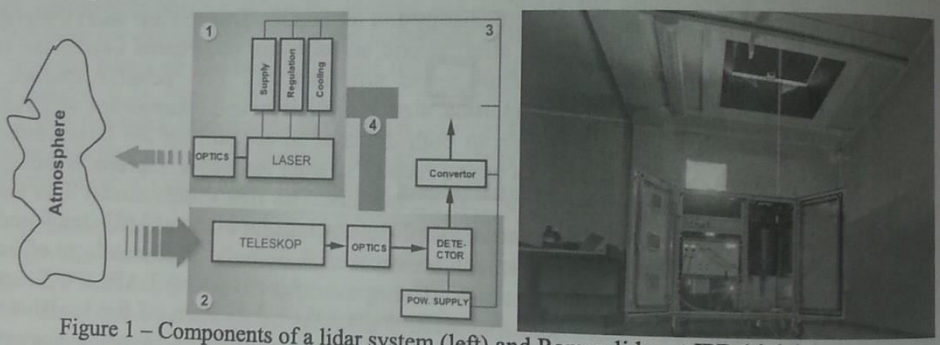

Figure 1 – Components of a lidar system (left) and Raman lidar at IPB (right)

Besides vertical profiles of aerosols backscatter and extinction coefficients lidar measurements can be used to estimate PBL height and aerosol elevated layers using different approaches [3]. In this study, the gradient method was used to determine the position of the strongest gradient of the aerosol vertical distribution, associated with the PBL height [4]. The height of a strong negative peak which can be identified as the absolute minimum of the range corrected signal's (RCS) derivative, determines the PBL top height. Other local minima in the signal derivative, with absolute values above a specified threshold and with transition intervals including a minimum of five points, are associated with elevated aerosol layer top heights in the free troposphere [4]. Differences between PBL and free troposphere can be also observed using vertical profiles of thermodynamic quantities and wind from radiosounding measurements. The bulk Richardson number is used for PBL height estimation from radiosounding measurements [5] at a weather station (Belgrade Košutnjak, WMO number 13275), 10 km away from the lidar measurement site.

3. RESULTS AND DISCUSSION

Within the lidar network, quality assurance program has been developed for both hardware and retrieval algorithms. One of the basic setup tests is system alignment since the incomplete overlap between the laser beam and the receiver field of view affects significantly lidar observations of particle optical properties.

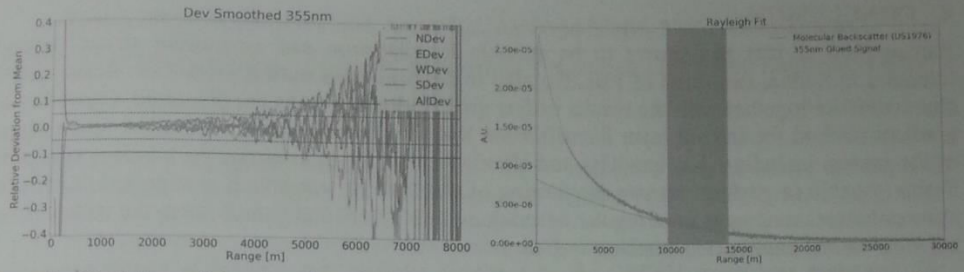

Figure 2 – Deviations of signals collected with four telescope sectors compared to the mean signal (left) and Rayleigh fit and fitting interval for 355 nm elastic channel, Raman lidar at IPB

Thus, quality assurance of the lidar measurement requires to test the alignment of the lidar system i.e. to determine overlap function. Procedure developed by Freudenthaler [6] involves a set of measurements with partially covered telescope (four sectors named N, E, W and S) so that each measurement is in fact collection of the backscattered light at a certain sector of the telescope. The deviation of each sector signal compared to the average of all signals below 10% is acceptable and from Figure 2 it is clear that the system is well aligned in the near field starting from 400 m. To assure lidar alignment in the far range the Rayleigh fit procedure can be used which is a normalization of the lidar signal to the calculated Rayleigh backscatter coefficient in a range where we assume clean conditions and where the calculated signal fits the lidar signal sufficiently good. From Figure 2–right panel it can be seen that the lidar system is well aligned up to the 12 km. Once the system is properly aligned it can be used for systematic aerosol measurements. In Figure 3 time series of RCS measured on July 6 2014 is presented.

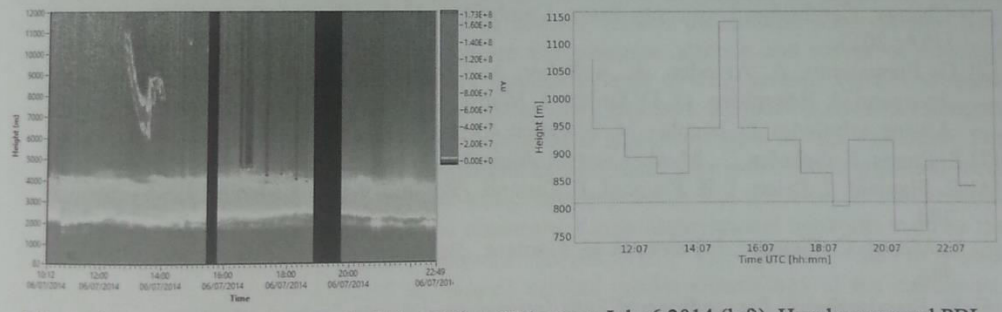

Figure 3 – Colormaps represent the lidar RCS at 355 nm on July 6 2014 (left). Hourly averaged PBL height (right). Horizontal red line represents PBL height retrieved from radiosounding at 00 UTC (dashed line) on July 7 2014

The gradient method was used to analyze the evolution of the PBL height during its diurnal cycle, and estimate elevated aerosol layer heights. Hourly averaged values of PBL show decrease of the PBL height from 1070 m to 860 m after the local noon (10 UTC). Significant increase in PBL height, reaching above 1100 m around 15 UTC can be attributed to strong convective motions which could have influenced formation of clouds between 16 UTC and 18 UTC, visible in the RCS plot. Gradient method shows decrease of the PBL heights until the end of the

measurement period to about 840 m. This value, is similar to the one estimated from 00 UTC radiosounding – 810 m. Two elevated aerosol layers were identified, one with its top reaching height of 2 – 2.2 km in the morning and reducing its height to below 1800 m in the afternoon. Another layer with top height ranging from 3.1 to 3.5 km was present during the whole measurement period.

4. CONCLUSION

Raman lidar at IPB has shown to be suitable for detection and monitoring aerosol layers' intrusion in Serbia, evolution of PBL but also to describe their optical properties. Basic system characteristics together with the results of few quality checks results are presented. Capability of gradient method for aerosol layer identification has been demonstrated. Additional optimization of the system including data handling and algorithm tests are in progress. As a unique system in Serbia capable to perform remote monitoring of atmospheric aerosols it is expected to perform systematic measurements on a regular schedule in near future and contribute to the collection of aerosol vertical distribution database in Europe.

ACKNOWLEDGEMENTS

This paper was realized as a part of the project III43007 financed by the Ministry of Education and Science of the Republic of Serbia within the framework of integrated and interdisciplinary research for the period 2011-2017. The publication was supported by the project GEO-CRADLE (Coordinating and integRating state-of-the-art Earth Observation Activities in the regions of North Africa, Middle East, and Balkans and Developing Links with GEO related initiatives towards GEOSS), Grant Agreement No. 690133, funded under European Union Horizon 2020 Programme - Topic: SC5-18b-2015, Integrating North African, Middle East and Balkan Earth Observation capacities in GEOSS.

REFERENCES

[1] T. F. Stocker, D. Qin, G.-K. Plattner, M. Tignor, S. K. Allen, J. Boschung, A. Nauels, Y. Xia, V. Bex, P. M. Midgley, IPCC: The Physical Science Basis, Contribution of Working Group I to the Fifth Assessment Report of the Intergovernmental Panel on Climate Change, Cambridge University Press, Cambridge, United Kingdom and New York, NY, USA, 2013.

[2] G. Pappalardo, A. Amodeo, A. Apituley, A. Comeron, V. Freudenthaler, H. Linné, A. Ansmann, J. Bösenberg, G. D'Amico, I. Mattis, L. Mona, U. Wandinger, V Amiridis, L. Alados Arboledas, D. Nicolae, M. Wiegner. Atmos. Meas. Tech. 7 (2014) 2389.

[3] S. Emeis, K. Schafer, C., Munkel Meteorologische Zeitschrift, 17(5) (2008) 621-630.

[4] C. Flamant, J. Pelon, P.H. Flamant, P. Durand., Boundary-Layer Meteorol. 83 (1997) 247-284.

[5] L. Menut, C. Flamant, J. Pelon, P. H. Flamant., Boundary-Layer Meteorol. 93 (1999) 269–286.

[6] V. Freudenthaler, Proceedings of 24th International Laser Radar Conference, 23-27 June, Boulder, USA, 2008.

University of Belgrade
Technical Faculty in Bor and
Mining and Metallurgy Institute Bor

49th International October Conference on Mining and Metallurgy

PROCEEDINGS

Editors:
Nada Štrbac
Ivana Marković
Ljubiša Balanović

Bor Lake, Serbia
October 18-21, 2017

IOC 2017
International October Conference

PROCEEDINGS,
49th INTERNATIONAL OCTOBER CONFERNCE
on Mining and Metallurgy

Editors:
Prof. dr Nada Štrbac
Doc. dr Ivana Marković
Doc. dr Ljubiša Balanović
University of Belgrade, Technical Faculty in Bor

Technical Editor:
M. Sc. Uroš Stamenković
University of Belgrade, Technical Faculty in Bor

Publisher: University of Belgrade, Technical Faculty in Bor
For the publisher: Dean Prof. dr Nada Štrbac
Circulation: 200 copies

Printed by "Happy trend DOO", Zaječar, 2017

ISBN 978-86-6305-066-2

CIP - Каталогизација у публикацији - Народна библиотека Србије, Београд

622(082)
669(082)

INTERNATIONAL October Conference on Mining and Metallurgy (49 ; 2017 ; Bor Lake)
Proceedings / 49th International October Conference on Mining and Metallurgy - IOC 2017, Bor Lake, Serbia, October 18-21, 2017;
[organized by] University of Belgrade, Technical Faculty Bor and Mining and Metallurgy Institute Bor;
editors Nada Štrbac, Ivana Marković, Ljubiša Balanović. - Bor : University of Belgrade, Technical Faculty, 2017 (Zaječar : Happy trend). - XXIII, 664 str. : ilustr. ; 25 cm

Tiraž 200. - Bibliografija uz svaki rad. - Registar.

ISBN 978-86-6305-066-2

a) Рударство - Зборници b) Металургија - Зборници

COBISS.SR-ID 246349324

Bor Lake, Serbia, October 18-21, 2017

SCIENTIFIC COMMITTEE

Prof. dr Nada Štrbac (Serbia) - president
Prof. dr Radoje Pantović (Serbia) - vice-president
Prof. dr Grozdanka Bogdanović (Serbia)- vice-president
Prof. dr Dragoslav Gusković (Serbia) - vice-president
Prof. dr Aleksandar Dimitrov (Macedonia)
Dr Ana Kostov (Serbia)
Dr Andrei Rotaru (Romania)
Prof. dr Anđelka Mihajlov (Serbia)
Prof. dr Batrić Pešić (USA)
Prof. dr Boštjan Markoli (Slovenia)
Prof. dr Boyan Boyanov (Bulgaria)
Prof. dr Branka Jordović (Serbia)
Prof. dr Carl Heinz Spitzer (Germany)
Prof. dr Costas Matis (Greece)
Prof. dr Dejan Tanikić (Serbia)
Prof. dr Desimir Marković (Serbia)
Prof. dr Dimitris Panias (Greece)
Prof. dr Dimitriu Sorin (Romania)
Prof. dr Dragan Manasijević (Serbia)
Prof. dr Duško Minić (Serbia)
Prof. dr Endre Romhanji (Serbia)
Prof. dr Fathi Habashi (Canada)
Prof. dr Guven Onal (Turkey)
Prof. dr György Kaptay (Hungary)
Prof. dr Heikki Jalkanen (Finland)
Prof. dr Iwao Katayama (Japan)
Prof. dr Jakob Lamut (Slovenia)
Prof. dr Jelena Penavin Škundrić (B&H)
Prof. dr Jožef Medved (Slovenia)
Prof. dr Karlo Raić (Serbia)
Prof. dr Kemal Delijić (Montenegro)
Prof. dr Krzystof Fitzner (Poland)
Prof. dr Luis Filipe Malheiros (Portugal)
Dr Magnus Ericsson (Sweden)
Prof. dr Milan Antonijević (Serbia)
Prof. dr Milan Trumić (Serbia)
Prof. dr Mile Dimitrijević (Serbia)
Prof. dr Mirjana Rajčić Vujasinović (Serbia)
Prof. dr Mirko Gojić (Croatia)
Dr Mile Bugarin (Serbia)
Dr Milenko Ljubojev (Serbia)
Dr Mirjam Jan-Blažić (Slovenia)
Dr Miroslav Sokić (Serbia)
Prof. dr Mirsada Oruč (B&H)
Dr Nadežda Talijan (Serbia)
Prof. dr Nenad Radović (Serbia)
Prof. dr Nenad Vušović (Serbia)
Prof. dr Nobuyuki Masuda (Japan)
Prof. dr Onuralp Yucel (Turkey)
Prof. dr Petr M. Solozhenkin (Russia)
Prof. dr Rodoljub Stanojlović (Serbia)
Prof. dr Sanda Krausz (Romania)
Prof. dr Seshadri Seetharaman (Sweden)
Dr Slavomir Hredzak (Slovakia)
Prof. dr Snežana Šerbula (Serbia)
Prof. dr Stoyan Groudev (Bulgaria)
Prof. dr Sulejman Muhamedagić (B&H)
Prof. dr Svetlana Ivanov (Serbia)
Dr Srećko Stopić (Germany)
Prof. dr Tamara Holjevac Grgurić (Croatia)
Prof. dr Tatjana Volkov-Husović (Serbia)
Prof. dr Tomaš Havlik (Slovakia)
Prof. dr Velizar Stanković (Serbia)
Prof. dr Velimir Radmilović (USA)
Prof. dr Vitomir Milić (Serbia)
Dr Vladan Ćosović (Serbia)
Prof. dr Vladimir Krstić (Canada)
Prof. dr Vladislav Kecojević (USA)
Prof. dr Vlastimir Trujić (Serbia)
Prof. dr Yong Du (China)
Prof. dr Zoran Marković (Serbia)
Prof. dr Žarko Radović (Montenegro)
Prof. dr Željko Kamberović (Serbia)
Prof. dr Živan Živković (Serbia)
Dr Walter Valery (Australia)
Dr Zvonko Gulišija (Serbia)

ORGANIZING COMMITTEE

Doc. dr Ivana Marković - president
Doc. dr Ljubiša Balanović - vice-president
Doc. dr Saša Stojadinović - vice-president
Prof. dr Svetlana Ivanov
Prof. dr Dragan Manasijević
Prof. dr Snežana Urošević
Dr Ana Kostov (IRM Bor)
Doc. dr Vesna Grekulović
Doc. dr Aleksandra Mitovski
Doc. dr Dejan Petrović
Doc. dr Milan Gorgievski
Doc. dr Ana Simonović
Doc.dr Tanja Kalinović
Doc.dr Marija Petrović Mihajlović
M.Sc. Uroš Stamenković
M.Sc. Oliver Marković
Slavica Stevanović, prof. engl.
Sandra Vasković, prof. engl.
Predrag Stolić, dipl. ing.
Dr Ana Radojević
M.Sc. Jelena Milosavljević

Marko Pavlović, Ljubiša Andrić, Dragan Radulović, Zoran Čeganjac *(Serbia)*
The influence of mechanical activation of talc- filler on the quality of the refractory coatings 53

Vesna Angelevska, Vasko Stojanovski, Cvete Dimitrieska, Sevde Stavreva *(Macedonia)*
Metodology for measuring of the transfer conveyor BRs 5500 load coordinates 57

Vasko Stojanovski, Vesna Angelevska, Cvete Dimitrieska, Sevde Stavreva *(Macedonia)*
Stability of transfer conveyor BRs 5500 after reconstruction 61

Zoran Mijić, Luka Ilić, Maja Kuzmanoski *(Serbia)*
Raman lidar for atmospheric aerosol profiling in Serbia 65

Zoran Mijić, Mirjana Perišić, Luka Ilić, Andreja Stojić, Maja Kuzmanoski *(Serbia)*
Air mass transport over Balkans region identified by atmospheric modeling and aerosol lidar technique 69

Alexander Udovsky, Dmitry Vasilyev *(Russia)*
Manifestation of ferro-, anti-ferro and paramagnetic phase diagram as specific heat singularities of Fe-Cr alloys 73

Alexander Udovsky, Mikhail Kupavtsev, Dmitry Vasilyev *(Russia)*
Application of a three-sublattice model for consistent calculations of the structural and thermodynamic properties of the σ-phase of Fe-Cr and Fe-V alloys for T=0K 77

Krsto Mijanović *(Bosnia and Herzegovina)*
Enhancement parameters workability with changes tribological characteristics of tools 81

Alina Badulescu, Daniel Badulescu *(Romania)*
Privatization and corporate governance in the metallurgical industry of cee economies: a review 85

Kemal Arslan, Kaan Soysal, Ömer Faruk Murathan *(Turkey)*
Surface characterization of boron nitride nanotubes (BNNT) 89

Georgi Patronov, Irena Kostova *(Bulgaria)*
Influence of rare earth dopants on zinc borophosphate materials 93

Alexander Udovsky *(Russia)*
Magnetism and size factor as main reasons of the birth of segregation at grain boundaries in bcc- Fe - Me alloys 97

Victor Grafutin, Irene Evstyukhina, Vladimir Kolotushkin, Victor Miloserdin, Andrew Mischenko, Serge Rudakov, Antony Sharapov, Alexander Udovsky, Yury Funtikov *(Russia)*
Investigations of short-range order and defects in iron- chromium alloys by nuclear physics methods 102

Ivan Saenko, Alexander Udovsky, Olga Fabrichnaya *(Russia, Germany)*
Experimental investigation of the Fe_2O_3–Y_2O_3 system and thermodynamic calculations 106

Erduan Mehmed, Vladislava Stefanova, Nadezhda Kazakova *(Bulgaria)*
Effect of impurities Co, Sb and Ge on current efficiency and energy consumption during zinc electrowinning 110

Can Çivi, Tuğçe Yağci, Enver Atik *(Turkey)*
Induction sintering of different shaped powder metal parts 114

AIR MASS TRANSPORT OVER BALKANS REGION IDENTIFIED BY ATMOSPHERIC MODELING AND AEROSOL LIDAR TECHNIQUE

Zoran Mijić, Mirjana Perišić, Luka Ilić, Andreja Stojić, Maja Kuzmanoski

Institute of Physics Belgrade, University of Belgrade, Pregrevica 118, 11080 Belgrade, Serbia

Abstract

This study combines atmospheric modeling with lidar measurements in order to assess the origin of aerosols traveling over Balkan region, having an impact on regional radiative budget and air quality. Particulate matter potential source regions and transport pathways were investigated using hybrid receptor modeling and mass concentrations measured in Belgrade, Serbia. In addition, the case study evidencing transport of Saharan dust particles simulated by the DREAM model was presented. The capability of the lidar technique to derive range-resolved vertical profiles of aerosol optical parameters was used to analyze the aerosol layers altitude and temporal evolution.

***Keywords**: atmospheric modeling, transport, PM*

1. INTRODUCTION

Suspended particulate matter (PM) in the atmosphere, commonly known as aerosol, plays an important role in the climate system. Besides significant effect on climate change, air quality and human health, aerosols affect long-range transport and deposition of toxics and nutrients. The complexity of aerosol processes in the atmosphere leads to large uncertainties in understanding of their role in many of the major environmental issues [1]. The direct (scattering and absorbing incoming solar radiation) and indirect aerosol effects (as they act as a cloud condensation nuclei) make the two largest contributions to the total uncertainty of radiative forcing. Regarding the impact of aerosols on air quality, the same processes that govern the global distribution, control the aerosol properties on regional and local scales. While *in situ* measurements are most adequate for air quality monitoring at the ground level, the assessment of impact of remote sources and transformation processes requires aerosol vertical distribution observations. Key parameters to be observed for this purpose are the presence, altitude and extent of elevated aerosol layers, the height of the planetary boundary layer (PBL), aerosol type, and mass concentration. Since long-range transport occurs at elevated layers, surface-based measurements of aerosol properties, such as chemical composition and size distribution are not sufficient. For global coverage including all relevant parameters, an integrated approach including ground-level and airborne in-situ measurements, ground-based remote sensing, and space-borne observations in combination with advanced modeling is necessary. Large observational networks such as the European Aerosol Research Lidar Network (EARLINET) [2], provide the long-term measurement series needed to build an aerosol vertical profile climatology at the continental scale. The capability of the lidar system (Light Detection And Ranging) to derive range-resolved aerosol vertical profiles with high spatial and temporal resolution is used to identify layers altitude and temporal evolution of intrusions. Using altitudes as inputs in air mass back-trajectories tracing method identification of aerosol sources at large distances from the measurement point, if their contribution is important, can be conducted. In this study hybrid receptor models for identification of potential source regions of PM affecting air quality in Belgrade are presented together with a case study evidencing transport of Saharan dust particles.

2. METHODOLOGY

Lidar technique is an active remote sensing method based on laser emission of the short-duration light pulses to the atmosphere and the analysis of the return signal. The intensity of the light backscattered by atmospheric molecules and particles is measured versus time – through the telescope receiver, collimating optics, a bandpass filter for daylight suppression – by an appropriate detector. For vertical profiling and remote sensing of atmospheric aerosol layers, Raman lidar at the Institute of Physics Belgrade (44.860 N, 20.390 E) has been used. It is bi-axial system with combined elastic and Raman detection designed to perform continuous measurements of aerosols in the PBL layer and the lower free troposphere. It is based on the third harmonic frequency of a compact, pulsed Nd:YAG laser, emitting pulses of 65 mJ output energy at 355 nm with a 20 Hz repetition rate. The optical receiver is a Cassegrain reflecting telescope with a primary mirror of 250 mm diameter and a focal length of 1250 mm. Photomultiplier tubes are used to detect elastic backscatter lidar signal at 355 nm and Raman signal at 387 nm. The detectors are operated both in the analog and photon-counting mode with lidar profiles averaging time of the order of 1 min and the spatial raw resolution of the detected signals of 7.5 m. Lidar measurements can be used in synergy with numerical models in order to validate and compare information about aerosols. In this paper DREAM (Dust Regional Atmospheric Model) model, designed to simulate and/or forecast the atmospheric cycle of mineral dust aerosol [3], is used to analyze dust transport. To estimate potential PM remote emission sources and their impact at the receptor site, concentration weighted trajectory (CWT) hybrid receptor model [4] was applied to the data set comprised of hourly PM_{10} mass concentrations obtained from Belgrade suburban location "Ovča" during the period 2012-14, and 72-h air masses back-trajectories, calculated according to Perišić et al. [5]. Furthermore, to obtain the vertical profile of PM, concentration weighted boundary layer (CWBL) hybrid receptor model [6], which uses a two-dimensional grid and a planetary boundary layer height, or any altitude in general, as a frame of reference, was used. Although the model can be applied for analyzing the pollutant concentration vertical distribution along the transport pathway, in this paper we present its usage for the receptor site solely.

3. RESULTS AND DISCUSSION

According to the CWT analysis, the most prominent PM_{10} sources were located in neighboring countries and in the areas NW, E and S of Belgrade. Significant impact of Central and Eastern European sources was registered during the autumn season (Figure 1–left panel).

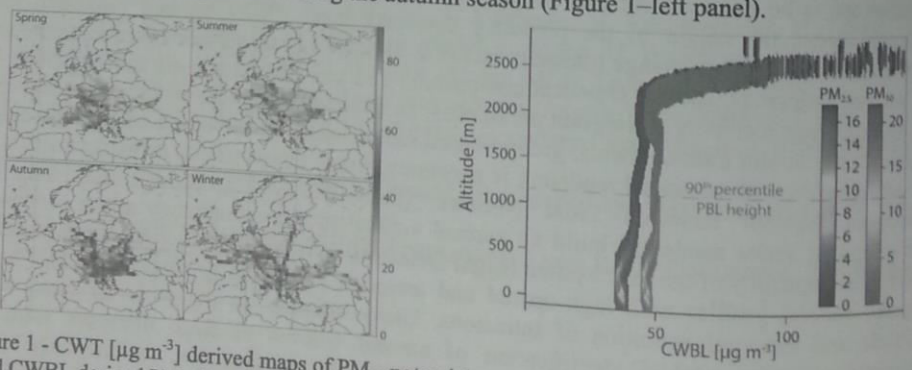

Figure 1 - CWT [μg m^{-3}] derived maps of PM_{10} potential sources in Europe – seasonal variations (left), and CWBL derived PM altitude distribution above the receptor site (right) – color scales indicate the number of events

Very similar, almost constant PM altitude distribution over the receptor site was observed for both coarse and fine particles (Figure 1–right panel), and the most common PBL heights (within 90th percentile). However, given the number of events (colored scale), it can be seen that concentrations exhibit decreasing trend to the height of about 400 m because the species emitted or generated near the ground level are mostly trapped and concentrated within the PBL, whereas free atmosphere concentrations remain low. Large CWBL values at higher altitudes correspond to rare PBL fluctuations which are not statistically significant, so the model results cannot be taken into consideration.

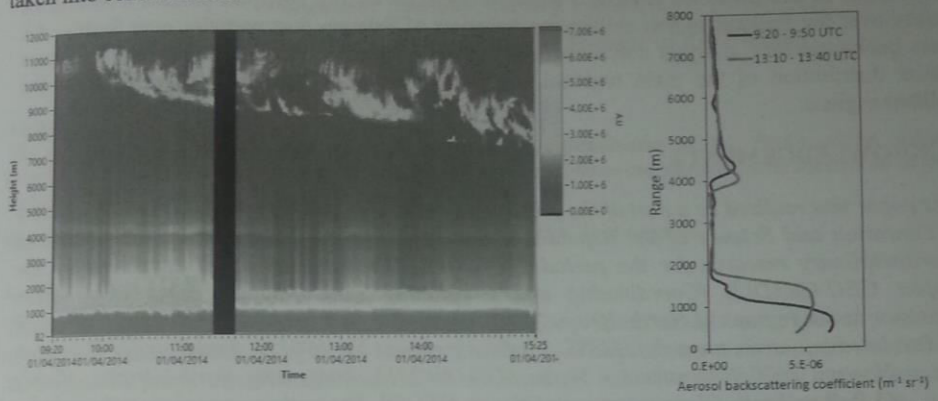

Figure 2 – Lidar range corrected signal (left) and backscatter coefficient at 355 nm (right) in Belgrade

Another aspect of aerosol climatology over Balkans region is related to the intrusions of Saharan dust which usually occurs during spring and summer periods. Such a case study evidencing transport of Saharan dust on 1st April 2014 is presented. From the RCS lidar time series (Figure 2), but also from the calculated backscatter coefficients profiles, the direct presence of an aerosol layer around 4-5 km altitude over Belgrade can been seen. This event was also successfully forecasted by DREAM model (Figure 3-left panel).

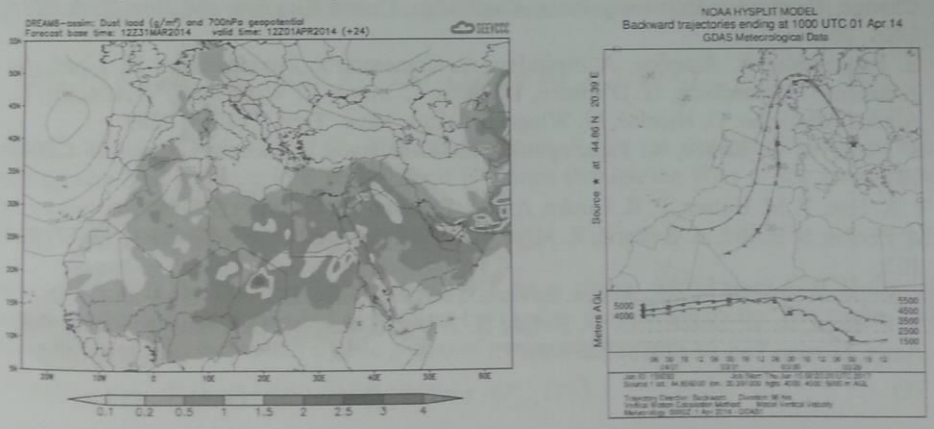

Figure 3 – Dust load over South Europe, estimated by the DREAM model (left) and air mass back-trajectories ending over Belgrade on 1st April, 2014 (righ)

Since the aerosols serve as a valuable tracer of air motion, using lidar observed altitudes of aerosol layer as inputs in the HYSPLIT [7] back-trajectory tracing method the source of aerosols was confirmed. As shown in Figure 3 (right panel) air masses reaching Belgrade traveled over

South Europe (Mediterranean Sea, Spain) and West Europe being influenced by continental pollution too.

4. CONCLUSION

The main advantage of lidar – real time observation of aerosol layering is that it can be used for air mass origin and path identification. Furthermore, in combination with statistical and numerical modeling, this technique can provide important information about aerosol type and distribution. In this paper we presented a case analysis of aerosol transport process affecting air quality over the Balkans region evidencing transport of Saharan dust particles over Serbia. Air mass back-trajectory analysis combined with hybrid receptor modeling were used to assess spatial distribution of the main regional sources for aerosols affecting air quality over the Balkans regions.

ACKNOWLEDGEMENTS

This paper was realized as a part of the projects III43007 and III41011 financed by the Ministry of Education and Science of the Republic of Serbia within the framework of integrated and interdisciplinary research for the period 2011-2017. The publication was supported by the project GEO-CRADLE (Coordinating and integRating state-of-the-art Earth Observation Activities in the regions of North Africa, Middle East, and Balkans and Developing Links with GEO related initiatives towards GEOSS), Grant Agreement No. 690133, funded under European Union Horizon 2020 Programme - Topic: SC5-18b-2015, Integrating North African, Middle East and Balkan Earth Observation capacities in GEOSS. The authors gratefully acknowledge the NOAA Air Resources Laboratory (ARL) for the provision of the HYSPLIT transport and dispersion model and/or READY website (http://www.ready.noaa.gov) used in this publication.

REFERENCES

[1] T. F. Stocker, D. Qin, G.-K. Plattner, M. Tignor, S. K. Allen, J. Boschung, A. Nauels, Y. Xia, V. Bex, P. M. Midgley, IPCC: The Physical Science Basis, Contribution of Working Group I to the Fifth Assessment Report of the Intergovernmental Panel on Climate Change, Cambridge University Press, Cambridge, United Kingdom and New York, NY, USA, 2013.

[2] G. Pappalardo, A. Amodeo, A. Apituley, A. Comeron, V. Freudenthaler, H. Linné, A. Ansmann, J. Bösenberg, G. D'Amico, I. Mattis, L. Mona, U. Wandinger, V. Amiridis, L. Alados Arboledas, D. Nicolae, M. Wiegner, Atmos. Meas. Tech. 7 (2014) 2389.

[3] S. Nickovic, G. Kallos, A. Papadopoulos, O. Kakaliagou, J. Geophys. Res. 106 (2001) 1813.

[4] Y. K. Hsu, T. M. Holsen, P. K. Hopke, Atmos. Environ. 37(4) (2003) 545-562.

[5] M. Perišić, S. Rajšić, A. Šoštarić, Z. Mijić, A. Stojić, Air Qual Atmos Health 10 (2017) 93-103.

[6] A. Stojić, S. Stanišić Stojić., Atmos. Environ. 164 (2017) 216-223.

[7] A. F. Stein, R. R. Draxler, G. D. Rolph, B. J. B. Stunder, M. D. Cohen, F. Ngan, Bull. Amer. Meteor. Soc. 96 (2015) 2059-2077.

WeBIOPATR2017

Particulate Matter: Research and Management

Proceedings from the
6th WeBIOPATR
Workshop & Conference
Belgrade, Serbia
6.-8.9.2017

Milena Jovašević-Stojanović
and Alena Bartoňová, eds.

Belgrade 2019

WeBIOPATR

The 6th WeBIOPATR Workshop and Conference,
Particulate Matter: Research and Management,
***WEBIOPATR2017 is organized by**:*

Vinča Institute of Nuclear Sciences, Serbia
Public Health Institute of Belgrade, Serbia
NILU Norwegian Institute for Air Research, Norway

The 6th WeBIOPATR Workshop and Conference,
Particulate Matter: Research and Management,
***WeBIOPATR2017 is supported by**:*

Ministry of Education, Science and Technological Development of

Republic of Serbia

PROCEEDINGS

The Sixth International WeBIOPATR Workshop & Conference
Particulate Matter: Research and Management
WeBIOPATR2017

6 - 8 September 2017
Belgrade, Serbia

Editors
Milena Jovašević-Stojanović
Alena Bartoňová

Publisher
Vinča Institute of Nuclear Sciences
Dr Zlatko Rakočević, Director
P.O. Box 522
11001 Belgrade, Serbia

Printed by
Vinča Institute of Nuclear Sciences

Number of copies
150

ISBN: 978-86-7306-152-8

Vinča Institute of Nuclear Sciences
www.vin.bg.ac.rs

SCIENTIFIC COMMITTEE

Dr Alena Bartoňová, Norway

Dr Bojan Radak, Serbia

Prof. Dr David Broday, Israel

Dr Med Elizabeta Paunović, Germany

Dr Maria Cruiz Min, Spain

Dr Milena Jovašević-Stojanović, Serbia

Prof. Dr Nenad Živković, Serbia

Prof. Dr Radim Šrám, Czech Republic

Dr Renata Kovačević, Serbia

Dr Slobodan Nićković, Serbia

Prof. Dr Simone Barreira Morais, Portugal

Zoran Mijić, Serbia

Prof. Dr Zoran Ristovski, Australia

Dr Zorana Jovanović-Andersen, Denmark

ORGANIZING COMMITTEE

Vinča Institute of Nuclear Sciences, Belgrade: Serbia
Dr Dragan Alavantić, Serbia
MS Ivan Lazović, Serbia
MS Maja Jovanović, Serbia (Secretary)
Dr Milena Jovašević-Stojanović (Co-chair)
Dr Miloš Davidović, Serbia (Secretary)
Dr Snežana Pašalić, Serbia

NILU - Norwegian Institute for Air Research, Kjeller
Dr Alena Bartoňová, Norway (Co-chair)

Public Health Institute of Belgrade, Belgrade
Dr Anka Cvetković, Serbia
MS Andrej Šoštarić, Serbia
Vesna Slapčević, Serbia

Ministry of Environmental Protection of RS
Ms Biljana Filipović, Serbia

Serbian Environmental Protection Agency
Mr Dejan Lekić, Serbia
Mr Tihomir Popović, Serbia

National Institute of Public Health "Dr Milan Jovanović-Batut", Belgrade
Dr Med Branislava Matić, Serbia

Military Medical Academy, Belgrade
Prof. Dr Jasmina Jović-Stošić, Serbia

Institute of Physics, Belgrade
Dr Mira Aničić Urošević, Serbia

Faculty of Occupational Protection, University of Niš
Prof. Dr Nenad Živković, Serbia

Medical Faculty, University of Niš
Prof. Dr Aleksandra Stanković, Serbia

Institute of Metallurgy and Mining, Bor
Dr Viša Tasić, Serbia

Mechanical Faculty, University of Belgrade
Prof. Dr Aleksandar Jovović, Serbia

CONFERENCE TOPICS

ATMOSPHERIC PARTICULATE MATTER - PHYSICAL AND CHEMICAL PROPERTIES	• *sources and formation of particulate matter* • *particulate matter composition and levels outdoors and indoors* • *environmental modeling* • *nanoparticles in the environment*
PARTICULATE MATTER AND HEALTH	• *exposure to particulate matter* • *health aspects of atmospheric particulate matter* • *full chain approach*
PARTICULATE MATTER AND REGULATORY ISSUES	• *issues related to monitoring of particulate matter* • *legislative aspects* • *abatement strategies*

PREFACE

The International Workshop and Conference, Particulate Matter: Research and Management – WeBIOPATR is a biennial event held in Serbia since 2007. The conference addresses air quality in general and particulate matter specifically. Atmospheric particulate matter arises both from primary emissions and from secondary formation in the atmosphere. It is one of the least well-understood local and regional air pollutants, has complex implications for climate change, and is perhaps the pollutant with the highest health relevance. It also poses many challenges to monitoring.

By WeBIOPATR, we aim to link the research communities with relevance to particulate matter with the practitioners of air quality management on all administrative levels, in order to facilitate professional dialogue and uptake of newest research into practice. The workshops usually draw an audience of about 70, and attract media attention in Serbia. It enjoys support of the responsible authorities, Ministry of Health, Ministry of Environment, and the Serbian Environmental Agency whose sponsorship is indispensable and gratefully acknowledged. We enjoy also support of international bodies such as the WHO.

The 1st WeBIOPATR Workshop was held in Beograd, 20.-22. May 2007, associated with a project funded by the Research Council of Norway. The 2nd workshop was held in Mecavnik, Serbia, 28.8.-1.9. 2009. WeBIOPATR2011 was held in Beograd 14.-17. 11. 2011 and for the first time, included a dedicated student workshop. WeBIOPATR2013 was held in Beograd 2.-4. 10. 2013. It covered the traditional PM research and management issues, discussions on how to encourage citizens to contribute to environmental governance, and how to develop participatory sensing methods. WeBIOPATR2015 was held in Beograd 14.-16.10. 2015. Own sessions were devoted to sensor technologies for air quality monitoring, utilizing information and input from the EU FP7 funded project CITI-SENSE (http://co.citi-sense.eu) and the EU COST action EuNetAir (www.eunetair.it).

We have now the pleasure to present to you the proceedings of the 6th conference held in Beograd 6.-8.9. 2017. We are excited to have contributions from old friends and new acquaintances, and we are especially pleased with a wider than before Western Balkan participation. The contributions were reviewed. The language editing was performed by Dr Simon Smith, PhD, to whom we would like to extend out sincere thanks. Technical manuscript preparation was graciously done by Dr Milos Davidovic, PhD, to whom we are very grateful.

We are hoping that you, the reader, will extend your support to WeBIOPATR also in the future. The issues of atmospheric pollution, with their wide implications for climate change, human health and ecosystem services, are no less important today than before. Addressing them requires a strong scientific community and commitment of all societal actors. Your contribution will make a difference.

Milena Jovašević-Stojanović and Alena Bartoňová

CONTENTS

1. PM COMPOSITION AND MODELING I 9

1.1. Black Carbon Measurements: Methodology, Sources, and Relevance on a Local, Regional and Global Scale 10

1.2. Source Analysis of Particle-Associated Polycyclic Aromatic Hydrocarbons (PAHs) in the Vicinity of a Steelmaking Industry (Smederevo, Serbia) 11

1.3. Source Apportionment Study Near Cooper Smelter Complex in Serbia Using Positive Matrix Factorization 18

1.4. Spatial Distribution of Carbon Mass Concentrations in Croatia 24

1.5. Characterization of Suspended Particles in the University Classrooms and Offices in Bor, Serbia 32

2. ADVANCES IN PM CHARACTERIZATION I 37

2.1. Electroanalytical Methods in Aerosols Particulate Matter Characterization 38

2.2. Time Series Analysis of Low Molecular Weight Organic Acids in Atmospheric Aerosols by Ion Chromatography 44

2.3. Polycyclic Aromatic Hydrocarbons: The Importance of (Bio)Monitorization 49

2.4. Leaves of Common Urban Tree Species as a Measure of Particle Pollution 56

2.5. Node-to-Node Field Calibration of Wireless Distributed Air Pollution Sensor Network 62

3. HEALTH EFFECTS I 63

3.1. Health Impacts of Air Pollution in Serbia 64

3.2. Comparative Analysis of Air Pollution and the Incidence of Diseases in the Exposed Population in Serbia 65

3.3. Exposure to Biomass Fuel Smoke and Use of Primary HealthCare in Women 66

3.4. Cytotoxic and Genotoxic Effects of Combustion-Derived Particles from Different Emission Sources 71

4. SCIENCE, POLICY & EDUCATION 77

4.1. The Activities of WHO Regional Office for Europe in Supporting the Development of Policies and Interventions in Improving Air Quality Related to PM 78

4.2. Urban Particulate Matter: Technologies for Assessment and Need for Information 79

4.3. A Dusty Road to Gardaland - Turning School's Science Projects Fun 80

5. PM COMPOSITION AND MODELING II 86

5.1. Atmospheric Mineral Dust as the Most Abundant Aerosol: Impacts and Modelling - A Review 87

5.2. Analysis of Regional Atmospheric Conditions Associated With Higher Ozone Days in Northwest Anatolia of Turkey 98
5.3. A Study of a Dust Intrusion Event Over Belgrade, Serbia 103
5.4. Relative Importance of Gaseous Pollutants and Aerosol Constituents for Identification of PM_{10} Sources of Variability 109
6. POSTER SESSION 113
6.1. Multiscale Multifractal Analysis of Nonlinearity in Particulate Matter Time Series 114
6.2. Modeling of PM_{10} Dispersion from Coal Thermal Power Plants Kostolac A and B 118
6.3. PM_{10} and $PM_{2.5}$ Emission During the Process of Preparing the Material for TIG Welding . 131
6.4. Convergence Chromatography as an Emerging Technique For Determination of PAHs in Biomonitors 132
6.5. Presentation of Current Atmospheric Particulate Matter Levels Within National Network for Air Quality Monitoring in Serbia 137
6.6. A Candidate Measurement System for the Standardized Routine Monitoring of Particle Number Concentration in Ambient Air 138
6.7. Preliminary Characterization of Carbonaceous Aerosols Collected Close to a Busy Tunnel in Belgrade, Serbia 140
6.8. Scope of Ambient Air PM_{10} Monitoring Within the Network of Local Public Health Institutions in Serbia 144
6.9. Evaluation of the Traffic Density and Meteorological Conditions Influence on $PM_{2.5}$ Concentration Levels in Ambient Air on Highway E75 148
6.10. Impact Of Street Level Traffic Emissions (CO_2, CO, NO_X, PM and VOC) on Outdoor Temperature and Thermal Comfort in a Complex Urban Environment 149
7. HEALTH EFFECTS II 155
7.1. Health Effects of Short- and Long-Term Exposure to Air Pollution in Denmark: An Overview of Epidemiological Methods and Major Findings 156
7.2. Particulate Matter in Nis, Serbia: Levels, Sources and Major Health Effects 157
7.3. The Development of Who Airq+ Tool to Assess the Impacts of Air Pollution on Health ... 161
8. PM COMPOSITION AND MODELING III 162
8.1. Concentration Weighted Boundary Layer Hybrid Receptor Model for Analyzing Particulate Matter Altitude Distribution 163
8.2. Estimation of PM emissions from Cruise ships in Kotor Bay 167
8.3. Practical Application of Short-Range Calpuff Modelling for $PM_{2.5}$ Assessment from Pulp and Paper Mill in Canada 174
8.4. Efficient Tools for the Creation and Validation of LUR Based Maps 175
9. EXPOSURE TO TOXIC AND INFECTIVE PM AGENTS 180
9.1. Microbiological Quality of Air in Pharmaceutical Laboratories 181
9.2. Development of an Evidence Base for Respirator Selection for Bioaerosols 186

9.3. Aerosol Transmission of Infective Agents: Possible Impacts 191
10. ADVANCES IN PM CHARACTERIZATION II..... 199
10.1. An instrument for the rapid quantification of PM-bound ROS: the Particle Into Nitroxide Quencher (PINQ) 200
10.2. Comparison of Low-Cost And Conventional PM Sizers and Counters in Indoor Ambient Environment 207
10.3. Artificial Intelligence Models With Multivariate Inputs for Calibration of Low-Cost PM Sensors - Proof of Concept and Preliminary Analysis 216
10.4. Analysis of Particulate Matter and Small Ion Concentration in the Indoor Environment Based on a Balance Equation 223
10.5. Current Status of Applicability of Low-Cost Particulate Matter Sensors for Ambient Air Pollution and Exposure Assessment 228
AUTHOR INDEX 237

5.3. A STUDY OF A DUST INTRUSION EVENT OVER BELGRADE, SERBIA

M. Kuzmanoski, L. Ilić, M. Todorović, Z. Mijić
Institute of Physics Belgrade, University of Belgrade, Belgrade, Serbia
maja.kuzmanoski@ipb.ac.rs

ABSTRACT

This paper is to present the results of aerosol measurements from a dust intrusion episode in Belgrade during the period of July 5-7, 2014. A vertical profile of the aerosol backscattering coefficient, obtained from ground-based LIDAR measurements in Belgrade, showed a distinct elevated dust layer at altitudes of 2-5 km on July 5, 2014. The altitude of the layer decreased later in the episode, with its centre of mass decreasing from approximately 4 km to below 3 km. On the last day of the episode, an entrainment of the dust layer into the planetary boundary layer was observed, consistent with the observed change of PM_{10} concentration at the surface level. The PM_{10} concentration increased by 15-17 μg m^{-3} at three monitoring sites in Belgrade, as the dust plume was settling down during the episode. The DREAM model simulations reproduced well the observed dust layer altitude. Dust surface concentrations from the model showed an increase of 11 μg m^{-3} during the episode. The difference from observed PM_{10} increase was attributed to contributions of other aerosol types to observations.

INTRODUCTION

Mineral dust is one of the most abundant components of the global aerosol burden (Kinne et al., 2006). Saharan dust originates from the world's primary dust source region, and can be transported over long distances (Prospero, 1999; Ansmann et al., 2003). It mixes with other aerosol types along the transport path, affecting their physical, optical and radiative properties. Mineral dust affects the Earth's radiative budget by scattering and absorbing solar and terrestrial radiation (direct effect), by modifying cloud properties due to their role in cloud formation (indirect effect) or by changing the thermal structure of the atmosphere (semi-direct effect). However, there is significant uncertainty in estimating role of dust in the Earth's climate system (IPCC, 2013). Dust impacts air quality, even at locations distant from the source region (Prospero, 1999), and has harmful effects on human health (Giannadaki et al., 2014). To address these problems, it is important to improve the understanding of dust properties on temporal and spatial scales. This requires the synergistic use of ground-based and satellite measurements, along with a regional dust model, for the analysis of dust spatial and temporal variability.

Here we present a case study of a dust intrusion episode observed in Belgrade from July 5-7, 2014. The analysis of the temporal variability of the dust layer was based on ground-based LIDAR measurements in Belgrade, while satellite measurements were used in the discussion of the spatial distribution of dust. Furthermore, the impact of the dust intrusion episode on PM_{10} concentrations in Belgrade was analysed. The measurement results were compared with results of Dust REgional Atmospheric Model DREAM (Ničković et al., 2001).

METHODOLOGY

The aerosol backscattering coefficient at 355 nm was derived from LIDAR measurements in Belgrade. A combined Raman elastic backscatter LIDAR has been operating at the Institute of Physics Belgrade since February 2014. It is based on the Nd:YAG laser operating at a fundamental wavelength of 1064 nm, and second and third harmonics at 532 and 355 nm. The laser pulses of 5 nm duration are transmitted at repetition rate of 20 Hz, with the output energies of 105, 45 and 65 mJ at these three wavelengths. The receiver is based on a 250 mm Cassegrain telescope in a biaxial arrangement, with adjustable field of view in the range from 0.5 to 3 mrad. Photomultiplier tubes are used to detect the backscatter signal in photon counting and analogue mode. The signals are detected at 355 and 387 nm, with a vertical resolution of 7.5 m and a temporal resolution of 1 minute. In this work we analysed the elastic backscatter signal at 355 nm. The analysis of the LIDAR signal to obtain the aerosol backscattering coefficient was performed using Fernald-Klett retrieval method (Fernald, 1984; Klett, 1985), assuming a LIDAR ratio value of 50 sr. Due to incomplete overlap of the laser and telescope fields of view, the LIDAR signal registering below 500 m was not considered in the analysis.

Daily PM_{10} mass concentrations at surface level, at three stations in Belgrade, were obtained from the State network for automatic monitoring of air quality (https://data.gov.rs/sr/datasets/kvalitet-vazdukha-u-republitsi-srbiji/).

Dust REgional Atmospheric Model DREAM (Ničković et al., 2001) embedded into the NCEP/NMME non-hydrostatic atmospheric model (Janjić et al., 2011) was used to provide horizontal and vertical distribution of dust concentration. The model domain covers Northern Africa, the Middle East and a large part of the European

continent, with a horizontal resolution of 1/5° (~ 30 km) and 28 vertical levels. It uses 8 particle size bins within the 0.1-10 μm radius range.

Additionally, we used an aerosol optical depth (AOD) at 550 nm from combined Deep Blue and Dark Target algorithms and the Deep Blue Ångström exponent (AE) at 412-470 nm products from the MODIS (Moderate Resolution Imaging Spetroradiometer) instrument aboard the NASA Aqua satellite. We used Collection 6, Level 3 data products. It should be noted, that the increase in AOD indicates an increase in aerosol load, while the AE parameter is used as a qualitative measure of particle size (the smaller AE values indicate predominantly coarse particles).

CALIOP (Cloud-Aerosol Lidar with Orthogonal Polarization) on board the CALIPSO satellite, was used to obtain vertical profiles of aerosols and clouds. It is an elastic backscatter LIDAR operating at two wavelengths: 532 nm and 1064 nm, with a depolarization channel at 532 nm. Here we used Level 2 Vertical Feature Mask product, which provides information on the aerosol types present in the detected layers (Omar et al., 2009).

Air-mass back trajectories ending at different altitudes over the LIDAR measurement site were calculated using the Hybrid Single-Particle Lagrangian Integrated Trajectory (HYSPLIT) model (Draxler and Hess, 1998; http://ready.arl.noaa.gov/HYSPLIT.php), with meteorological input from the Global Data Assimilation System (GDAS). The backtrajectories were used to provide an indication of the origin and pathways of air-masses arriving at altitudes of interest over Belgrade.

RESULTS AND DISCUSSION

We present an analysis of a dust episode that was observed over Belgrade from July 5-7, 2014. The beginning of the episode can be seen in MODIS data shown in Figure 1. MODIS values of AOD and AE indicate an increase of aerosol load and an increased contribution of coarse particles on July 5th compared to the previous day; this is typical for dust episodes.

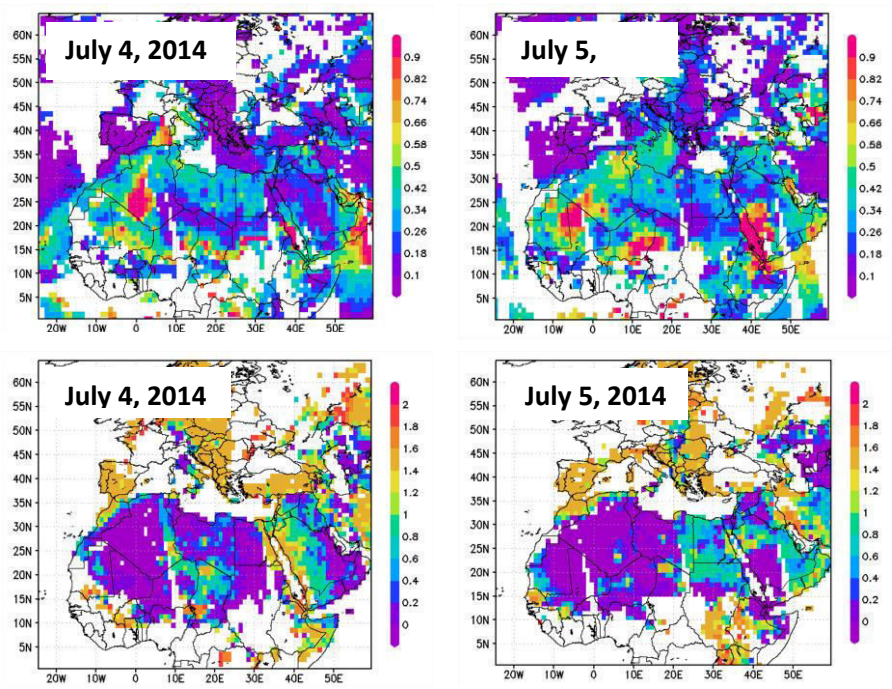

Figure 1. *MODIS aerosol data for July 4-5, 2014: (upper panels) MODIS aerosol optical depth (AOD) at 550 nm from combined Deep Blue and Dark Target algorithms; (lower panels) Deep Blue Angström exponent (AE) at 412-470 nm.*

The observed AOD at 550 nm over Belgrade increased from below 0.1 on July 4th, to about 0.3 on July 5th (the first day of the dust episode), with a decrease in the AE value from 1.4 to 0.4. Moderate AOD values were observed

over Belgrade during the dust episode. MODIS data also showed that the dust event affected parts of western and central Europe.

A close CALIPSO overpass over Belgrade occurred during the peak of the dust episode, on July 6th, at approximately 12 UTC. The CALIOP Vertical Feature Mask data, along the satellite ground track, is presented in Figure 2. We also showed the dust load over the area of interest and a vertical profile of the dust concentration along the CALIPSO ground track, resulting from DREAM model simulations. Both CALIOP data and the DREAM model results indicated that the dust plume extended north to Poland. The concentrations resulting from the model were largest around 40°N, at altitudes between 2 and 3 km, and decreased towards the north. At the part of the track within a 100 km distance from Belgrade, the DREAM model dust concentrations showeda maximum at a similar altitude range. CALIOP data suggested the presence of polluted dust (a mixture of pure dust with smoke or anthropogenic pollution) in this layer.

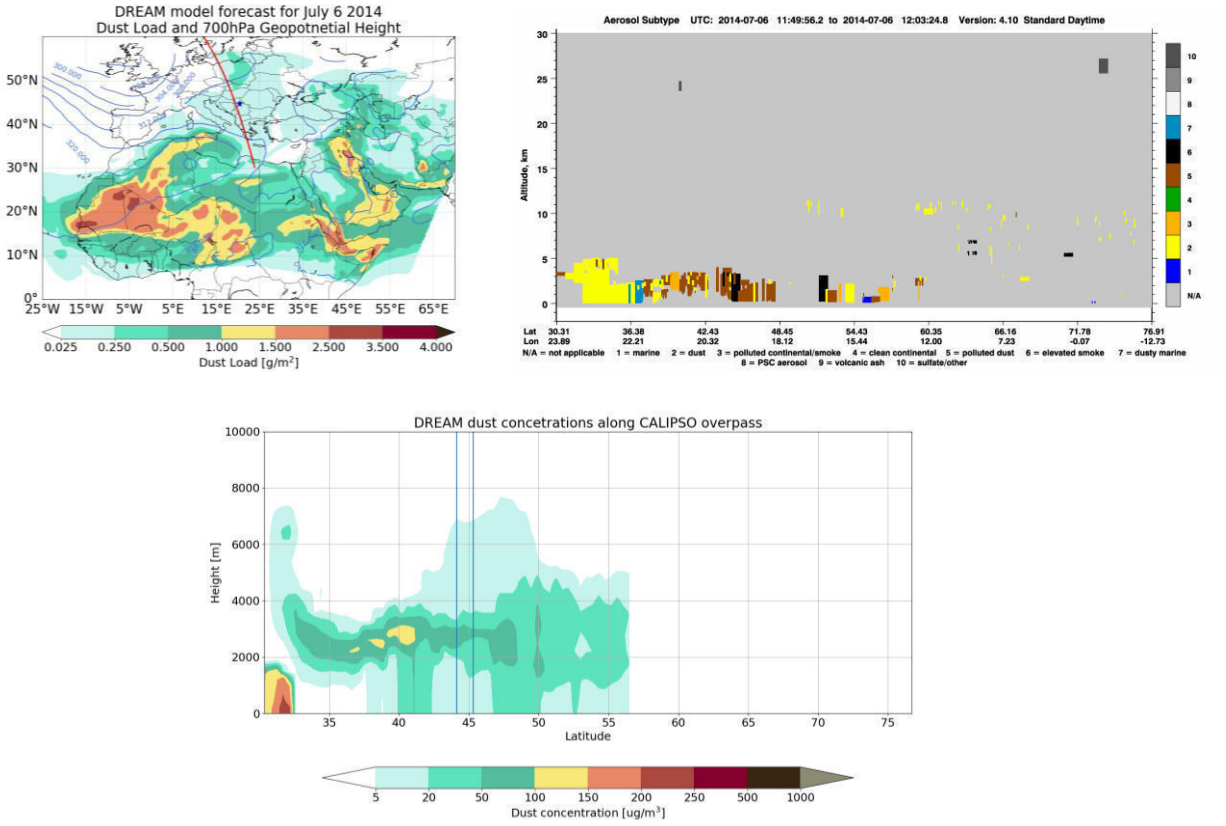

Figure 2. *(upper panels) Map of dust load calculated from DREAM model on July 6, 2014 at 12 UTC, with CALIPSO ground track and Belgrade LIDAR station marked; and the corresponding results of CALIOP aerosol classification. (lower panel) Dust concentration vertical profiles along the CALIPSO ground track obtained from DREAM model. Data between the two vertical lines corresponds to the part of the track within 100 km distance from Belgrade LIDAR station.*

Ground-based LIDAR measurements in Belgrade were analyzed to characterize the aerosol vertical profile during the dust episode. The profile of the aerosol backscattering coefficient showed a distinctly elevated aerosol layer on July 5th, at altitudes between approximately 2 and 5 km, with a maximum at about 4.5 km. It was identified as a dust layer, based on the air-mass backtrajectory was calculated to find the corresponding aerosol source region. Selected vertical profiles of the aerosol backscattering coefficient, and of the corresponding profiles of dust mass concentration obtained from DREAM model simulations, are presented in Figure 3. It should be noted that their comparison is only qualitative as we did not attempt to calculate the backscattering coefficient from the DREAM model results due to its high sensitivity to aerosol chemistry. The averaging of LIDAR signals for the analysis of the presented data was performed in 30minute intervals centered at the time of the model result. The dust layer boundaries were determined following the procedure described by Mona et al. (2006). The backscattering

coefficients showed that the layer descended during the course of the dust episode, and indicated an entrainment of dust into the PBL on July 7th. Dust mass concentrations resulting from the DREAM model showed a similar vertical pattern as the LIDAR measurements and a notable increase of dust concentration at altitudes below 2 km on July 7th.

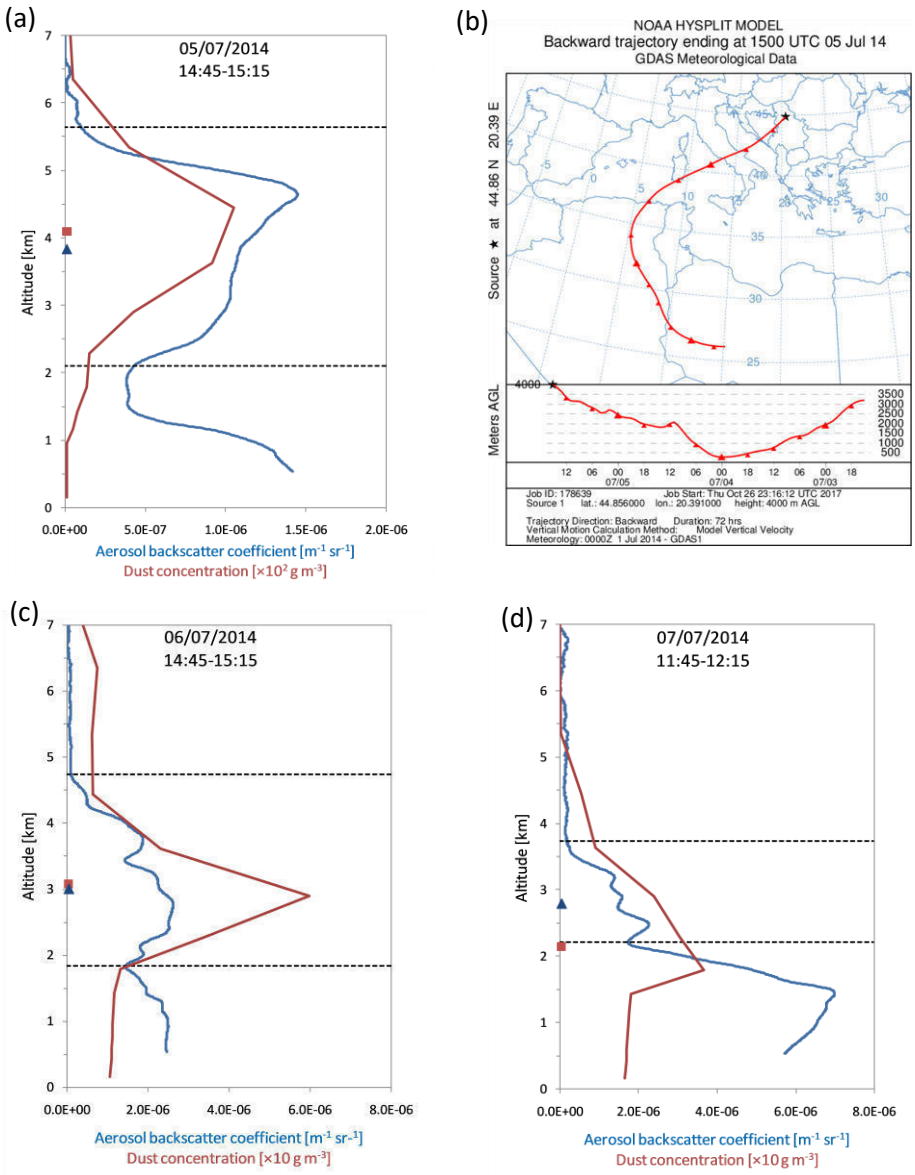

Figure 3. *(a, c, d) Vertical profile of aerosol backscattering coefficient from LIDAR measurements in Belgrade (blue line) and the corresponding profile of dust concentration from the DREAM model (red line); horizontal lines indicate dust layer base and top, while symbols show the positions of the dust layer's center of mass as calculated from LIDAR measurements and the DREAM model (b) 72hour airmass backtrajectory arriving at a 4 km altitude over Belgrade on July 5, 2014, at 15 UTC (corresponding to profile (a)).*

Figure 3 also shows altitudes of the dust layer center of mass, based on LIDAR measurements and the DREAM model. In the case of LIDAR measurements, it was calculated as a backscattering-coefficient-weighted altitude, according to:

$$z_c = \frac{\int_{z_b}^{z_t} z \cdot \beta(z) dz}{\int_{z_b}^{z_t} \beta(z) dz}$$

where z_b and z_t are the altitudes of the base and the top of the dust layer and $\beta(z)$ is the aerosol backscattering coefficient at altitude z. To minimize the effect of anthropogenic pollution, the center of mass from the LIDAR measurements was calculated only for the elevated layer. The dust's centre of mass from the DREAM model was calculated taking into account the entire dust profile.

Daily mass concentration of PM_{10} at ground level showed a similar trend at three air quality monitoring stations in Belgrade, with an increase during the dust episode (Figure 4). The increase started on July 6th, and the maximum was reached on July 7th, exceeding the 95th percentile of the summer (June, July and August) 2014 values. However, the daily limit value of 50 μg m^{-3}, set by the EU Air Quality Directive 2008/50/EC, was not exceeded. The increase of PM_{10} concentration is in agreement with the results of the LIDAR measurements, and the DREAM model, which indicated a settling of the dust plume (as shown in Figure 3). For comparison, daily average dust mass concentrations at the surface, obtained from the DREAM model, are also shown in Figure 4. They showed a similar trend as measured PM_{10} concentrations, increasing by 11 μg m^{-3} during the dust episode, while measured PM_{10} increased by 15 to 17 μg m^{-3} at the three monitoring stations. Larger measured PM_{10} concentrations, compared to surface dust concentrations from the model, were attributed to sources other than mineral dust.

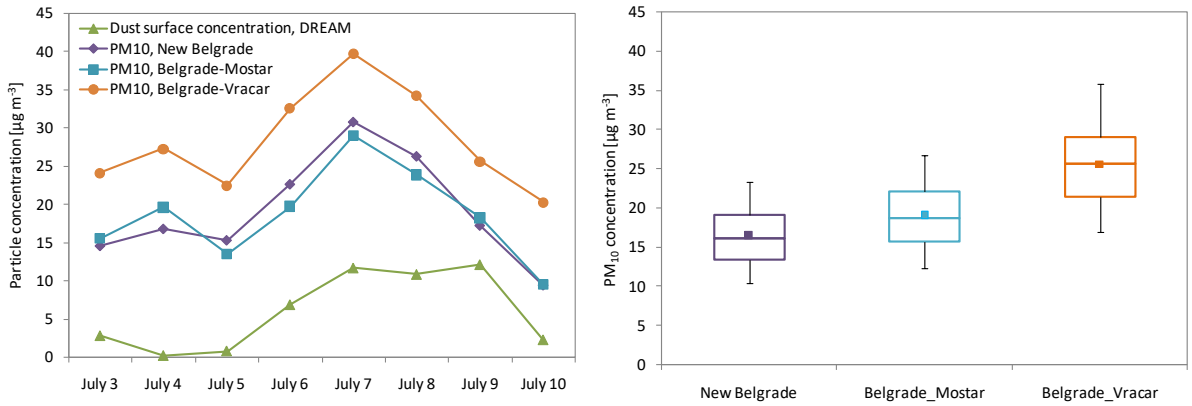

Figure 4. *(left panel) Daily average dust surface concentration values from the DREAM model and PM_{10} concentrations from three air quality monitoring stations in Belgrade. (right panel) Boxplot of PM_{10} concentrations during summer (June, July, August) of 2014 at three monitoring stations in Belgrade; the extent of the box indicates the 25th and 75th percentiles, the central line represents the median value, while the whiskers indicate the 5th and 95th percentiles; the points represent the mean values.*

CONCLUSION

We present analysis of a dust intrusion episode that was observed over Belgrade on July 5-7, 2014. The satellite measurements showed that the dust plume extended to western and central Europe. A distinctly elevated dust layer, extending at altitudes of approximately 2-5 km, was observed on July 5th using ground-based LIDAR in Belgrade. The layer altitude decreased during the dust episode, with the centre of mass altitude decreasing from approximately 4 km to below 3 km. The LIDAR measurements indicated entrainment of dust into the PBL on July 7th, the last day of the episode. The vertical distribution of dust and its temporal evolution over Belgrade was reproduced well by the DREAM model. The observed daily PM_{10} concentrations at three monitoring stations in Belgrade showed an increase of 15-17 μg m^{-3}, while dust was settling down during the episode as indicated by LIDAR measurements. Dust surface concentrations obtained from the DREAM model showed the same trend as measured PM_{10} concentrations, with a smaller increase (11 μg m^{-3}), during the episode: This difference was attributed to the contribution of other aerosol types to the observed PM_{10} concentrations.

ACKNOWLEDGEMENTS

This research was realized as a part of the project no. III43007, financed by the Ministry of Education, Science and Technological Development of the Republic of Serbia within the framework of integrated and interdisciplinary research for the period 2011-2020. The authors acknowledge support by the project GEO-CRADLE, Grant Agreement No. 690133, funded under European Union Horizon 2020 Programme. The authors gratefully acknowledge the NOAA Air Resources Laboratory (ARL) for the provision of HYSPLIT transport and dispersion

model and READY website (http://www.ready.noaa.gov), used in this publication. Analyses and visualizations of MODIS data used in this study were produced with the Giovanni online data system, developed and maintained by the NASA GES DISC. CALIPSO data were obtained from the NASA Langley Research Center Atmospheric Science Data Center.

REFERENCES

1. Ansmann, A., Bösenberg J., Chaikovsky, A., Comeron, A., Eckhardt, S., Eixmann, S. et al., 2003. Long-range transport of Saharan dust to northern Europe: The 11-16 October 2001 outbreak observed with EARLINET, Journal of Geophysical Research 108, 4783, doi:10.1029/2003JD003757.
2. Draxler, R. R. and Hess, G. D., 1998. An overview of the HYSPLIT 4 modeling system for trajectories, dispersion, and deposition, Australian Meteorology Magazine, 47, 295-308.
3. Fernald, F. G., 1984. Analysis of atmospheric lidar observations: some comments, Applied Optics 23,652-653.
4. Giannadaki, D., Pozzer, A., Lelieveld, J., 2014. Modeled global effects of airborne desert dust on air quality and premature mortality, Atmospheric Chemistry and Physics 14, 957-968.
5. IPCC: Climate Change 2013: The physical science basis. Contribution of Working Group I to the Fifth Assessment Report of the Intergovernmental Panel on Climate Change, edited by: Stocker, T.F., Qin, D., Plattner, G.-K., Tignor, M., Allen, S.K., Boschung, J., Nauels, A., Xia, Y., Bex, V., Midgley, P.M., Cambridge University Press, Cambridge, UK and New York, USA.
6. Janjić, Z. I., Gerrity Jr, J. P., Ničković, S., 2011. An alternative approach to non-hydrostatic modelling, Monthly Weather Review 129, 1164-78.
7. Kinne, S., Schulz, M., Textor, C., Guilbert, S., Balkansky, Y., Bauer, S. E. et al., 2006. An AeroCom initial assessment - optical properties in aerosol component modules of global models, Atmospheric Chemistry and Physics 6, 1815-1834.
8. Klett, J. D. 1985. Lidar inversion with variable backscatter/extinction ratios, Applied Optics 24, 1638-1643.
9. Mona, L., Amodeo, A., Pandolfi, M., Pappalardo, G., 2006. Saharan dust intrusions in the Mediterranean area: Three years of Raman lidar measurements, Journal of Geophysical Research, 111, D16203, doi:10.1029/2005JD006569.
10. Ničković, S., Kallos, G., Papadopoulos, A., Kakaliagou, O., 2001. A model for prediction of desert dust cycle in the atmosphere, Journal of Geophysical Research 106, 18113-18130.
11. Omar, A. H., Winker, D. M., Kittaka, C., Vaughan, M. A., Liu, Z., Hu, et al., 2009. The CALIPSO automated aerosol classification and Lidar Ratio Selection Algorithm, Journal of Atmospheric and Oceanic Technology 26, 1994-2014, doi:10.1175/2009JTECHA1231.1.
12. Prospero, J. M., 1999. Long-term measurements of the transport of African mineral dust to the southeastern United States: Implications for regional air quality, Journal of Geophysical Research 104, 15917-15927, doi:10.1029/1999JD900072.

5.4. RELATIVE IMPORTANCE OF GASEOUS POLLUTANTS AND AEROSOL CONSTITUENTS FOR IDENTIFICATION OF PM_{10} SOURCES OF VARIABILITY

M. Perišić (1), G. Vuković (1), Z. Mijić (1), A. Šoštarić (2) and A. Stojić (1)
(1) Institute of Physics, University of Belgrade, Pregrevica 118, Serbia
(2) Institute of Public Health of Belgrade, Boulevard of Despot Stefan 54a, Belgrade, Serbia
mirjana.perisic@ipb.ac.rs

ABSTRACT

This study combines advanced statistical methods including time series decomposition, source apportionment and supervised learning algorithms, to identify the main sources of particulate matter (PM_{10}) variability in an urban area within Belgrade. The analyses indicated that the season, (i.e., meteorological conditions) strongly influenced daily and annual PM_{10} variations particularly during the colder part of the year. A guided regularized random forest model estimated that As, Cd, BaP, CO, and benzene have the highest relative importance for the prediction of PM_{10}. Polar plot source apportionment revealed common sources of pollution at specific directions. Specifically, emissions of PM_{10}, CO and benzene could be attributed to heating and gasification processes, while processes in oil refineries and chemical industries produced PM_{10} and toluene.

INTRODUCTION

Due to adverse effects on human health and the increased risk of morbidity and mortality, particulate matter (PM) is one of the most studied atmospheric pollutants, and perhaps, the most pressing issue in worldwide air quality regulation (Fuzzi et al, 2015, Stanišić Stojić et al, 2016). Even though significant progress has been made through the integration of different scientific approaches, modelling of air pollution data remains a challenge due to the complexity and non-linear nature of atmospheric phenomena and processes (Pai et al, 2013). During the last decade, poor air quality in Belgrade, with many PM_{10} limit value exceedances (Directive 2008/50/EC), has been identified as an important environmental risk factor (Perišić et al, 2015, 2017). Identification of factors affecting PM_{10} concentration variability could provide better insight into the aerosol spatiotemporal distribution and source composition, revealing their dominant sources in an urban area (Stojić et al, 2016).

Apart from the commonly used methods for data analysis, this study adopts the advanced statistical classifier, guided regularized random forest (GRRF), widely applied in many fields for feature selection. Moreover, the study demonstrates the possibilities of source apportionment analysis, which combines correlation and regression statistics with the bivariate polar plot analysis, to offer considerably more insight into air pollution sources.

METHODOLOGY

The analysed dataset, comprised of daily PM_{10} and its constituent concentrations (As, Cd, Cr, Mn, Ni, Pb, BaP, Cl^-, NO_3^-, NH_4^+, SO_4^{2-}, Na^+, K^+, Mg^{2+} and Ca^{2+}), and hourly PM_{10} and gaseous pollutant concentrations (CO, SO_2, NO, NO_2, NO_x, benzene, toluene, o- and m, p xylene) have been obtained from an Institute of Public Health regular monitoring station located within an urban area in Belgrade (Longitude 20.470, Latitude 44.817) from 2011 - 2016. The time series of PM_{10} concentrations was resolved into the additive components of the multi-year and seasonal trends, as well as the remainders using the Loess smoothing decomposition model (LSD) (Li et al, 2014). Daily, weekly and seasonal periodicity was analyzed by the use of Lomb-Scargle periodogram (*Lomb* package within the statistical software environment *R*) (Ruf, 1999; Team, 2014). Bivariate polar plot analysis was used for identification of the main PM_{10} emission sources (Carslaw and Ropkins, 2012), while the advanced bivariate polar plots, coupled with pair-wise statistics, were applied to distinguish specific sources and to gain information about pollutant relationships. The model includes a weighted Pearson correlation, linear regression slope and Gaussian kernel to locally weight the statistical calculations on a wind speed-direction surface together with variable-scaling (Grange et al, 2016). Feature selection was implemented using a GRRF ensemble learning method (Deng and Runger, 2013). GRRF can select compact feature subsets revealing higher order variable interactions, thus moderating the problem of dimensionality and avoiding the effort to analyze irrelevant or redundant features.

RESULTS AND DISCUSSION

Annual concentrations of PM_{10} and BaP exceeded prescribed limit values of 50 μg m^{-3} and 1 ng m^{-3}, respectively (Directive 2000/69/EC, Directive 2008/50/EC) every year of the period examined. The most abundant aerosol constituents were Cr, Pb and Mn (Figure 1), while SO_4^{2-} and NO_3^- were the ions with the highest concentrations.

In an urban area, the dominance of sulfate and nitrate ions is related to fossil fuel burning and traffic exhaust emission of SO_2 and NO_x, which, in the presence of water, transform into these ions. In addition, NH_4^+ and Ca^{2+} cations are usually presented as neutralizing agents for SO_4^{2-} and NO_3^- in heterogeneous atmospheric chemical reactions.

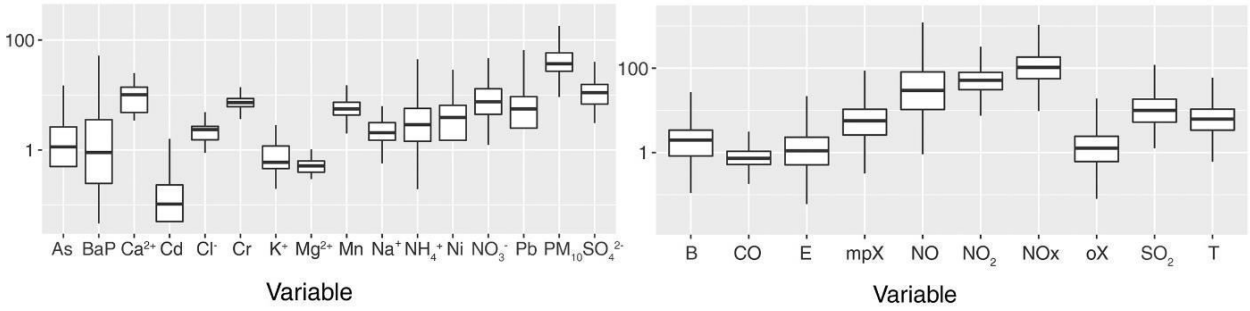

Figure 1. *PM_{10} concentration [μg m^{-3}], its chemical constituent (ions and BaP [μg m^{-3}], metals [ng m^{-3}]) (left) and gaseous pollutant [μg m^{-3}] (right) whisker plots*

Spectral analysis (Figure 2, left) reveals the highest normalized power values are attributed to the periods of 12 and 24 h, 7 days, and 1 and 3 months. This implies that meteorological conditions and anthropogenic emissions are strongly affected by aerosol daily and seasonal variations, and weekly periodicity, respectively (Bigi, 2016).

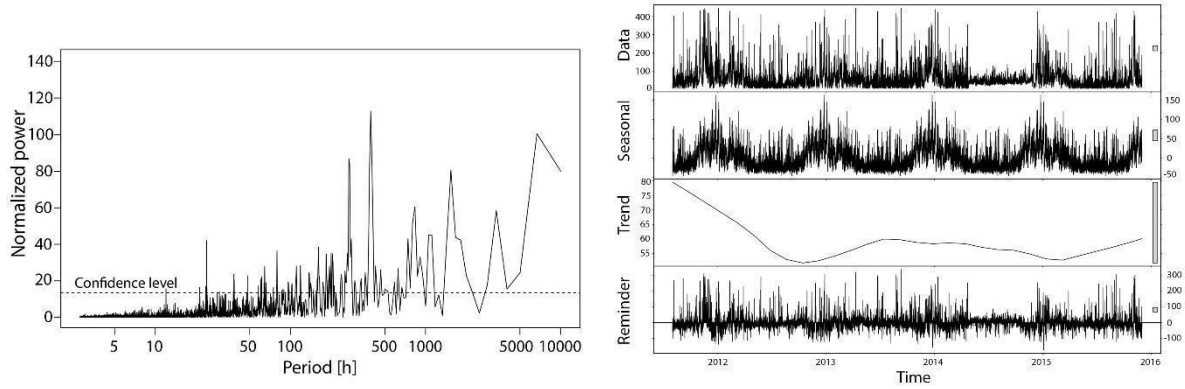

Figure 2. *PM_{10} Lomb-Scargle periodogram (left) and PM_{10} time series decomposition [μg m^{-3}] (right)*

Decomposed PM_{10} time series indicates a decreasing multi-year trend and significant impact of the seasonal component. Large variance of the remainder component possibly occurs as a result of short-term air pollution episodes (Figure 2, right). The conventional bivariate polar plot approach reveals the pronounced influence of both local and remote sources on PM_{10} variability (Figure 3).

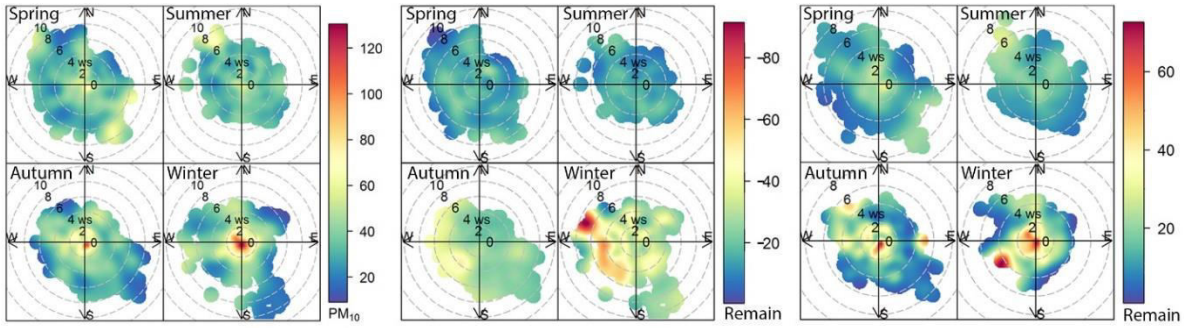

Figure 3. *Bivariate polar plot of PM_{10} concentrations (left) and its remainder components: negative (middle) and positive (right) [μg m^{-3}]*

Bivariate polar plot analysis of the remainder component, separately applied on positive and negative values, confirms that the episodes of the highest variations mainly occur during the colder part of the year. Positive variations related to SW and negative related to NW winds with speeds greater than 6 m s^{-1}.

The highest Pearson's correlation coefficients were obtained between concentrations of PM_{10} and its constituents (BaP (0.83), As (0.81), Cd (0.79) and Pb (0.66)), as well as for the gaseous pollutants: CO (0.56), benzene (0.46), NO (0.35), and NO_x (0.35). Similarly, the GRRF estimated the highest relative importance of As, Cd, BaP, CO and benzene for the prediction of PM_{10}, indicating that the environmental burden is mainly associated with fossil fuel combustion, particularly pronounced during the colder part of the year. An inconsistency between the correlation and GRRF analysis was observed for toluene. This compound had a higher importance for PM_{10} prediction than NO_x, but its correlation coefficient was among the lowest (0.25).

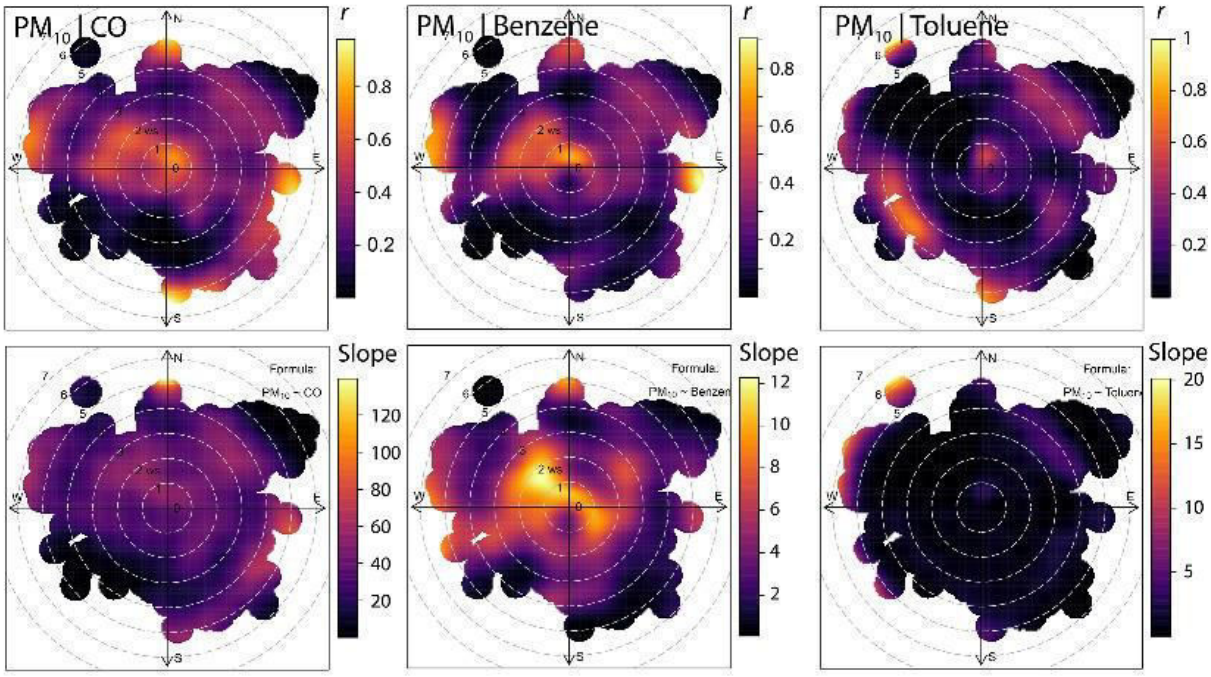

Figure 4. *Bivariate polar source apportionment*

Even though Pearson's coefficients did not indicate a significant correlation between PM_{10} and gaseous pollutants ($r < 0.6$), the bivariate polar source apportionment (Figure 4) showed that during episodes of north-westerly winds, concentrations of PM_{10} and benzene and CO were more correlated ($r \approx 0.7$) probably because of several common sources in the vicinity of the sampling site. Source composition obtained from slope diagrams reveals a 1:0.1 and 1:12 contribution of PM_{10}, CO and benzene, respectively. This could be associated with various biomass combustion processes (traffic activities, heating plants and individual heating units) (Yokelson et al, 2007). Besides the vicinity of the sampling site, particulate matter and toluene shared prominent sources located in the SW, S, NE and SE directions ($r > 0.8$, wind speed > 4 m s-1). Unlike southern and western sources, characterized by PM_{10} to toluene ratio of 1:1 which could be related to mineral oil and gas refineries, the source located on the north-east is characterized by the ratio of 1:6 indicating influences from the chemical industry, and chemical installations for production, on an industrial scale, of basic organic chemicals including aromatic hydrocarbons (European Commission, 2006).

CONCLUSIONS

Due to the pronounced nonlinearity and complexity of atmospheric processes in the troposphere of an urban environment, the application of multivariate and nonlinear methods is required to gain reliable information for a better understanding of the underlying factors which determine the air pollution phenomena. Methods such as feature selection based on advanced supervised learning algorithms, advanced source apportionment techniques and time series decomposition and detailed component analysis, are capable of providing this information, particularly for characterization of variable pollution sources. Summarizing this study, it has been shown that

locally emitted and transported pollution, as well as meteorological factors, have the highest impact on urban air quality.

ACKNOWLEDGMENTS

This paper was completed as part of the project titled “Studying climate change and its influence on the environment: impacts, adaptation and mitigation" (III43007) financed by the Ministry of Education and Science of the Republic of Serbia within the framework of integrated and interdisciplinary research for the period 2011-2017. The publication was supported by the project GEO-CRADLE (Coordinating and integRating state-of-the-art Earth Observation Activities in the regions of North Africa, Middle East, and Balkans and Developing Links with GEO related initiatives towards GEOSS), Grant Agreement No. 690133, funded under European Union Horizon 2020 Programme - Topic: SC5-18b-2015, Integrating North African, Middle East and Balkan Earth Observation capacities in GEOSS.

REFERENCES

1. Bigi, A. and Ghermandi, G. 2016. Trends and variability of atmospheric $PM_{2.5}$ and $PM_{10-2.5}$ concentration in the Po Valley, Italy. Atmospheric Chemistry and Physics 16, 15777-15788.
2. Carslaw, D.C., Ropkins, K. 2012. Openair - an R package for air quality data analysis. Environmental Modelling and Software 27-28, 52-61.
3. Deng, H. and Runger, G. 2013. Gene selection with guided regularized random forest. Pattern Recognition 46, 3483-3489.
4. Directive 2000/69/EC of the European Parliament and of the council of 16 November 2000 relating to limit values for benzene and carbon monoxide in ambient air. Official Journal of the European Communities L313, 12-21 (13/12/2000).
5. Directive 2008/50/EC of the European Parliament and of the Council of 21 May 2008 on ambient air quality and cleaner air for Europe. Official Journal of the European Union L152/3, 6-15 (11/06/2008).Fuzzi, S., Baltensperger, U., Carslaw, K., Decesari, S., Denier Van Der Gon, H., Facchini, M.C., Fowler, D., Koren, I., Langford, B., Lohmann, U. and Nemitz, E. 2015. Particulate matter, air quality and climate: lessons learned and future needs. Atmospheric Chemistry and Physics 15, 8217-8299.
6. European Commission, 2006. Guidance Document for the implementation of the European Pollutant Release and Transfer Register (E-PRTR).
7. Grange S.K., Lewis A. and Carslaw D. 2016. Source apportionment advances using polar plots of bivariate correlation and regression statistics. Atmospheric Environment 145, 128-134.
8. Li, L., Qian, J., Ou, C. Q., Zhou, Y. X., Guo, C. and Guo, Y. 2014. Spatial and temporal analysis of Air Pollution Index and its timescale-dependent relationship with meteorological factors in Guangzhou, China, 2001-2011. Environmental Pollution 190, 75-81.
9. Ruf, T. 1999. The Lomb-Scargle periodogram in biological rhythm research: analysis of incomplete and unequally spaced time-series. Biological Rhythm Research 30, 178-201.
10. Pai, T.Y., Hanaki, K., Chiou, R.J. 2013. Forecasting hourly roadside particulate matter in Taipei County of Taiwan based on firstorder and one-variable grey model. CLEAN Soil Air Water 41, 737-742.
11. Perišić, M., Rajšić, S., Šoštarić, A., Mijić, Z. and Stojić, A. 2017. Levels of PM_{10}-bound species in Belgrade, Serbia: spatio-temporal distributions and related human health risk estimation. Air Quality, Atmosphere and Health 10, 93-103.
12. Perišić, M., Stojić, A., Stojić, S. S., Šoštarić, A., Mijić, Z., and Rajšić, S. (2015). Estimation of required PM_{10} emission source reduction on the basis of a 10-year period data. *Air Quality, Atmosphere & Health*, *8*(4), 379-389.
13. Stanišić Stojić, S., Stanišić, N., Stojić, A., and Šoštarić, A. 2016a. Single and combined effects of air pollutants on circulatory and respiratory system-related mortality in Belgrade, Serbia, Journal of Toxicology and Environmental Health, Part A 79, 17-27.
14. Stojić, A., Stojić, S. S., Reljin, I., Čabarkapa, M., Šoštarić, A., Perišić, M. and Mijić, Z. 2016. Comprehensive analysis of PM_{10} in Belgrade urban area on the basis of long-term measurements. Environmental Science and Pollution Research 23, 10722-10732.
15. R Core Team, 2014. R: A language and environment for statistical computing. R Foundation for Statistical Computing, Vienna, Austria. http://www.R-project.org/.
16. Yokelson, R. J., Urbanski, S. P., Atlas, E. L., et. al, 2007. Emissions from forest fires near Mexico City. Atmospheric Chemistry and Physics 7, 5569-5584.

6.1. MULTISCALE MULTIFRACTAL ANALYSIS OF NONLINEARITY IN PARTICULATE MATTER TIME SERIES

A. Stojić (1), S. Stanišić Stojić (2), M. Perišić (1), Z. Mijić (1)

(1) Institute of Physics, University of Belgrade, Belgrade, Serbia, (2) Faculty of Physical Chemistry, University of Belgrade, Belgrade, Serbia

andreja.stojic@ipb.ac.rs

ABSTRACT

In this study the multiscale multifractal method was used with aim of capturing the fractal behaviour of the particulate matter time series obtained from an urban area in Belgrade, Serbia, as well as investigating their persistence properties and heterogeneity features. As shown, the $PM_{2.5}$ time series exhibited persistency, slightly affected by the concentrations occurring randomly only at the level of small fluctuations and small scales. Compared to $PM_{2.5}$, PM_{10} concentrations were shown to display more stochastic behaviour with more frequent random fluctuations being observed at small scales. The results herein presented contribute to the current understanding of the structural complexity of the temporal evolution of particulate matter and provide a theoretical background for enhanced air pollution modelling.

INTRODUCTION

Comprehensive analyses, conducted over the past few years, of air pollutant emission sources, their subsequent distribution and relationship to mortality caused by circulatory, respiratory and malignant diseases suggest that the exposure to particulate matter (PM) has detrimental effects on human health in the Belgrade area (Stanišić Stojić et al, 2016a, 2016b). Besides the fact that PM levels in Serbia are higher than in most European cities, with a significant number of air quality standard exceedances, our studies have shown that suspended particles also contain high concentrations of carcinogenic contaminants, such as arsenic and benzo(a)pyrene (Stojić et al, 2015a, 2015b, 2016, Perišić et al, 2015, 2017).

Diverse methods have been implemented to provide relevant information for efficient air quality management, including deterministic models, statistical analysis, neural networks, fuzzy models, geographic information system, remote sensing and trend analysis (Yu et al, 2011). Multifractality is one of the inherent properties that can be recognized in physical, chemical, biological, social and other systems, that are described as very complex at different spatial and temporal scale levels (Glushkov et al, 2014). The atmosphere is a complex system that exhibits nonlinear behavior involving both deterministic and stochastic components (Lorenz and Haman, 1996). In previous studies, the multifractal approach has been applied to analyse average ozone concentrations (Kocak et al, 2000), nonlinearity in NO_2 and CO time series (Kumar et al, 2008) and the daily air pollution index (Sivakumar et al, 2007). The aim was to provide information essential to better understand the behaviour of pollution and to forecast the temporal evolution of the species (Dong et al, 2017). The multifractal method was used herein to reveal PM fluctuation properties, *i.e.* to investigate to what extent, and on which time scale, changes in $PM_{2.5}$ and PM_{10} concentration levels can be considered random or persistent.

METHODOLOGY

In this study, multiscale multifractal analysis (MMA) was used to investigate the presence of fractal behaviour in the complex time series of $PM_{2.5}$ and PM_{10} concentrations. Data was obtained during a period of almost three years (2012-2014) of regular pollutant monitoring in Belgrade (suburban site Ovča, Longitude 20.528, Latitude 44.884, Serbia) provided by the Institute of Public Health Belgrade. MMA is a generalization of the standard multifractal detrended fluctuation analysis (MF-DFA), which adds the dependence on scale, providing a broader analysis of the fluctuation properties, as well as, more general and stable results (Gierałtowski et al, 2012).

RESULTS AND DISCUSSION

Measured PM concentrations are presented in Figure 1. According to the results, multiscale multifractal derived Hurst surfaces confirmed the non-linear behavior of PM time series (Figure 2).

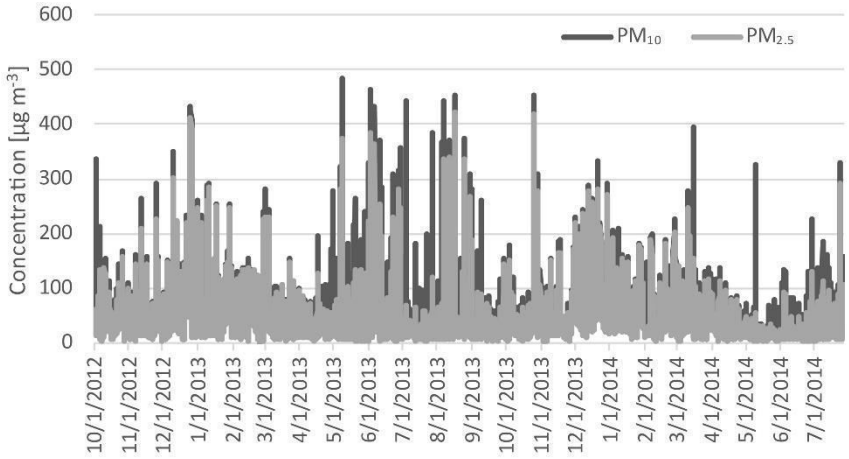

Figure 1. *Measured $PM_{2.5}$ and PM_{10} concentrations.*

For most of the scale and multifractal parameter values, the local Hurst exponent remains in the interval between 1 and 1.5 indicating persistency of the $PM_{2.5}$ time series, while slightly affected by the concentrations occurring randomly. Such random concentration values occur only at the level of small fluctuations for scales below 44, which corresponds to a period of about 2 days. At this scale, there emerges a clear crossover resulting from the different correlation properties. Given that the sampling site was not directly exposed to intense PM bursts, the occurrence of concentrations in narrow bands (Hurst exponent equals 2) was not recorded. The PM_{10} Hurst surface reveals similar features, except that in the area of small variance and scales below 90, its growth to a maximum of approximately 1.9 is steeper, almost reaching black noise area values of local Hurst exponent. Compared to $PM_{2.5}$, the PM_{10} Hurst structure around its maximum corresponds to visibly more pronounced peaks in the time series (Figure 1). However, unlike $PM_{2.5}$, the PM_{10} Hurst surface shows no crossover.

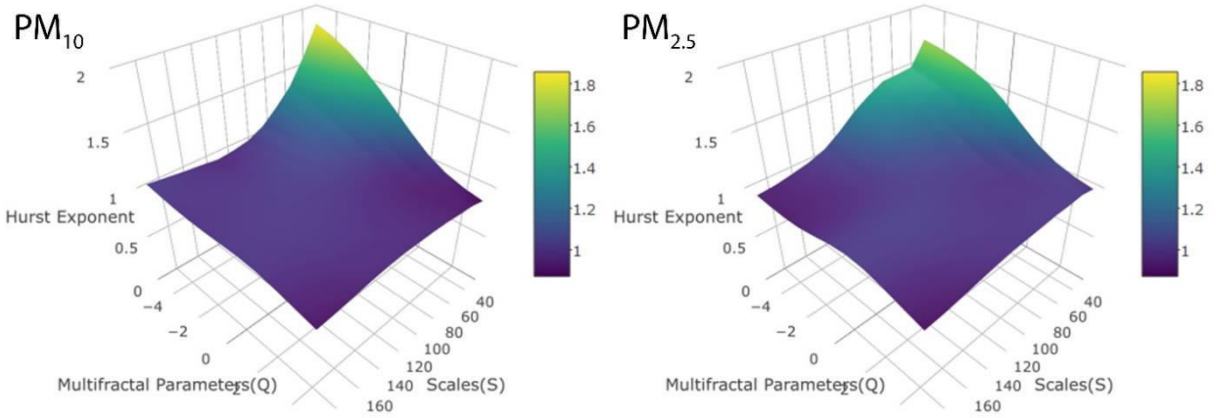

Figure 2. *MMA derived particulate matter Hurst surfaces.*

In addition, the generalized distance coefficient (0.069) between Hurst surfaces of PM fractions is higher than the threshold value (0.065) and implies that the $PM_{2.5}$ and PM_{10} time series must be considered statistically different. The difference is particularly pronounced in the area of small fluctuations and medium scales (Figure 3).

Furthermore, it is shown that the source of multifractality, examined by PM time series randomization, originates from both nonlinear correlations and a fat-tailed probability distribution (Figure 4).

The findings of Lalwani (2016) and Liu et al. (2015) confirmed the existence of multifractality in the PM time series and found that daily pollutant concentrations exhibited high persistence in a period of approximately one

year. As argued, the persistence in the air pollutant concentrations over longer period of time may be governed by the impact of background levels, seasonal trend or intrinsic evolution of the system.

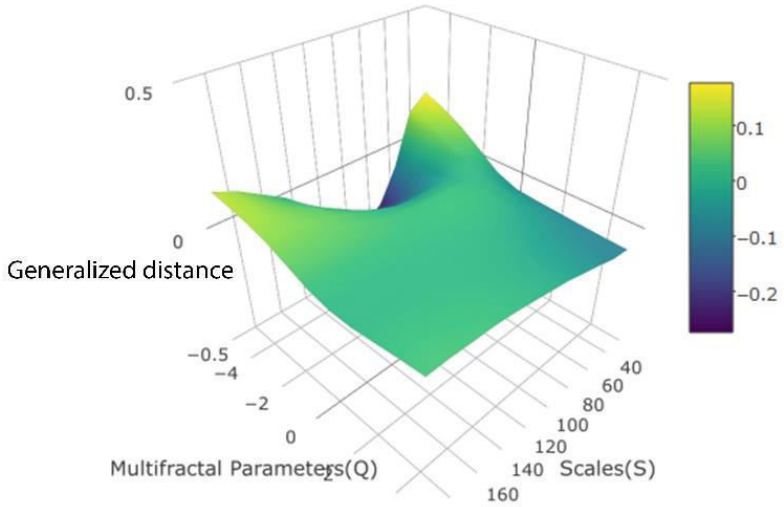

***Figure 3**. Generalized $PM_{10}/PM_{2.5}$ Hurst surface distance.*

The difference in the behavior of the $PM_{2.5}$ and PM_{10} time series was proven by Xue et al. (2015), who employed a multifractal analysis to explore temporal fluctuations and self-similarities within the PM time series and to understand their behaviour associated with diffusion, spreading and coagulation processes. Using the multifractal detrended fluctuation analysis method, the researchers registered the pronounced multifractality and long-term persistence of the $PM_{2.5}$ time-series, whereas the PM_{10} time series were shown to have stochastic behaviour.

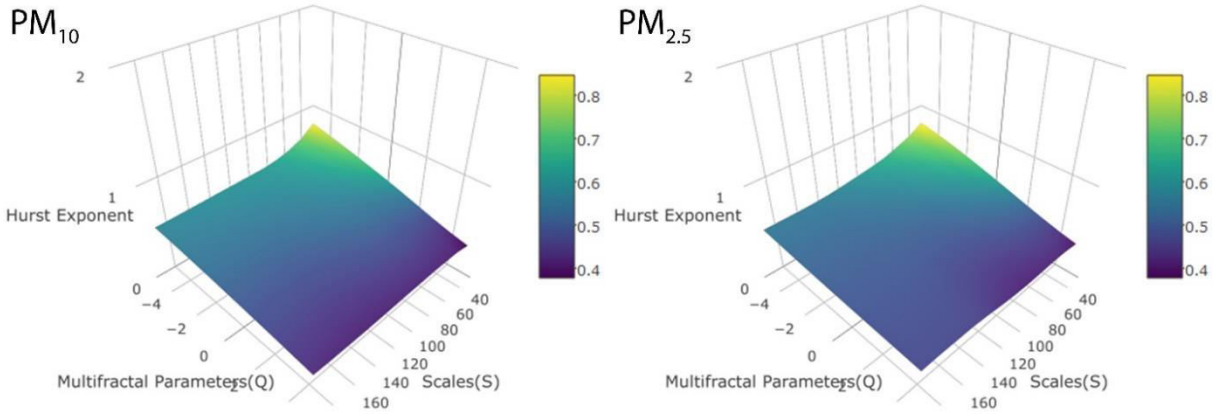

***Figure 4**. MMA derived Hurst surfaces for randomized PM time series.*

CONCLUSIONS

In this study, the multifractal approach was used to analyse the temporal dynamics of $PM_{2.5}$ and PM_{10} concentrations on the basis of a regular monitoring of data over a three-year period. As shown, the particulate matter time series possess a long-term memory of distant past events and require a large number of exponents, the so-called fractal dimensions, to be described. The presented analysis provides essential information for better understanding of the PM behaviour and the underlying factors, as well as for more accurate and reliable pollutant forecasting and efficient mitigation policy.

ACKNOWLEDGEMENTS

This study was performed as part of the projects Grant No III43007 and No III41011, which were supported by the Ministry of Education, Science and Technological Development of the Republic of Serbia within the framework of integrated and interdisciplinary research for the period 2011-2017. The publication was supported by the project GEO-CRADLE (Coordinating and integRating state-of-the-art Earth Observation Activities in the regions of North Africa, Middle East, and Balkans and Developing Links with GEO related initiatives towards GEOSS), Grant Agreement No. 690133, funded under European Union Horizon 2020 Programme - Topic: SC5-18b-2015, Integrating North African, Middle East and Balkan Earth Observation capacities in GEOSS.

REFERENCES

1. Dong, Q., Wang, Y. and Li, P. 2017. Multifractal behaviour of an air pollutant time series and the relevance to the predictability, Environmental Pollution 222, 444-457.
2. Gierałtowski, J., Żebrowski, J. J. and Baranowski, R. 2012. Multiscale multifractal analysis of heart rate variability recordings with a large number of occurrences of arrhythmia, Physical Review E 85(2), 021915.
3. Glushkov, A. V., Svinarenko, A. A., Buyadzhi, V. V., Zaichko, P. A. and Ternovsky, V. B. 2014. Chaosgeometric attractor and quantum neural networks approach to simulation chaotic evolutionary dynamics during perception process, Advances in Neural Networks, Fuzzy Systems and Artificial Intelligence, Series: Recent Advances in Computer Engineering, Ed. J. Balicki. Gdansk, WSEAS Pub.
4. Koçak, K., Şaylan, L. and Şen, O. 2000. Nonlinear time series prediction of O_3 concentration in Istanbul, Atmospheric Environment 34(8), 1267-1271.
5. Kumar, U., Prakash, A. and Jain, V. K. 2008. Characterization of chaos in air pollutants: A Volterra-Wiener-Korenberg series and numerical titration approach, Atmospheric Environment 42(7), 1537-1551.
6. Lalwani, A. 2016. Long-Range Correlations in Air Quality Time Series: Effect of Differencing and Shuffling, Aerosol and Air Quality Research 16(9), 2302-2313.
7. Liu, Z., Wang, L. and Zhu, H. 2015. A time-scaling property of air pollution indices: a case study of Shanghai, China, Atmospheric Pollution Research 6(5), 886-892.
8. Lorenz, E. N. and Haman, K. 1996. The essence of chaos, Pure and Applied Geophysics 147(3), 598-599.
9. Sivakumar, B., Wallender, W. W., Horwath, W. R. and Mitchell, J. P. 2007. Nonlinear deterministic analysis of air pollution dynamics in a rural and agricultural setting, Advances in Complex Systems 10(04), 581-597.
10. Stojić, A., Stojić, S. S., Šoštarić, A., Ilić L., Mijić Z. and Rajšić S. 2015a. Characterization of VOC sources in an urban area based on PTR-MS measurements and receptor modelling, Environmental Science and Pollution Research 1-16.
11. Stojić, A., Stojić, S. S., Mijić, Z., Šoštarić, A. and Rajšić S. 2015b. Spatio-temporal distribution of VOC emissions in urban area based on receptor modelling, Atmospheric Environment 106, 71-79.
12. Stojić, A., Stojić, S. S., Reljin, I., Čabarkapa, M., Šoštarić, A., Perišić, M. and Mijić, Z. 2016. Comprehensive analysis of PM_{10} in Belgrade urban area on the basis of long-term measurements, Environmental Science and Pollution Research 23(11), 10722-10732.
13. Stojić, S. S., Stanišić, N., Stojić, A., and Šoštarić, A. 2016a. Single and combined effects of air pollutants on circulatory and respiratory system-related mortality in Belgrade, Serbia, Journal of Toxicology and Environmental Health, Part A 79(1), 17-27.
14. Stojić, S. S., Stanišić, N., and Stojić, A. 2016b. Temperature-related mortality estimates after accounting for the cumulative effects of air pollution in an urban area, Environmental Health 15(1), 73.
15. Perišić, M., Stojić, A., Stojić, S. S., Šoštarić, A., Mijić, Z. and Rajšić, S. 2015. Estimation of required PM_{10} emission source reduction on the basis of a 10-year period data, Air Quality, Atmosphere & Health 8(4), 379-389.
16. Perišić, M., Rajšić, S., Šoštarić, A., Mijić, Z. and Stojić, A. 2017. Levels of PM_{10}-bound species in Belgrade, Serbia: spatio-temporal distributions and related human health risk estimation, Air Quality, Atmosphere & Health 10(1), 93-103.
17. Xue, Y., Pan, W., Lu, W. Z. and He, H. D. 2015. Multifractal nature of particulate matters (PMs) in Hong Kong urban air, Science of the Total Environment 532, 744-751.
18. Yu, B., Huang, C., Liu, Z., Wang, H. and Wang, L. 2011. A chaotic analysis on air pollution index change over past 10 years in Lanzhou, Northwest China, Stochastic Environmental Research and Risk Assessment 25(5), 643-653.

CIP - Каталогизација у публикацији
Народна библиотека Србије, Београд

502.3:502.175(082)
66.071.9(082)
613.15(082)

INTERNATIONAL WeBIOPATR Workshop Particulate Matter: Research and Management (6; 2017; Beograd)

Proceedings [Elektronski izvor] /
The Sixth International WeBIOPATR Workshop & Conference Particulate Matter: Research and Management, WeBIOPATR2017, 6-8 September 2017, Belgrade;
editors Milena Jovašević-Stojanović and Alena Bartoňová. –
Belgrade: Vinča Institute of Nuclear Sciences, 2019
(Belgrade: Vinča Institute of Nuclear Sciences). -
1 elektronski optički disk (CD-ROM); 12 cm

Sistemski zahtevi: Nisu navedeni. –
Nasl. sa naslovne strane dokumenta. -
Tiraž 150. –
Bibliografija uz svaki rad.

ISBN 978-86-7306-152-8

a) Ваздух - Контрола квалитета - Зборници

b) Отпадни гасови – Штетно дејство - Зборници

c) Здравље - Заштита - Зборници

COBISS.SR-ID 278918412

WeBIOPATR

ПУБЛИКАЦИЈЕ АСТРОНОМСКОГ ДРУШТВА "РУЂЕР БОШКОВИЋ" Св. 20
PUBLICATIONS OF THE ASTRONOMICAL SOCIETY "RUDJER BOŠKOVIĆ" No. 20

PROCEEDINGS
OF THE XII SERBIAN-BULGARIAN ASTRONOMICAL CONFERENCE

Sokobanja, Serbia, September 25-29, 2020

Eds. Luka Č. Popović, Vladimir A. Srećković, Milan S. Dimitrijević and Anđelka Kovačević

BELGRADE, 2020

ПУБЛИКАЦИЈЕ АСТРОНОМСКОГ ДРУШТВА "РУЂЕР БОШКОВИЋ"
PUBLICATIONS OF THE ASTRONOMICAL SOCIETY "RUDJER BOŠKOVIĆ"
Св. 20 No. 20

PROCEEDINGS OF THE XII SERBIAN-BULGARIAN ASTRONOMICAL CONFERENCE

Sokobanja, Serbia, September 25-29, 2020

Eds. Luka Č. Popović, Vladimir A. Srećković,
Milan S. Dimitrijević and Anđelka Kovačević

Б Е О Г Р А Д
2020

PUBL. ASTRON. SOC. "RUDJER BOŠKOVIĆ" No. 20, 1-192 BELGRADE, DECEMBER 2020

SCIENTIFIC COMMITTEE

Luka Č. Popović (Co-chairman)
Vladimir A. Srećković (Co-chairman)
Ognyan Kounchev (Co-chairman)

Milan S. Dimitrijević (Co-vice chairman)
Milcho K. Tsvetkov (Co-vice chairman)

Robert Beuc (Croatia)
Svetlana Boeva (Bulgaria)
Momchil Dechev (Bulgaria)
Dragana Ilić (Serbia)
Andjelka Kovačević (Serbia)
Jelena Kovačević Dojčinović (Serbia)
Maša Lakićević (Serbia)
Petko Nedialkov (Bulgaria)
Nikola Petrov (Bulgaria)
Branko Predojević (Bosnia and Herzegovina)
Milan Radovanović (Serbia)
Saša Simić (Serbia)
Nikolaj Samus (Russia)
Georgi Simeonov (Bulgaria)
Katya Tsvetkova (Bulgaria)
Dejan Urošević (Sebia)
Jan Vondrák (Czech Republic)

LOCAL ORGANIZING COMMITTEE

Andjelka Kovačević (Chairperson)

Maša Lakićević (Scientific secretary)

Members:
Milan S. Dimitrijević
Jelena Kovačević Dojčinović
Slađana Marčeta Mandić
Saša Simić
Vladimir A. Srećković

ORGANIZER:
Astronomical Observatory Belgrade, Serbia

Co-organizers:
Institute of Mathematics and Informatics - BAS, Sofia, Bulgaria
Institute of Physics Belgrade, Belgrade, Serbia
Faculty of Mathematics and Department of Astronomy, University of Belgrade, Serbia

Logo on the front cover: Saša Simić

Text arrangement by computer: Tatjana Milovanov

Financially supported by the Ministry of Education, Science and Technological Development of Serbia

ISBN 978-86-89035-15-5

Production: Skripta Internacional, Mike Alasa 54, Beograd, in 100 copies

CONTENTS

Goran Damljanović
GAIA DR3 AND SOME RESULTS OF SERBIAN-BULGARIAN COOPERATION 5

Goran Damljanović, Rumen Bachev, Svetlana Boeva, Georgy Latev, Milan Stojanović, Miljana D. Jovanović, Oliver Vince, Zorica Cvetković, Rade Pavlović and Gabrijela Marković
SERBIAN-BULGARIAN OBSERVATIONS OF GAIA ALERTS (GAIA-FUN-TO) DURING 2019 15

Miljana D. Jovanović, Goran Damljanović, Zorica Cvetković, Rade Pavlović and Milan Stojanović
COLOR VARIABILITY OF SOME QUASARS IMPORTANT TO THE ICRF – GAIA CRF LINK 23

Jelena Kovačević-Dojčinović, Ivan Dojčinović, Maša Lakićević and Luka Č. Popović
THE SPECTRAL PROPERTIES OF THE AGN TYPE 2 SAMPLE: THE SEARCH FOR THE SIGMA* SURROGATE 33

Daniela Kirilova and Mariana Panayotova
INFLATIONARY MODELS, REHEATING AND SCALAR FIELD CONDENSATE BARYOGENESIS 39

Jelena Petrovic
EVOLUTION OF MASSIVE BINARY SYSTEMS: PRIMARY STAR EVOLUTION INTO A NEUTRON STAR 43

Lyubov Marinkova, Todor V. Veltchev and Sava Donkov
ANALYSIS OF THE DENSITY DISTRIBUTION IN STAR-FORMING CLOUDS: EXTRACTION OF A SECOND POWER-LAW TAIL 51

Mariyana Bogdanova, Orlin Stanchev and Todor V. Veltchev
STUDY OF THE FRACTAL DIMENSIONS IN THE MOLECULAR CLOUD ROSETTE BY USE OF DENDROGRAM ANALYSIS 61

Orlin Stanchev, Todor V. Veltchev and Mariyana Bogdanova
TRACING THE LOCAL MORPHOLOGY OF THE MOLECULAR CLOUD ROSETTE USING MOLECULAR-LINE DATA 69

Ruslan Zlatev, Nikola Petrov, Tsvetan Tsvetkov, Emil Ivanov, Rositsa Miteva, Velimir Popov, Yoana Nakeva and Ljube Bojevski
SHADOW BANDS AND RELATED ATMOSPHERIC PHENOMENA REGISTERED DURING TOTAL SOLAR ECLIPSES 79

Miroslava Vukcevic and Luka Č. Popović
SOLITONS IN THE IONOSPHERE – ADVANTAGES AND PERSPECTIVES 85

Aleksandra Kolarski
STORM ACTIVITY OVER BALKAN REGION DURING MAY 2009 93

Aleksandra Nina, Milan Radovanović, Luka Č. Popović, Ana Černok, Bratislav P. Marinković, Vladimir A. Srećković, Anđelka Kovačević, Jelena Radović, Vladan Čelebonović, Ivana Milić Žitnik, Zoran Mijić, Nikola Veselinović, Aleksandra Kolarski and Alena Zdravković
ACTIVITIES OF SERBIAN SCIENTISTS IN EUROPLANET 107

Natalija Janc, Milivoj B. Gavrilov, Slobodan B. Marković, Vojislava Protić Benišek, Luka Č. Popović and Vladimir Benišek
MILUTIN MILANKOVIĆ AND ASSOCIATES IN THE CREATION OF THE "*KANON*" 123

Milan S. Dimitrijević and Aleksandra Bajić
MYTHOLOGICAL ORIGIN OF CONSTELLATIONS AND THEIR DESCRIPTION: ARATUS, PSEUDO-ERATOSTHENES, HYGINUS 129

Aleksandra Bajić and Milan S. Dimitrijević
A PAIR OF STEĆAKS FROM DONJA ZGOŠĆA 139

Александра Бајић
ВЕНЕРА У МИТОЛОГИЈИ ЈУЖНИХ СЛОВЕНА
VENUS IN THE MYTHOLOGY OF THE SOUTHERN SLAVES 155

Петар В. Вуца
СУНЧАНИ ВАЉЦЕР
SUNDIAL WALTZ 169

LIST OF PARTICIPANTS 181

AUTHORS' INDEX 185

PROGRAMME OF THE CONFERENCE 186

Proceedings of the XII Serbian-Bulgarian Astronomical Conference (XII SBAC) Sokobanja, Serbia, September 25-29, 2020
Editors: L. Č. Popović, V. A. Srećković, M. S. Dimitrijević and A. Kovačević
Publ. Astron. Soc. "Rudjer Bošković" No 20, 2020, 107-121

ACTIVITIES OF SERBIAN SCIENTISTS IN EUROPLANET

ALEKSANDRA NINA[1], MILAN RADOVANOVIĆ[2], LUKA Č. POPOVIĆ[3], ANA ČERNOK[4], BRATISLAV P. MARINKOVIĆ[1], VLADIMIR A. SREĆKOVIĆ[1], ANĐELKA KOVAČEVIĆ[5], JELENA RADOVIĆ[6], VLADAN ČELEBONOVIĆ[1], IVANA MILIĆ ŽITNIK[3], ZORAN MIJIĆ[1], NIKOLA VESELINOVIĆ[1], ALEKSANDRA KOLARSKI[7] and ALENA ZDRAVKOVIĆ[8]

[1]*Institute of Physics Belgrade, University of Belgrade, Pregrevica 118, 11080 Belgrade, Serbia*
[2]*Geographical Institute Jovan Cvijić SASA, 11000 Belgrade, Serbia*
[3]*Astronomical Observatory, Volgina 7, 11060 Belgrade, Serbia*
[4]*Royal Ontario Museum, Center for the applied planetary mineralogy, Toronto, ON, Canada*
[5]*Department of astronomy, Faculty of Mathematics, University of Belgrade Studentski trg 16, 11000 Belgrade, Serbia*
[6]*Charles University, Faculty of Mathematics and Physics, Ke Karlovu 3, 12116, Prague 2*
[7]*Technical Faculty "Mihajlo Pupin", University of Novi Sad, 23000 Zrenjanin, Serbia*
[8]*Faculty of Mining and Geology, University of Belgrade, Belgrade*
E-mail: sandrast@ipb.ac.rs, bratislav.marinkovic@ipb.ac.rs, vlada@ipb.ac.rs, vladan@ipb.ac.rs, zoran.mijic@ipb.ac.rs, veselinovic@ipb.ac.rs
E-mail: m.radovanovic@gi.sanu.rs, lpopovic@aob.rs, ivana@aob.rs, acernok@rom.on.ca, andjelka@matf.bg.ac.rs, radovicj95@gmail.com, aleksandrakolarski@gmail.com, alena.zdravkovic@rgf.bg.ac.rs

Abstract. The Europlanet Society, an organization which promotes the advancement of European planetary science and related fields, has 10 hubs. The Serbian Europlanet Group (SEG) is included in the Europlanet South Eastern European Hub (ESEEH) and, currently, has 20 active scientists.

In this work, we present activities of SEG. Primarily, we describe two Europlanet workshops organized in the Petnica Science Center: "Geology and geophysics of the solar system bodies" and "Integrations of satellite and ground-based observations and multi-disciplinarity in research and prediction of different types of hazards in Solar system" that occurred in 2018 and 2019, respectively, and the Europlanet session during XII Serbian-

Bulgarian Astronomical Conference that occurred in Sokobanja 2020. In addition, we present other activities that were primarily aimed at connecting SEG members coming from six institutions as well as the promotion of the Europlanet and ESEEH organizations.

1. INTRODUCTION

The Europlanet society is an organization which promotes the European planetary science and related fields. Its aims are to support the development of planetary science at a national and regional level, particularly in countries and areas that are currently under-represented within the community, and early career researchers who establish their network within the Europlanet: the Europlanet Early Career (EPEC) network (https://www.europlanet-society.org/early-careers-network/).

Two Europlanet projects (the Europlanet 2020 Research Infrastructure and the Europlanet 2024 Research Infrastructure (RI)) are funded through the European Commission's Horizon 2020 programme. The first one, lasting 4 years, ended 2020, while the second one runs for four years from February 2020 until January 2024. The latest is led by the University of Kent, UK, and has 53 beneficiary institutions from 21 countries in Europe and around the world, with a further 44 affiliated partners. It provides free access to the world's largest collection of planetary simulation and analysis facilities, data services and tools, a ground-based observational network and programme of community support activities.

The Europlanet consists of 10 Regional Hubs:

- Benelux
- Central Europe: Austria, Czech Republic, Hungary, Poland, Slovenia and Slovakia
- France
- Germany
- Ireland and UK
- Italy
- Northern Europe: Denmark, Estonia, Finland, Iceland, Latvia, Lithuania, Norway and Sweden
- Southeast Europe: Bulgaria, Croatia, Cyprus, Greece, Romania, and Serbia
- Spain and Portugal
- Switzerland

As one can see, Serbia is one of, current six countries included in the Southeast European Hub that is established in 2019.

More information about organization and activities of this society can be found at the website https://www.europlanet-society.org/.

2. SERBIAN EUROPLANET GROUP

The Serbian Europlanet Group (SEG) currently consists of 20 members from 6 institutions. Details of members and activities of SEG can be found at

https://www.europlanet-society.org/europlanet-society/regional-hubs/southeast-europe/.

The main activities of Serbian scientists in the Europlanet were:

- Organization of two Europlanet meetings and one session,
- Establishing of SEG webpage,
- Participations in the Europlanet science congresses and meetings,
- Participations in the Europlanet NA1 Expert Exchange Program, and
- Participations in the Europlanet commities.

In this paper we describe these activities and present scientific research of SEG members related to the Europlanet fields.

3. EUROPLANET MEETING ORGANIZATIONS

Serbian scientist organized two Europlanet workshops in Petica Science Center near Valjevo in Serbia:

- "Geology and geophysics of the solar system bodies" (24 June– 1 July, 2018), and
- “Integrations of satellite and ground-based observations and multidisciplinarity in research and prediction of different types of hazards in the Solar system” (10-13 May, 2019),

and Europlanet session during the XII Serbian-Bulgarian Astronomical Conference (XII SBAC) in Sokobanja, Serbia 25-29 September, 2020.

3.1. Europlanet workshops

3.1.1. Workshop in Geology and Geophysics of the Solar System

The workshop took place in Petnica Science Center, Petnica, Serbia (23 June – 1 July 2018) and further details can be found at http://petnica.rs/planetary2017. It was designed to cover a wide range of topics related to the formation, structure and dynamics of the Solar System and aimed to attract students and young researchers of various backgrounds and of different levels of experience in the fields of planetary sciences and space exploration. The workshop attended 43 participants, of which 24 PhD, 13 master and 6 undergraduate students. They were from 19 different home countries, including 15 from Eastern Europe, 3 from Russia and 4 from Northern Afrika. Other participants came from as far as India, Australia, and USA. The scientific organizers of the workshop were Dr. Katarina Miljkovic (Curtin University, Australia), Dr. Ana Cernok (The Open University, UK) and Dr. Matija Cuk (SETI Institute, USA), supported by the local organizers Dusan Pavlovic (Petnica Science Centre, Serbia) and Andrea Rajsic, deputy (University of Belgrade, Serbia). In total, there were 14 lecturers (7 female and 7 male). Although there was only one lecturer from a Serbian institution (University of Bel-

grade), there were 5 other lecturers (including the organizers) who were originally from Serbia. This planetary sciences workshop was supported by the Europlanet 2020 RI NA1 (Innovation through Science Networking) Task 5 (Coordination of ground-based observations) and Europlanet 2020 RI NA2 (Impact through outreach and engagement).

3.1.2. Workshop in Hazards in the Solar system

This workshop was focused on integrations of satellite and ground-based observations and multidisciplinarity in research and prediction of different types of hazards in the Solar system. The main of this meeting was connection of young researchers and scientists from under-represented countries, and experts in corresponding scientific fields. The organizer was the Geographical Institute "Jovan Cvijic" of Serbian Academy of Sciences and Arts. The chairs of the Scientific committee were Aleksandra Nina, Milan Radovanović from Serbia and Giovanni Nico from Italy. In this committee participated 11 scientists from 9 countries. Aleksandra Nina and Milan Radovanović were co-chairs, and Gorica Stanojević, Vladimir Čadež, Dejan Doljak, Vladimir Srećković and Dragoljub Štrbac were members of the Local Organizing Committee. The meeting attended 33 participants (of which 11 early career scientists) from 8 European countries: Bulgaria, Croatia, Greece, Hungary, Italy, Russia, Ukraine and Serbia. Their research fields relate to different theoretical and observation areas as well as to data sciences. In addition, two participants were from industry. This event was supported by the Europlanet 2020 RI NA1 - Innovation through Science Networking, Task 2: Scientific working groups (Europlanet 2020 RI has received funding from the European Union's Horizon 2020 research and innovation programme under grant No. 654208) and the Ministry for Education, Science and Technological Development of Republic of Serbia. More information about this event can be found at http://www.gi.sanu.ac.rs/site/index.php/en/activities/conferences-organisation/998-hazards-sos.

3.3. Europlanet session organised by SEG

Serbian scientists organized a Europlanet session during XII Serbian-Bulgarian Astronomical Conference (SBAS 12) that was held in Sokobanja from 25-29 of September 2020 (see Popović et al. 2020). Several lectures were held, a discussion, as well as the report of work of our group in the previous period was presented. At this Europlanet special session and during SBAC 12, possible directions for expanding cooperation were discussed with Bulgarian colleagues and also with colleagues from Europlanet Southeast HUB countries.

3.4. Participations in the Europlanet Science Congresses

Serbian scientists participated at the Europlanet Science Congresses (EPSC). The number of participants from Serbia is increasing. 7 scientists from Serbia participated in the EPSC-2020 and presented 3 lectures.

Figure 1: Participants of the workshop "Integrations of satellite and ground-based observations and multidisciplinarity in research and prediction of different types of hazards in the Solar system" held in Petnica Science Center on 10-13 May, 2019 (photo: Veljko Vujičić). From left to right:
Upper row: Konstantinos Kourtidis (Greece) , Pál Gábor Vizi (Hungary), Jelena Petrović (Serbia), Anđelka Kovačević (Serbia), Duško Borka (Serbia), Gorica Stanojević (Serbia), Zorica Marinković (Serbia), Bratislav Marinković (Serbia) and Dejan Doljak (Serbia);
Middle row: Georgi Simeonov (Bulgaria), Inna Pulinets (Russia), Bozhidar Srebrov (Bulgaria), Dejan Vinković (Croatia), Yaroslav Vyklyuk (Ukraine), Pier Francesco Biagi (Italy), Aleksandra Kolarski (Serbia), Lelica Popović (Serbia), Nikola Veselinović (Serbia) and Zoran Mijić (Serbia);
Bottom row: Predrag Jovanović (Serbia), Vesna Borka Jovanović (Serbia), Sergey Pulinets (Russia), Milan Radovanović (Serbia), Aleksandra Nina (Serbia), Vladimir Srećković (Serbia), Giovanni Nico (Italy), Milan S. Dimitrijević (Serbia), Luka Č. Popović (Serbia), Nataša Todorović (Serbia), Slavica Malinović-Milićević (Serbia) and Dragoljub Štrbac (Serbia).

3.5. Participations in the Regional Hubs Meetings

On the 4th and 5th June 2019, in Hotel Gellért, Budapest the Regional Hubs Meeting was organized by Melinda Dósa from Wigner RCP with the presence of the representatives from the Europlanet Society, Benelux Hub (represented by Ann Carine Vandaele, vice-president of Europlanet Society), Central European Hub, France, Italy, Northern European Hub, Spain & Portugal and Southeast European Hub, in total there were 23 researchers present. After the participants introduced themselves, the talk by Anita Heward, communication officer, was given on the Role of the hubs in the Europlanet Society and building a sustainable future from Europlanet 2020 RI. Following discussion was about the importance of widening.in Europlanet. The focus of the meeting was on Planetary science – technology – industry synergy: aims and possibilities & Towards a strategy definition. As a result of this meeting the participation and formal enrollment in Europlanet Society by Serbian researchers has been substantially increased.

3.6. Participation in the Europlanet NA1 Expert Exchange Program

Supported through the Europlanet NA1 Expert Exchange Program, Dr. Alena Zdravković, curator of the Mineral and Rock Collection of the Faculty of Mining and Geology in Belgrade, Serbia, visited The Open University in October 2017 to work with Dr. Ana Cernok and other experts in meteorite science. During this visit, six meteorite samples from the Marquis de Mauroy collection of the Mineral and Rock Collection (01. Lancon, 02. Bath, 03. Powder Mill Creek, 04.Morrisyown Hamblen, 05. Merceditas and 06. Hex River, with numbers representing a handing number at the Open University) were used for polished thin- and thick-section preparation at the Open University, Milton Keynes, UK. Lancon and Bath are fragmented chondrite meteorites, Powder Mill Creek and Morrisyown Hamblen are mesosiderites, and Merceditas and Hex River are iron meteorites. Since the meteorite samples belong to a very old collection, dating from 1899, due to inadequate equipment and unprecise preparation facilities in the laboratory of Faculty of Mining and Geology in Belgrade, those kind of samples were never used for utilizing cut and polishing preparations. This visit aimed at meteorite thin-section preparation was an important milestone for this Serbian collection. It was the first such opportunity to open and present the collection to an international scientific community. More importantly, those are the only thin sections of meteorite samples available at Belgrade University, and will therefore serve as precious teaching material for students educating, as well as for initiating meteorite research.

3.7. Participations in the Europlanet committees

As a member of the Southeastern European Hub Committee, Aleksandra Nina participated in two teleconferences and one meeting of the Selection committee for Europlanet funding.

3.8. Other activities

Lecture during XIX Serbian astronomical conference (19 SAC) held at the Serbian Academy of Sciences and Arts in Belgrade, from October 13 – 17, 2020 (see Kovačević et al. 2020).

4. SOME STUDIES OF SEG MEMBERS

SEG members are scientists in four research fields: astronomy, geophysics, physics and geography. Here we present a few research that are in Europlanet areas.

4.1. Astronomy

4.1.1. The functional relation between mean motion resonances and Yarkovsky force on small eccentricities

We examined asteroid's motion with orbital eccentricity in the range (0.1, 0.2) across the 2-body mean motion resonance (MMRs) with Jupiter due to the Yarkovsky effect. We calculated time delays dtr caused by the resonance on the mobility of an asteroid with the Yarkovsky drift speed. We derived a functional relation that accurately describes dependence between the average time lead/lag dtr, the strength of the resonance SR, and the semimajor axis drift speed da/dt with asteroids' orbital eccentricities in the range (0.1, 0.2). We analysed average values of dtr using this functional relation comparing with obtained values of dtr from the numerical integrations. On the basis of the obtained results and analyses, we conclude that our equation can be used for the 2-body MMRs with strengths in the range $[1.3\times10^{-8}, 2.2\times10^{-4}]$, for Yarkovsky drift speeds in the range $[2.6\times10^{-4}, 2\times10^{-3}]$ au/Myr and for asteroids' orbital eccentricities in the range (0.1, 0.2) (Milić Žitnik 2020a).

4.1.2. The specific property of motion of resonant asteroids with very slow Yarkovsky drift speeds

We examined the specific characteristics of the motion of asteroids with very slow Yarkovsky drift speeds across the 2-body MMRs with Jupiter, whose strengths cover a wide range. It was found that the test asteroids with very small Yarkovsky drift speeds moved extremely rapidly across MMRs (order of magni-

tude 10^{-5} au/Myr or less). This result may indicate that, below a certain boundary value of da/dt asteroids typically move quickly across MMRs. From the obtained results, it is concluded that the boundary value of the Yarkovsky drift speed is 7×10^{-5} au/Myr (Milić Žitnik 2019).

4.1.3. The relationship between the 'limiting' Yarkovsky drift speed and asteroid families' Yarkovsky *V*-shape

We examined the relationship between asteroid families' *V*-shapes and the 'limiting' diameters in the (a, 1/D) plane. Following the recently defined 'limiting' value of the Yarkovsky drift speed at 7×10^{-5} au/Myr, we decided to investigate the relation between the asteroid family Yarkovsky *V*-shape and the 'limiting' Yarkovsky drift speed of asteroid's semi-major axes. We have used the known scaling formula to calculate the Yarkovsky drift speed in order to determine the inner and outer 'limiting' diameters (for the inner and outer *V*-shape borders) from the 'limiting' Yarkovsky drift speed. The method was applied to 11 asteroid families of different taxonomic classes, origin type and age, located throughout the Main Belt. Our main conclusion is that the 'breakpoints' in changing *V*-shape of the very old asteroid families, crossed by relatively strong MMRs on both sides very close to the parent body, are exactly the inverse of 'limiting' diameters in the a versus 1/D plane. This result uncovers a novel interesting property of asteroid families' Yarkovsky *V*-shapes (Milić Žitnik 2020b).

4.1.4. Improvement of modelling of atmospheres using A&M data

We continued to work on topics of modelling various atmospheres (using new software packages and supercomputers) and diagnostic of the astrophysical (terrestrial and space) and laboratory plasma using A&M datasets e.g. rate coefficients, Stark broadening parameters, line profiles (the shape of atomic spectral lines in plasmas contains information on the plasma parameters, and can be used as a diagnostic tool), etc. Results which are of interest for Europlanet community are presented in our recently published papers (see e.g. Ignjatović et al. 2019, Srećković et al. 2020, Majlinger et al. 2020, Dimitrijević et al. 2020) as well as in database MolD http://servo.aob.rs/mold (Marinković et al. 2019) hosted on SerVO at AOB.

4.1.5. Correlation of solar wind parameters with cosmic rays observed with ground station

It has been well known for more than half a century that solar activity has a strong influence on galactic cosmic ray (GCR) flux reaching Earth (anti-correlation). Coronal mass ejections (CMEs) structure and shockwave can additionally modulate GCRs, which could results in a transient decrease in observed GCR intensity, known as Forbush decrease (FD). These FDs can be detected even

with ground muon detector (Savić et al. 2019). Variation of GCR can be analyzed correlating in situ measurement of the particles species present in solar wind with ground observations. Correlation between the 1-hour variations of GCR and several different one-hour averaged particle fluxes was found during FDs and it depends on energy of the particles of the solar wind as well as cut-off rigidities of secondary cosmic rays detectors on ground.

4.1.6. Habitability of exoplanets

Balbi, Hami and Kovačević (2020) present a new investigation of the habitability of the Milky Way bulge, that expands previous studies on the Galactic Habitable Zone. This work discusses existing knowledge on the abundance of planets in the bulge, metallicity and the possible frequency of rocky planets, orbital stability and encounters, and the possibility of planets around the central supermassive black hole. The paper focuses the two aspects that can present substantial differences with respect to the environment in the disk: (i) the ionizing radiation environment, due to the presence of the central black hole and to the highest rate of supernovae explosions and (ii) the efficiency of putative lithopanspermia mechanism for the diffusion of life between stellar systems. Authors devised analytical models of the star density in the bulge to provide estimates of the rate of catastrophic events and of the diffusion timescales for life over interstellar distances.

This article has been published as an invited contribution in the Special Issue "Frontiers of Astrobiology" edited by Manasvi Lingam.

Another concern for habitability is the presence of the supermassive black hole in the Galactic center, but also in nearby Active galactic nuclei, that could have resulted in a substantial flux of ionizing radiation during its past active phase, causing increased planetary atmospheric erosion and potentially harmful effects to surface life as shown by Wisłocka, Kovačević, Balbi (2019).

The goal of this paper is to improve our knowledge of the erosion of exoplanetary atmospheres through radiation from supermassive black holes (SMBHs) undergoing an active galactic nucleus (AGN) phase.

Authors extended the well-known energy-limited mass-loss model to include the case of radiation from AGNs. In the paper was calculated the possible atmospheric mass loss for 54 known exoplanets (of which 16 are hot Jupiters residing in the Galactic bulge and 38 are Earth-like planets, EPs) due to radiation from the Milky Way's (MW) central SMBH, Sagittarius A* (Sgr A*), and from a set of 107 220 AGNs generated using the 33 350 AGNs at $z < 0.5$ of the Sloan Digital Sky Survey database.

It was found that planets in the Galactic bulge might have lost up to several Earth atmospheres in mass during the AGN phase of Sgr A*, while the EPs are at a safe distance from Sgr A* (>7 kpc) and have not undergone any atmospheric erosion in their lifetimes. It was also found that the MW EPs might experience a mass loss up to 15 times the Mars atmosphere over a period of 50 Myr as the result of exposure to the cumulative extreme-UV flux FXUV from the AGNs up to z

= 0.5. This work was featured in famous *Forbes Magazine* in their section Innovation.

4.2. Geophysics

4.2.1. Investigation of a possible new type of lower ionosphere precursor of earthquakes

Analysis of the signal transmitted in Italy and received by the AbsPAL receiver in Belgrade in the period around the earthquake that occurred in the vicinity of Kraljevo on November 3, 2010 indicated a change in the amplitude of the signal less than an hour before this event. Although this change has not been reported in the literature, an additional study of several earthquakes indicates the existence of this change in other cases as well. The first study of this phenomenon is presented in Nina et al. (2020), and a broader statistical analysis is underway.

4.2.2. Modelling of solar X-ray flare influence on propagation of satellite signals

Due to the low electron density, the unperturbed D-region has practically no effect on the propagation of satellite signals. Therefore, it is generally not involved in modeling of signal propagation path or, if it is, its influence is given by analytical expressions based on observational data from higher altitudes. In Nina et al. (2020b), it is shown that during intense perturbations of this ionospheric layer due to the influence of solar X-ray flares (they do not perturb significantly higher ionospheric layers except when their intensity is very strong) it is necessary to include observational data for the D-region in modeling the propagation of satellite signals.

4.2.3. Satellite radar technique for atmospheric water vapor measurement and modelling effects of the ionospheric disturbances

Atmospheric water vapor measurement can be carried out in many different ways. One of the techniques for observing and measuring atmospheric water vapor is through satellite radars, precisely the Synthetic Aperture Radar (SAR) used and carried on the platform of many active satellites. In Radović (2020) are introduced four of such satellites and the water vapor modelling technique called SAR Interferometry is described as well. Along with the above mentioned in Radović (2020) it is demonstrated how neglecting the ionospheric disturbances that can occur during the satellite radar measurement of the water vapor can influence the modelling of certain parameters which are connected to the measured atmospheric water vapor.

4.2.4. Remote sensing of the atmospheric aerosol

Atmospheric aerosol plays one of the most important roles in climate changes and environmental issues through direct (scattering and absorption of solar and terrestrial radiation) and indirect (modification of cloud condensation nuclei through aerosol-cloud interaction) effects. In Mijić and Perišić (2019), study the relationship between satellite aerosol optical depth (AOD) measurements by Moderate Resolution Imaging Spectroradiometer (MODIS) and PM (Particulate Matter) concentrations data set from the Belgrade region was investigated. The preliminary results showed that AOD retrieved from a satellite sensor can be considered as a good proxy for ground observed PM mass concentrations. Within the EARLINET (European Aerosol Research Lidar Network) network a stand-alone lidar-based method (Papagiannopoulos et al. 2020) for detecting airborne hazards for aviation in near real time (NRT) is developed. In addition, Belgrade lidar station has been involved in ESA ADM-Aeolus mission (the first high-spectral resolution lidar in space) Cal/Val activity through validation of L2A products of aerosol and cloud profiles of backscatter, extinction and lidar-ratio.

4.2.5. Atmospheric disturbances due to severe stormy weather over Balkan region

Strong release of energy by atmospheric lightning discharges induced ionization changes along the propagation path of several Very Low Frequency (VLF) radio signals that had been received and recorded by Absolute Phase and Amplitude Logger (AbsPAL) system located in Belgrade (44.85^{o} N, 20.38^{o} E), at the Institute of Physics Belgrade, University of Belgrade, Serbia. Increased ionization is apparent in the perturbation of the signal amplitude and phase delay with respect to regular undisturbed ionospheric conditions. Integrated ground-based observations were performed with the aim to find coincidence and possible relationship between phenomena of VLF signal perturbations, optically documented Transient Luminous Events (TLEs) and documented lightning stroke events, during the stormy night of 27th-28th of May, 2009. The survey enclosed data from three independent sources: 1) VLF signal records from Belgrade Institute for Physics database, 2) video records of sprite events from ITALIAN METEOR and TLE NETWORK (I.M.T.N.) database and 3) detected lightning strokes from European Cooperation for Lightning Detection (EUCLID) network database. In most cases, the correspondence between VLF perturbations and CG strokes and on the other hand, VLF perturbations and TLE events, was found. In some cases the correspondence between all three phenomena was found (Kolarski 2019, 2020).

4.3. Physics

4.3.1. V. Čelebonović has been working on the problem of impact craters on the surfaces of solid planetary and satellite bodies. He showed that using standard solid state physics and measured properties of the craters, one can derive various parameters of the impactors. The calculations were checked on several known examples, and the agreement is reasonable.
4.3.2. The role of electron induced dissociation in the comet's coma and the findings during Rosetta spacecraft mission have been the subject of investigation published in Marinković et al. (2017). Data needs for modelling electron processes in cometary coma and their influence on the interpretation of the observed data by Rosetta instruments, have been discussed together with the currently available data and databases, where BEAMDB (Belgrade Electron/Atom(Molecule) DataBase - http://servo.aob.rs/emol) is given as an example (Marinković et al. 2019).

4.4. Geography

4.4.1. Our research was devoted to the determination of the causal relationship between the flow of particles that are coming from the Sun and the hurricanes Irma, Jose, and Katia. As a result of the preliminary analysis, using 12,274,264 linear models by parallel calculations, six of them were chosen as best. The identified lags were the basis for refinement of models with the artificial neural networks. Multilayer perceptrons with back propagation and recurrent LSTM have been chosen as commonly used artificial neural networks. Comparison of the accuracy of both linear and artificial neural networks results confirmed the adequacy of these models and made it possible to take into account the dynamics of the solar wind. Sensitivity analysis has shown that F10.7 has the greatest impact on the wind speed of the hurricanes. Despite low sensitivity of pressure to change the parameters of the solar wind, their strong fluctuations can cause a sharp decrease in pressure, and therefore the appearance of hurricanes (Vyklyuk, et al. 2019).

4.4.2. Forest fires that occurred in Portugal on 18 June 2017 caused several tens of human casualties. The cause of their emergence, as well as many others that occurred in Western Europe at the same time remained unknown. Taking into account consequences, including loss of human lives and endangerment of ecosystem sustainability, discovering of the forest fires causes is the very significant question. The heliocentric hypothesis has indirectly been tested, according to which charged particles are a possible cause of forest fires. We must point out that it was not possible to verify whether in this specific case the particles by reaching the ground and burning the plant mass create the initial phase of the formation of the flame. Therefore, we have tried to determine whether during the critical period, i.e. from 15–19 June there is a certain statistical connection between certain parameters of the solar wind and meteorological elements. Based on the 2 hourly values of the charged particles flow, a correlation analysis was performed with

hourly values of individual meteorological elements including time lag at Monte Real station. The application of the Adaptive Neuro Fuzzy Inference System models has shown that there is a high degree of connection between the flow of protons and the analysed meteorological elements in Portugal. However, further verification of this hypothesis requires further laboratory testing (Radovanović et al. 2019).

5. CONCLUSION

In this paper we present activities of Serbian scientists in the Europlanet. We describe two Europlanet workshops organized in the Petnica Science Center: "Geology and geophysics of the solar system bodies" and “Integrations of satellite and ground-based observations and multi-disciplinarity in research and prediction of different types of hazards in Solar system” that occurred in 2018 and 2019, respectively, and the Europlanet session during XII Serbian-Bulgarian Astronomical Conference that occurred in Sokobanja 2020. In addition, we present other activities that were primarily aimed at connecting SEG members coming from six institutions as well as the promotion of the Europlanet and ESEEH organizations. Several studies relevant for the Europlanet research fields are presented in the second part of this paper.

Acknowledgments

This research is supported by the Europlanet. The authors acknowledge funding provided by the Institute of Physics Belgrade, Astronomical Observatory (the contract 451-03-68/2020-14/200002), Faculty of Mathematics University of Belgrade (the contract 451-03-68/2020-14/200104) through the grants by the Ministry of Education, Science, and Technological Development of the Republic of Serbia.

References

Balbi A., Hami M., Kovačević A.: 2020, The Habitability of the Galactic Bulge, *Life*, 10, 132-145.

Čelebonović V.: 2020, The origin of impact craters, some ideas. *Bulg. Astron. J*, 33, 21.

Drimitrijević M. S., Srećković V. A., Ignjatović Lj. M., Marinković B. P.: 2021, The role of some collisional processes in AGNs: rate coefficients needed for modeling, *New Astronomy*, 84, 101529.

Ignjatović Lj. M., Srećković V. A., Dimitrijević M. S.: 2019. The collisional atomic processes of Rydberg alkali atoms in geo-cosmical plasmas. *Monthly Notices of the Royal Astronomical Society*, 483(3), 4202-4209.

Kolarski A.: 2019, *Atmospheric disturbances due to severe stormy weather*, Book of Abstracts, “Integrations of satellite and ground-based observations and multi-disciplinarity in research and prediction of different types of hazards in Solar system”, Petnica, Science Center, May 10-13, 2019, Valjevo, Serbia, Geographical Institute “Jovan Cvijić” SASA, Belgrade, Serbia, p. 42.

Kolarski A.: 2020, *Storm activity over Balkan region during May 2009*, Book of Abstracts, "XII Serbian-Bulgarian Astronomical Conference (XII SBAC)" September 25-29, 2020, Sokobanja, Serbia, Astronomical Observatory, Belgrade, Serbia, p. 75.

Kovačević A., Kovačević Dojčinović A., Marčeta D., Onić D: 2020, Book of abstracts XIX Serbian Astronomical Conference October 13 - 17, 2020, Belgrade, Serbia.

Majlinger Z., Dimitrijević M. S., Srećković V. A.: 2020, Stark broadening of Co II spectral lines in hot stars and white dwarf spectra, *Monthly Notices of the Royal Astronomical Society*, 496(4), 5584-5590.

Marinković B. P., Bredehöft J. H., Vujčić V., Jevremović D., Mason N. J.: 2017, Rosetta Mission: Electron Scattering Cross Sections - Data Needs and Coverage in BEAMDB Database, *Atoms*, 5(4), 46 [18pp].

Marinković B. P., Srećković V. A., Vujčić V., Ivanović S., Uskoković N., Nešić M., Ignjatović Lj. M., Jevremović D., Dimitrijević M. S., Mason N. J.: 2019, BEAMDB and MOLD – Databases at the Serbian Virtual Observatory for collisional and radiative processes, *Atoms*, 7(1), 11 [14pp].

Mijić Z., Perišić M.: 2019, *Comparison of Modis aerosol observations and ground-based PM measurement for the Belgrade region*, Book of abstracts, "Integrations of satellite and ground-based observations and multi-disciplinarity in research and prediction of different types of hazards in Solar system", pp.51-52, Petnica Science Center, 10-13 May, 2019, Geographical Institute "Jovan Cvijić" SASA, Belgrade.

Milić Žitnik I.: 2019, The specific property of motion of resonant asteroids with very slow Yarkovsky drift speeds, *MNRAS*, 486, 2435-2439.

Milić Žitnik I.: 2020a, The functional relation between mean motion resonances and the Yarkovsky force for small eccentricities, *MNRAS*, 498(3), 4465-4471.

Milić Žitnik I.: 2020b, The relationship between the 'limiting' Yarkovsky drift speed and asteroid families' Yarkovsky V-shapes, *SAJ*, 200, 25-41.

Nina A., Radovanović M., Srećković V. A.: 2019, Book of abstracts, "Integrations of satellite and ground-based observations and multi-disciplinarity in research and prediction of different types of hazards in Solar system", Petnica Science Center, 10-13 May, 2019, Geographical Institute "Jovan Cvijić" SASA, Belgrade.

Nina A, Pulinets S., Biagi P. F., Nico G., Mitrović S. T., Radovanović M., Popović L. Č.: 2020a, *Sci. Total Environ*., 710, 136406.

Nina A., Nico G., Odalović O., Čadež M., V., Todorović Drakul M., Radovanović M., Popović L. Č.: 2020b, *IEEE Geosci. Remote Sens. Lett*., 17(7), 1198 – 1202.

Papagiannopoulos N., D'Amico G., Gialitaki A., Ajtai N., Alados-Arboledas L., Amodeo A., Amiridis V., Baars H., Balis D., Binietoglou I., Comerón A., Dionisi D., Falconieri A., Fréville P., Kampouri A., Mattis I., Mijić Z., Molero F., Papayannis A., Pappalardo G., Rodríguez-Gómez A., Solomos S., Mona L.: 2020, An EARLINET early warning system for atmospheric aerosol aviation hazards, *Atmos. Chem. Phys.*, 20, 10775–10789.

Popović L. Č., Srećković V. A., Dimitrijević M. S., Kovačević A.: 2020, *Book of Abstracts,* "XII Serbian-Bulgarian Astronomical Conference (XII SBAC)" September 25 - 29, 2020, Sokobanja, Serbia, Astronomical Observatory, Belgrade, Serbia

Radovanović M. M, Vyklyuk Y, Stevančević T, M, Milenković Đ. M, Jakovljević D, Petrović M, Malinović Milićević S, Vuković N, Vujko A, Yamashkin A, Sydor P, Vuković D, Škoda M.: 2019, Forest fires in Portugal — case study, 18 June 2017, *Thermal Science*, 23(1), 73-86.

Radović J.: 2020, *Satellite radar technique for atmospheric water vapor measurement and modelling effects of the ionospheric disturbances*, Master thesis, Faculty of Physics, University of Belgrade, Serbia.

Savić M., Veselinović N., Dragić A., Maletić D., Joković D., Banjanac R., Udovičić V.: 2019, Rigidity dependence of Forbush decreases in the energy region exceeding the sensitivity of neutron monitors, *Advances in Space Research*, 63(4), 1483-1489.

Srećković V. A., Dimitrijević M. S., Ignjatović Lj. M.: 2020, The influence of collisional-ionization and recombination processes on spectral line shapes in stellar atmospheres and in the hydrogen clouds in broad-line region of AGNs, *Contrib. Astron. Obs. Skalnaté Pleso*, 50, 171-178.

Vyklyuk Y, Radovanović M. M, Milovanović B, Milenković M, Petrović M, Doljak D, Malinovic Milićević S, Vuković N, Vujko A, Matsiuk N, Mukherjee S.: 2019, Space weather and hurricanes Irma, Jose and Katia, *Astrophys Space Sci,* 364, 154.

Wisłocka A. M., Kovačević A. B., Balbi A.: 2019, Comparative analysis of the influence of Sgr A* and nearby active galactic nuclei on the mass loss of known exoplanets, *Astron. Astrophys*., 624, A71 [17 pp].

WeBIOPATR 2021

The Eighth International WEBIOPATR
Workshop & Conference
Particulate Matter: Research and Management

Abstracts of Keynote Invited Lectures and Contributed Papers

Milena Jovašević-Stojanović,

Alena Bartoňová,

Miloš Davidović and Simon Smith, Eds

Vinča Insitute of Nuclear Sciences

Vinča, Belgrade 2021

ABSTRACTS OF KEYNOTE INVITED LECTURES AND CONTRIBUTED PAPERS

The Eighth WeBIOPATR Workshop & Conference

Particulate Matter: Research and Management

WeBIOPATR 2021

29th November to 1st December 2021

Vinča, Belgrade, Serbia

Editors

Milena Jovašević-Stojanović

Alena Bartoňová

Miloš Davidović

Simon Smith

Publisher

Vinča Institute of Nuclear Sciences

Prof. Dr Snežana Pajović, Director

P.O.Box 522

11001 Belgrade, Serbia

Printed by

Vinča Institute of Nuclear Sciences

ISBN 978-86-7306-164-1

www.vin.bg.ac.rs/

SCIENTIFIC COMMITTEE

Aleksandar Jovović, Serbia
Alena Bartoňová, Norway
Antonije Onjia, Serbia
David Broday, Israel
Dikaia Saraga, Greece
Griša Močnik, Slovenia
Ivan Gržetić, Serbia
María Cruz Minguillón, Spain
Milena Jovašević-Stojanović, Serbia
Miloš Davidović, Serbiac
Saverio de Vito, Italy
Selahattin Incecik, Turkey
Slobodan Ničković, Serbia
Simone Barreira Morais, Portugal
Zoran Mijić, Serbia
Zoran Ristovski, Australia
Zorana Jovanović-Andersen, Denmark

ORGANIZING COMMITTEE

Aleksandra Stanković, Serbia
Alena Bartoňová, Norway
Andrej Šoštarić, Serbia
Anka Cvetković, Serbia
Biljana Filipović, Serbia
Branislava Matić, Serbia
Lidija Marić-Tanasković, Serbia
Uzahir Ramadani, Serbia
Ivan Lazović, Serbia
Sonja Dmitrašinović (Secretary), Serbia
Marija Živković (Secretary), Serbia
Milena Jovašević-Stojanović, Serbia
Miloš Davidović, Serbia
Mira Aničić Urošević, Serbia
Mirjana Perišić, Serbia
Nenad Živković, Serbia
Tihomir Popović, Serbia
Vesna Slepčević, Serbia
Viša Tasić, Serbia

CONFERENCE TOPICS

1. **Atmospheric Particulate Matter - Physical and Chemical Properties**
    i. Sources and formation of particulate matter
    ii. Particulate matter composition and levels outdoors and indoors
    iii. Environmental modeling
    iv. Nanoparticles in the environment
2. **Particulate Matter and Health**
    i. Exposure to particulate matter
    ii. Health aspects of atmospheric particulate matter
    iii. Full chain approach
    iv. COVID-19 and particulate matter
3. **Particulate Matter and Regulatory Issues**
    i. Issues related to monitoring of particulate matter
    ii. Legislative aspects
    iii. Abatement strategies

Organizers

Vinča Institute of Nuclear Sciences, Serbia

Public Health Institute of Belgrade, Serbia

NILU Norwegian Institute for Air Research, Norway

The 8th WeBIOPATR Workshop and Conference,

Particulate Matter: Research and Management, WEBIOPATR 2021

is supported by:

EC H2020 Framework Program for Research and Innovation, area "Spreading excellence and widening participation", VIDIS project (2020-2023) coordinated by Vinca Institute of Nuclear Sciences, Grant agreement number 952433.

Ministry of Education, Science and Technological Development of Republic of Serbia

PREFACE

Dear Colleagues,

Welcome to the 8th WeBIOPATR Conference, to be held at the premises of the Vinca Institute of Nuclear Sciences, Serbia, 29.11.–1.12.2021, as a combination of online and face-to-face event.

The International Workshop and Conference, Particulate Matter: Research and Management – WeBIOPATR is a biennial event held in Serbia since 2007. The conference addresses air quality in general and particulate matter specifically. Atmospheric particulate matter arises both from primary emissions and from secondary formation in the atmosphere. It is one of the least well understood local and regional air pollutants, has complex implications for climate change, and is perhaps the pollutant with the highest health relevance. It also poses many challenges to monitoring.

By WeBIOPATR, we aim to link the research communities with relevance to particulate matter with the practitioners of air quality management on all administrative levels, in order to facilitate professional dialogue and uptake of newest research into practice. The workshops usually draw an audience of about 70 and attract media attention in Serbia. It enjoys support of the responsible authorities, Ministry of Education, Science and Technological Development, Ministry of Health, Ministry of Environment, and the Serbian Environmental Agency whose sponsorship is indispensable and gratefully acknowledged. We also enjoy support of international bodies such as the WHO.

The 1st WeBIOPATR Workshop was held in Beograd, 20.-22. May 2007, associated with a project funded by the Research Council of Norway. The 2nd workshop was held in Mećavnik, Serbia, 28.8.-1.9.2009. WeBIOPATR2011 was held in Beograd 14.-17.11.2011 and for the first time, included a dedicated student workshop. WeBIOPATR2013 was held in Beograd 2.-4.10. 2013. It covered the traditional PM research and management issues, discussions on how to encourage citizens to contribute to environmental governance, and how to develop participatory sensing methods. WeBIOPATR2015 was held in Beograd 14.-16.10. 2015. Dedicated sessions were devoted to sensor technologies for air quality monitoring, utilizing information and input from the EU FP7 funded project CITI-SENSE (http://co.citi-sense.eu) and the EU COST action EuNetAir (www.eunetair.it). WeBIOPATR2017, the 6th conference, was held in Beograd 6.-8.9. 2017, with a wider than before Western Balkan participation. The 7th WeBIOPATR2019 was held 1.-4.10. 2019 at the Mechanical Faculty, University of Belgrade. It has attracted a record of over 50 contributions, and brought together scientists from 12 countries, documenting that the issues of atmospheric pollution, with their wide implications for climate change, human health and ecosystem services, are no less important today. This year's event will be with similar number of contributions that have been accepted.

In the past two years, all our lives were affected by the COVID-19 pandemic. We have adapted our ways of life and work – and now we hope that the new format of the conference

will be a success, for the participants physically present as well as for those who will participate online.

We are very grateful to our unrelenting national and international partners for their financial and scientific support for this event. In addition, WeBIOPATR2021 is supported by the VIDIS project, https://vidis-project.org/, funded by the EC H2020 Framework Programme for Research and Innovation, area "Spreading excellence and widening participation". VIDIS (2020-2023) is coordinated by Vinca Institute, Grant agreement number 952433.

Welcome to Vinca and online and have a stimulating and productive time!

Milena Jovašević-Stojanović and Alena Bartoňová

TABLE OF CONTENTS

1. INDOOR, VENTILATION, PROTECTION 11

1.1 COVID-19, Particles in the Air and Ventilation 12

1.2 Applying Aerosol Science to the Current Needs: Particle Removal Efficiency of Face Masks During the COVID-19 Pandemic 13

1.3 Personal Protection Against Airborne Particulate Matter 14

1.4 The Role of Microclimate in the Formation of Indoor Air Pollution 15

2. LOW-COST SENORS 17

2.1 PM Low-Cost Sensors Calibration in the Wild: Methods and Insights From AirHeritage Project 18

2.2 Schools for Better Air Quality: Citizens-Based Monitoring, Stem Education, and Youth Activism in Serbia *UNICEF in Serbia* 19

2.3 Assessing Air Pollution from Wood Burning Using Low-Cost Sensors and Citizen Science 20

2.4 Potential for Using Low-Cost Sensor Measurements in Outdoor Environmental Quality Particulate Matter Measurements 21

3. SCIENCE – POLICY 23

3.1 How Do We Understand Interdisciplinarity in Environment and Climate Research: Results From a Recent Study in Norway 24

3.2 The Hybrid Computational Approach in Revealing Particulate Matter Related Processes 25

4. HEALTH AND EXPOSURE I 27

4.1 Long-term Exposure to Air Pollution and Mortality: Overview with Focus on the Low-exposure Areas 28

4.2 Air Pollution and the Growth of Children – Is There a Connection? 29

4.3 Health Risk Assessment of Particulate Matter Emissions from Natural Gas and Fuel Oil Heating Plants Using Dispersion Modelling 30

4.4 Assessment of Increased Individual-Level Exposure to Airborne Particulate Matter During Periods of Atmospheric Thermal Inversion 31

4.5 How Will the New Who Air Quality Guidelines for PM2.5 Affect the Health Risk Assessment by the European Environment Agency 32

5. HEALTH AND EXPOSURE II 33

5.1 Biomarkers of Exposure to Particulate Matter Air Pollutants: A Precious Tool for Studying Health-Related Effects 34

5.2 Experimental Approaches for Studying Viral infectivity, RNA Presence and Stability in Environmental PM: Dedicated Sampling, Biosensors, and Adaptation of Standard TECHNIQUES 35

5.3 Exposure to Particulate Matter in Fire Stations: Preliminary Results 36

5.4 A Numerical Model for Pollen Prediction: Thunderstorm Asthma Case Study 37

6. PM MONITORING AND MODELLING I 39

6.1 Introduction to Transboundary Particulate Matter in Europe 40

6.2 SAMIRA-Satellite Based Monitoring Initiative for Regional Air Quality – Lessons Learned and Plans 41
6.3 Chemical Composition of PM particles Inside the Laboratory and in the Ambient Air Near the Copper Smelter in Bor, Serbia 42
6.4 Planning and Conducting Mobile Aerosol Monitoring Campaign: Experiences from Belgrade and Novi Sad 43
6.5 Assessment of Detected In Situ and Modelled PM Concentration Levels During Urban Transformation Processes in Novi Sad, Serbia 44
7. PM MONITORING AND MODELLING II 45
7.1 Accounting for Spatiotemporal Information Improves the Imputation of Missing PM2.5 Monitoring Records 46
7.2 A Method for Tracing the Sources of AirBorne Dust Using Source-Simulation and Multivariate PLS Modelling of Chemical Analytical Data 47
7.3 Seasonal Variation in Ambient PM10 Concentrations Over the Novi Sad Aglomeration 48
7.4 An Overview of Monitoring and Research of Atmospheric Particulate Matter in Serbia in the Past Half Decade 49
8. OXIDATIVE STRESS 51
8.1 Real-time Reactive Oxygen Species Measurements in Chinese Cities 52
8.2 Source Apportionment of Oxidative Potential – What We Know So Far 53
8.3 A Study on Tropospheric Aerosols Change During the COVID-19 Lock-down Period: Experience From EARLINET Measurement Campaign 54
8.4 Comparative Statistical Analysis of Particulate Matter Pollution and Traffic Intensity on a Selected Location in the City of Novi Sad 55
9. AEROSOL CHARACTERIZATION I 57
9.1 Measuring Aerosol Absorption – The Advantage of Direct Over Other Methods, and Multi-Wavelength Calibration 58
9.2 Apportionment of Primary and Secondary Carbonaceous Aerosols Using an Advanced Total Carbon – Black Carbon (TC-$BC_{7\text{-}\lambda}$) Method 59
9.3 Variation of Black Carbon Concentration in Cold and Warm Seasons in Skopje Urban Area 60
10. AEROSOL CHARACTERIZATION II 61
10.1 Secondary Organic Aerosol Formation From Direct Photolysis and OH Radical Reaction of Nitroaromatics 62
10.2 Emerging Pollutants in Atmospheric Aerosols in Latvia: Present Situation Overview 63
10.3 Chemical Composition and Source Apportionment of PM2.5 at a Suburban Site in the Northwestern Part of Turkey 64
10.4 Key Factors Governing Particulate Matter Environmental Fate in an Urban Environment 65
10.5 Harmonization of UFP Measurements: A Novel Solution for Microphysical Characterization of Aerosols 66
11. POSTER SESSION 67
11.1 Effects of Biomass Fuel Smoke on Maternal Health and Pregnancy Outcomes 68

5.4 A NUMERICAL MODEL FOR POLLEN PREDICTION: THUNDERSTORM ASTHMA CASE STUDY

S. Ničković (1,2), L. Ilić(1), S. Petković (2), G. Pejanović (2), A. Huete (3), Z. Mijić (1)
(1) Institute of Physics Belgrade, University of Belgrade, Belgrade, Serbia, (2) Republic Hydrometeorological Service of Serbia, Belgrade, Serbia, (3) School of Life Sciences, University of Technology Sydney, Sydney,NSW Australia, zoran.mijic@ipb.ac.rs

More than 300 million people worldwide have asthma - resulting, at the global scale, in approximately 180,000 deaths annually (To et al., 2012). Approximately 50% of adults and 90% of children with asthma had an allergic form of the disease (Palomares et al., 2017). The allergy occurrence is often caused by pollen, representing one of the major healthcare problems. The strongest risk factors for developing asthma are inhaled particles; pollen grains emitted by trees, grasses, and ragweed are among the most commonly present particles. The pollen dispersion process starts with the pollen emission which depends on plant phenology and on near-surface atmospheric conditions. Emitted pollen is dispersed by vertical air mixing and by free-atmospheric horizontal transport. In the final phase of the pollen atmospheric process, pollen grains settle down to the Earth's surface by wet and by dry deposition (due to gravity and near-surface turbulence). In order to predict the atmospheric pollen process, several pollen models have been developed over the last decade (e.g., Siljamo et al., 2013; Luvall et al., 2013). The prediction of extreme pollen episodes generated by thunderstorm processes is of particular interest. Thunderstorm-caused asthma, usually called "thunderstorm asthma" (TA) is a striking event in which patients could experience life-threatening asthma attacks caused by extreme numbers of pollen grains. If a thunderstorm occurs during a pollen season, favourable conditions for intense pollen uptake and transport are fulfilled. In the TA Melbourne case occurred on November 21st 2016, high near-surface concentrations of grass pollen caused instant allergic reactions in predisposed persons. As a result, within 30 hours there was a 672% increase in visits to emergency services due to respiratory difficulties, and a 992% increase of asthma-related hospital admissions compared with the occurrences in previous 3 years (Thien et al., 2018). In this study, the capacity of the PREAM (Pollen Regional Atmospheric Model) model to predict excessive TA events is examined. PREAM is a version of the DREAM regional dust aerosol atmospheric model (Ničković et al., 2001) modified in our study to predict pollen dispersion. In our study we implemented a regional Euler-type pollen prediction model over the Australian state of Victoria in order to explore its capability to predict the Melbourne pollen event. We set up the model with a horizontal resolution below 10km, sufficiently fine to confidently resolve pollen sources and to adequately represent atmospheric features essential for pollen storm generation (such as non-hydrostatic and convection processes). Furthermore, we introduced an advanced pollen emission scheme which takes into account different near-surface turbulence conditions. The model simulation covering the period 16-22 November 2016 was verified against available pollen counts observed at a Melbourne site. The model correctly identified the increased pollen concentrations from the weaker observed peak on 16th November. The extreme pollen concentrations on the 21st November, which triggered the epidemic asthma, was quite well represented by the model, in terms of both timing and location, thus demonstrating its high potential to successfully simulate extreme pollen events.

REFERENCES

Luvall, J. C., NASA/MSFC, Huntsville, AL; and W. A. Sprigg, E. Levetin, A. Huete, S. Ničković, et.al., 2013. Use of MODIS Satellite Data to Evaluate Juniperus spp. Pollen Phenology to Support a Pollen Dispersal Model, PREAM, to Support Public Health Allergy Alerts Earth Observation Systems and Applications for Public Health Models and Decisions, 93rd American Meteorological Society Annual Meeting January 05 – 10.

Palomares Ó, Sánchez-Ramón S, Dávila I, Prieto L, Pérez de Llano L, Lleonart M, et al. 2017. dIvergEnt: How IgE Axis Contributes to the Continuum of Allergic Asthma and Anti-IgE Therapies, International Journal of Molecular Sciences 18(6):E1328.

Ničković, S., Kallos, G., Papadopoulos, A., Kakaliagou, O., 2001. A model for prediction of desert dust cycle in the atmosphere. Journal of Geophysical Research 106, 18113-18130.

Siljamo, P., Sofiev, M., Filatova, E., Grewling, L., Jager, S., Khoreva, E., et al. 2013. A numerical model of birch pollen emission and dispersion in the atmosphere Model evaluation and sensitivity analysis, International Journal of Biometeorology 57, 125-136.

Thien, F., Beggs, P. J, Csutoros, D., Darvall, J., Hew, M., et al. 2018. The Melbourne epidemic thunderstorm asthma event 2016: an investigation of environmental triggers, effect on health services, and patient risk factors, Lancet Planet Health 2, e255–263.

To, T., Stanojevic, S., Moores, G., Gershon, A.S., Bateman, E.D., Cruz, A.A., Boulet, L., 2012. Global asthma prevalence in adults: findings from the cross-sectional world health survey, BMC Public Health. 12:204.

8.3 A STUDY ON TROPOSPHERIC AEROSOLS CHANGE DURING THE COVID-19 LOCK-DOWN PERIOD: EXPERIENCE FROM EARLINET MEASUREMENT CAMPAIGN

Z. Mijić, M. Kuzmanoski, L. Ilić
Institute of Physics Belgrade, University of Belgrade, Belgrade, Serbia
zoran.mijic@ipb.ac.rs

To slow down the rate of spread of corona virus, most of the countries in Europe have followed partial-to-complete lockdown measures in 2020. The lockdown period provided a unique opportunity to examine the effects of reduced anthropogenic activities on changes in the atmospheric environment. Aerosol lidars with their high temporal and vertical resolution, provide reliable information on the atmospheric structure, its dynamics, and its optical properties. The European Aerosol Research Lidar Network, EARLINET, was established in 2000 as a research project with the goal of creating a quantitative, comprehensive, and statistically significant database for the horizontal, vertical, and temporal distribution of aerosols on a continental scale (Pappalardo et al., 2014). EARLINET is part of ACTRIS (Aerosols, Clouds and Trace gases Research Infrastructure) a pan-European initiative consolidating actions among European partners producing high-quality observations of aerosols, clouds and trace gases.

As a part of the ACTRIS initiative for studying the changes in the atmosphere during the COVID-19 lockdown period in May 2020 a dedicated EARLINET measurement campaign was organized in order to: monitor the atmosphere's structure during the lockdown and early relaxation period in Europe, and to identify possible changes due to decreased emissions by comparison to the aerosol climatology in Europe. During the campaign the near-real-time (NRT) operation of the EARLINET was demonstrated following previous experience from the EUNADICS-AV exercise (Papagiannopoulos et al., 2020). The Belgrade lidar station (Ilić et al., 2018) participated in the campaign together with 21 EARLINET stations providing vertical aerosol profiles twice per day (minimum two hours measurements at noon, and minimum two hours after sunset). The measurements were submitted and processed by the Single Calculus Chain (SCC) in the near-real-time. The SCC is a tool for the automatic analysis of aerosol lidar measurements developed within EARLINET network (D'Amico et al., 2015, D'Amico et al., 2016). The main aim of SCC is to provide a data processing chain that allows all EARLINET stations to retrieve, in a fully automatic way, the aerosol backscatter and extinction profiles (measures of the aerosol load) together with other aerosol products. This first analysis was based on the data processed by the SCC and directly published on the THREDDS server in NRT. The preliminary analysis made on aerosol lidar data shows that by simply comparing the observed backscatter values with the climatological values from 2000-2015 is not sufficient to extract a clear conclusion on how much the COVID-19 lock-down has impacted the aerosols in the atmosphere, but a certain effect for low troposphere can be seen. Beyond the scientific goals of this campaign, the actions organized by EARLINET/ACTRIS (NRT delivery of the data and fast analysis of the data products) proved that aerosol lidars are useful for providing information not only for climatological purposes, but also in emergency situations. A more quantitative analysis based on re-analyzing additional data products will be made to consolidate the conclusions.

REFERENCES

Pappalardo, G., Amodeo, A., Apituley, A., Comeron, A., Freudenthaler, V., Linné, H., Ansmann, A., Bösenberg, J., D'Amico, G., Mattis, I., Mona, L., Wandinger, U., Amiridis, V., Alados-Arboledas, L., Nicolae, D., and Wiegner, M., 2014. EARLINET: towards an advanced sustainable European aerosol lidar network, Atmospheric Measurement Techniques 7, 2389–2409.

D'Amico, G., Amodeo, A., Baars, H., Binietoglou, I., Freudenthaler, V., Mattis, I., Wandinger, U., and Pappalardo, G., 2015. EARLINET Single Calculus Chain – overview on methodology and strategy, Atmospheric Measurement Techniques 8, 4891-4916.

D'Amico, G., Amodeo, A., Mattis, I., Freudenthaler, V., and Pappalardo, G., 2016. EARLINET Single Calculus Chaintechnical– Part 1: Pre-processing of raw lidar data, Atmospheric Measurement Techniques 9, 491-507.

Ilić, L., KuzmanoskiM., KolaržP., NinaA., SrećkovićV., MijićZ., BajčetićJ., AndrićM., 2018. Changes of atmospheric properties over Belgrade, observed using remote sensing and in situ methods during the partial solar eclipse of 20 March 2015,Journal of Atmospheric and Solar-Terrestrial Physics171,250-259.

Papagiannopoulos, N., D'Amico, G., Gialitaki, A., Ajtai, N., Alados-Arboledas, L., Amodeo, A., Amiridis, V., Baars, H. et al., 2020. An EARLINET early warning system for atmospheric aerosol aviation hazards, Atmospheric Chemistry and Physics 20, 10775–10789.

CIP - Каталогизација у публикацији
Народна библиотека Србије, Београд

WeBIOPATR

Integrations of satellite and ground-based observations and multi-disciplinarity in research and prediction of different types of hazards in Solar system

May 10-13, 2019, Petnica Science Center, Valjevo, Serbia

BOOK OF ABSTRACTS

Edited by Aleksandra Nina, Milan Radovanović and Vladimir A. Srećković

europlanet NA1 – Innovation Through Science Networking
Task 2 – Scientific Working Groups

Geographical Institute "Jovan Cvijić" SERBIAN ACADEMY OF SCIENCES AND ARTS

Venue: Petnica Science Center, Valjevo, Serbia

Organizers: Europlanet 2020 RI NA1 – Innovation through Science Networking and Geographical Institute "Jovan Cvijić" of Serbian Academy of Sciences and Arts

Published by: Geographical Institute "Jovan Cvijić" of Serbian Academy of Sciences and Arts, 2019

The publication of this issue is financially supported by the Ministry for Education, Science and Technological Development of Serbia

Picture on the first cover: Aleksandra Nina

ISBN 978-86-80029-77-1

Printed by: Skripta Internacional, Mike Alasa 54, Beograd
Number of copies: 50

CONTENTS

Abstracts of Invited Lectures

Darko Jevremović
SOLAR SYSTEM OBJECTS IN THE LSS ERA (ASSESSING THE HAZARDS) 9–9

Pál Gábor Vizi, Péter Szutor, Szaniszló Bérczi, Szilárd Csizmadia, Tibor Hegedűs
TRAJECTORY AND ANALYSIS OF LOCAL FIREBALL-METEORITE EVENTS AND EXTENDED METEOR HUNTING WITH SMARTPHONES AS 'SKY EVENT' CAMERAS 10–12

Sergey Pulinets, Dimitar Ouzounov
INTEGRATION OF SATELLITE AND GROUND-BASED OBSERVATIONS AND MULTI-DISCIPLINARITY IN EARTHQUAKE AND VOLCANO ERUPTION FORECAST BASED ON THE LAIC PHYSICAL MODEL 13–14

Pier Francesco Biagi
THE INFREP VLF/LF RADIO NETWORK FOR STUDYING EARTHQUAKE PRECURSORS: PRESENT SITUATION AND RECENT RESULTS 15–16

Konstantinos Kourtidis, Veronika Barta, Jozsef Bor, Evgeny Mareev, Christina Oikonomou, Colin Price, Sergey Pulinets
WORK WITHIN THE COST ACTION ELECTRONET ON THE COUPLING OF THE ATMOSPHERIC ELECTRIC CIRCUIT TO EARTHQUAKES, LIGHTNING AND THE SUN-EARTH ENVIRONMENT 17–17

Giovanni Nico, Weike Feng, Olimpia Masci, Motoyuki Sato, Luciano Garramone
RADAR INTERFEROMETRY AS A NEW TOOL FOR EARTHQUAKE GEOTECHNICAL ENGINEERING 18–19

Nikola Veselinović, Mihailo Savić, Aleksandar Dragić, Dimitrije Maletić, Dejan Joković, Radomir Banjanac, Vladimir Udovičić, David Knežević
CORRELATION OF SOLAR WIND PARAMETERS WITH COSMIC RAYS OBSERVED WITH GROUND STATION 20–20

Dejan Vinković, Maria Gritsevich
THE CHALLENGES OF HYPERVELOCITY MICROPHYSICS RESEARCH IN METEOROID IMPACTS INTO THE ATMOSPHERE 21–22

Slavica Malinović-Milićević, Zoran Mijatović, Ilija Arsenić, Zorica Podrašćanin, Ana Firanj Sremac, Milan Radovanović, Nusret Drešković
THE IMPORTANCE OF GROUND-BASED AND SATELLITE OBSERVATIONS FOR MONITORING AND ESTIMATION OF UV RADIATION IN NOVI SAD, SERBIA 23–23

Yaroslav Vyklyuk, Milan Radovanović, Slavica Malinović-Milićević
DEEP LEARNING LSTM RECURRENT NEURAL NETWORK FOR CONSEQUENCE FORECASTING OF THE SOLAR WIND DISTURBANCE 24–25

Milan S. Dimitrijević
MILUTIN MILANKOVIĆ AND CLIMATE CHANGES LEADING TO ICE AGES 26–27

Aleksandar Valjarević, Nikola Bačević, Marko Ivanović
DIGITAL AND NUMERICAL METHODS IN ESTIMATION OF A HAZARD FLOODS IN THE MUNICIPALITY OF OBRENOVAC 28–28

Abstracts of Progress Reports

Aleksandra Nina, Giovanni Nico, Luka Č. Popović, Vladimir M. Čadež, Milan Radovanović
NATURAL DISASTERS AND LOW IONOSPHERIC DISTURBANCES DETECTED BY BELGRADE VLF/LF RECEIVER STATION 31–32

Sergey Pulinets
THE ROLE OF GALACTIC COSMIC RAYS IN DYNAMICS OF HURRICANES AND TYPHOONS AND GLOBAL CHANGE 33–34

Bozhidar Srebrov, Ognyan Kounchev, Georgi Simeonov
ANALYSIS OF BIG DATA IN GEOMAGNETISM VIA WAVELET ANALYSIS 35–35

Nataša Todorović
DYNAMICAL ORIGIN OF TWO POTENTIALLY HAZARDOUS ASTEROIDS 36–36

Andjelka B. Kovačević

PLANETARY ATMOSPHERES EROSION DUE TO Sgr A AND (z<0.5) ACTIVE GALACTIC NUCLEI RADIATION 37–37

Dušan Marčeta, Bojan Novaković

STARDUST-RELOADED: THE ASTEROID AND SPACE DEBRIS NETWORK 38–38

Abstracts of Posters

Veljko Vujčić, Darko Jevremović

NEO DETECTION USING COMPLEX EVENT PROCESSING 41–41

Aleksandra Kolarski

ATMOSPHERIC DISTURBANCES DUE TO SEVERE STORMY WEATHER 42–42

Jelena Petrović, Snežana Dragović

RADON AS POTENTIAL EARTHQUAKE PRECURSOR 43–44

Predrag Jovanović, Duško Borka, Vesna Borka Jovanović

CONSTRAINING YUKAWA GRAVITY FROM PLANETARY MOTION IN THE SOLAR SYSTEM 45–46

Bratislav P. Marinković, Stefan Ivanović, Nebojša Uskoković, Milutin Nešić

ELECTRON-IMPACT CROSS SECTIONS FOR THOLINS: COVERAGE WITHIN BEAMDB DATABASE 47–48

Milan Radovanović, Aleksandra Nina, Vladimir A. Srećković

EXTREME SOLAR RADIATION AND NATURAL DISASTERS: CROSS DISCIPLINARY APPROACHES 49–49

Vladimir A. Srećković

SOLAR ACTIVITY, NATURAL HAZARDS, LOW IONOSPHERIC PERTURBATIONS AND SATELLITE AND GROUND-BASED OBSERVATIONS 50–50

Zoran Mijić, Mirjana Perišić

COMPARISON OF MODIS AEROSOL OBSERVATIONS AND GROUND-BASED PM MEASUREMENT FOR THE BELGRADE REGION 51–52

Integrations of satellite and ground-based observations and multi-disciplinarity in research and prediction of different types of hazards in Solar system
Petnica Science Center, Valjevo, Serbia, May 10-13, 2019
Book of Abstracts, Eds. Aleksandra Nina, Milan Radovanović and Vladimir A. Srećković

Poster

COMPARISON OF MODIS AEROSOL OBSERVATIONS AND GROUND-BASED PM MEASUREMENT FOR THE BELGRADE REGION

Zoran Mijić[1], *Mirjana Perišić*[1]

[1] Institute of Physics Belgrade, University of Belgrade, Serbia;
e-mail: zoran.mijic@ipb.ac.rs, mirjana.perisic@ipb.ac.rs

Suspended particulate matter in the atmosphere, commonly known as atmospheric aerosol, plays one of the most important role in climate changes and environmental issues. Numerous epidemiological studies in recent years have shown detrimental effects of aerosol pollution on human health, causing respiratory and cardiovascular disease and even premature death (Kim, Oh, Park, & Cheong, 2018). Additionally, scattering and absorption of solar and terrestrial radiation as direct, and modification of cloud condensation nuclei through aerosol-cloud interaction as indirect effects of aerosols, make the largest contribution to the total uncertainty of the radiative forcing (Intergovernmental Panel on Climate Change, 2007).

Assessment of air quality primarily relies on ground-based measurements of the concentrations of airborne particulate matter (PM) with aerodynamic diameter less than 10 μm (PM_{10}) and 2.5 μm ($PM_{2.5}$), and for this purpose, all European countries were established regulatory monitoring networks. Because this kind of observation provides limited spatial PM information, various studies have been conducted to obtain PM estimates from satellite measurements (Kumar, Chu, & Foster, 2007; Li, Carlson, & Lacis, 2015). Aerosol optical depth (AOD) is one of the most important aerosol product retrieved from satellite measurements, and represent the attenuation of solar radiation caused by aerosols. The relationship between AOD (integration of the aerosol extinction coefficient from the Earth's surface to the top of the atmosphere) and surface PM concentrations depends on various factors: aerosol type and its chemical composition, vertical distribution, spatial and temporal variability - all governed by emissions and meteorological conditions (Kong, Xin, Zhang, & Wang, 2016; Sayer, Hsu, Bettenhausen, & Jeong, 2013).

In this study, we investigated the relationship between AOD and, $PM_{2.5}$ and PM_{10} concentrations data set from the Belgrade region. We obtained Level 2 AOD data at 0.55 μm based on measurements by Moderate Resolution Imaging Spectroradiometer (MODIS) aboard *Terra* (MOD04) and *Aqua (*MYD04) platforms with the resolution of 10x10 km^2 for three years period 2012-2014. Hourly average $PM_{2.5}$ and PM_{10} mass concentrations for the investigating period were obtained from urban and suburban monitoring stations of the Institute of Public Health Belgrade. The analyses included the impact of ambient relative humidity (RH) on PM concentration due to the hygroscopic growth of aerosol particles, as well as vertical correction of AOD with respect to the mixing layer height (MLH). The preliminary results showed that AOD retrieved from satellite sensor can be considered as a good proxy for ground observed PM mass concentrations. It is found that the relationship between AOD and PM is practically linear and strongly influenced by RH and MLH. The increase in the correlation coefficient (of around 20%) is indicative for vertical corrected AOD parameter and dry PM. Further investigation should examined influences of the other

meteorological parameters, different season and types of monitoring stations at the examined PM-AOD relationship. Also, the study based on the analyses of satellite aerosol products and ground-based measured pollutants concentrations may be used for air quality assessment and PM prediction in the region of the City of Belgrade.

Acknowledgments

This paper was realized as a part of the projects III43007 and III41011 financed by the Ministry of Education and Science of the Republic of Serbia within the framework of integrated and interdisciplinary research for the period 2011-2019. The MODIS data were obtained from NASA Atmosphere Archive and Distribution System (LAADS) at the Goddard Space Flight Center (GSFC) and we would like to thanks MODIS team for developing the AOD product.

References

Intergovernmental Panel on Climate Change. (2007). Climate Change 2007: The Physical Science Basis. Contribution of Working Group I to the Fourth Assessment Report of the Intergovernmental Panel on Climate Change. Cambridge, UK; New York, NY: Cambridge University Press.

Kim, J.-H., Oh, I.-H., Park, J.-H., & Cheong, H.-K. (2018). Premature Deaths Attributable to Long-term Exposure to Ambient Fine Particulate Matter in the Republic of Korea. *Journal of Korean Medical Science, 33*(37). https://doi.org/10.3346/jkms.2018.33.e251

Kumar, N., Chu, A., & Foster, A. (2007). An empirical relationship between PM2. 5 and aerosol optical depth in Delhi Metropolitan. *Atmospheric Environment, 41*(21), 4492–4503. https://doi.org/10.1016/j.atmosenv.2007.01.046

Li, J., Carlson, B. E., & Lacis, A. A. (2015). How well do satellite AOD observations represent the spatial and temporal variability of PM2. 5 concentration for the United States? *Atmospheric Environment, 102*, 260–273. https://doi.org/10.1016/j.atmosenv.2014.12.010

Kong, L., Xin, J., Zhang, W., & Wang, Y. (2016). The empirical correlations between PM2. 5, PM10 and AOD in the Beijing metropolitan region and the PM2. 5, PM10 distributions retrieved by MODIS. *Environmental pollution, 216*, 350–360. https://doi.org/10.1016/j.envpol.2016.05.085

Sayer, A. M., Hsu, N. C., Bettenhausen, C., & Jeong, M. J. (2013). Validation and uncertainty estimates for MODIS Collection 6 "Deep Blue" aerosol data. *Journal of Geophysical Research: Atmospheres, 118*(14), 7864–7872. https://doi.org/10.1002/jgrd.50600

PROGRAMME

Friday, May 10

13:00 - 15:00 **Arrival, registration and lunch**

Chairs: Aleksandra Nina and Milan Radovanović
15:30 – 15:45 **Opening ceremony**

Chair: Sergey Pulinets
15:45 – 16:30 **Darko Jevremović:** *SOLAR SYSTEM OBJECTS IN THE LSST ERA (ASSESSING THE HAZARDS)*
16:30 – 17:00 **Pál Gábor Vizi, Péter Szutor, Szaniszló Bérczi, Szilárd Csizmadia, Tibor Hegedűs:** *TRAJECTORY AND ANALYSIS OF LOCAL FIREBALL-METEORITE EVENTS AND EXTENDED METEOR HUNTING WITH SMARTPHONES AS 'SKY EVENT' CAMERAS*

18:00 – 19:30 **Welcome cocktail**
20:00 – Dinner time

Saturday, May 11

Chair: Bratislav P. Marinković
9:00 – 9:45 **Sergey Pulinets, Dimitar Ouzounov:** *INTEGRATION OF SATELLITE AND GROUND-BASED OBSERVATIONS AND MULTI-DISCIPLINARITY IN EARTHQUAKE AND VOLCANO ERUPTION FORECAST BASED ON THE LAIC PHYSICAL MODEL*
9:45 – 10:30 **Pier Francesco Biagi:** *THE INFREP VLF/LF RADIO NETWORK: PRESENT SITUATION AND RECENT RESULTS*

10:30 – 11:00 Coffee break

Chair: Pier Francesco Biagi
11:00 – 11:45 **Konstantinos Kourtidis, Veronika Barta, Jozsef Bor, Evgeny Mareev, Christina Oikonomou, Colin Price, Sergey Pulinets:** *WORK WITHIN THE COST ACTION ELECTRONET ON THE COUPLING OF THE ATMOSPHERIC ELECTRIC CIRCUIT TO EARTHQUAKES, LIGHTNING AND THE SUN-EARTH ENVIRONMENT*
11:45 – 12:30 **Aleksandra Nina, Giovanni Nico, Luka Č. Popović, Vladimir M. Čadež, Milan Radovanović:** *NATURAL DISASTERS AND LOW IONOSPHERIC DISTURBANCES DETECTED BY BELGRADE VLF/LF RECEIVER STATION*

Chair: Ognyan Kounchev

12:30 – 14:00 **Discussions – integration of observation methods and models in research of earthquakes and volcanoes**

14:00 – 15:00 Lunch break

Chair: Luka Č. Popović

15:00 – 15:45 **Giovanni Nico, Weike Feng, Olimpia Masci, Motoyuki Sato, Luciano Garramone:** *RADAR INTERFEROMETRY AS A NEW TOOL FOR EARTHQUAKE GEOTECHNICAL ENGINEERING*

15:45 – 16:30 **Nikola Veselinović, Mihailo Savić, Aleksandar Dragić, Dimitrije Maletić, Dejan Joković, Radomir Banjanac, Vladimir Udovičić, David Knežević:** *CORRELATION OF SOLAR WIND PARAMETERS WITH COSMIC RAYS OBSERVED WITH GROUND STATION*

16:30 – 17:00 **Sergey Pulinets:** *THE ROLE OF GALACTIC COSMIC RAYS IN DYNAMICS OF HURRICANES AND TYPHOONS AND GLOBAL CHANGE*

17:00 – 17:30 Coffee break

Chair: Darko Jevremović

17:30 – 18:15 **Dejan Vinković, Maria Gritsevich:** *THE CHALLENGES OF HYPERVELOCITY MICROPHYSICS RESEARCH IN METEOROID IMPACTS INTO THE ATMOSPHERE*

18:15 – 19:00 **Bozhidar Srebrov, Ognyan Kounchev, Georgi Simeonov:** *ANALYSIS OF BIG DATA IN GEOMAGNETISM VIA WAVELET ANALYSIS*

20:00 – **Meeting dinner**

Sunday, May 12

Chair: Konstantinos Kourtidis

9:00 – 9:30 **Slavica Malinović-Milićević, Zoran Mijatović, Ilija Arsenić, Zorica Podrašćanin, Ana Firanj Sremac, Milan Radovanović, Nusret Drešković:** *THE IMPORTANCE OF GROUND-BASED AND SATELLITE OBSERVATIONS FOR MONITORING AND ESTIMATION OF UV RADIATION IN NOVI SAD, SERBIA*

9:30 – 10:00 **Nataša Todorović:** *DYNAMICAL ORIGIN OF TWO POTENTIALLY HAZARDOUS ASTEROIDS*

10:00 – 10:30 Coffee break

Chair: Giovanni Nico

10:30 – 12:00 **Discussions – integration of observation methods and models in research of hurricanes, meteors and climatic changes**

12:00 **Meeting photo**

12:05 – 14:00 **Guided tour of Petnica's vicinity**

14:00 – 15:00 Lunch break

Chair: Milan S. Dimitrijević

15:15 – 16:00 Yaroslav Vyklyuk, **Milan Radovanović, Slavica Malinović-Milićević**: *DEEP LEARNING LSTM RECURRENT NEURAL NETWORK FOR CONSEQUENCE FORECASTING OF THE SOLAR WIND DISTURBANCE*

16:00 – 16:30 **Andjelka B. Kovačević**: *PLANETARY ATMOSPHERES EROSION DUE TO Sgr A AND (z<0.5) ACTIVE GALACTIC NUCLEI RADIATION*

16:30 – 17:00 **Dušan Marčeta, Bojan Novaković:** *STARDUST-RELOADED: THE ASTEROID AND SPACE DEBRIS NETWORK*

17:00 – 17:30 Coffee break

17:30 – 19:00 **Posters**

19:00 – Dinner time

20:30 – **Networking event**

Monday, May 13

Chair: Yaroslav Vyklyuk

9:00 – 9:45 **Milan S. Dimitrijević:** *MILUTIN MILANKOVIĆ AND CLIMATE CHANGES LEADING TO ICE AGES*

9:45 – 10:30 **Aleksandar Valjarević, Nikola Bačević, Marko Ivanović:** *DIGITAL AND NUMERICAL METHODS IN ESTIMATION OF A HAZARD FLOODS IN THE MUNICIPALITY OF OBRENOVAC*

10:30 – 10:45 Closing ceremony

11:15 – Departure

LIST OF POSTERS

P1. Veljko Vujčić, Darko Jevremović: *NEO DETECTION USING COMPLEX EVENT PROCESSING*

P2. Aleksandra Kolarski: *ATMOSPHERIC DISTURBANCES DUE TO SEVERE STORMY WEATHER*

P3. Jelena Petrović, Snežana Dragović: *RADON AS POTENTIAL EARTHQUAKE PRECURSOR*

P4. Predrag Jovanović, Duško Borka, Vesna Borka Jovanović: *CONSTRAINING YUKAWA GRAVITY FROM PLANETARY MOTION IN THE SOLAR SYSTEM*

P5. Bratislav P. Marinković, Stefan Ivanović, Nebojša Uskoković, Milutin Nešić: *ELECTRON-IMPACT CROSS SECTIONS FOR THOLINS: COVERAGE WITHIN BEAMDB DATABASE*

P6. Milan Radovanović, Aleksandra Nina, Vladimir A. Srećković: *EXTREME SOLAR RADIATION AND NATURAL DISASTERS: CROSS DISCIPLINARY APPROACHES*

P7. Vladimir A. Srećković: *SOLAR ACTIVITY, NATURAL HAZARDS, LOW IONOSPHERIC PERTURBATIONS AND SATELLITE AND GROUND-BASED OBSERVATIONS*

P8. Zoran Mijić, Mirjana Perišić: *COMPARISON OF MODIS AEROSOL OBSERVATIONS AND GROUND-BASED PM MEASUREMENT FOR THE BELGRADE REGION*

CIP - Каталогизација у публикацији - Народна библиотека Србије, Београд

523:504.4(048)

INTEGRATIONS of satellite and ground-based observations and multi-disciplinarity in research and prediction of different types of hazards in Solar system (2019 ; Valjevo)
Book of abstracts / Integrations of satellite and ground-based observations and multi-disciplinarity in research and prediction of different types of hazards in Solar system, May 10-13, 2019, Valjevo, Serbia ; edited by Aleksandra Nina, Milan Radovanović, and Vladimir A. Srećković. - Belgrade : Geographical Institute "Jovan Cvijić" SASA, 2019 (Beograd : Skripta Internacional). - 59 str. : ilustr. ; 24 cm

Tiraž 50.

ISBN 978-86-80029-77-1

a) Сунчев систем - Безбедност - Апстракти b) Природне катастрофе - Апстракти
COBISS.SR-ID 275944460

Book of abstracts

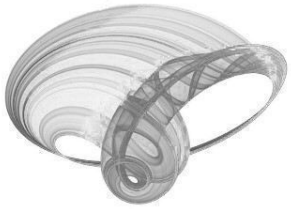

PHOTONICA2017

The Sixth International School and Conference on Photonics

& COST actions: MP1406 and MP1402

&H2020-MSCA-RISE-2015 CARDIALLY workshop

28 August – 1 September 2017

Belgrade, Serbia

Editors

Marina Lekić and Aleksandar Krmpot

Institute of Physics Belgrade, Serbia

Belgrade, 2017

ABSTRACTS OF TUTORIAL, KEYNOTE, INVITED LECTURES, PROGRESS REPORTS AND CONTRIBUTED PAPERS

of

The Sixth International School and Conference on Photonics PHOTONICA2017

28 August – 1 September 2017
Belgrade Serbia

Editors
Marina Lekić and Aleksandar Krmpot

Technical assistance
Marko Nikolić and Danica Pavlović

Publisher
Institute of Physics Belgrade
Pregrevica 118
11080 Belgrade, Serbia

Printed by
Serbian Academy of Sciences and Arts

Number of copies
300

ISBN 978-86-82441-46-5

PHOTONICA 2017 (The Sixth International School and Conference on Photonica - www.photonica.ac.rs) is organized by Institute of Physics Belgrade, University of Belgrade (www.ipb.ac.rs), Serbian Academy of Sciences and Arts (www.sanu.ac.rs), and Optical Society of Serbia (www.ods.org.rs).

Other institution that helped the organization of this event are: Vinča Institute of Nuclear Sciences, University of Belgrade (www.vinca.rs), Faculty of Electrical Engineering, University of Belgrade (www.etf.bg.ac.rs), Institute of Chemistry, Technology and Metallurgy, University of Belgrade (www.ihtm.bg.ac.rs), Faculty of Technical Sciences, University of Novi Sad (www.ftn.uns.ac.rs), Faculty of Physics, University of Belgrade (www.ff.bg.ac.rs), and Faculty of Biology, University of Belgrade (www.bio.bg.ac.rs).

PHOTONICA 2017 is organized under auspices and with support of the Ministry of Education, Science and Technological Development, Serbia (www.mpn.gov.rs). PHOTONICA 2017 is supported and recognized by The Integrated Initiative of European Laser Research Infrastructures LaserLab-Europe (www.laserlab-europe.eu) and European Physical Society (www.eps.org).

The support of the sponsors of PHOTONICA 2017 is gratefully acknowledged:

Committees

Scientific Committee

Aleksandar Krmpot, Serbia
Antun Balaž, Serbia
Arlene D. Wilson-Gordon, Israel
Bojan Resan, Switzerland
Boris Malomed, Israel
Branislav Jelenković, Serbia
Dejan Gvozdić, Serbia
Detlef Kip, Germany
Dragan Indjin, United Kingdom
Edik Rafailov, United Kingdom
Feng Chen, China
Francesco Cataliotti, Italy
Giannis Zacharakis, Greece
Goran Isić, Serbia
Goran Mašanović, United Kingdom
Isabelle Philippa Staude, Germany
Jelena Radovanović, Serbia
Jerker Widengren, Sweden
Jovana Petrović, Serbia
Laurent Sanchez, France
LjupčoHadžievski, Serbia
Marco Santagiustina, Italy
Milan Mashanović, United States of America
Milan Trtica, Serbia
Miloš Živanov, Serbia
Milutin Stepić, Serbia
Milivoj Belić, Qatar
Nikola Stojanović, Germany
Pavle Anđus, Serbia
Peđa Mihailović, Serbia
Radoš Gajić, Serbia
Schaaf Peter, Germany
Sergei Turitsyn, United Kingdom
Suzana Petrović, Serbia
Ticijana Ban, Croatia
Vladana Vukojević, Sweden
Zoran Jakšić, Serbia
Željko Šljivančanin, Serbia

Organizing Committee

Aleksandar Krmpot, (Chair)
Marina Lekić (Secretary)
Stanko Nikolić (webmaster)
Marko Nikolić,
Vladimir Veljić
Danica Pavlović

Technical Organizer

O.M.P.16 Subwavelength nickel-copper multilayers as an alternative plasmonic material……199
Ivana Mladenović, Zoran Jakšić, Marko Obradov, Slobodan Vuković, Goran Isić, Dragan Tanasković, Jelena Lamovec
O.M.P.17 Nontrivial nonradiating all-dielectric anapole sources……200
Nikita A. Nemkov, Ivan V. Stenishchev, Alexey A Basharin
O.M.P.18 Metamaterials with broken symmetry: general approach, experiment and multipolar decomposition……201
Anar K. Ospanova and Alexey A. Basharin
O.M.P.19 Titanium nitride plasmonic resonator Fabry-Perot for Raman lasing on nanoscale……202
A. V. Kharitonov, S. S. Kharintsev and M. Kh. Salakhov
O.M.P.20 Phase and amplitude tunability in planar THz metamaterials with toroidal response……203
Maria V. Cojocari, Kristina Schegoleva, Alexey A. Basharin
O.M.P.21 Laser induced ultrafast switching processes in diamond……204
T. Apostolova and B. Obreshkov
O.M.P.22 Plasmonic Transmission Gratings for biosensors and atomic physics……205
A. Sierant, B. Jany, D. Bartoszek-Bober, J. Fiutowski, J. Adam and T. Kawalec
O.M.P.23 Flat lenses with continuously graded metamaterials designed using transformation optics: anexact analytical solution of field equations……206
M. Dalarsson, R. Mittra and Z. Jakšić

11. Other topics in photonics

O.P.1 Fresnel diffraction of a Laguerre-Gaussian LG(l,n) laser beam by a combination of a fork-shaped grating and an axicon……207
S. Topuzoski
O.P.2 Manipulation of the topological charges of vortices within large optical vortex lattices: Far-field beam reshaping……208
L. Stoyanov, G. Maleshkov, I. Stefanov, A. Dreischuh
O.P.3 Characterization of liquid-phase epitaxy grown thick GaInAs (Sb)N layers……209
V Donchev, I Asenova, M Milanova, D Alonso-Álvarez, K Kirilov, N Shtinkov, I G Ivanov, S Georgiev, E Valcheva and N Ekins-Daukes
O.P.4 Vertical Raman LIDAR profiling of atmospheric aerosol optical propertis over Belgrade……210
Z. Mijić, L. Ilić and M. Kuzmanoski
O.P.5 Planar versus three-dimensional growth of metal nanostructures at 2D heterostructures……211
S. Stavrić, M. Belić, Ž. Šljivančanin
O.P.6 *Ab initio* study of superconducting properties of $NbSe_2$monolayer in the DFPT formalism using Wannier interpolation……212
Tatjana Agatonović Jovinand Radoš Gajić
O.P.7 Characterization of magnetron sputtered transparent hole conducting layers for organic solar cells……213
M. Sendova-Vassileva, R. Gergova, Hr. Dikov, G. Popkirov, V. Gancheva and G. Grancharov
O.P.8 Post-processing synchronization and characterization of generated signals by a repetitive Marx generator……214
A. Redjimi, Z. Nikolić, D. Knežević and D. Vasiljević
O.P.9 Cryogenic slab CO laser with RF discharge pumping: sealed-off plasma chemistry of the active medium……215
A.A. Ionin, I.V. Kochetov, A.Yu. Kozlov, A.K. Kurnosov, A.P. Napartovich, L.V. Seleznev, D.V. Sinitsyn
O.P.10 Organic Nanocrystals for Quantum Nanophotonic Applications……216

Vertical Raman LIDAR profiling of atmosphericaerosol optical properties over Belgrade

Z. Mijić, L. Ilić and M. Kuzmanoski
Institute of Physics,Belgrade, Serbia
e-mail:luka.ilic@ipb.ac.rs

The direct radiative effect due to aerosol–radiation interactions is the change in radiative flux caused by the combined scattering and absorption of radiation by anthropogenic and natural aerosols. Due to their short lifetime and the large variability in space and time atmospheric aerosols are considered one of the major uncertainties in climate forcing and atmospheric processes [1]. For radiative studies it is necessary to measure aerosol optical properties, size, morphology and composition as a function of time and space, with a high resolution in both domains to account for the large variability. Lidar (Light Detection And Ranging), an active remote sensing technique, represents the optimal tool to provide range-resolved aerosol optical parameters. Large observational networks such as the European Aerosol Research Lidar Network (EARLINET) [2], the Aerosol Robotic Network (AERONET), provide the long-term measurement series needed to build a climatology of aerosol optical properties at the continental and global scales.

In order to assess the origin and type of aerosols which travel over Balkan region, having an impact on modification of the regional radiative budget, case studies combining measurements at the EARLINET joining lidar station in Belgrade with atmospheric modeling have been analyzed. For vertical profiling and remote sensing of atmospheric aerosol layers the Raman lidar system at the Institute of Physics Belgrade (44.860 N, 20.390 E) has been used. It is bi-axial system with combined elastic and Raman detection designed to perform continuous measurements of aerosols in the planetary boundary layer and the lower free troposphere. It is based on the third harmonic frequency of a compact, pulsed Nd:YAG laser, emitting pulses of 65 mJ output energy at 355 nm with a 20 Hz repetition rate. The optical receiver is a Cassegrain reflecting telescope with a primary mirror of 250 mm diameter and a focal length of 1250 mm. Photomultiplier tubes are used to detect elastic backscatter lidar signal at 355 nm and Raman signal at 387 nm. The detectors are operated both in the analog and photon-counting mode and the spatial raw resolution of the detected signals is 7.5 m. Averaging time of the lidar profiles is of the order of 1 min corresponding to 1200 laser shots. Lidar measurements can be used in synergy with numerical models in order to validate and compare information about aerosols. In this paper DREAM (Dust Regional Atmospheric Model) model, designed to simulate and/or predict the atmospheric cycle of mineral dust aerosol [3], will be used to analyze dust transport. The capability of the lidar technique to derive range-resolved vertical profiles of aerosol optical parameters (backscatter and extinction coefficient) with very high spatial and temporal resolution will be used to identify the altitude of layers and the temporal evolution of intrusions. Using these altitudes as inputs in air mass trajectory model, the source of aerosols can be identified. The additional techniques (satellite remote sensing) will be also discussed for selected case-studies.

REFERENCES

[1] IPCC: The Physical Science Basis, Contribution of Working Group I to the Fifth Assessment Report of the Intergovernmental Panel on Climate Change, edited by: Stocker, T. F., Qin, D., Plattner, G.-K., Tignor, M., Allen, S. K., Boschung, J., Nauels, A., Xia, Y., Bex, V., and Midgley, P. M., Cambridge University Press, Cambridge, United Kingdom and New York, NY, USA, (2013).

[2] G. Pappalardo, A. Amodeo, A. Apituley, A. Comeron, V. Freudenthaler, H. Linné, A.Ansmann, J. Bösenberg, G. D'Amico, I.Mattis, L. Mona, U. Wandinger, V Amiridis, L. Alados Arboledas, D. Nicolae, and M. Wiegner,: EARLINET: towards an advanced sustainable European aerosol lidar network, Atmos. Meas. Tech. 7, 2389 (2014).

[3] S. Nickovic, G. Kallos, A. Papadopoulos, O. Kakaliagou, J. Geophys. Res. 106, 1813 (2001).

III Meeting on Astrophysical Spectroscopy - A&M DATA

December 6 to 9, 2021, Palić, Serbia

BOOK OF ABSTRACTS AND CONTRIBUTED PAPERS

Edited by Vladimir A. Srećković, Milan S. Dimitrijević and Nikola Cvetanović

A&M DATA

UNIVERSITY OF BELGRADE | INSTITUTE OF PHYSICS | BELGRADE
NATIONAL INSTITUTE OF THE REPUBLIC OF SERBIA

Belgrade 2021

Scientific Committee

Milan S. Dimitrijević, **Co-Chairman**
Vladimir A. Srećković, **Co-Chairman**

Nebil Ben Nessib, Saudi Arabia
Nikolai N. Bezuglov, Russia
Vesna Borka Jovanović, Serbia
Magdalena Christova, Bulgaria
Nikola Cvetanović, Serbia
Rafik Hamdi, Tunisia
Dragana Ilić, Serbia
Darko Jevremović, Serbia
Predrag Jovanović, Serbia
Andjelka Kovačević, Serbia
Jelena Kovačević, Serbia
Evaggelia Lyratzi, Greece
Bratislav Marinković, Serbia
Zoran Mijić, Serbia
Luka Č. Popović, Serbia
Branko Predojević, Republic of Srpska
Sylvie Sahal Bréchot, France
Saša Simić, Serbia

Local Organizing Committee

Vladimir A. Srećković, Institite of Physics, Belgrade, **Chairman**

Jovan Aleksić, Astronomical Observatory, Belgrade
Nikola Cvetanović, Faculty of Transport and Traffic Engineering, Belgrade
Milan S. Dimitrijević, Astronomical Observatory, Belgrade
Aleksandra Kolarski, Institute of Physics, Belgrade
Aleksandra Nina, Institute of Physics, Belgrade
Nikola Veselinović, Institute of Physics, Belgrade
Veljko Vujčić, Astronomical Observatory, Belgrade

Organizers:

Institute of Physics Belgrade, Serbia and
Astronomical Observatory Belgrade, Serbia

Text arrangement by computer: Tanja Milovanov

ISBN 978-86-82441-54-0

Financially supported by the Ministry of Education, Science and Technological Development of Serbia

Production: Skripta Internacional, Mike Alasa 54, Beograd in 50 copies

Lower ionosphere under high-energy events: observations and model parameters

Aleksandra Kolarski [1], Vladimir A. Srećković[2] and Zoran R. Mijić[2]

[1]Technical Faculty Mihajlo Pupin, University of Novi Sad, Đure Đakovića bb, 23000 Zrenjanin, Serbia
E-mail: aleksandra.kolarski@tfzr.rs
[2]Institute of Physics Belgrade, University of Belgrade, PO Box 57, 11000 Belgrade, Serbia
E-mail: vlada@ipb.ac.rs, zoran.mijic@ipb.ac.rs

Analysis of lower ionospheric response and electron density altitude profile variations in lower ionosphere induced by high-energy events during daytime and during nighttime was carried out. Sudden events induced changes in ionosphere and consequently electron density height profile. All data are recorded by BEL radio stations system and the model computation is used to obtain the atmospheric parameters induced by these perturbations. According to perturbed conditions, variation of estimated parameters, sharpness and reflection height differ for analyzed cases. The data and results are useful for Earth observation, telecommunication and other applications in modern society.

References

[1] Šulić, D. M., Srećković, V. A., & Mihajlov, A. A. (2016). A study of VLF signals variations associated with the changes of ionization level in the D-region in consequence of solar conditions. *Advances in Space Research*, 57(4), 1029-1043.

[2] Srećković, V. A., Šulić, D. M., Ignjatović, L., & Vujčić, V. (2021). Low Ionosphere under Influence of Strong Solar Radiation: Diagnostics and Modeling. *Applied Sciences*, *11*(16), 7194.

Demonstration of the EARLINET Capacity to Provide Near Real Time Data

Zoran Mijić

Institute of Physics Belgrade, University of Belgrade, Pregrevica 118, 11080 Belgrade, Serbia

The European Aerosol Research Lidar Network, EARLINET, was established in 2000 with the goal of creating a quantitative, comprehensive, and statistically significant database for the horizontal, vertical, and temporal distribution of aerosols on a continental scale [1]. EARLINET is part of ACTRIS (Aerosols, Clouds and Trace gases Research Infrastructure) a pan-European initiative consolidating actions amongst European partners producing high-quality observations of atmospheric aerosols, clouds and trace gases. Aerosol lidars with their high temporal and vertical resolution, provide reliable information on the atmospheric structure, its dynamics, and its optical properties. The Belgrade lidar station [2] participated in the several campaigns providing vertical aerosol profiles measurements which were submitted and processed by the Single Calculus Chain (SCC) in the near-real time (NRT). The SCC is a tool for the automatic analysis of aerosol lidar measurements developed within EARLINET network [3,4]. The main aim of SCC is to provide a data processing chain that allows all EARLINET stations to retrieve, in a fully automatic way, the aerosol backscatter and extinction profiles together with other aerosol products. Beyond the scientific goals of this campaign, the actions organized by EARLINET/ACTRIS (NRT delivery of the data and fast analysis of the data products) proved that aerosol lidars are useful for providing information not only for climatological purposes, but also in emergency situations [5].

References

[1] Pappalardo, G., Amodeo, A., Apituley, A., Comeron, A., Freudenthaler, V., Linné, H., Ansmann, A., Bösenberg, J., D'Amico, G., Mattis, I., Mona, L., Wandinger, U., Amiridis, V., Alados-Arboledas, L., Nicolae, D., and Wiegner, M., 2014. EARLINET: towards an advanced sustainable European aerosol lidar network, Atmospheric Measurement Techniques 7, 2389–2409.

[2] Ilić, L., Kuzmanoski M., Kolarž P., Nina A., Srećković V., Mijić Z., Bajčetić J., Andrić M., 2018. Changes of atmospheric properties over Belgrade, observed using remote sensing and in situ methods during the partial solar eclipse of 20 March 2015, Journal of Atmospheric and Solar-Terrestrial Physics171,250-259.

[3] D'Amico, G., Amodeo, A., Baars, H., Binietoglou, I., Freudenthaler, V., Mattis, I., Wandinger, U., and Pappalardo, G., 2015. EARLINET Single Calculus Chain – overview on methodology and strategy, Atmospheric Measurement Techniques 8, 4891-4916.

[4] D'Amico, G., Amodeo, A., Mattis, I., Freudenthaler, V., and Pappalardo, G., 2016. EARLINET Single Calculus Chaintechnical– Part 1: Pre-processing of raw lidar data, Atmospheric Measurement Techniques 9, 491-507.

[5] Papagiannopoulos, N., D'Amico, G., Gialitaki, A., Ajtai, N., Alados-Arboledas, L., Amodeo, A., Amiridis, V., Baars, H. et al., 2020. An EARLINET early warning system for atmospheric aerosol aviation hazards, Atmospheric Chemistry and Physics 20, 10775–10789.

Usage of High-Resolution Satellite Products in Atmospheric modeling

Zoran Mijić

Institute of Physics Belgrade, University of Belgrade, Pregrevica 118, 11080 Belgrade, Serbia

Aerosol optical depth (AOD) is one of the most important aerosol products retrieved from satellite measurements, and represent the attenuation of solar radiation caused by aerosols. The direct radiative effect due to aerosol–radiation interactions is the change in radiative flux caused by the combined scattering and absorption of radiation by anthropogenic and natural aerosols. Due to their short lifetime and the large variability in space and time atmospheric aerosols are considered one of the major uncertainties in climate forcing and atmospheric processes [1]. The relationship between AOD (integration of the aerosol extinction coefficient from the Earth's surface to the top of the atmosphere) and surface aerosol concentrations depends on various factors: aerosol type and its chemical composition, vertical distribution, spatial and temporal variability. In this study the potential of Level 2 AOD data at 0.55 μm based on measurements by Moderate Resolution Imaging Spectroradiometer (MODIS) aboard Terra (MOD04) and Aqua (MYD04) platforms for PM modeling will be discussed [2]. In addition, recently lunched ESA Aeolus mission products intended for assimilation in Numerical Weather Prediction (NWP) models in Near-Real-Time together with its optical products will be introduced.

References

[1] IPCC (2007), IPCC Fourth Assessment Report Climate Change 2007 - The Physical Science Basis Contribution of Working Group I to the Fourth Assessment Report of the IPCC

[2] Fu, D., Xia, X., Wang, J. et al. Synergy of AERONET and MODIS AOD products in the estimation of PM2.5 concentrations in Beijing. Sci Rep 8, 10174 (2018).

CIP - Каталогизација у публикацији
Народна библиотека Србије, Београд

52-355.3(048)
533.92:537.228.5(048)
539.184.27(048)

MEETING on Astrophysical Spectroscopy - A&M DATA (3 ; 2021 ; Palić)
Book of abstracts and contributed papers / III Meeting on Astrophysical Spectroscopy - A&M DATA, December 6 to 9, 2021, Palić, Serbia ; edited by Vladimir A. Srećković, Milan S. Dimitrijević and Nikola Cvetanović. - Belgrade : Institute of Physics, 2021 (Beograd : Skripta Internacional). - 56 str. ; 24 cm

Tiraž 50. - Registar.

ISBN 978-86-82441-54-0

a) Астрофизика - Апстракти b) Плазма - Спектрална анализа - Апстракти
c) Штарков ефекат - Апстракти

COBISS.SR-ID 52784137

Publ. Astron. Obs. Belgrade No. 100 (2021), 315 - 321 *Progress Report*

ACTIVITIES OF THE SERBIAN EUROPLANET GROUP WITHIN EUROPLANET SOCIETY

I. MILIĆ ŽITNIK[1], A. NINA[2], V. A. SREĆKOVIĆ[2], B. P. MARINKOVIĆ[2], Z. MIJIĆ[2]
D. ŠEVIĆ[2], M. BUDIŠA[3], D. MARČETA[4], A. KOVAČEVIĆ[4], J. RADOVIĆ[5]
and A. KOLARSKI[6]

[1] *Astronomical Observatory, Volgina 7, 11000 Belgrade, Serbia*
E–mail: ivana@aob.rs

[2] *Institute of Physics Belgrade, University of Belgrade,*
Pregrevica 118, 11080 Belgrade, Serbia

[3] *University of Belgrade School of Electrical Engineering,*
Bulevar kralja Aleksandra 73, 11000 Belgrade, Serbia

[4] *Faculty of Mathematics, University of Belgrade, Studentski Trg 10, 11000 Belgrade, Serbia*

[5] *Department of Atmospheric Physics, Faculty of Mathematics*
and Physics, Charles University, Prague, Czech Republic

[6] *Technical Faculty Mihajlo Pupin, University of Novi Sad, 23000 Zrenjanin, Serbia*

Abstract. Europlanet society connects many different scientific institutions all over the world. The Serbian Europlanet Group (SEG) was established at 2019. It currently has 20 active scientists from 6 institutions working in Serbia in different fields of planetary science as well as related fields. Here are presented activities of SEG in 2020.

1. INTRODUCTION

The European society promotes the European planetary science as well as related fields. Its aims are to support the development of planetary science at a national and regional level, particularly in countries and areas that are currently under–represented within the community, and early career researchers who established their network within the Europlanet: the Europlanet Early Career (EPEC) network ($https://www.europlanet-society.org/early-careers-network/$). The Europlanet consists of 10 Regional Hubs. More information about organization and activities of this society can be found at the website $https://www.europlanet-society.org/$.

Serbia is one of six countries included in the Southeast European Hub that was established in 2019. The Serbian Europlanet Group (SEG) currently consists of 20 members from 6 institutions. Details of members and activities of SEG can be found at the website $https://www.europlanet-society.org/europlanet-society/regional-hubs/southeast-europe/$. In this paper are described main activities and presented scientific research of SEG members related to the Europlanet fields in 2020.

2. CONFERENCES AND WORKSHOPS OF SEG 2020

2. 1. PARTICIPATION IN THE EUROPLANET SCIENCE CONGRESSES

The Europlanet Science Congress (EPSC) is the annual meeting of the Europlanet Society. In the Europlanet Science Congress 2020, seven scientists from Serbia participated with several lectures. It was first virtual EPSC congress attended by 1168 participants from 49 countries. Here, will be mentioned two of SEG participants.

Dušan Marčeta presented research about population of interstellar asteroids and possibility that one of the observational selection effects, known as Holetschek's effect, could be used for preliminary estimation of the size-frequency distribution of this population. Aleksandra Nina presented research on new methodology for earthquake prediction which was partially realized within the Europlanet workshop in Petnica Science Center in 2019.

2. 2. PARTICIPATION IN THE XII SERBIAN–BULGARIAN ASTRONOMICAL CONFERENCE

Serbian scientists organized a Europlanet session with several lectures during the XII Serbian–Bulgarian Astronomical Conference (SBAC 12). SBAC 12 was held in Sokobanja from September 25 to 29, 2020 (Popović et al. 2020). SEG presented its work (Nina et al. 2020a) and discussed with Bulgarian colleagues and with colleagues from Europlanet Southeast HUB countries about expanding of their cooperation.

2. 3. PARTICIPATION IN THE XIX SERBIAN ASTRONOMICAL CONFERENCE

The work of SEG was presented during the XIX Serbian Astronomical Conference (19 SAC), held at the Serbian Academy of Sciences and Arts in Belgrade from October 13 to 17, 2020 (Kovačević et al. 2020). Aleksandra Nina participated with invited lecture about investigation of the lower ionosphere disturbances as possible earthquake precursors and application of research of the lower ionosphere influences in Earth observations by satellite during influence a solar X-ray flare. Ivana Milić Žitnik gave progress report about asteroid's motion with orbital eccentricity in the range (0, 0.2) across the 2-body mean motion resonances with Jupiter with different strengths due to the Yarkovsky effect (Milić Žitnik & Novaković 2016, Milić Žitnik 2020a).

3. RESEARCHES OF SEG MEMBERS AT 2020

SEG members are scientists in different research fields. Here are a few researches that are in the areas of Europlanet.

3. 1. ASTRONOMY

3.1.1. Model of interstellar asteroids and expected predominance of retrograde object among the discovered objects

Dušan Marčeta and Bojan Novaković examined the model of interstellar asteroids and comets and found analytical expressions for the distributions of their orbital elements (Marčeta & Novaković 2020). They payed special attention to objects which could be detectable by future LSST survey. Also, they found that majority of these objects should move along retrograde orbits resulting in asymmetry of the distribution of

their orbital inclinations. Finally, they found that this asymmetry is a result of the Holetschek effect. Since this effect is size-dependant, its influence is stronger for populations with steeper size-frequency distributions since they are comprised of larger number of smaller objects. This fact could be used for preliminary estimation of the size-frequency distribution of the underlying true population of interstellar objects once when sufficient number of objects become discovered.

3.1.2 The relationship between the 'limiting' Yarkovsky drift speed and asteroid families' Yarkovsky V-shape

Ivana Milić Žitnik examined the relationship between asteroid families' V-shapes and the 'limiting' diameters in the $(a, 1/D)$ plane. Following the recently defined 'limiting' value of the Yarkovsky drift speed at 7×10^{-5} au/Myr (Milić Žitnik 2019), she decided to investigate the relation between the asteroid family Yarkovsky V-shape and the 'limiting' Yarkovsky drift speed of asteroid's semi-major axes. She has used the known scaling formula to calculate the Yarkovsky drift speed in order to determine the inner and outer 'limiting' diameters (for the inner and outer V-shape borders) from the 'limiting' Yarkovsky drift speed. The method was applied to 11 asteroid families of different taxonomic classes, origin type and age, located throughout the Main Belt. Her main conclusion was that the 'breakpoints' in changing V-shape of the very old asteroid families, crossed by relatively strong mean motion resonances on both sides very close to the parent body, are exactly the inverse of 'limiting' diameters in the a versus $1/D$ plane. This result uncovers a novel interesting property of asteroid families' Yarkovsky V-shapes (Milić Žitnik 2020b).

3.1.3 Astrobiology-habitability of exoplanets

Balbi, Hami and Kovačević (2020) present a new investigation of the habitability of the Milky Way bulge, that expands previous studies on the Galactic Habitable Zone. This work discusses existing knowledge on the abundance of planets in the bulge, metallicity and the possible frequency of rocky planets, orbital stability and encounters, and the possibility of planets around the central supermassive black hole. Another concern for habitability is the presence of the supermassive black hole in the Galactic center, but also in nearby Active galactic nuclei, that could have resulted in a substantial flux of ionizing radiation during its past active phase, causing increased planetary atmospheric erosion and potentially harmful effects to surface life as shown by Wislocka, Kovačević, Balbi (2019). This work was featured in famous Forbes Magazine in their section Innovavations. Andjelka Kovačević is a member of Working group of habitability of exoplanets of European astrobiology institute.

3. 2. GEOPHYSICS

3.2.1 Atmospheric aerosol remote sensing and modelling

The EARLINET lidar network was established with the goal of creating a quantitative, comprehensive, and statistically significant database for the horizontal, vertical, and temporal distribution of aerosols on a continental scale. Within the network Belgrade lidar station was involved in initiative for studying the changes in the atmosphere's structure, its dynamics, and its optical properties during the COVID-19 lock-down by comparison to the aerosol climatology in Europe. Near real time de-

livery of the data and fast analysis of the data products proved that aerosol lidars are useful for providing information not only for climatological purposes, but also in emergency situations like detecting airborne hazards for aviation (Papagiannopoulos et al. 2020). The preliminary results indicate that the lock-down did not affected the high troposphere, but for the low troposphere a certain effect can be seen. In addition, ongoing activities are related to the participation in ESA ADM-Aeolus mission (the first high-spectral resolution lidar in space) Cal/Val activity through validation of L2A products of aerosol profiles and studying the relationship between satellite AOD measurements and ground PM concentrations (Mijić & Perišić 2019).

3.2.2 Lower ionosphere

The lower ionosphere research was a continuation of research related to a possible new type of earthquake precursor in the form of signal noise amplitude reduction (Nina et al. 2020b) and examinations of the effects of the D-region which is disturbed by a solar X-ray flare on satellite signals (Nina et al. 2020c). Also, a new model for determining ionospheric parameters in the unperturbed D-region was developed.

3.2.3 Investigation of a possible lithosphere-ionosphere coupling through seismo-ionospheric effect

Possible relationship between amplitude and phase delay characteristics of the NWC/19.8 kHz signal transmitted from H. E. Holt in Australia (φ = 21.8° S, Λ = 114.16° E) towards Belgrade AbsPAL receiver (φ = 44.85° N, Λ = 20.38° E) in Serbia and seismic activity reported by Helmholtz-Zentrum Potsdam - Deutsches GeoForschungsZentrum GFZ in period from December 2005 to June 2007 was investigated with the main result presented in Kolarski and Komatina (2020).

3.2.4 Satellite radar technique for atmospheric water vapor measurement and modelling effects of the ionospheric disturbances

Satellite observation and measurements performed by the Synthetic Aperture Radar (SAR) and the Interferometric Synthetic Aperture Radar (InSAR) technique can be used for acquiring more information about the water vapor present within the atmosphere. The methodology of the SAR instrument and the InSAR technique is described in Radović (2020). Additionally, the focus is set on the four different satellites with SAR instruments working on different frequencies. Apart from that, in Radović (2020) is presented how neglecting the ionospheric perturbations which took place during the satellite measurements can influence modelling of the water vapor parameters derived from such measurements acquired by the SAR instruments carried by the mentioned satellites.

3. 3. ASTROPHYSICS

3.3.1. Atomic Molecular and Optical Physics group of researchers at the Laboratory for Atomic Collision Processes

LACP[1], Institute of Physics Belgrade, University of Belgrade, has been studying several collisional processes that involve electron scattering by atomic particles (e.g. for

[1] *http : //mail.ipb.ac.rs/ centar3/acp.html*

helium Jureta et al. (2014)) and laser interactions with gases (Rabasović et al. 2019), nanopowders (Šević et al. 2020a,b) and single crystal phosphors (Šević et al. 2021). Electron impact cross sections are relevant parameters in modelling of processes that occur in cometary coma (Marinković et al. 2017), collisional processes in AGNs (Dimitrijević et al. 2021) or Earth' s and other planets' atmospheres (Vukalović et al. 2021). Due to the immense importance of having full survey and accurate data of electron cross sections, there are several databases that maintain large sets of electron collisional data and even more, a unique portal for accessing such kind of data have been created through European framework programs (for a recent update of the Virtual Atomic and Molecular Data Centre[2] – VAMDC see e.g. Albert et al. (2020)).

BeamDB (Belgrade electron-atom/molecule DataBase[3]) is a collisional database that is maintained by the researchers of the LACP and it covers interactions of electrons with atoms and molecules in the form of differential (DCS) and integral cross sections for the processes such as elastic scattering, excitation and ionization (Jevremović et al. 2020). At present the output files that come from the search of BeamDB are present in the xml format of specific syntax developed by the International Atomic Energy Agency (IAEA)[4]. These so called "xsams" files contain full record of data sets including bibliographical entities, but the process of extracting values of cross sections is hard for researchers. That is why this group started to develop a converter which will convert xsams file into textual format file with simple columns that list values of impact energy, scattering angle, DSC and corresponding uncertainty. The next step would be adding a graphical presentation to the webpage of the BeamDB database. The graphics should present logarithm of DCS data points with error bars associated to the uncertainty versus impact energy and scattering angle in 3D graph.

Exploiting the fact that BeamDB contains large sets of DCS values obtained both experimentally and theoretically, they are in the process of developing machine learning algorithms for determining extrapolated DCS in the regions which are not accessed by experiments (Ivanović et al. 2020). The primary goal is to determine extrapolated values toward zero scattering angle as well as to large angles, usually from 150° to 180°.

It is envisaged that the BeamDB will contain electron spectroscopy data as well, beside the cross section data. At present, there is only a single threshold photoelectron spectrum of argon curated in the BeamDB, but the plans are to add energy loss spectra, presumably obtained in the LACP. This would allow them to develop tools for spectral classification and particular spectra identification based on data-mining methods. An overview of various data mining methods has been recently presented by Yang et al. (2020).

3.3.2. A&M data for stellar atmosphere modelling

Work on topics of modelling various astrophysical and laboratory plasma which are of interest for Europlanet community is continued. A&M datasets e.g. rate coefficients, Stark broadening parameters, line profiles, etc. are published during this year (see

[2] $https://portal.vamdc.eu/vamdc_portal/$
[3] $http://servo.aob.rs/emol$
[4] $https://www-amdis.iaea.org/xsams/documents/$

some of the papers: Srećković et al. 2020; Majlinger et al. 2020; Dimitrijević et al. 2020). Part of the data are hosted on SerVO at AOB[5].

4. CONCLUSION AND FURTHER WORK

In this paper are presented activities of Serbian scientists within Europlanet society. In the first part of the paper, are described briefly conferences that occurred in 2020 which promoted work of Serbian Europlanet Group. In the second part are presented several studies of SEG important for the Europlanet research fields. Serbian scientists plan to continue work within Europlanet society in the following years and to promote the Europlanet and SEG activities, as well as to expand SEG.

Acknowledgments

This research is supported by the Europlanet. The authors acknowledge funding provided by the Institute of Physics Belgrade, Astronomical Observatory (the contract 451-03-68/2020-14/200002), Faculty of Mathematics University of Belgrade (the contract 451-03-68/2020-14/200104) through the grants by the Ministry of Education, Science, and Technological Development of the Republic of Serbia.

References

Albert, D., Antony, B. K., Ba, Y. A. et al.: 2020, *Atoms*, **8(4)**, 76.
Balbi, A., Hami, M., Kovačević, A.: 2020, *Life*, **10(8)**, 132.
Dimitrijević, M. S., Srećković, V. A., Zalam, A. A., Miculis, K., Efimov, D. K., Bezuglov, N. N., Klyucharev, A. N.: 2020, *Contrib. Astron. Obs. Skaln. Pleso*, **50(1)**, 66.
Dimitrijević, M. S., Srecković, V. A., Ignjatović, Lj. M., Marinković, B. P.: 2021, *New Astronomy*, **84**, 101529.
Ivanović, S., Uskoković, N., Marinković, B. P., Mason, N. J.: 2020, *Publ. Astron. Obs. Belgrade*, **99**, 43.
Jevremović, D., Srećković, V. A., Marinković, B. P., Vujičić, V.: 2020, *Contrib. Astron. Obs. Skalnaté Pleso*, **50(1)**, 44.
Jureta, J. J., Milosavljević, A. R., Marinković, B. P.: 2014, *Int. J. Mass Spectrom.*, **365-366**, 114.
Kolarski, A., Komatina, S.: 2020, *Book of Abstracts*, International Symposium GEOSCIENCE 2020, November 20 - 22 2020, Bucharest, Romania, 81.
Kovačević, A., Kovačević Dojčinović, J., Marčeta, D., Onić, D.: 2020, *Book of Abstracts*, XIX Serbian Astronomical Conference, October 13 - 17, 2020, Belgrade, Serbia.
Majlinger, Z., Dimitrijević, M. S., Srećković, V. A.: 2020, *Mon. Not. R. Astron. Soc.*, **496(4)**, 5584.
Marinković, B. P., Bredehöft, J. H., Vujčić, V., Jevremović, D., Mason, N. J.: 2017, *Atoms*, **5(4)**, 46.
Marčeta, D., Novaković, B.: 2020, *Mon. Not. R. Astron. Soc.*, **498(4)**, 5386.
Mijić, Z., Perišić, M.: 2019, *Book of abstracts*, "Integrations of satellite and ground-based observations and multi-disciplinarity in research and prediction of different types of hazards in Solar system", Petnica Science Center, May 10-13, 2019, Geographical Institute "Jovan Cvijić" SASA, Belgrade, 51.
Milić Žitnik, I., Novaković, B.: 2016, *Aphys. Journ. lett.*, **816**, L31.
Milić Žitnik I.: 2019, *Mon. Not. R. Astron. Soc.*, **486**, 2435.
Milić Žitnik I.: 2020a, *Serb. Astron. Journ.*, **200**, 25.
Milić Žitnik I.: 2020b, *Mon. Not. R. Astron. Soc.*, **498(3)**, 4465.

[5]see e.g. *http : //servo.aob.rs/mold*

Nina, A., Radovanović, M., Popović, L. Č., Černok, A., Marinković, B., Srećković, V., Kovačević, A., Radović, J., Čelebonović, V., Milić Žitnik, I., Mijić, Z., Veselinović, N., Kolarski, A., Zdravković, A.: 2020a, *Proceedings of the XII Serbian-Bulgarian Astronomical Conference (XII SBAC)*, Sokobanja, Serbia, September 25-29, 2020, Eds: L. Č. Popović, V. A. Srećković, M. S. Dimitrijević, A. Kovačević, Publ. Astron. Soc. Rudjer Bošković, **20**, 107.

Nina, A., Pulinets, S., Biagi, P. F., Nico, G., Mitrović, S. Dj., Radovanović, M., Popović, L. Č.: 2020b, *Science of the Total Environment*, 710, 136406.

Nina, A., Nico, G., Odalović, O., Čadež, V. M., Todorović, M. D., Radovanović, M., Popović, L. Č.: 2020c, *IEEE Geoscience and Remote Sensing Letters*, **17(7)**, 1198.

Papagiannopoulos, N., D'Amico, G., Gialitaki, A., Ajtai, N., Alados-Arboledas, L., Amodeo, A., Amiridis, V., Baars, H., Balis, D., Binietoglou, I., Comerón, A., Dionisi, D., Falconieri, A., Fréville, P., Kampouri, A., Mattis, I., Mijić, Z., Molero, F., Papayannis, A., Pappalardo, G., Rodríguez-Gómez, A., Solomos, S., Mona, L.: 2020, *Atmos. Chem. Phys.*, **20**, 10775.

Popović, L. Č., Srećković, V. A., Dimitrijević, M. S., Kovačević, A.: 2020, *Book of Abstracts*, XII Serbian–Bulgarian Astronomical Conference (XII SBAC) September 25 - 29, 2020, Sokobanja, Serbia, Astronomical Observatory, Belgrade, Serbia.

Rabasović, M. S., Rabasović, M. D., Marinković, B. P., Šević, D.: 2019, *Atoms*, **7(1)**, 6.

Radović, J.: 2020, Master thesis, Faculty of Physics, University of Belgrade, Serbia.

Srećković, V. A., Dimitrijević, M. S., Ignjatović, L. M.: 2020, *Contrib. Astron. Obs. Skaln. Pleso*, **50**, 171.

Šević, D., Rabasović, M. S., Križan, J., Savić-Šević, S., Rabasović, M. D., Marinković, B. P., Nikolić, M. G.: 2020a, *Opt. Quant. Electron.* **52**, 232.

Šević, D., Vlasić, A., Rabasović, M. S., Savić-Šević, S., Rabasović, M. D., Nikolić, M. G., Marinković, B. P., Križan, J.: 2020b, *Tehnika*, **75(3)**, 279.

Šević, D., Križan, J., Rabasović, M. S., Marinković, B. P.: 2021, "Temperature sensing using YAG:Dy single crystal phosphor", *Eur. Phys. J. D.*, submitted.

Vukalović, J., Maljković, J. B., Tökési, K., Predojević, B., Marinković, B. P.: 2021, *Int. J. Molec. Sci.* **22(2)**, 647.

Yang, P., Yang, G., Zhang, F., Jiang, B., Wang, M.: 2020, *Arch. Computat. Methods. Eng.*, accepted, $https://doi.org/10.1007/s11831-020-09401-9$.

Wislocka, A. M., Kovačević, A. B., Balbi, A.: 2019, *Astron. Astroph.*, 624, A71.

Citation overview

Self citations of selected authors are excluded. ×

Back to author results Export Print

This is an overview of citations for this author. Author *h*-index : 11 View *h*-graph

29 Cited Documents from "Mijić, Zoran" + Save to list

Date range: 2008 to 2022 Exclude self citations of selected author Exclude self citations of all authors Exclude citations from books Update

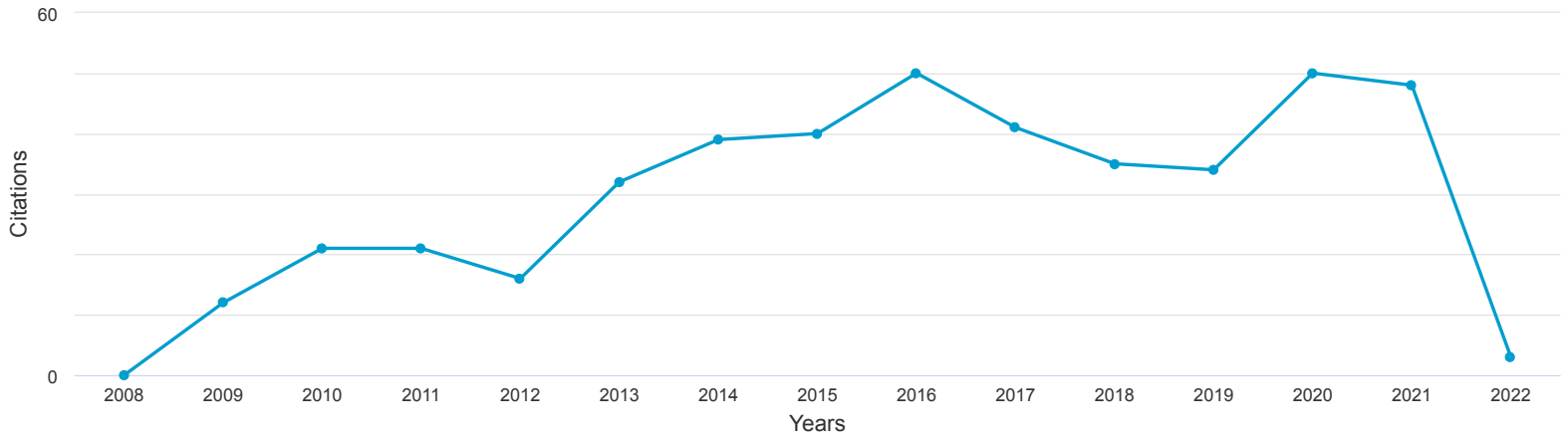

Sort on: Citation count (descending)

Page Remove

	Documents	Citations	<2008	2008	2009	2010	2011	2012	2013	2014	2015	2016	2017	2018	2019	2020	2021	2022	**Subtotal**	>2022	**Total**
		Total	0	0	**12**	**21**	**21**	**16**	**32**	**39**	**40**	**50**	**41**	**35**	**34**	**50**	**48**	**3**	**442**	0	**442**
1	Seasonal variability and source apportionment of metals in t...	2010					4	4	7	11	6	8	7	9	11	8	6	1	**82**		**82**
2	Active moss biomonitoring of trace elements with Sphagnum gi...	2009			3	4	5	3	13	10	9	11	4	4	5	3	7		**81**		**81**
3	Evaluation of the levels and sources of trace elements in ur...	2008			6	4	3	1	4	8	8	5	3	1		3	5		**51**		**51**
4	Determination of O_3, NO_2, SO_2	2008			2	6	1	2	2	7	5	2	4	2	3	6	3	1	**46**		**46**
5	The statistical characters of PM_{10} in Belgrade ar...	2009				1	2	3	5	1	2		2	2		3	1		**22**		**22**

	Documents	Citations	<2008	2008	2009	2010	2011	2012	2013	2014	2015	2016	2017	2018	2019	2020	2021	2022	Subtotal	>2022	Total
		Total	0	0	**12**	**21**	**21**	**16**	**32**	**39**	**40**	**50**	**41**	**35**	**34**	**50**	**48**	**3**	**442**	0	**442**
☐	6 Characterization of VOC sources in an urban area based on PT...	2015										6	1	2	4	4	4		**21**		**21**
☐	7 Physico-chemical characterization of PM_{10} and PM<...	2006				2	2		1	1	3	3	3	2		2			**19**		**19**
☐	8 Forecasting of VOC emissions from traffic and industry using...	2015										2	3	3	4	4	1		**17**		**17**
☐	9 Traffic contribution to air pollution in urban street canyon...	2016											3	2	1	6	4		**16**		**16**
☐	10 Spatio-temporal distribution of VOC emissions in urban area ...	2015									1	4	3	1	1	2	2		**14**		**14**
☐	11 [Receptor modeling studies for the characterization of PM	2012									5	4		1		2			**12**		**12**
☐	12 Comprehensive analysis of PM_{10} in Belgrade urban ...	2016										2	3			2	3		**10**		**10**
☐	13 Levels of PM_{10}-bound species in Belgrade, Serbia:...	2017											1	4	1	1	3		**10**		**10**
☐	14 An assessment of air quality in Belgrade urban area: PM...	2007			1	2	1	2					1	1	1	1			**10**		**10**
☐	15 An EARLINET early warning system for atmospheric aerosol avi...	2020														1	5		**6**		**6**
☐	16 Source apportionment of atmospheric bulk deposition in the B...	2009					2			1			1					1	**5**		**5**
☐	17 PM10 and PM2.5 mass concentration measurements in Belgrade U...	2005				2	1	1											**4**		**4**
☐	18 Estimation of required PM_{10} emission source reduc...	2015									1	1	1			1			**4**		**4**
☐	19 Rainwater capacities for BTEX scavenging from ambient air	2017													2		2		**4**		**4**
☐	20 Assessment of PM $_{10}$ pollution level and required ...	2015										1	1				1		**3**		**3**
☐	21 Changes of atmospheric properties over Belgrade, observed us...	2018													1	1	1		**3**		**3**
☐	22 Comprehensive analysis of VOC emission sources in Belgrade u...	2015										1							**1**		**1**
☐	23 Some characteristic air back trajectories for high PM_{10}...	2007												1					**1**		**1**
☐	24 Air quality study in belgrade: Particulate matter and volati...	2013																	0		0
☐	25 A study of airborne trace elements in belgrade urban area: I...	2012																	0		0
☐	26 Response of the Earth's Lower Ionosphere to Solar Flares and...	2022																	0		0
☐	27 Novel modelling approach for obtaining the parameters of low...	2021																	0		0
☐	28 Activities of serbian scientists in europlanet	2020																	0		0
☐	29 Physical characterization of PM_{10} and $PM_{2.5<...}$	2007																	0		0

BACK TO SEARCH RESULTS

Citation Report

Analyze Results

Export Full Report

Publications
23
Total
From 1980 to 2022

Citing Articles
390 Analyze
Total
375 Analyze
Without self-citations

Times Cited
463
Total
20.13
Average per item
417
Without self-citations

11
H-Index

Times Cited and Publications Over Time

DOWNLOAD

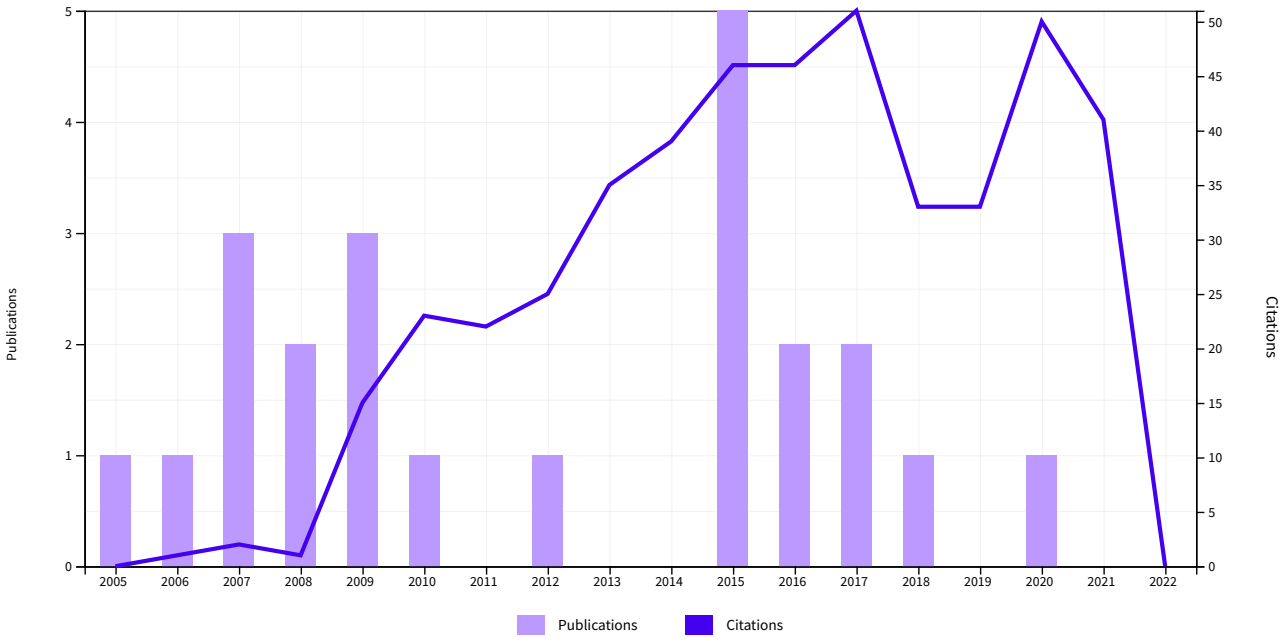

23 Publications

Citations: highest first 1 of 1

		Citations						
		Back				Forward	Average per year	Total
		2018	2019	2020	2021	2022		
	Total	33	33	50	41	0	28.94	463
1	Seasonal variability and source apportionment of metals in the atmospheric deposition in Belgrade Mijic, Z; Stojic, A; (...); Joksic, J Sep 2010 | ATMOSPHERIC ENVIRONMENT 44 (30) , pp.3630-3637	9	11	8	5	0	7	84
		4	5	3	5	0	6.08	79

2	Active moss biomonitoring of trace elements with Sphagnum girgensohnii moss bags in relation to atmospheric bulk deposition in Belgrade, Serbia Anicic, M; Tasic, M; (...); Popovic, A Feb 2009 | ENVIRONMENTAL POLLUTION 157 (2) , pp.673-679							
3	Evaluation of the levels and sources of trace elements in urban particulate matter Rajsic, S; Mijic, Z; (...); Joksic, J May 2008 | ENVIRONMENTAL CHEMISTRY LETTERS 6 (2) , pp.95-100	1	0	3	3	0	3.86	54
4	Determination of O-3, NO2, SO2, CO and PM10 measured in Belgrade urban area Markovic, DM; Markovic, DA; (...); Mijic, Z Oct 2008 | ENVIRONMENTAL MONITORING AND ASSESSMENT 145 (1-3) , pp.349-359	2	2	5	4	0	3.07	43
5	Physico-chemical characterization of PM10 and PM2.5 in the Belgrade urban area Tasic, M; Duric-Stanojevic, B; (...); Novakovic, V 2006 | ACTA CHIMICA SLOVENICA 53 (3) , pp.401-405	2	1	2	0	0	1.63	26
6	The statistical characters of PM10 in Belgrade area Mijic, Z; Tasic, M; (...); Novakovic, V Jun 2009 | ATMOSPHERIC RESEARCH 92 (4) , pp.420-426	2	0	4	0	0	1.85	24
7	Characterization of VOC sources in an urban area based on PTR-MS measurements and receptor modelling Stojic, A; Stojic, SS; (...); Rajsic, S Sep 2015 | ENVIRONMENTAL SCIENCE AND POLLUTION RESEARCH 22 (17) , pp.13137-13152	2	3	4	4	0	3	21
8	Traffic contribution to air pollution in urban street canyons: Integrated application of the OSPM, moss biomonitoring and spectral analysis Lazic, L; Urosevic, MA; (...); Ilic, L Sep 2016 | ATMOSPHERIC ENVIRONMENT 141 , pp.347-360	3	2	6	4	0	3.17	19
9	Spatio-temporal distribution of VOC emissions in urban area based on receptor modeling Stojic, A; Stojic, SS; (...); Rajsic, S Apr 2015 | ATMOSPHERIC ENVIRONMENT 106 , pp.71-79	1	1	3	2	0	2.71	19
10	Forecasting of VOC emissions from traffic and industry using classification and regression multivariate methods Stojic, A; Maletic, D; (...); Sostaric, A Jul 15 2015 | SCIENCE OF THE TOTAL ENVIRONMENT 521 , pp.19-26	2	3	4	1	0	2.29	16
11	RECEPTOR MODELING STUDIES FOR THE CHARACTERIZATION OF PM10 POLLUTION SOURCES IN BELGRADE Mijic, Z; Stojic, A; (...); Tasic, M Oct-dec 2012 | CHEMICAL INDUSTRY & CHEMICAL ENGINEERING QUARTERLY 18 (4) , pp.623-634	1	0	2	0	0	1.4	14
12	Levels of PM10-bound species in Belgrade, Serbia: spatio-temporal distributions and related human health risk estimation Perisic, M; Rajsic, S; (...); Stojic, A Jan 2017 | AIR QUALITY ATMOSPHERE AND HEALTH 10 (1) , pp.93-103	4	1	1	3	0	2	10
13	Comprehensive analysis of PM10 in Belgrade urban area on the basis of long-term measurements Stojic, A; Stojic, SS; (...); Mijic, Z International Conference on Contaminated Sediments (ContaSed-2015) Jun 2016 | ENVIRONMENTAL SCIENCE AND POLLUTION RESEARCH 23 (11) , pp.10722-10732	0	0	2	2	0	1.67	10
14	An assessment of air quality in Belgrade urban area: PM10, PM2.5 and trace metals Tasic, M; Rajsic, S; (...); Mijic, Z 1st International Workshop on Nonequilibrium Processes in Plasma Physics and Studies of Environment 2007 | FIRST INTERNATIONAL WORKSHOP ON NONEQUILIBRIUM PROCESSES IN PLASMA PHYSICS AND STUDIES OF ENVIRONMENT 71	0	1	1	0	0	0.6	9

15	Estimation of required PM10 emission source reduction on the basis of a 10-year period data Perisic, M; Stojic, A; (...); Rajsic, S Aug 2015 | AIR QUALITY ATMOSPHERE AND HEALTH 8 (4) , pp.379-389	0	0	1	0	0	1	7
16	Source Apportionment of Atmospheric Bulk Deposition in the Belgrade Urban Area Using Positive Matrix Factorization Tasic, M; Mijic, Z; (...); Joksic, J 2nd International Workshop on Non-Equilibrium Processes in Plasmas and Environmental Science 2009 | SECOND INTERNATIONAL WORKSHOP ON NON-EQUILIBRIUM PROCESSES IN PLASMAS AND ENVIRONMENTAL SCIENCE 162	0	0	0	0	0	0.54	7
17	PM10 and PM2.5 mass concentration measurements in Belgrade urban area Tasic, MD; Rajsic, SF; (...); Tomasevic, MN 1st International Meeting on Applied Physics 2005 | PHYSICA SCRIPTA T118 , pp.29-30	0	0	0	0	0	0.41	7
18	An EARLINET early warning system for atmospheric aerosol aviation hazards Papagiannopoulos, N; D'Amico, G; (...); Mona, L Sep 15 2020 | ATMOSPHERIC CHEMISTRY AND PHYSICS 20 (18) , pp.10775-10789	0	0	0	4	0	2	4
19	Changes of atmospheric properties over Belgrade, observed using remote sensing and in situ methods during the partial solar eclipse of 20 March 2015 Ilic, L; Kuzmanoski, M; (...); Andric, M Jun 2018 | JOURNAL OF ATMOSPHERIC AND SOLAR-TERRESTRIAL PHYSICS 171 , pp.250-259	0	1	1	2	0	1	4
20	Rainwater capacities for BTEX scavenging from ambient air Sostaric, A; Stojic, SS; (...); Grzetic, I Nov 2017 | ATMOSPHERIC ENVIRONMENT 168 , pp.46-54	0	2	0	1	0	0.6	3
21	Assessment of PM10 pollution level and required source emission reduction in Belgrade area Todorovic, MN; Perisic, MD; (...); Rajsic, SF Nov 10 2015 | JOURNAL OF ENVIRONMENTAL SCIENCE AND HEALTH PART A-TOXIC/HAZARDOUS SUBSTANCES & ENVIRONMENTAL ENGINEERING 50 (13) , pp.1351-1359	0	0	0	1	0	0.43	3
22	Some characteristic air back trajectories for high PM10 and PM2.5 concentration episodes in Belgrade Mijic, ZR; Lazic, LA; (...); Novakovic, VT 6th International Conference of the Balkan-Physical-Union 2007 | SIX INTERNATIONAL CONFERENCE OF THE BALKAN PHYSICAL UNION 899 , pp.741-741	0	0	0	0	0	0	0
23	Physical characterization of PM10 and PM2.5 in Belgrade atmosphere by SEM/EDX and image analysis system Novakovic, VT; Tasic, MD; (...); Mijic, ZR 6th International Conference of the Balkan-Physical-Union 2007 | SIX INTERNATIONAL CONFERENCE OF THE BALKAN PHYSICAL UNION 899 , pp.743-743	0	0	0	0	0	0	0

Citation Report Publications Table

Република Србија
МИНИСТАРСТВО ПРОСВЕТЕ,
НАУКЕ И ТЕХНОЛОШКОГ РАЗВОЈА
Комисија за стицање научних звања

Број: 660-01-00001/512
26.04.2017. године
Б е о г р а д

На основу члана 22. став 2. члана 70. став 5. Закона о научноистраживачкој делатности ("Службени гласник Републике Србије", број 110/05, 50/06 – исправка, 18/10 и 112/15), члана 3. ст. 1. и 2. тачке 1) – 4) (прилози), став 3. и члана 40. Правилника о поступку, начину вредновања и квантитативном исказивању научноистраживачких резултата истраживача ("Службени гласник Републике Србије", број 24/16, 21/17 и 38/17) и захтева који је поднео

Институт за физику у Београду

Комисија за стицање научних звања на седници одржаној 26.04.2017. године, донела је

ОДЛУКУ
О СТИЦАЊУ НАУЧНОГ ЗВАЊА

Др Зоран Мијић

стиче научно звање

Виши научни сарадник

у области природно-математичких наука - физика

О Б Р А З Л О Ж Е Њ Е

Институт за физику у Београду

утврдио је предлог број 1546/1 од 13.09.2016. године на седници Научног већа Института и поднео захтев Комисији за стицање научних звања број 1573/1 од 21.09.2016. године за доношење одлуке о испуњености услова за стицање научног звања ***Виши научни сарадник***.

Комисија за стицање научних звања је по претходно прибављеном позитивном мишљењу Матичног научног одбора за физику на седници одржаној 26.04.2017. године разматрала захтев и утврдила да именовани испуњава услове из члана 70. став 5. Закона о научноистраживачкој делатности ("Службени гласник Републике Србије", број 110/05, 50/06 – исправка,18/10 и 112/15), члана 3. ст. 1. и 2. тачке 1) – 4) (прилози), став 3. и члана 40. Правилника о поступку, начину вредновања и квантитативном исказивању научноистраживачких резултата истраживача ("Службени гласник Републике Србије", број 24/16, 21/17 и 38/17) за стицање научног звања ***Виши научни сарадник***, па је одлучила као у изреци ове одлуке.

Доношењем ове одлуке именовани стиче сва права која му на основу ње по закону припадају.

Одлуку доставити подносиоцу захтева, именованом и архиви Министарства просвете, науке и технолошког развоја у Београду.

ПРЕДСЕДНИК КОМИСИЈЕ

Др Станислава Стошић-Грујичић,
научни саветник

С. Стошић-Грујичић

МИНИСТАР

Младен Шарчевић